Refractive Integrated Nonimaging Solar Collectors

Design and Analysis of a Novel Solar-Daylighting-Technology

A thesis submitted in partial fulfilment of the requirements for the degree of Doctor of Philosophy (Ph.D.)

by

Alexandre Vieira Pelegrini

M.Eng., B.Sc.

School of Engineering and Design

Brunel University

October 2009

Refractive Integrated Nonimaging Solar Collectors: Design and Analysis of a Novel Solar-Daylighting-Technology

A Ph.D. thesis by Alexandre Vieira Pelegrini (*)

(*) Supported by the Brazilian National Council for Scientific and Technological Development (CNPq), under the scholarship grant 200663/2004-6 (GDE), from 01/03/2005 to 28/02/2009.

Brunel University / School of Engineering and Design
Uxbridge, Middlesex, UB8 3PH, Greater London - UK

Abstract

A novel and original category of low-cost static solar-daylighting-collectors named Refractive Integrated Nonimaging Solar Collectors (RINSC) has been designed and thoroughly tested. The RINSC category is based on nonimaging optics and integrates several optical elements, such as prismatic arrays and light guides, into a single-structured embodiment made of solid-dielectric material. The RINSC category is sub-divided in this thesis into four distinctive and original sub-categories/systems: Prismatic Solar Collectors (PSC), Multi-Prismatic Solar Collectors (MPSC), Integrated Multi-Prismatic Solar Collectors (IMPSC) and Vertically Integrated Nonimaging Solar Collectors (VINSC). The optical configuration and compact embodiment of these systems allows them to be integrated into a building façade without creating any protrusion, indicating that they can lead to solar collector systems with high building integration potential. Laboratory and outdoor experimental tests conducted with a series of demonstration prototypes made of clear polymethyl-methacrylate (PMMA) and manufactured by laser ablation process, yield peak transmission efficiencies T_E varying from 2% to 8%. Computer simulations indicated that transmission efficiencies $T_E > 30\%$ are possible. The design and development of the innovative optical systems introduced in this thesis were backed-up with extensive computer ray-tracing analysis, rapid-prototyping, laboratory and outdoor experimental tests. Injection moulding computer simulations and surface analysis concerning the development of the RINSC systems were also conducted. Basic theory and comprehensive literature review are presented. This research has also resulted in the design and prototyping of a novel optical instrumentation named Angular Distribution Imaging Device (ADID), specially developed to analyse the spatial distribution of light emerging from the exit aperture of solar collectors/concentrators. The systems and knowledge described in this thesis may find application in areas such as solar collector systems to harvest sunlight for natural illumination in buildings, solar-photovoltaic and solar-thermal.

Keywords**:** solar energy, solar collectors, daylighting systems, nonimaging optics, renewable energy, sustainable design.

"*What I cannot create, I do not understand*",
Richard Feynman

TABLE OF CONTENTS

Acknowledgements

Some may argue that the acknowledgments are the most difficult part of the thesis.
I couldn't agree more. I would like to thank:

My supervisors, Dr. Peter Evans and Prof. David Harrison, for their effort and time dedicated to this long work. Dr. John Shackleton, who co-supervised the first part of my research at Brunel University.

The School of Engineering and Design staff, in especial: Ian Kay, Lyn Edgecock, Paul Barrett, Paul Josse, Paul Yates and Wendy Dean.

My colleagues at Brunel University: Gareth Hay, Richard Young, Sam Duby, Julian Woods, Jonas Pettersson, Daniel Lockton, Alexander Plant, Alexander Komashie, Vahid Pazeshki and Dehong Huo.

My former professors in Curitiba / Brazil, Dr. Virginia Borges Kistmann and Dr. Aguinaldo dos Santos, for their recommendation letters.

My friend Raquel and her sons Sol and Mylo.

My parents, Fernando and Eliane, for their support and understanding.

And finally, my wife Vanessa, for her endless patience.
This work is dedicated to her.

(*) This research was funded in part by the Brazilian National Council for Scientific and Technological Development (CNPq), under the scholarship grant 200663/2004-6 (GDE), from 01/03/2005 to 28/02/2009.

List of Figures

List of Tables

Nomenclature and Abbreviations

μ	conversion factor from primary energy to electricity
A_1	entrance aperture area
A_2	exit aperture area
ADID	angular distribution imaging device
AILG	asymmetrical integrated light guide
ASTM	American Society for Testing and Materials
BS	British Standard
$C0_2$	carbon-dioxide
CCD	charge-coupled device
CIE	International Commission on Illumination
C_{max}	maximum concentration ratio
CMOS	complimentary metal-oxide semiconductor
CO_2	carbon dioxide
CPC	Compound Parabolic Concentrator
C_R	geometric concentration ratio
d	distance
DF	daylight factor
DLC	deconcentrator light cone
DTIRC	Dielectric Total Internal Reflection Concentrator
E (or E_v)	Illuminance (measured in lux, lx)
E_{el}	gross electric energy consumption
E_{eo}	Solar Constant
E_{in}	illuminance input (measured in lux, lx)
E_{out}	illuminance output (measured in lux, lx)
E_{prim}	primary energy requirements for buildings
E_{sp}	surplus electricity generated by photovoltaic panels
E_{th}	auxiliary thermal energy for heating
E_{vc}	luminous solar constant (measured in lux, lx)
E_{vo}	luminous solar constant
FDM	fluid-deposition machine
HOE	holographic optical element
h_s	solar altitude angle
I_s	Solar irradiance (measured in W/m^2)
I_0	total solar radiation (measured in W/m^2)
i_{max}	maximum number of internal reflections
IMPSC	Integrated Multi-Prismatic Solar Collector(s)

K	luminous efficacy of solar radiation (measured in lm/W)
L	length
LAN	light at night
LCP	laser cut panels
LSC	luminescent solar concentrator(s)
Lx	lux (unit of illuminance)
MPSC	Multi-Prismatic Solar Collector(s)
N	refractive index
NIR	near-infrared radiation (λ > 780nm)
NO	nitric oxide
NO_2	nitrogen oxide
N_R	number of reflections
N_{TIR}	number of total internal reflections
Ø	diameter
OPL	optical path length
PA1	first prismatic array
PA2	second prismatic array
PC	polycarbonate
PM_{10}	Particulate Matter of less than 10μm in diameter (air pollutant particle)
$PM_{2.5}$	Particulate Matter of less than 2.5μm in diameter (air pollutant particle)
PMMA	polymethyl-methacrylate
PSC	Prismatic Solar Collector(s)
ROPS	“RINSC optical profile section”
RVS	“RINSC volumetric space”
SILG	symmetrical integrated light guide
SPD	spectral power distribution
S_θ	angular increment
T_E	transmission efficiency
TIR	total internal reflection
TS_θ	total angular increment
UDI	useful daylight illuminances (measured in lux, lx)
UV	ultraviolet radiation (λ < 400nm)
v(λ)	photopic luminous efficacy function
UFO	Universal Fibre Optics (from: Tsangrassoulis et al, 2005)
VINSC	Vertically Integrated Nonimaging Solar Collector(s)
VIS	visible light (λ = 400nm to 780nm)
WMO	World Meteorological Organization
α_{PA1}	first prismatic array apex angle
α_{PA2}	second prismatic array apex angle
α_{SILG}	symmetrical integrated light guide apex angle

γ_s	solar azimuth angle
δ	total angular deviation (light deflected by a prism)
δ_{sun}	solar declination
$\Delta\theta$	angular distribution
$\delta\theta_{exit}$	angular distribution at exit aperture interface
η_0	optical efficiency
θ_{accept}	acceptance angle
θ_c	critical angle
θ_i	incident angle
λ	wavelength
ρ	surface reflectivity
σ	surface absorption
Φ	luminous flux

Chapter 1 - Introduction

1.1 Foreword

It has been estimated that buildings account for 20% to 40% of total final energy consumption and around 40% of the carbon dioxide (CO_2) emissions in most developed countries (Jenkins and Newborough, 2007; Pérez-Lombard et al, 2007; Pérez-Lombard et al, 2008). Of this total, about 10% to 30% corresponds to artificial lighting (Pérez-Lombard et al, 2008; Loe, 2003). Increasing evidence for anthropogenic global warming has meant that issues relating to the design of low-energy and energy-efficient buildings are gaining support among builders, architects, society and governments (De Vries et al, 2007; Jenkins and Newborough, 2007). However, despite innovations and the development of more energy-efficient appliances and building systems, energy demand continues to rise due to the fact that there are more buildings being constructed and higher comfort levels are required by occupants (Addington 2003; Jenkins and Newborough, 2007; Pérez-Lombard et al, 2008; EIA, 2009). As highlighted by Osbourn (1997, pp.4), "*modern buildings are expected to be a life-support machine*". In this context, increasing the applications of solar radiation is viewed as a fundamental issue in the design of sustainable buildings and also for sustainable development (Eicker, 2003; Goldemberg, 2006; Okoro and Madueme, 2006; Omer, 2008; Pelegrini et al, 2007). .

Exploitation of solar radiation can have a significant impact in the development of a clean and sustainable energy mix, resulting in several benefits for society and the environment and leading to a low-carbon economy (Omer, 2008). Solar-photovoltaics, solar-thermal-heating and core daylighting systems are some examples of promising solar technologies applications (De Vries et al, 2007; Omer, 2008; EIA, 2009). Among these examples, core daylighting systems, which aim to deliver natural illumination into areas deep inside buildings, are advocated by many authors as a potential clean and energy-efficient solution for sustainable buildings (IEA, 2000; Leslie, 2003; Rosemann et al, 2008; Chen, 2004; Cutler et al, 2008; Pelegrini et al, 2007).

The increase in daylighting in buildings can lead to several direct and indirect benefits. Research has shown that strategic daylighting can reduce 20% to 75% of

electric lighting demand, leading to an estimated 15% to 20% reduction on buildings overall energy consumption (Loe, 2003; Loe, 2009; Ihm et al, 2008). Recent studies also indicate that natural illumination can have a very positive contribution on buildings occupants' well-being, satisfaction, productivity, and even help to combat depression and seasonal-affect-disorders (Olders, 2003; Berson, 2003; Pauley, 2004; Webb, 2006). The disadvantage of increasing direct sunlight for indoor illumination is that, if not properly managed, it can introduce excessive heat into the building, and hence, increase cooling demand (Bodart and De Herde, 2002; Sezgen and Koomey, 2000; Pelegrini et al, 2007; Li and Tsang, 2005).

A large number of solar collectors, solar concentrators and sunlight transportation systems have been designed and tested for a variety of applications over the last decades, including solar-photovoltaic and solar-daylighting (Scharlack, 1977; Welford and Winston, 1978; Fraas et al, 1983; Feuermann and Gordon, 1999; IEA, 2000; Bazilian et al, 2001; Kandilli et al, 2008).

Swanson (2000) reports on the significant effort to develop cost-effective solar concentrator systems for solar-photovoltaic applications. According to Swanson (2000, pp.93-94), this research-led effort took place from the mid-1970s to the beginning of the 1990s, and it involved several world-wide companies, research institutions and large universities. However, after more than 15 years of research and despite successfully demonstrating prototypes, no system with wide-market commercial potential was achieved (Swanson, 2000). A series of yet unsolved problems that range from technical to economical issues have kept these systems at prototype stage (Swanson, 2000; Antón et al, 2003; Kandilli and Ulgen, 2009).

A similar fate has also marked the development of daylighting systems. The basic idea of collecting and guiding sunlight into core-building areas has been around for more than a century. Some of the earliest patents describing daylighting technologies can be traced back to the end of the 19th century (Ewen, 1897; Wadsworth, 1898). According to Selkowitz (1998) the idea of natural illumination in buildings periodically re-emerges in the academic and industry arenas always when a major energy crisis seems imminent. In a review on the subject, the author argued that in the 1970s world oil crises, daylighting emerged as a promising option to reduce energy demand (Selkowitz, 1998). The current energy and environmental crises are also the main motivation behind the research and investment in renewable energy nowadays (Bodart and De Herde, 2002; Block, 2006; Omer, 2008).

Daylighting systems have been proposed and tested all over the world under all types of weather and climate conditions (Chirarattananon et al, 2000; Callow, 2003; Canziani et al, 2004). However, few of the current commercial daylighting systems

provide what they are expected to do at an acceptable cost (Selkowitz, 1998; IEA, 2000; Matusiak, 2004; Rosemann et al, 2008).

In the field of solar concentrators it has been argued that static nonimaging concentrators can achieve higher concentration than static imaging concentrators (Welford and Winston, 1978; Mallick et al, 2007). Compact nonimaging optical devices have already been developed and applied to concentrate solar radiation for photovoltaic applications (Luque, 1986; Ning et al, 1987). However, for applications where sunlight has to be transported through longer distances, such as to increase natural illumination in core-building areas, most existing solar collectors for daylighting application do not provide a cost-effective solution (Selkowitz, 1998; Reinhart and Selkowitz, 2006). Furthermore, technical problems such as the lack of building and architecture integration attributes, makes it more difficult for these systems to be widely used and succeed in the market (Nicoletti, 1998; Hestnes, 1999; IEA, 2000).

Figure 1.1 shows a schematic illustration of four existing commercial types of daylighting systems. A comprehensive review is described in IEA (2000).

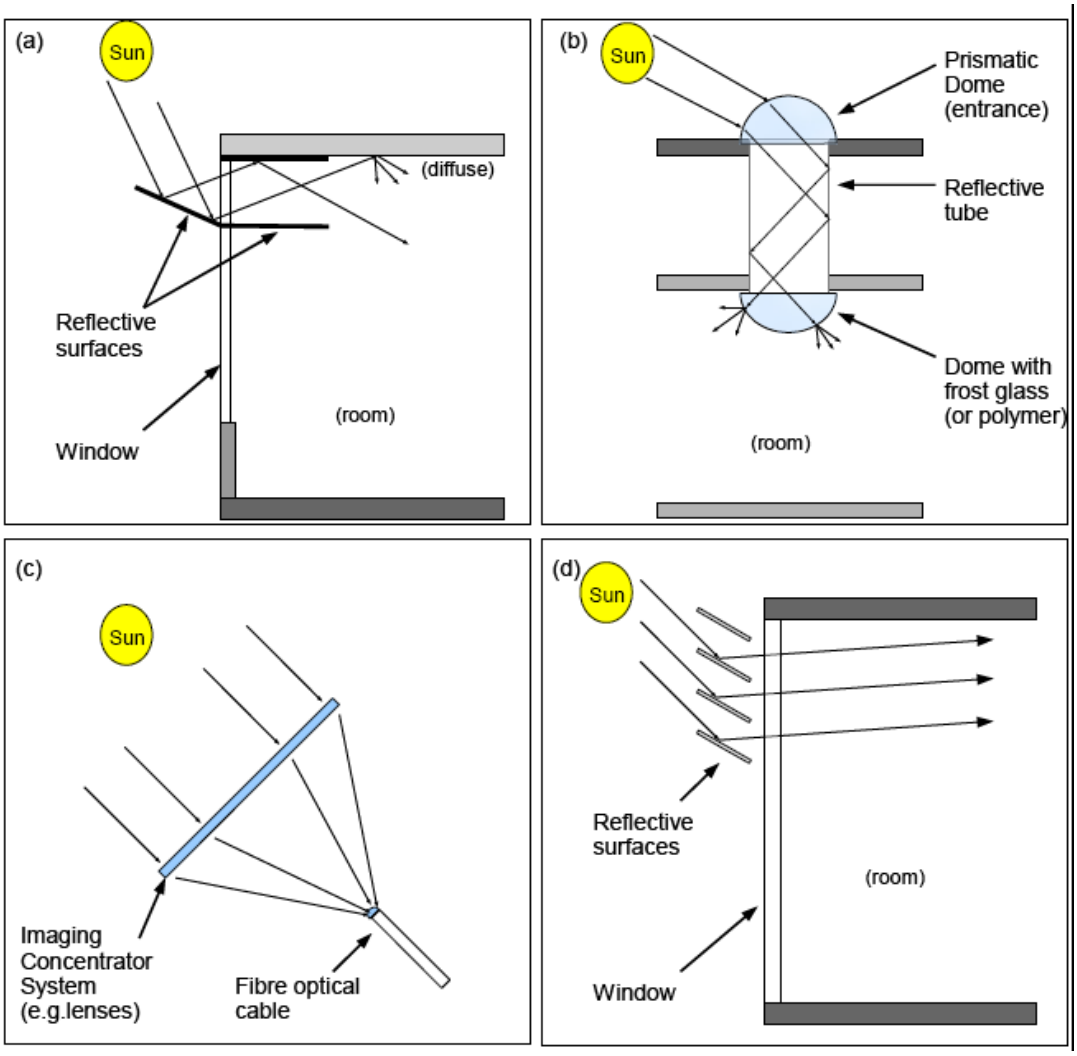

Figure 1.1 – Schematic illustration of existing commercial daylighting systems.

1.2 Aim and objectives of the research

The aim of this design-focused research is to design and analyse a novel category of compact nonimaging-optical-systems that can lead to the development of low-cost solar-daylighting-collectors, with emphasis on the development of innovative nonimaging optical configurations concepts that can lead to the development of cost-effective mass-produced systems with high building integration potential. Considering this, the main objectives of this work are:

- The design and analysis of novel configurations of nonimaging optical geometries suitable to be applied in the development of compact static solar collectors/concentrators for solar energy related systems used in buildings, and more specifically for applications such as to harvest direct sunlight for core-daylighting application;
- The design, simulation, prototyping and experimental tests on a series of low-cost compact single-structure-configuration solar-daylighting-collectors based on nonimaging optics and total internal reflection (TIR); and
- The proof-of-concept and basic description of the working principle of the designed systems.

1.3 Statement of thesis and original contributions to the field

This research has resulted in the development and test of a novel category of solar-daylighting-collectors, named Refractive Integrated Nonimaging Solar Collectors (RINSC). The RINSC systems category is further sub-divided into four distinct original categories also introduced and tested in this thesis, named: Prismatic Solar Collectors (PSC), Multi-Prismatic Solar Collectors (MPSC), Integrated Multi-Prismatic Solar Collectors (IMPSC) and Vertically Integrated Nonimaging Solar Collectors (VINSC).

A series of innovative nonimaging optical systems designed to harvest and trap incident sunlight by means of refractive-optics and total internal reflection (TIR) has been developed and thoroughly tested. The RINSC systems and sub-categories are characterised by integrating distinct geometric optical features, such as prismatic arrays and light guides, into single-structure-configurations. Static, low-cost and compact optical configurations with relatively high concentration ratios are possible, resulting in systems with high building integration potential. The original designs are backed-up by computer simulations, prototyping and experimental tests, including photometric measurements, spectral analysis and surface analysis.

This research has also resulted in the design, prototyping and experimental test of a novel optical instrumentation device conceived to analyse the angular distribution of light emerging from the exit aperture of the solar-collectors demonstration prototypes. The device, named Angular Distribution Imaging Device (ADID), provided a qualitative evaluation of the spatial distribution of the collected light in order to assess the potential of the system and indicate possible improvements.

Until the submission date of this thesis, two journal papers had been submitted to scientific journals. One of the papers, related to the RINSC-PSC system, had already been accepted (Pelegrini et al, 2009a). The second journal paper, describing the RINSC-IMPSC system, was still being peered reviewed. The abstracts of the submitted and the accepted papers are presented in the Appendix section of this thesis (Pelegrini et al, 2009a; Pelegrini et al, 2009b). Further papers concerning the results of this research are still expected to be published.

The abstract of a third paper, named "Splitting and managing the solar spectrum for energy efficiency and daylighting", published in the proceedings and presented at the international conference "*Portugal SB07 Sustainable Construction, Materials and Practices: Challenge of the Industry for the New Millennium*", is also included in the Appendix section (Pelegrini et al, 2007). This paper relates to the first part of this research, developed in the beginning of the doctorate course.

1.4 Summary of chapters and thesis structure

This thesis is divided into ten chapters:

Chapter 1 (current) presented a general introduction to the thesis, its objectives, the research statement and original contributions to the field. A general introduction to the main problems related to the design and implementation of solar collector systems for daylighting application in buildings has been outlined. A brief review on the increase in building energy demand and the potential benefits of solar-daylighting was also presented.

Chapter 2 presents a comprehensive literature review on the main topics related with this work. The benefits and advantages of solar-daylighting in buildings are described. The current state-of-the-art in solar collectors/concentrators technologies are presented and discussed. A discussion on the justification for this work and the identification of a gap in the literature are presented at the end of the Chapter 2.

Chapter 3 describes the main research methods, optical analysis techniques and instrumentation applied during the development of this research. It also describes the instrumentation apparatus specially designed and manufactured for this work,

including: hollow cylindrical light pipes to function as light luminous flux integrating devices, and a novel optical measuring device to analyse the spatial distribution of light emerging from the solar-collectors demonstration prototypes, named Angular Distribution Imaging Device (ADID).

Chapter 4 introduces the conceptual model, general design considerations and the basic theory for the development of the Refractive Integrated Nonimaging Solar Collectors (RINSC) category and systems. The RINSC category is further sub-divided into four distinct sub-categories: the Prismatic Solar Collectors (PSC), the Multi-Prismatic Solar Collectors (MPSC), the Integrated Multi-Prismatic Solar Collectors (IMPSC) and the Vertically Integrated Nonimaging Solar Collectors (VINSC). These sub-categories are analysed in more detail in Chapters 5, 6, 7 and 8, respectively.

Chapter 5 the Prismatic Solar Collectors (PSC) systems are introduced and thoroughly tested. The main design issues and parameters related to the application of prismatic arrays with combined light guide to harvest direct sunlight are presented. The PSC concept was designed in order to analyse the potential to harvest and trap light by means of TIR inside a prismatic array system with combined light guide.

Chapter 6 the Multi-Prismatic Solar Collectors (MPSC) systems are introduced and thoroughly tested. The MPSC systems were derived from the PSC basic concept. The MPSC considers the introduction of a series of parallel prismatic arrays with combined light guides in order to increase the acceptance angle θ_{accept} and the efficiency (in comparison with the PSC system from Chapter 5).

Chapter 7 the Integrated Multi-Prismatic Solar Collectors (IMPSC) systems are introduced and thoroughly tested. The IMPSC was derived from the MPSC basic concept of applying a group of parallel prismatic arrays in order to deflect and harvest direct incident light. However, in the design of IMPSC systems it was considered the inclusion of at least one independent solid-dielectric light guide positioned in between a set of two prismatic arrays.

Chapter 8 the Vertically Integrated Nonimaging Solar Collectors (VINSC) systems are introduced and thoroughly tested. The VINSC systems present a more complex geometric configuration than the systems previously described.

Chapter 9 discusses and compares the main results from this thesis. The main contributions to knowledge resulting from this work are presented in technical terms.

Chapter 10 concludes the thesis and presents a series of topics for possible future work in the area.

Chapter 2 - Literature Review

2.1 Introduction

This chapter presents a review of the main topics investigated during this research. The most relevant factors in the development of solar-daylighting-collectors and daylighting systems are discussed. Several solar collectors and solar concentrator technologies, applied for both solar-daylighting and/or for solar-photovoltaic systems are investigated in order to understand their basic optical working principles. The chapter concludes with a discussion of the main problems with current solar-daylighting of technologies and the justification for this work. A gap in the literature and a research opportunity are defined.

2.2 Solar radiation and the solar spectrum

Solar irradiance on a perpendicular plane (in relation to solar radiation incident angle) outside the Earth atmosphere is normalised to a constant value, known as the Solar Constant E_{eo}, standardized by the World Meteorological Organisation (WMO) as E_{eo} = 1367 W/m^2 (BS EN ISO 9488:2000, pp.11; Eicker, 2003). An alternative to the Solar Constant E_{eo}, which measures solar irradiance in radiometric terms (W/m^2), is the luminous solar constant E_{vo}, which measures the solar illuminance in the photometric quantity *lux* (lx). On a perpendicular plane (in relation to solar radiation incident angle) at the top of the Earth atmosphere the luminous solar constant E_{vo} = 133.800 lx (Kittler and Darula, 2002, pp.178-179; Darula et al, 2005). However, it is important to note that both the Solar Constant E_{eo} and the luminous solar constant E_{vo} are not actually real constants. Variations in the solar activity lead to variations in the "Solar Constant". Continuous satellite measurements during a period of 25 years (from late 1978 to 2004) measured variations of the Solar Constant E_{eo} from 1362 W/m^2 to 1374 W/m^2 (Fröhlich, 2006).

According to the standard ASTM G173-03 (2003), solar radiation wavelength composition at the Earth's surface varies from around 250nm to 4000nm. Approximately 99% of this energy is contained in the spectrum range between 300nm

to 3300nm, corresponding to: 48% of visible light (VIS: 380nm to 780nm), 6% of ultraviolet radiation (UV: < 380nm), and 45% of near-infrared radiation (NIR: > 780nm). In power terms this translates to: 660 W/m^2 related to visible light (VIS); 92.6 W/m^2 related to ultraviolet (UV), and 614.4 W/m^2 related to the near-infrared (NIR) – (Eicker, 2003, pp.16). In the tropical regions of the planet, solar irradiance I_o can reach up to 1000 W/m^2 and solar illuminance around 100,000 lx under direct sunlight (clear sky). In countries located at high latitude, such as the United Kingdom, the amount of solar radiation received in a year corresponds to about half of what a tropical country receives (Pearsall, 1998, pp.553; BS EN ISO 9488:2000, pp.10; Chandra, 1996).

The standard ASTM G173-03 is internationally adopted a reference for terrestrial solar spectral irradiance (ASTM, 2003; BS EN 60904-3-2008). It is important to note that the standard ASTM G173-03 (ASTM, 2003) stresses that its measurements for the terrestrial solar spectral irradiance are only valid for a specific orientation, under a specific direct solar incident angle, received on an inclined plane at 37° tilt toward the equator, under an air mass[1] of 1.5 and specific atmospheric conditions, as described in the standard (ASTM, 2003).

Solar radiation at the Earth's surface is usually divided into two components: direct sunlight and diffuse sunlight. Direct sunlight is also referred in the literature as direct component, and diffuse sunlight as diffuse component. Diffuse radiation gradually increases toward the solar disk. This effect, known as degree of isotropy, is higher in the proximity of industrial and urban areas, where dust, aerosols and pollution particles are more concentrated. Their presence increases the turbidity of local atmospheric conditions (Welford and Winston, 1978, pp.125). A third component is the albedo, or the amount of radiation that is reflected by the ground and immediate surroundings (IEA, 2001; Messenger and Ventre, 2000).

According to Chandra (1996, pp.1623), "*the amount of illumination for a given amount of radiation can be calculated as*":

$$E = K I_s \qquad [2.1]$$

where E is the illuminance, or illumination (measured in *lux*, lx), I_s the incident solar radiation, or solar irradiance (measured in W/m^2), and K is the luminous efficacy of solar radiation (measured in lm/W) – (Chandra, 1996, pp.1623).

[1] Air mass corresponds to the thickness of the atmosphere that solar radiation travels before reaching the ground. It varies according to solar angular displacement, site geographic locations and altitude (Messenger and Ventre, 2000, pp.21).

Schneider and Young (in DeCusatis, 1998, pp.243) defines the term luminous efficacy for monochromatic radiation of wavelength λ as the "*ratio of the total luminous flux Φ_v to the total radiant flux Φ_e (measured in lumens per Watt, lm/W)*". For most photometric applications, the luminous efficacy for the photopic vision and the scotopic vision is standardized as 683 lm/W for monochromatic radiation normalized at the wavelength λ = 555nm (Schneider and Young, 1998, pp.243; British Standard BS ISO 23539:2005, pp.3; Robledo and Soler, 2001).

The mix of wavelengths in the visible part of the spectrum gives sunlight its characteristic white colour appearance. Intensity peaks in the visible light range at wavelength λ=555nm, which corresponds to the human photopic response (Ohno, in DeCusatis, 1998; Chandra, 1996).

2.3 Sun-Earth geometry, sun path and solar incident angles

Earth is inclined around its own polar axis by an angle of 23.45°. Due to this inclination the Sun appears to be higher in the sky during the summer than in the winter (Messenger and Ventre, 2000, pp.25). It is also for this reason that the Earth receives more hours of direct solar radiation during the summer than during the winter (Messenger and Ventre, 2000; Eicker, 2003).

The apparent movement of the Sun across the sky is usually described by two angles: (1) the solar altitude angle h_s, which measures the vertical displacement of the Sun; (2) and the solar azimuth angle γ_s, which measures the horizontal displacement of the Sun (Messenger and Ventre, 2000, pp.26; BS EN ISO 9488:2000, pp.2).

The angle of deviation of the Sun in relation to the Equator line is called solar declination δ_{sun}. At north of the Equator, the solar declination δ_{sun} is conventionally considered positive, and, symmetrically, negative at the south of the Equator (Messenger and Ventre, 2000, pp.24; British Standard BS 8206-2:2008).

2.4 Atmospheric conditions and the CIE Standard Skies

The atmosphere plays an important role in governing the intensity, spectral composition and distribution of solar radiation that reaches the Earth surface. Absorption and scattering reduces the intensity of solar radiation as it travels through the atmosphere (Chandra, 1996; Rahoma, 2001). Vapour water molecules, dust, aerosols and other pollution particles attenuate significant part of the direct solar radiation intensity spectral composition, contributing to a moderate increase in the

diffuse solar radiation component (Jacovides et al, 2000, pp 215). According to Rahoma (2001, pp.338), the main absorbing molecules and components in the atmosphere are: O_2, O_3, H_20, CO_2, N_2, N, NO, N_20, CO, CH_4.

Total global and sky illuminances value varies greatly throughout the day and year. The CIE (*International Commission on Illumination*)[2] has adopted a standard classification to evaluate sky conditions (CIE, 2003). It serves as a reference to define and categorise a type of sky. Factors such as availability of direct sunlight, weather patterns and cloud distribution are applied in the classification process. The CIE standard sky model, as it is known, is composed by a set of 15 different types of skies, grouped in three main categories: (A) five types of clear skies; (B) five types of overcast skies; and (C) five types of intermediate skies (CIE, 2003; Li and Cheung, 2006; Li et al, 2008).

Table 2.1 presents an overview of the 15 types of standard skies recognised by the CIE standard skies reference (Li, 2007, pp.747; Li et al, 2008; CIE, 2003).

Table 2.1 – Brief description of the 15 CIE standard skies (Li, 2007, pp.747; CIE, 2003; Li et al, 2008).

No. (code)	Type of sky
1 (I1)	CIE standard overcast sky, steep luminance gradation towards zenith, azimuthal uniformity
2 (I2)	Overcast, with steep luminance gradation and slight brightening towards the sun
3 (II1)	Overcast, moderately graded with azimuthal uniformity
4 (II2)	Overcast, moderately graded and slight brightening towards the sun
5 (III1)	Sky of uniform luminance
6 (III2)	Partly cloudy sky, no gradation towards zenith, slight brightening towards the sun
7 (III3)	Partly cloudy sky, no gradation towards zenith, brighter circumsolar region
8 (III4)	Partly cloudy sky, no gradation towards zenith, distinct solar corona
9 (IV2)	Partly cloudy, with the obscured sun
10 (IV3)	Partly cloudy, with brighter circumsolar region
11 (IV4)	White-blue sky with distinct solar corona
12 (V4)	CIE standard clear sky, low luminance turbidity
13 (V5)	CIE standard clear sky, polluted atmosphere
14 (VI5)	Cloudless turbid sky with broad solar corona
15 (VI6)	White-blue turbid sky with broad solar corona

2.5 Solar energy and daylighting for sustainable buildings

Buildings have a significant environmental impact. Several studies have estimated that buildings account for a 20-40% of total energy consumption in most developed nations (EIA, 2009; Pérez-Lombard et al, 2008). Of this total, artificial lighting corresponds to about 10-30% (Pérez-Lombard et al, 2008; Loe, 2003).

[2] The International Commission on Illumination is also known as the CIE from its French name: *Commission Internationale de l´Eclairage* (http://www.cie.co.at/) – [Accessed 10th April 2006].

It has been estimated that 30% to 40% of energy-related CO_2 emissions in developed nations are generated by energy use in buildings (Jenkins and Newborough, 2007; Omer, 2008; Pérez-Lombard et al, 2008; EIA, 2009). Several authors stress that the reduction of building energy consumption is paramount to reduce CO_2 emissions (Jenkins and Newborough, 2007; De Vries et al, 2007; Omer, 2008).

According to Peippo et al (1999, pp.193) the annual net primary energy requirement E_{prim} for buildings can be estimated by the equation:

$$E_{prim} = E_{th} + E_{el} – E_{sp} / \mu \quad [2.2]$$

Where:

- E_{th} is the annual auxiliary thermal energy used for space and water heating;
- E_{el} represents the gross electric energy consumption acquired from the electricity grid;
- E_{sp} is the surplus electricity generated by photovoltaic panels (if any);
- μ is the conversion factor from primary energy to electricity.

Considering the literature, the increase in natural illumination can lead to a direct decrease in the E_{th} and E_{el} factors (from Equation 2.2) up to 10-40% (Leslie, 2003; Loe, 2003; Lee and Selkowitz, 2006; Ihm et al, 2009).

Natural illumination (or daylighting) can be categorised as a building service (McMullan, 2002). In this sense, daylighting should be seen in a broader context, where issues relating renewable energy and building energy efficiency are considered together with building integration issues and the importance of natural illumination for human well being. This view is gaining support among many researchers (Fontoynont, 2002; Gratia and De Herde, 2003; Webb, 2006; Reinhart and Selkowitz, 2006).

Energy and economic benefits from the use of core-daylighting systems in buildings is described in the literature. According to Loe (2003, pp.319; 2009, pp.209) artificial lighting energy consumption in the UK demands around 20% of the total electric energy generated country. Lighting management with artificial lighting dimming as a function of daylighting can result in lighting energy savings from 20% to 70%, depending on several factors such as the building design, orientation and local climate conditions (Bodart and De Herde, 2002; Ihm et al, 2009). It has been argued that overall building energy consumption can be reduced by 10% to 40% if daylighting is used strategically (Ihm et al, 2009; Leslie, 2003; Loe, 2003; Loe, 2009).

However, it is important to note that the analysis of the real impact of daylighting on artificial lighting dimming and overall building energy consumption is a very complex task. To accomplish such a task it is necessary to apply a comprehensive strategy that considers an optimum equilibrium in building cooling, heating and lighting balance, which "*can only be reached by an integrated approach combining daylighting, artificial lighting and thermal analysis*" (Bodart and De Herde, 2002, pp.421).

According to Leslie (2003) and Fontoynont (2002), the distribution of natural illumination inside a room is a crucial factor to achieve a low-energy consumption level. Freewan et al (2009) argues that the interactions of indoors architectural features and daylighting systems are a main issue to achieve an even distribution of natural light indoors.

The spectral power distribution (SPD) and wavelength (λ) composition of natural illumination has a higher luminous efficiency than most types of artificial lighting (Schanda, 2002; Webb, 2006). For example, the relative intensity distribution of most tungsten filament light bulbs increases with the wavelength λ until it peaks at around 1000nm, in the near-infrared portion of the spectrum (Webb, 2006, pp.722). This means that most of the electric energy used to generate light with a tungsten filament light bulb is actually being used to produce heat. On the other hand, the spectral composition of white natural light carries less energy in the infrared and more in the visible range of the spectrum. As a result natural light is more suitable for indoors illumination than artificial light (Webb, 2006; Bodart and Herde, 2002).

2.5.1 Solar energy and daylighting systems building integration

In the literature, solar building integration relates to the potential and feasibility to "integrate" a solar-energy-system (including solar-thermal panels, solar-photovoltaic panels and solar-daylighting-collectors) into the building outside structure without compromising the buildings architectural and aesthetics qualities (Nicoletti, 1998; Hestnes, 1999). One of the key aspects for the commercial success of daylighting systems and solar collectors in general, is that they should preferably have a small footprint, that is, they should occupy a small volume when installed into the building (Hestnes, 1999; Pearsall, 1998; Prasad and Snow, 2005; Probst and Roecker, 2007).

Most existing solar energy systems, including solar-photovoltaic panels, solar-thermal collectors and solar-daylighting collectors, are designed to be installed on buildings roofs (Prasad and Snow, 2005). Façade-integrated solar energy systems are a more recent trend (Hestnes, 1999; Prasad and Snow, 2005; Probst and Roecker, 2007). Current photovoltaic-façade and solar-thermal façade systems are now being

designed to blend and integrate with most buildings architectural composition (Nicoletti, 1998; Reijenga, 2003; Matuska and Sourek, 2006; Probst and Roecker, 2007).

The British Standard BS 7543:1992 defines the "normal life-time expectancy" for building main components and materials as a minimum of 60 years. For solar-daylighting-collectors and other solar energy systems installed on building facades and roofs, this means that they should be expected to last as long (as possible) as other ordinary building materials and components. Therefore, the use of durable materials, such as glass and polycarbonate, in the development of solar-daylighting-collectors designed for building-façade integration may provide a potential strategy to achieve long-lasting products (Nicoletti, 1998; IEA, 2000; Hestnes, 1999; Smith, 2004).

2.5.2 Daylighting assessment methods

According to Rosenfeld and Selkowitz (1977):

"*Daylighting reaching an interior position is the sum of: (A) direct light from the sky; (B) light reflected from external objects, and; (C) inter-reflected light which has been scattered from surfaces and objects inside the room*". Inside a building "*total available daylight declines exponentially as one moves away from the window – actual value depend on window size and location, room dimensions, etc*" (Rosenfeld and Selkowitz, 1977, p.44).

The daylight factor (DF) is a relation that describes the ratio of outside illuminance over indoor illuminance. Li and Cheung (2006), defines the daylight factor as:

"The ratio of the internal illuminance simultaneously available on a horizontal plane from the whole of an unobstructed sky (excluding direct sunlight), expressed as a percentage" (Li and Cheung, 2006, pp.138).

The daylight factor (DF) measurements are always in relation to the CIE standard overcast sky with 10.000lx (CIE, 2003; Li, 2007). Current standards recommend an average DF of 2% to 5% as a satisfactory level to provide the sensation of well lit room (IEA, 2000, pp.3-4; Li, 2007; British Standard BS 8206-2:2008).

British Standard BS 8206-2:2008 recommends a daylight factor between 1% to 5%, depending on the type of room and/or activity. The standard states that a daylight factor ≥ 5% is enough to enable the switching-off of electric lighting in the daytime.

Daylight factors between 2% and 5% may require supplementary artificial lighting depending on the type of room/activity (British Standard BS 8206-2:2008).

A simplified form to estimate the daylight factor (DF) is given by the equation:

$$DF = (E_{indoor} / E_{outdoor}) \times 100(\%) \quad [2.3]$$

Where:

- DF is the daylight factor (measured as a percentage value, %);
- E_{indoor} is the indoors illuminance (measured in *lux*, lx);
- $E_{outdoor}$ is the outdoor illuminance (measured in *lux*, lx).

Nabil and Mardaljevic (2006) proposed an alternative to the daylight factor (DF). Their method, called useful daylight illuminances (UDI), aims to define and classify the distribution of daylight illuminances according to a predefined range of four utility levels:

- Low or no utility level (low UDI): daylight illuminances less than 100 lx.
- Acceptable utility level (acceptable UDI): daylight illuminances between 100-500 lx.
- Desirable level (desirable UDI): daylight illuminances between 500-2000 lx.
- Undesirable level (UDI): daylight illuminances higher than 2000 lx (Nabil and Mardaljevic, 2006).

It is important to stress that both the DF and the UDI method were developed in order to estimate the distribution of natural illumination inside a room as a fraction of outdoor illuminances (CIE, 2003; Li and Cheung 2006; Nabil and Mardaljevic, 2006). They are not suitable to directly measure the optical efficiency of solar-daylighting-collectors. However, they are useful as a comparison reference to estimate the utility level of a solar-daylighting-collector.

2.5.3 Lighting impact on human health and indoors activities

Light and solar radiation in general is extremely important for human health and daily activities. The utility of daylight for illumination application in buildings can be divided in three areas: (A) visual-task needs; (B) physiological needs; (C) subjective needs (Schanda et al, 2002; Fontoynont, 2002; Webb, 2006; Durak et al, 2007).

Research in the area of human visual acuity has shown that people usually prefer natural illumination over artificial lighting (Webb, 2006; Fontoynont, 2002). Visual-task lighting needs relates to the required illuminance level for a specific activity or a specific area/room inside a building (IEA, 2000; British Standard BS 8206-2:2008). Visual-task lighting needs are directly related to physiological and subjective needs.

They are also age related and time-dependent (Webb, 2006). For example, Galasiu and Veitch (2006) found that office workers working on computers preferred lower light levels (100-300 lx) when they were working for longer hours, and higher light levels (300-600 lx) when they worked for short periods (Galasiu and Veitch, 2006, pp.773).

Lighting (including artificial and natural) also affects human spatial perception, moods and well-being (Fontoynont, 2002; Reinhart and Selkowitz, 2006). Durak et al (2007) investigate the subjective response of building occupants when exposed to a series of different interior lighting arrangements with illuminance levels of 320 lx (considered low level) and 500 lx (high level). They concluded that "*lighting can affect the mood setting in a space by arousing different impressions with the use of different arrangements at different illuminances*" (Durak et al, 2007, pp.3482).

Galasiu and Veitch (2006) presented a comprehensive literature review on the subject of building occupants preferences and satisfaction in indoors lighting. For visual-task orientated activities in office buildings, daylight illuminances less than 100 lx are in general too low to be considered as a sole source of illumination for most working tasks. However, it may still be useful in other building areas, such as corridors. Daylighting illuminances between 100 lx to 500 lx are considered useful for most office-work tasks (British Standard BS 8206-2:2008). Daylighting illuminances between 500 lx to 2000 lx are considered effective for most office-working tasks, enabling a significant reduction in artificial lighting and building energy consumption (Nabil and Mardaljevic, 2006). Daylight illuminances above 2000 lx can cause visual discomfort and increase building thermal loads, which could potentially increase building energy consumption by increasing cooling demand (Nabil and Mardaljevic, 2006, pp.907; Bodart and Herde, 2002; Schanda et al, 2002; British Standard BS 8206-2:2008).

According to Pauley (2004) and Webb (2006), the excessive exposure to blue light (464-484 nm) and light at night (LAN) can disrupt the human body circadian-rhythm and suppress the production of melatonin. The consequences of all this are not yet totally known, but recent research is linking it to depression, seasonal affective disorder (SAD), and even some types of cancer, such as breast cancer (Pauley, 2004, pp.590; Berson, 2003; Olders, 2003; Webb, 2006). As a direct result, Pauley (2004) suggests that "*lighting is becoming a public health issue*" (Pauley, 2004, pp.588).

2.6 Optics: basic theory and design principles

2.6.1 Light representation and ray optics

Light is one of the most complex physical phenomenon. In classical physics, light is described as a part of the electromagnetic radiation. Quantum mechanics analyses light through the dualistic concept of particle-wave, where the *photon* is the particle of light (Cannon, in DeCusatis, 1998; Hecht, 1998).

An early geometric treatment of light is presented by Huygens (1690)[3] in his classic book "*Treatise on Light*", firstly published in the late 17th century. He describes the propagation of light as "straight lines" (Huygens, 1690, pp.1) and applies trigonometric relations to formulate a "geometric view" on the behaviour of light. His treatment, although purely geometric, already contained the notion of light propagating as a "wave-front" (Huygens, 1690, pp.16).

For most practical applications in optical design, the propagation of light can be represented as a stream of straight lines. This form of representation is known as *ray optics*. One of the most powerful methods used in ray optics is ray-tracing analysis (Hecht, 1998; Smith, 2000). Considering the interactions of light with matter, it is important to highlight here some relevant terms in ray optics and ray-tracing analysis:

- Incident ray: corresponds to the ray (or beam) of light that hits the surface/interface of the material (Hecht, 1998; Smith, 2000);
- Reflected ray: corresponds to the ray that is reflected by the surface (Hecht, 1998; Smith, 2000);
- Refracted or transmitted ray: corresponds to the ray that is transmitted through the material, in case of a transparent solid dielectric material (glass or transparent polymers, for example) – (Hecht, 1998; Smith, 2000).

2.6.2 Law of Reflection

The reflected ray is described by the Law of Reflection (Huygens, 1690; Hecht, 1998). Considering a perfectly smooth surface with mirror-like specular reflection, the angle of the reflected ray θ_r is equal to the angle of the incident ray θ_i, in relation to the surfaces normal (Huygens, 1690; Hecht, 1998). This law can be simply stated as "*the*

[3] **Important note on reference**: the referred Huygens book used in this thesis is a more recent edition, published in 1962, that is an exact copy of the original book, firstly published in the late 17th century.

angle of reflection is equal to the angle of incidence" (Huygens, 1690; Hecht, 1998), or, expressed as:

$$\theta_r = \theta_i \qquad [2.4]$$

However, for most materials, part of the incident radiation is scattered due to surface imperfections (Ashby et al, 2007, pp.370). Figure 2.1 illustrates the most general types of reflection of a beam of light on a reflective surface (Hecht, 1998; Serra, 1998).

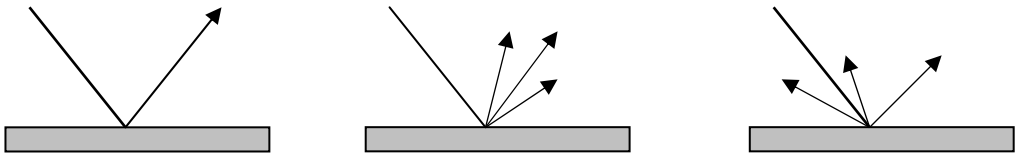

Figure 2.1 – General types of light reflection.

2.6.3 Snell's Law of Refraction

Refraction happens when light passes through the interface between two transparent mediums with different densities (Hecht, 1998, pp.100). The speed of light inside a transparent medium varies according to the density of the medium. As a result, a denser medium has a higher the refractive index n (Mouroulis and Macdonald, 1997; Hecht, 1998). Thus, it is possible to calculate the refractive index of a material by calculating the speed of light inside of it. This is given by the equation:

$$n = c / v \qquad [2.5]$$

Where,

- n is the refractive index of the material
- c is the speed of light in vacuum (299,997 km/s, in vacuum)
- v is the speed of light inside the material

In a gas, the density is a relation between pressure, temperature and volume. Changes in any of these parameters will influence the refractive index of the medium. The refractive index of air is for practical reasons defined as n = 1,0 (one). Changes in atmospheric conditions will result in small changes in the refractive index n of the air (Freeman, 1990; Mouroulis and Macdonald, 1997; Hecht, 1998).

Snell's Law of Refraction states that a ray of light entering a denser medium (with higher refractive index n) will approach the normal to the incident surface (Huygens, 1690, pp.35; Hecht, 1998, pp.101). When leaving the denser medium to a lower density medium it will move away from the normal to the exit surface (Hecht, 1998; Mouroulis and Macdonald, 1997, pp.9). This relation is given by the equation:

$$n_1 \sin \theta_1 = n_2 \sin \theta_2 \qquad [2.6]$$

Where:

- n_1 is the refractive index of the first medium;
- θ_1 is the incident angle formed between the ray and the entrance surface;
- n_2 is the refractive index of the second medium;
- θ_2 is the incident angle formed between the ray and the exit surface.

Figure 2.2 presents a schematic illustration of the general types of transmission of an incident beam of light through a transparent solid dielectric medium. Note that the refractive index n_1 of the solid dielectric medium is considered to be larger than the refractive index n_2 of the surrounding medium (Hecht, 1998; Serra, 1998).

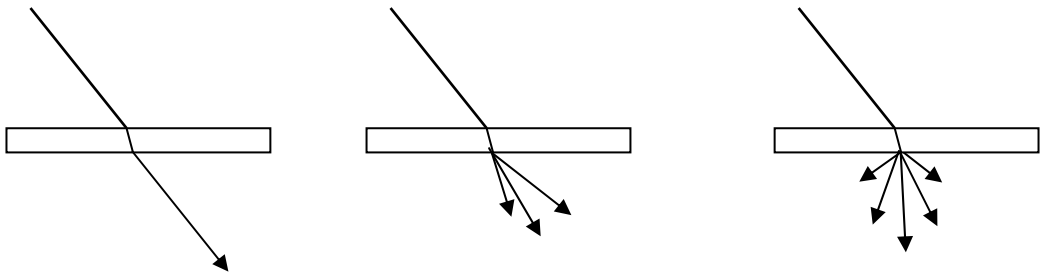

Figure 2.2 – General types of light transmission through a solid dielectric medium.

It is known that the refractive index n of any material is wavelength λ dependent (Hecht, 1998; Smith, 2000). This means that it varies according to the incident wavelength. Different wavelengths travel at slightly different speeds inside the denser medium which consequently will lead to different refractive angles, and also different critical angles θ_c for each specific wavelength (Hecht, 1998). Shorter wavelengths will refract most. Longer wavelengths will refract least (Hecht, 1998, pp101-103; Freeman, 1990, pp.362). For convenience the mean refractive index n is usually adopted, which relates to the measured refractive index n of a material for a wavelength λ of the visible part of the spectrum (Freeman, 1990, pp.362). In most cases, the refractive index n

generally decreases as the wavelength λ decreases. However, in regions of anomalous dispersion, which relates to the absorption bands of the material, the refractive index n will increase (Freeman, 1990; Hecht, 1998; Mouroulis and Macdonald, 1997, pp.7).

Thus, any optical device that is based on refractive optics is wavelength λ dependent (Smith, 2000). A practical example of the effect of the variation of the refractive index in relation to the wavelength can be observed through the dispersion of colours in a prism (Mouroulis and Macdonald, 1997, pp.7; Hecht, 1998). Prisms can be used to break down the white spectrum of sunlight into its basic colours, a phenomenon called dispersion (Hecht, 1998; Smith, 2000). It is also known that if a second prism is positioned next to the output beam of the first prism, the dispersed colours can blend together to form white light again, a phenomenon called light re-composition (Freeman, 1990; Hecht, 1998; Smith, 2000).

The refraction index n also varies according to the temperature of the material (Cariou et al, 1986). This is particularly important for polymers, since they exhibit a relatively high thermal volume expansion in response to the increase in the temperature (Cariou et al, 1986, pp.334).

2.6.4 Total internal reflection (TIR) and the critical angle

Light travelling inside a denser transparent medium surrounded by a medium with lower density may hit the internal walls of the denser medium and be totally reflected back into the denser medium instead of passing through the interface between both mediums (Freeman, 1990; Hecht, 1998, pp.121). For incident angles θ_i equal or larger than the critical angle θ_c of the material, light will remain trapped inside the denser medium by the optical phenomenon of total internal reflection (TIR) (Mouroulis and Macdonald, 1997, pp.10; Hecht, 1998).

The critical angle θ_c is wavelength λ dependent. It also depends on the density relation between the denser transparent medium and its surroundings (Hecht, 1998). The higher the difference between the densities of the two mediums the lower is the critical angle θ_c inside the denser medium. This means that it will trap and transmit more light by TIR (Freeman, 1990; Ries et al, 1997a; Hecht, 1998).

The critical angle θ_c can be calculated by using the Snell's Law of Refraction (Hecht, 1998; Smith, 2000). According to Hecht (1998), for the situation in which a denser medium is surrounded by air, the critical angle θ_c is given by:

$$\theta_c = \sin^{-1}(1/n) \qquad [2.7]$$

Where,

- θ_c is the critical angle
- 1 is density of air (temperature; pressure conditions)
- n is the refractive index of the denser medium

If the rare medium is not air, then the equation above becomes:

$$\theta_c = \sin^{-1} (n'/n) \qquad [2.8]$$

where n is the refractive index of the denser medium and n' is the refractive index of the rarer medium (Freeman, 1990; Hecht, 1998; Smith, 2000).

The graph presented in Figure 2.11 was built by using numerical data extracted from Hecht (1998, pp.122). It shows the gradual decrease of the critical angle θ_c with the increase of the refractive index n. The material considered is glass surrounded by air, forming an air-glass interface. The measurements of critical angle θ_c varies from θ_c = 50.284° for n = 1.30 to θ_c = 36.529° for n = 1.68, resulting in a decrease of 13.755° related to the corresponding increase of the refractive index n (Hecht, 1998, pp.122). As a result, total internal reflection (TIR) inside the solid-dielectric medium (in this case, glass) will increase with the increase in the refractive index n. Another way to say it would be: total internal reflection (TIR) increases with the decrease of the critical angle θ_c (Freeman, 1990; Ries et al, 1997a; Hecht, 1998, pp.122).

This might suggest that it may be a straight forward process to design a device to harvest and trap light: simply use solid-dielectric materials with higher refractive index so that more light can be trapped by TIR. However, as seen in Figure 2.3, an increase in the refractive index n leads to a decrease in the critical angle θ_c, meaning that it becomes increasingly difficult to extract light from solid-dielectric materials with higher refractive indices n (Welford and Winston, 1978, pp.73; Hecht, 1998, pp. 122; Ries et al, 1997a; Masui et al, 2008).

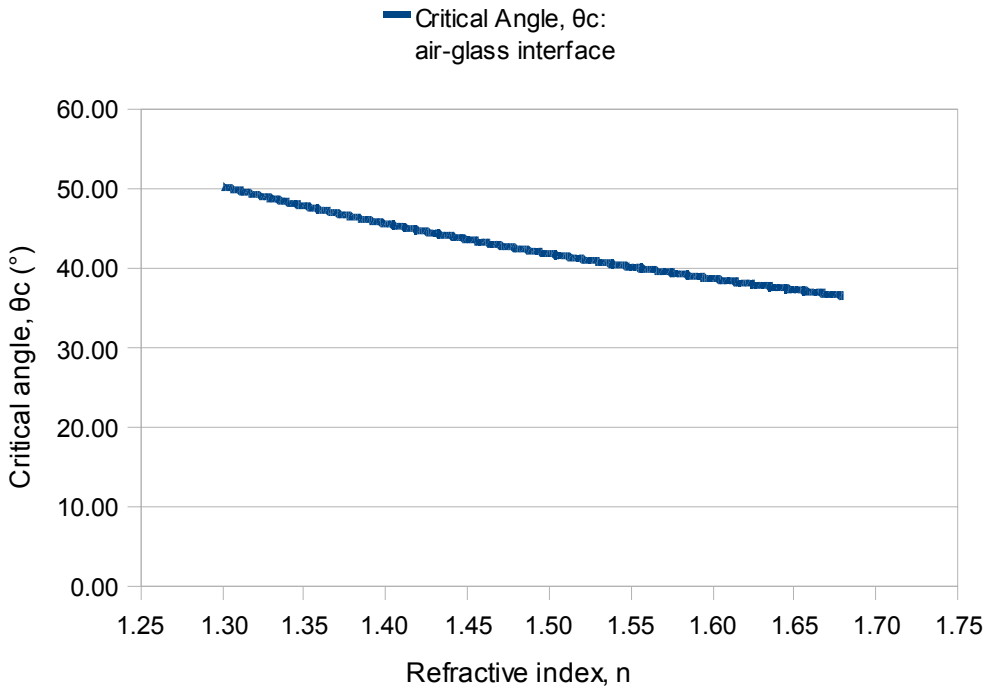

Figure 2.3 – Critical angle θ_c as a function of the refractive index n for an air-glass interface.

2.6.5 Fresnel-reflection (or dielectric reflection)

When sunlight hits the surface of a solid dielectric material, such as a glass window, for example, part of it is transmitted through the window, part is absorbed by the glass and part of it is reflected back to the outdoor environment. The reflected component is named dielectric reflection, or Fresnel-reflection (Hecht, 1998; Freeman, 1990; Smith, 2000).

Fresnel-reflections are material specific and angle dependent (Gordon and Feuermann, 2005, pp.2329). Fresnel-reflections are associated with losses in an optical system. In general, the higher the refractive index n the greater the component of Fresnel-reflections at its surface (Hecht, 1998; Smith, 2000).

According to Hecht (1998) and Freeman (1990), Fresnel's law quantifies the reflection loss, r_λ, at normal incidence between two media with different refractive indices, (n_λ = n' / n, the ratio of the refractive indices):

$$r_\lambda = (n_\lambda - 1) \times 2 / (n_\lambda + 1) \times 2 \qquad [2.9]$$

Where:

- r_λ is the Fresnel-reflection component;
- n' / n is the ratio between the refractive indices of the two mediums.

Fresnel-reflection increases as the incident angle θ_i increases (Hecht, 1998). This has serious implications for the performance of compact façade systems solar collectors with frontal glazing surfaces. Systems designed for low latitudes, where the apparent movement of the Sun reaches more than $h_s = 75°$ of angular altitude may lose 20% to 80% of incident sunlight due to Fresnel-reflections at the frontal glazing surface (Freeman, 1990; Hecht, 1998; Smith, 2000).

Fresnel-reflections losses (or Fresnel-transmission losses) are also highly dependent on surface finishing and coating choices (Fournier and Rolland, 2008). It is possible to reduce or minimise Fresnel-reflection losses by applying an anti-reflective coating over the frontal glazed-type surface of the collector/concentrator. The anti-reflective coating can be applied in the form of a film or spray. Usually, this type of coating consists of a layer of transparent material with a lower refractive index n such as magnesium fluoride MgF_2 (Dislich, 1979, pp.50; Smith, 2004). Optical films are usually applied inside a vacuum chamber (Smith, 2000, pp.201).

2.6.6 Attenuation of light in solid dielectric materials

Attenuation of light inside a transparent solid dielectric medium is generally a result of scattering, absorption and radiation. According to Hunsperger (1995, pp.74) the attenuation of electromagnetic waves (including visible light) by scattering is more predominant in glass and other types of transparent dielectric medium, such as optical polymers, while absorption is more significant in semiconductors and crystalline materials. According to Lin et al (1994, pp.5193) and Ashby et al (2007) the attenuation of electromagnetic waves inside a solid-dielectric material can be described as:

- *Attenuation = scattering losses + absorption losses + radiation losses*

Radiation losses become more significant for light travelling inside a curved or bent light guide, for example a curve along a fibre optical cable (Hunsperger, 1995, pp.74; Dislich, 1979). Both scattering and absorption losses tend to increase with the thickness of the material and also with the optical path length (OPL) of light propagating inside the material (Hunsperger, 1995; Hecht, 1998; Ashby et al, 2007).

2.6.6.1 Surface scattering and volume scattering

The scattering of light and other electromagnetic waves is a direct result of its interaction with matter (Kerker, 1969). Scattering leads to a change in the direction of incident light due to collisions. According to Liebert and Maniewski (2003), "*the incident light is deflected by collisions with particles or centres of inhomogeneity of the medium*" (Liebert and Maniewski, 2003, pp. 2545). Scattering can seriously compromise the performance of an optical component (British Standard BS ISO 10110-8:1997, pp.5).

Scattering losses are usually classified in two types: surface scattering and volume scattering (Hunsperger, 1995; Kerker, 1969). Surface scattering losses are usually associated to imperfections and surface roughness at the surface/interface of the material. Volume (or bulk) scattering is caused by imperfections and impurities inside a transparent dielectric medium (Smith, 2000; Liebert and Maniewski, 2003; Kerker, 1969).

Volume scattering can account for most of the losses in plastic light guides (Lin et al, 1994; Dislich, 1979, pp.55). Backscattering is also of particular concern for light propagation inside solid dielectric light guides (Ladouceur and Poladian, 1996).

2.6.6.2 Absorption losses

The absorption of light by any material is wavelength λ dependent. As a result, some materials will absorb and/or transmit more radiant energy at a particular band of the spectrum more than other materials (Hecht, 1998; Serra, 1998; Nicklov and Ivanov, 2000; Gross et al, 2007).

Huang et al (2002) presented a series of equations to calculate the absorption coefficients of optical dielectric materials by taking into account their transmissivities and refractive indices. Usually the transmissivity decreases as the refractive index n increases due to the increase of the density of the material (Hecht, 1998; Nicklov and Ivanov, 2000; Huang et al, 2002).

2.6.7 Optical surface

Specular (optically smooth) surfaces are usually produced by applying efficient polishing techniques or by moulding processes, such as injection moulding. According to British Standard BS ISO 10110-8:1997 (pp.1), the main effect of surface roughness on optical surfaces is light scattering (Ashby et al, 2007).

Surface roughness parameters are usually described in relation to their deviation from a smooth reference surface (Rao and Raj, 2003, pp.741). The increase of surface roughness of a solid-dielectric optical device leads to an increase of scattered transmitted and scattered reflected light components (Kerker, 1969; Hecht, 1998; Rao and Raj, 2003, 746).

2.6.7.1 Sub-surface defects and air-bubble concentration

Shen et al (2005) presented a review on the subject of sub-surface damages in optical materials. Most sub-surface damages are a result of machining and manufacturing techniques. Sub-surface damages include "*fractures, scratches, microcracks, air-bubbles, residual stress and remnants of polishing*" (Shen et al, 2005, pp.288). These defects will increase scattering, especially volume scattering, and result in a negative effect in the path of light beam that enters the material or that is propagating inside of it by total internal reflection (TIR) - (Ladouceur and Poladian, 1996; Shen et al, 2005).

Another possible defect inside an optical refractive material (glass or plastic) is the formation of air-bubbles, also usually a result from the manufacturing process. The British Standard BS ISO 10110-3:1996 defines the formation of bubbles in an optical component as "*gaseous voids, of generally circular cross section, which sometimes appear in glass or polymer materials as the result of the manufacturing process*" (British Standard BS ISO 10110-3:1996, pp.1). The presence of bubbles inside the bulk of the material and also close to its surface (sub-surface bubbles) has a significant impact on the propagation of light, resulting in a significant increase in volume (bulk) scattering, in particular backscattering (British Standard BS ISO 10110-3:1996; Hunsperger, 1995; Ladouceur and Poladian, 1996).

According to the British Standard BS ISO 10110-3:1996:

> "A *concentration occurs when more than 20 % of the number of allowed bubbles and other inclusions are found in any 5 % of the test region. For example, if the total number of bubbles and other inclusions is less than 10, then 2 or more bubbles or other inclusions falling within a 5 % sub-area constitute a concentration*" (British Standard BS ISO 10110-3:1996, pp.1).

The maximum number of air-bubbles recommended by the British Standard BS ISO 10110-3:1996 is given by the equation:

$$N \times A^2 \text{ (= maximum total area)} \qquad [2.10]$$

Where:

- N is the number of gaseous bubbles and other inclusions of maximum permitted size allowed; and
- A is the grade number that corresponds to the size of the bubbles and inclusions.

Using Equation 2.10 it is possible to estimate the level of defects and inclusions inside a solid-dielectric optical material. This is done by counting the number N of gaseous bubbles or/and inclusions in small areas of a material and multiplying this number by a grade number A that is recommended by the British Standard BS ISO 10110-3:1996. High concentration of air-bubbles and inclusions inside an optical dielectric material are not recommended because they increase volume scattering, resulting in significant optical losses (Hunsperger, 1995; British Standard BS ISO 10110-3:1996; Ashby et al, 2007).

2.7 Materials for solar collectors and concentrators

Materials are extremely important for the performance and durability of solar collectors and solar energy systems. It is often common to group optical materials in two categories: reflective materials (for reflective optics) and refractive materials (for refractive optics) – (Hecht, 1998; Fend et al, 2003; Smith, 2004; Ashby et al, 2007).

2.7.1 Reflective materials for solar collectors

Reflective solar-concentrators are usually electroplated with reflective metals. This technique provides a very smooth surface with high reflectivity but is limited to a certain group of metals that can be effectively applied (Nuwayhid et al, 2001). Electroplated aluminium is usually applied as a reflective solar concentrator material (Smith, 2004, Kaushika and Reddy, 2000).

Bodart et al (2008, pp.2049) presented a classification to evaluate and characterize materials according to reflected light angles. Fend et al (2003) investigated the long-term durability of a series of reflector materials (SolarBrite® 95 reflector, thin glass mirror, Alanod Miro2® and Flabeg® thick glass mirror) for solar energy systems in a variety of climatic conditions. Their measurements included outdoor on-site tests and accelerating aging inside an accelerated exposure chamber.

Kaushika and Reddy (2000) reported on the decay of reflectivity of a parabolic-mirror solar concentrator system. The diameter of the parabolic-mirror dish was 2.4m, and its focal length was approximately 1m. The surface of their system is covered by a silvered polymer reflector. The authors monitored the performance of the system during a period of 6 years. Their results show that reflectance of the mirror-like surface of the parabolic dish was reduced by 26%, resulting in 23% decrease in the systems optical efficiency (Kaushika and Reddy, 2000, pp.724).

2.7.2 Optical and commercial glasses

Commercial glasses used as glazing material in buildings present relatively high transmittance from the UV, VIS and NIR ranges of the spectrum (Serra, 1998; Smith, 2004). Soda-lime glass is widely used as commercial window glazing. Low-iron glass is a material commonly used for solar-thermal collectors covers (Zacharopoulos et al, 2000; Serra, 1998, pp.121).

According to the British Glass Manufacturers Confederation website (www.britglass.org.uk, accessed 20th June 2009), most commercial glasses have roughly similar chemical compositions of 70-74% SiO_2 (silica), 12-16% Na_2O (sodium oxide), 5-11% CaO (calcium oxide), 1-3% MgO (magnesium oxide) and 1-3% Al_2O_3 (aluminium oxide).

2.7.3 Optical plastics

According to Smith (2000), two of the most used optical plastics are polymethyl-methacrylate (PMMA) and polycarbonate (PC). Both are thermoplastics and present an amorphous molecular composition (Dislich, 1979; Askeland and Phulé, 2003, pp.670). According to Yalukova and Sarady (2006) polymers with amorphous molecular composition usually are more transparent to the visible range of the spectrum than polymers that are partially crystalline.

The transmittance ranges of optical plastics are more limited than optical glasses (Dislich, 1979, pp.50). Crystalline polymers present higher packing of molecules (density) than amorphous polymers. As a consequence they have a higher refractive index n. Thus, it is possible to say that in polymers the refractive index n increases with increasing crystallinity (degree of molecular structural order) of the material (Elias, 2003, pp.232; Dislich, 1979; Ashby et al, 2007).

Some suppliers of PMMA say that the material offers stability under weather conditions of up to 30 years (van Sark et al, 2008; Gross et al, 2007). PMMA can be

classified as an amorphous polymer. PMMA and polycarbonate are both already used as glazing material for buildings. Among their advantages it is highlighted: (A) impact resistance, making these materials more suitable to satisfy buildings standards related to safety glazing materials; and (B) good optical transmission in the visible range (Ashby et al, 2007; Gross et al, 2007).

According to Smith (2000, pp.191), the changes in the refractive index n of optical plastics as a function of temperature are about twenty times higher than glasses. The refractive index n of optical plastics decreases with an increase in the temperature (Cariou, 1986; Lin et al, 1994; Smith, 2000). The refractive index n of PMMA is strongly dependent on temperature variations (Lin et al, 1994; Gross et al, 2007). Based on experimental tests, Lin et al (1994) presented an equation to estimate the variations of the refractive index of PMMA according to temperature variations:

$$n_{PMMA}(T) = 1.4925 - 1.1 \times 10^{-4} (T - 25) \qquad [2.11]$$

Where: $n_{PMMA}(T)$ is the refractive index of PMMA as a function of temperature T (°C).

The durability of polycarbonate (PC) and PMMA components used in the building industry will be affected by the exposure to UV radiation and weather conditions. Some manufactures of building components (such as sky-lights and windows) made of polycarbonate estimate a useful life of up to 20-30 years for their products. After this period it is recommend that they should be replaced (Ashby et al, 2007; British Standard BS ISO 15686-5:2008; Askeland and Phulé, 2003; McMullan, 2002).

It is important to highlight that both PMMA and polycarbonate can be applied as building materials, such as window glazing, skylights and transparent roof covers (IEA, 2000; British Standard BS EN 13119:2007; www.Kingspan.co.uk, accessed 20th July 2008). The disadvantages of using polymers in solar collectors and concentrator systems relates to their thermal expansion and the real risk of fire (Rosemann, 2008). Therefore, it is not recommended the use of these materials as a viable commercial solution to manufacture solar concentrator/collector systems. However, polymers such as PMMA work well to build prototypes for preliminary tests and proof-of-concept (Welford and Winston, 1978, pp.137; Chien et al, 2009).

Table 2.2 shows a summary of the data analysed by Nikolov and Ivanov (2000, pp.2068) regarding the variation of the refractive index as a function of the wavelength for three types of optical plastics: polymethyl-methacrylate (PMMA), polystyrene (PS) and polycarbonate (PC). The graph displayed in Figure 2.4 was built with numerical data extracted from Table 2.2.

Table 2.2 – Numerical data of the refractive index n varying as a function of wavelength λ for three optical plastics: PMMA, PC and PS (polystyrene).

Plastic	Wavelengths (nm)										
	436	486	546	588	633	656	703	752	804	879	1052
PMMA	1.503	1.497	1.493	1.491	1.489	1.489	1.486	1.485	1.484	1.483	1.481
PS	1.617	1.606	1.596	1.592	1.587	1.586	1.582	1.579	1.578	1.576	1.572
PC	1.612	1.599	1.590	1.585	1.580	1.579	1.575	1.572	1.570	1.568	1.565

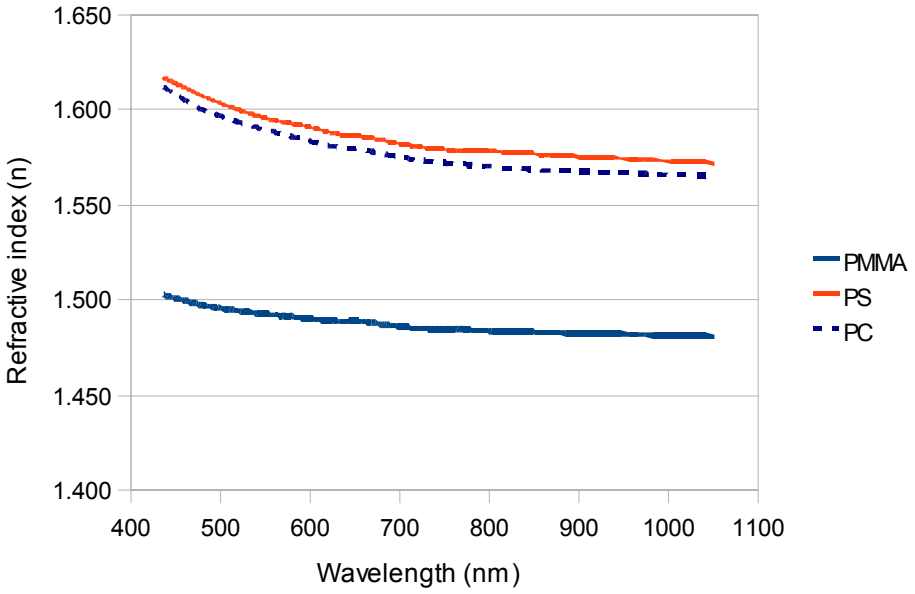

Figure 2.4 – Variation of the refractive index n as a function of wavelength λ (measured in nm) for three optical plastics: PMMA, PC and PS (polystyrene).

2.8 Important concepts in solar concentrator optics

The basic function of a solar concentrator system is to increase the flux density of incoming solar radiation by confining it to a smaller area (Ries et al, 1982; Welford and Winston, 1978). In general terms, most solar concentrator devices can be grouped into two categories: imaging optics concentrators and nonimaging optics concentrators. Subdivisions of these categories and also combinations between them are described in the literature (Welford and Winston, 1978; Ning et al 1987).

Winston (1970, pp.245) defines the fundamental problem of collecting light as:

> "*Given a set of light rays with a specified angular divergence θ_{max} distributed over an entrance aperture, how can we direct theses rays efficiently onto the smallest possible exit aperture?*" (Winston, 1970, pp.245).

An essential step to solve this problem is to distinguish between collecting light and imaging (Winston, 1970, pp.245; Welford and Winston, 1978; Timinger et al, 2000). As mentioned previously in Chapter 1 (pp.2), a large number of solar concentrators has been designed and tested for a variety of applications. However, several problems that range from technical to economical issues have kept most concentrators concepts at a prototype stage (Swanson, 2000; Antón et al, 2003; Kandilli and Ulgen, 2009).

2.8.1 Intercept factor and acceptance angle

Concentrators with large acceptance angles θ_{accept} can collect part of the diffuse radiation that they intercept, especially part of the diffused radiation resulted from the atmosphere turbidity (Welford and Winston, 1978, pp.125). Chaves and Collares-Pereira (2002) argued that it is possible to design an optical device that has two or more different acceptance angles θ_{accept}.

To simplify the analysis and characterisation process of solar collectors and solar concentrators it is also accepted to relate to only one solar displacement angle, normally the solar altitude angle h_s. In this situation the solar altitude angle h_s represents the incident angle θ_i of direct solar radiation at the optical meridional plane of the solar collector/concentrator (Welford and Winston, 1978; Smith, 2000; Messenger and Ventre, 2000).

2.8.2 Concentration ratio and concentration limits

According to Rabl and Winston (1976) and Rabl (1994), the maximum concentration ratio C_{max} achievable by a nontracking solar concentrator is related to the magnitude of the angular motion of the sun during the day and the year. The magnitude of the angular motion is equal to the maximum vertical displacement, measured by the solar altitude angle h_s, and the maximum horizontal displacement, measured by the solar azimuth angle γ_s (Rabl and Winston, 1976; Rabl, 1994; Messenger and Ventre, 2000).

In the literature there are three different definitions for the concentration ratio of a solar concentrator: the geometric concentration C_R, theoretical maximum concentration C_{max} and effective concentration factor C_F, which is the measured value of a real concentrator system (Welford and Winston, 1978; Luque, 1986; Nilsson, 2005; Chaves and Collares-Pereira, 2000).

The geometric concentration ratio C_R is actually a geometric relation (aspect ratio) between the area of the entrance aperture A_1 and the area of the exit aperture A_2 (or receiver) of a solar collector/concentrator device (Welford and Winston, 1978). It depends only on the geometric configuration of the concentrator/collector, and it can be calculated by the equation:

$$C_R = A_1 / A_2 \qquad [2.12]$$

where A_1 is the area of the entry aperture and A_2 is the area of exit aperture" (Nilsson, 2005, pp.21; Welford and Winston, 1978, pp.3).

The theoretical maximum concentration C_{max} is the ideal concentration ratio of an ideal system, with no losses. Considering a collimated isotropic distribution of radiant energy at the entrance aperture of a concentrator device, the maximum concentration C_{max} achievable in two dimensions (2D) is given by the equation:

$$C_{max} = 1 / \sin \theta_i \qquad [2.13]$$

where θ_i is the incident angle (Welford and Winston, 1978; Chaves and Collares-Pereira, 2000). The maximum concentration C_{max} achievable in three dimensions (3D) is given by the equation (Welford and Winston, 1978, pp.5; Chaves and Collares-Pereira, 2000):

$$C_{max} = 1 / \sin^2 \theta_i \qquad [2.14]$$

It has been demonstrated that an increase in the refractive index n of a solid-dielectric nonimaging concentrator can lead to an increase of its effective concentration ratio (Welford and Winston, 1978; Ning et al, 1987; Chien et al, 2009). In the situation where the exit aperture of the concentrator is embedded in a medium with higher refractive index n than its surroundings, the right hand terms in Equation 2.13 and Equation 2.14 are multiplied by n and n^2 respectively (Welford and Winston, 1978; Chaves and Collares-Pereira, 2000).

According to Timinger et al (2000, pp.156) there are two conflicting objectives in concentrating solar radiation: high average flux at the exit aperture and high optical efficiency. Large exit apertures lead to higher transmission but lower concentration, while small exit apertures lead to high concentration but lower transmission efficiency (Timinger et al, 2000, pp. 156; Welford and Winston, 1978).

The theoretical maximum concentration limit is analysed by many authors (Welford and Winston, 1978; Luque, 1986; Nilsson, 2005). For an ideal, a theoretical no-loss imaging system that is constantly facing the sun (using an active-3D-solar-tracking heliostat) the maximum concentration achievable at a focal point is about 45.400x (times) in air (Welford and Winston, 1978; Luque, 1986).

Rosemann et al (2008a) argued that there may be an optimum concentration ratio for solar collectors designed to harvest sunlight for natural illumination in building core areas. Considering technical and economical issues they suggest that a concentration ratio C_R of about 10X (ten times) might provide the best cost-benefit relation for most applications. Higher concentration ratios will require precise heliostats (solar tracking devices). Rosemann et al (2008a) also observed that high concentration optics also requires safety measures to reduce possible hazards (e.g. fire). This would include thermal isolation and fire-prevention features, adding up significant costs to the system (Rosemann et al, 2008a; Rosemann et al, 2008b).

2.8.3 Output flux angular distribution

The concentration power of a solar concentrator depends not only on the acceptance angle θ_{accept} of the system but also on the angular distribution of the output flux $\Delta\theta_{out}$. How this angular distribution is used and directed towards its final application will define the systems overall transmission efficiency. In the literature a greater emphases has been given on the influence of the incidence angle rather on the output flux angular distribution (Goodman et al, 1976; Gordon and Feuermann, 2005).

Most optical systems and devices are incidence-angle dependent. As a result they only perform at maximum efficiency for a specific range of incidence-angles. For example, Martin and Ruiz (2001) analyse the influence on the performance of photovoltaic modules as a function of the angular incidence and resulting angular losses. Ultimately the angular distribution of light emerging from the exit aperture (output flux) will define the most suitable application for the concentrated radiation and the optimum positioning and orientation for the application (Welford and Winston, 1978; Rabl and Winston, 1976; Gordon and Rabl, 1992; Martin and Ruiz, 2001).

2.8.4 Optical efficiency (η_0)

The optical efficiency (η_0) is a direct product of the optical system geometry and materials. For most solar collectors and concentrator systems it also varies according to the solar incident angle (h_s; γ_s). It is measured as the fraction of the solar radiation

intercepted by the entrance aperture of the solar concentrator that reaches the exit aperture or receiver (Welford and Winston, 1978; Luque, 1986). In general terms, the optical efficiency of a solar collector/concentrator can be calculated by the equation:

$$\eta_0 = \Phi_{out} / \Phi_{in} \quad [2.15]$$

Where:

- η_0 is the optical efficiency (measured in %);
- Φ_{in} is the radiant flux or luminous flux intercepted by the collector/concentrator at its entrance aperture (measured in W or lumens, lm); and
- Φ_{out} is the radiant flux or luminous flux at the exit aperture of the collector (measured in W or lumens, lm).

It is also possible to consider the optical efficiency η_0 in terms of illuminance transmission efficiency T_E (measured in lx), which can be convenient for solar-daylighting-collectors (Earp et al, 2003). This will be further discussed in Chapter 3.

2.9 Core daylighting technologies and light transport systems

Core-daylighting systems are basically systems that are designed to collect sunlight (preferably in the visible range of the spectrum) and transport it and distribute it in core-building areas. In recent years, many new technologies and materials have been developed to increase the use of daylight inside buildings. Technology advances include: fibre optical cables, dichroic materials, prismatic glass, integrated artificial/natural lighting systems, Holographic Optical Elements (HOE), nonimaging concentrators and luminescent solar concentrators (LSC) (Smith, 2004; IEA, 2000; Elmualin et al, 1999). Louvres and light-shelves are also being incorporated in some recent architectural and façade designs (IEA, 2000; Canziani et al, 2004).

However, as pointed by Selkowitz (1998) and Matusiak (2004), in spite of all the investment and recent advances there is still a great gap between what is expected by core-daylighting systems and what it actually does. It is possible to categorise the main types of solar-daylighting technologies into one of the following groups:

- Passive architectural systems, which include: windows, sky lights and fenestration systems (IEA, 2000; Freewan, 2009);
- Static solar collector systems: is form of collecting solar radiation that relays only on the optics of the system, having no moving parts (IEA, 2000); and
- Active-tracking systems: relays on the optics and mechanical-tracking system (heliostat) that allows it to follow the sun's path (IEA, 2000).

2.9.1 Prismatic panels and laser-cut panels

Prismatic panels have already been applied to divert and/or redirect sunlight into deeper areas of a building. According to Cutler et al (2008), prismatic panels were popular natural illumination solutions for buildings in the 1890s (Cutler, 2008; Ewen, 1897). With the advent of artificial lighting their use became less common and only recently are they regaining attention as a daylighting technology. Current commercially available prismatic panels are made of clear acrylic (PMMA) by using injection moulding manufacturing processes (IEA, 2000; Edmonds and Greenup, 2002).

Prismatic panels are usually positioned on the upper area of windows or glazed facades. Basic configurations are designed to function as a passive-static daylighting system, although some more advanced systems can be adapted to a moveable configuration (manually or mechanical/electrical). One of the disadvantages of using prismatic panels to redirect incident sunlight is that part of the transmitted light can be directed downwards, causing discomfort glare on building occupants (IEA, 2000, pp.4-39; Fontoynont, 2002; Nazzal, 2005). This can happen due to the geometric construction of the prismatic structures and also depends on the incidence angle θ_i of direct light at the surface of the panel (Hecht, 1998; Edmonds and Greenup, 2002).

Laser-cut prismatic panels are currently used as a form of relatively low-cost daylighting system (IEA, 2000). Laser cut panels (LCP) are manufactured by making linear cuts on a polycarbonate or PMMA sheet (Edmonds and Greenup, 2002).

2.9.2 Light pipes and light duct systems

Hollow light pipes with internal reflective surface can be defined as tubular structures through which natural light can reach deep inside the buildings interior (IEA, 2000; Matusiak, 2004). Most light pipes have circular cross-sections or rectangular cross-sections. In general terms, they can be classified as: (A) vertical light pipe, attached on the top of the building; and (B) horizontal light pipe, attached on the side of the building - usually the façade. Commercial light pipes usually have a gloss-white or specular mirror-reflective internal surface in order to minimise light scattering along its length (Rosemann e Kaase, 2005). The British company Monodraught manufactures commercial light pipes (http://www.monodraught.com/, accessed 25th June 2005).

Rosemann and Kaase (2005) reported on the development of natural illumination system named ARTHELIO. The ARTHELIO main focus was to combine the utilisation of daylight and artificial light in hollow prismatic light guides. From 1998-2001 the Institute of Lighting at the Technical University of Berlin was the co-ordinator of the

project. The ARTHELIO system used two tracking flat mirror to redirect sunlight into a system of prismatic light pipes (Rosemann and Kaase, 2005).

Rosemann et al (2006; 2008) described a "*solar canopy illumination system*" that can be integrated into a building façade and redirect sunlight indoors. The authors argued that their system is cost-effective due to the fact that it combines other energy-saving elements in addition to its main function of daylighting. However the system is not compact and occupies a considerable amount of space. It also requires an active-solar-tracking support system. Sunlight redirecting elements consists of a series of metallic slats with mirror finished surfaces. The slats are horizontally displaced and together they act like a kind of blind system. They can be adjusted to redirect light into the solar canopy (Canziani, et al 2004; Rosemann et al, 2008a; 2008b).

Canziani et al (2004) proposed a "light pipe equipped with a flat capitation *system suitable to be integrated in a building's façade, without any protrusion as to the architectural envelope*" (Canziani et al, 2004, pp.1163). Gupta et al (2001) introduced the concept of principle sections to analyse the propagation of light through light pipes of regular simple geometries, with symmetrical rectangular or elliptical cross-sections. The irradiance distribution inside hollow light pipes is analysed by Gupta et al (2001), Jenkins and Muneer (2004) and Cheng and Chern (2006).

One of the current problems with tubular sunpipes (light pipes, light ducts) is that they need to have a large diameter / cut-section in order to transport enough natural illumination indoors (Rosemann et al, 2008). This makes it unpractical and uneconomical to use them in most buildings because they occupy a large volume across the building. Ideally they should occupy the smallest volume possible, making them more suitable for building integration (Hestnes, 1998; Probst and Roecker, 2007). However, with current technology, a significant reduction in the light pipe diameter would result in a significant reduction in its light transport efficiency, since the entrance of the light pipe would be also reduced and less light would be captured (Gupta et al, 2001; Carter, 2002). Hence, there is a technical contradiction here that needs to be solved in order to allow the development of compact daylighting systems with higher building integration potential (Nicoletti, 1998; Reijenga, 2003; IEA, 2000).

2.9.3 Fibre optical cables

Another way to transport light is by fibre-optical cables. The use of optical fibre as a mean to conduct daylight into the interior of buildings has been investigated since the early 1980s (Fraas et al, 1983). A comprehensive review in the application of fibre-optic systems for natural illumination is presented by Kandilli and Ulgen (2009).

Fibre-optic systems for natural illumination require high concentration. To achieve such high values it is necessary to apply two-axis active-tracking mechanical systems (heliostats). These systems are very expensive and require periodic maintenance (Rosemann et al, 2008, pp.303). Attenuation of light in fibre-optical cables results in an exponential decrease of about 20% to 25% per meter (Andre and Schade, 2002, p.51; Kandilli and Ulgen, 2009).

Due to its relatively high costs, few concentrator systems apply fibre optical cables as a means to transport sunlight indoors (Andre and Schade, 2002; IEA, 2000). Japanese manufacturer Himawari® (http://www.himawari-net.co.jp/e_page-index01.html, accessed, 24th July 2005) and Swedish company Parans® (http://www.parans.com, accessed, 10th Sept. 2009) are two examples of companies that have adopted fibre optics as a core technology for their daylighting systems.

A fundamental issue in using fibre-optical cables to transport and distribute concentrated sunlight relates to the technical and optical aspects of coupling concentrated light into the fibre-optics (Kandilli et al, 2008; Kandilli and Ulgen, 2009).

2.10 Imaging solar concentrators

Imaging solar concentrators are usually classified as 3D concentrators, in the sense that they converge radiant energy to a focal-point. Examples of imaging concentrator devices used in solar optics are the Fresnel lens and the parabolic-dish reflector. To achieve high concentration in imaging systems it is necessary to maintain a constant focal point. As a result imaging concentrators require the support of mechanical active-tracking heliostat systems (IEA, 2000; Maxey et al, 2008; Rosemann et al, 2008). Current active-tracking solar collector/concentrator systems can follow the Sun path with high accuracy, making it possible to achieve extremely high concentration ratios (Feuermann and Gordon, 1999). However, most solar-tracking systems are cost prohibitive. As discussed earlier, high concentration of solar radiation can also result in serious damage (e.g. fire), requiring the application of fire-protective materials and making the final system even more expensive (Rosemann et al, 2008).

2.10.1 Fresnel lenses

The famous Fresnel lens was invented by French scientist *Augustin-Jean Fresnel* around 1822 (Hecht, 1998; Fresnel Technologies, 2001). The basic idea of Fresnel was to make a thinner lens by changing the usual curved profile a lens to a

concentric array of prisms that could focus light to its focal point. It was originally conceived to concentrate and collimate light for lighthouses. The simplicity of its design allows it to be manufactured by using a variety of materials (glasses, PMMA, PVC, polycarbonate) and processes (injection moulding, compression moulding, casting, embossing), which has many commercial advantages and low-cost implications. Since its creation, Fresnel lenses have been successfully applied and adapted to a wide range of applications, including solar concentrators (Fraas, 1983; Feuermann and Gordon, 1999; Sierra and Vazquez, 2005).

Fresnel lenses do not concentrate all the light that they intercept basically for three main reasons: (A) Fresnel-reflection losses at the optical interfaces (frontal surface and back surface), which may account for losses up to 8%; (B) transmission and absorption losses due to interactions with the material and (C) manufacturing limitations and imperfections. Current modern flat-facet Fresnel lenses, manufactured by compression-moulded process, can achieve an optical efficiency of about 85% under direct collimated light at normal incidence angle θ_i in relation to the lens surface (Swanson, in: Luque and Hegedus, 2003, pp.487; Fresnel Technologies, 2001).

Figure 2.5 presents a schematic section view of two Fresnel lenses with grooves facing outwards (Fig.2.5a) and inwards (Fig.2.5b) – (Fresnel Technologies, 2001; Hecht, 1998).

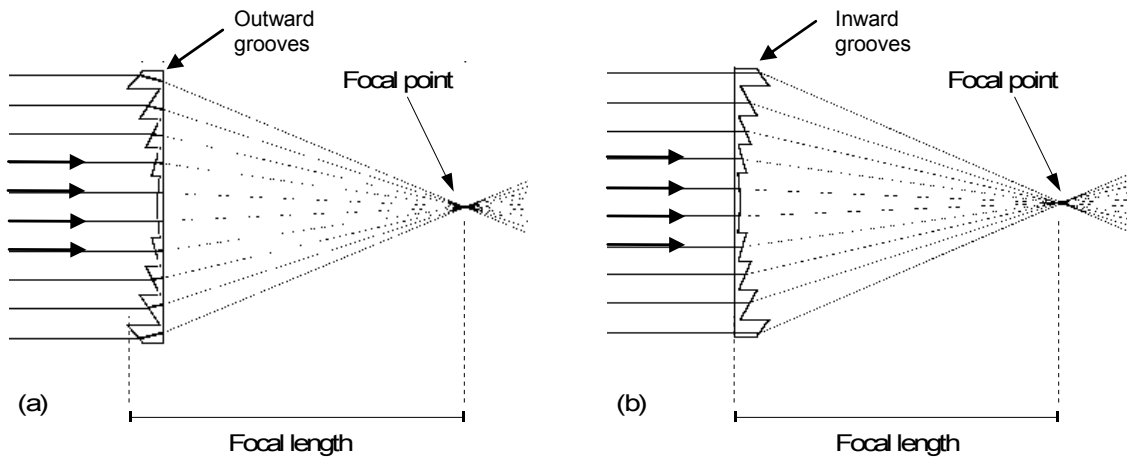

Figure 2.5 – Fresnel lens optical profile section.

The optical efficiency η_0 of a Fresnel lens is also reduced due to aberration losses (Welford and Winston, 1978; Lorenzo, 1981; Fresnel Technologies, 2001). Chromatic aberration is a fundamental problem in imaging systems (Lorenzo, 1981). Each wavelength λ converges to different focal point, resulting in a reduction of power concentration density and making it more difficult to collect all the concentrated

radiation (Welford and Winston, 1978; Lorenzo, 1981). Losses in concentration power density due to chromatic aberration will be very small between nearby wavelengths, but they may become more significant for wavelengths λ in further bands of the spectrum (Smith, 2000; Welford and Winston, 1978; Lorenzo, 1981). Lorenzo (1981) measured the effect of chromatic aberration using Fresnel lenses and concluded that:

> "The d*istance measured in the receiving plane between the far-violet wavelength (λ≈380nm) and the far-red wavelength (λ≈780nm) can become of the same order as the receiver size*" (Lorenzo, 1981, pp.3729).

However, some active-tracking solar concentrators systems that apply Fresnel lenses as primary optics use chromatic aberration to their advantage. For example, the Japanese *Himawari*® solar collector system (Figure 2.24) uses chromatic aberration effects to separate the near-infrared radiation (λ >780nm) from the visible (λ = 400nm to 780nm) part of the spectrum. This contributed to the reduction of building cooling demand by reducing the amount of near-infrared radiation (λ >780nm) that enters the building through the solar collector system (IEA, 2000; http://www.himawari-net.co.jp/e_page-index01.html, accessed 24th July 2005).

An alternative construction of the classic Fresnel lens is the line focus Fresnel lens, or 2D Fresnel lens. Instead of concentrating radiant energy at a focal point, the 2D Fresnel lens concentrates it along a focal line. Buie (2004) argues that "*line focus Fresnel concentrators show great potential in reducing capital costs of large scale solar concentrating systems*" (Buie, 2004, p.97). Some solar-thermal concentrators applied for water heating and solar-photovoltaic concentrators use line focus Fresnel lens in combination with a trough-like reflective system to increase concentration ratio (Swanson, 2000; Antón et al, 2003).

2.10.2 Fresnel lenses optics solar concentrators

Several solar concentrators that apply a single Fresnel lens or an array of Fresnel lenses to concentrate light have been developed and tested for a variety of applications (Swanson, 2000; IEA, 2000). Some existing commercial solar concentrators apply Fresnel lenses to concentrate solar radiation. Most of these systems are designed for solar-photovoltaic applications (Andreev et al, 2004; Sierra and Vazquez, 2005). However, some commercial solar concentrators, such as the Parans® solar panels (http://www.parans.com, accessed 10th Sept. 2009), apply arrays of small Fresnel lenses to concentrate sunlight for natural illumination application.

However, since Fresnel lenses are imaging optical devices, they have a relative small acceptance angle and require the support of active-tracking systems (heliostats) to follow the apparent movement of the Sun across the sky. This is fundamental to keep the lens surface constantly facing direct sunlight at normal angle position (90°), so that the focal point of the lens maintains its constant position in space. Without an active-tracking system, sunlight will not be concentrated at the expected focal point, making it more difficult to use the collected solar radiation for a practical application (Welford and Winston, 1978; Sierra and Vazquez, 2005).

The *Himawari® Collector* is an active solar tracking system with a sun collector made up of several hexagonal Fresnel lens attached in a honeycomb pattern structure. The sun tracking is possible due to a "sun detector" (heliostat), an internal microprocessor, mechanical devices and electric motor (Andre and Schade, 2002, p.21; http://www.himawari-net.co.jp/e_page-index01.html, accessed, 24th July 2005). Costs range from US$7000 to US$300.000, depending on the size and accuracy of the system, and the length of the required fibre-optical cables (Andre and Schade, 2002; Leslie, 2003; Lighting Research Center, 1998).

Tsangrassoulis et al (2005) presented the hybrid daylighting system named Universal Fibre Optics (UFO), which aims to integrate natural and artificial lighting into one single system that delivers light by fibre-optical cables. The UFO system is composed by a combination of other already well known systems: (A) an active-tracking heliostat system with based on Fresnel lens optics; (B) artificial lighting sources; (C) fibre-optical cables; (D) universal light emitter; and (E) control system. The authors claim that the UFO system contribution to artificial lighting energy savings reached 58.8% during summer (Tsangrassoulis et al, 2005).

2.10.3 Parabolic-dish solar concentrators

Feuermann and Gordon (1999) analysed the potential of miniaturization of solar-dish-concentrators rather than building large dishes. Their idea was to combine the power of a several arrays of mini-solar-dish-concentrators that concentrates light into fibre optical cables. The cables then transport concentrated light to a central receiver. They estimated collection efficiencies of up to 80% and argued that their system can achieve a concentration ratio of around 30.000 suns at the central receiver focal point. To do so, the system required the use of high-precision sun-tracking (heliostats) to keep the parabolic dishes constantly facing the Sun. However, such high concentration can become extremely dangerous, requiring special anti-fire protection and the use of materials with high thermal resistance. This all adds significant costs,

making it very expensive for mass-market orientated applications (Feuermann and Gordon, 1999).

Kandilli et al (2008) analysed the energy efficiency of an active-tracking solar parabolic-dish concentrator (diameter ≈ 1m) to beam concentrated light into fibre optical cables (length ≈ 3m) for daylight application in buildings. The system efficiency peaks at around 42% under direct sunlight (Kandilli et al, 2008). Maxey et al (2008a; 2008b) expect that a commercial version of their parabolic-dish hybrid concentrator system will be able to illuminate an area of approximately 75m^2 (≈ 800ft^2) at an initial cost of US$ 20,000 (Maxey et al, 2008b).

2.10.4 Ring-array concentrator (RAC)

Vasylyev (2005) reported on the development of a new concept of solar concentrator that applied a series of highly reflective metal slats displayed in a concentric ring-like configuration. Developed by SVV Technologies Innovations (http://www.svvti.com, accessed 15th March 2007), the system was named ring-array concentrator (RAC). The RAC system optical working-principle functions as a kind of "reflective-lens", converging incident sunlight to its focal point. The RAC system was initially conceived to concentrate solar radiation for solar-photovoltaic or solar-thermal applications (Vasylyev, 2005).

2.11 Nonimaging optics and nonimaging solar concentrators

Nonimaging optics is a relative new field of optics that deals with the transfer of radiation flux intensity rather than with image fidelity – a subject studied by classic geometric optics. It offers a different approach and concepts from those used in classic geometric optics (Luque, 1986; Timinger et al, 2000). Terms such as aberration, paraxial approximation, focal length and optical aperture are no longer relevant (Welford and Winston, 1978). New concepts are introduced: flow lines, geometric flux vector, and density of flux conservation, or étendue (Welford and Winston, 1978; Luque, 1986; Timinger et al, 2000; Chaves and Collares-Pereira, 2000).

Many authors argue that nonimaging optics is more suitable than imaging optics for the design of fixed/static solar concentrators/collectors (Welford and Winston, 1978; Ries and Rabl, 1994; Luque, 1986). One of the reasons is that nonimaging optics is more concerned with the transport of radiant energy (Welford and Winston, 1978; Ning et al, 1987; Timinger et al, 2000; Chaves and Collares-Pereira, 2000).

2.11.1 Nonimaging optics basic theory and design principles

Ries and Rabl (1994) argue that the main goal of nonimaging optics is to "*transfer radiant energy from an extended source to a target in such way as to achieve a specified distribution of radiation on the target*" (Ries and Rabl, 1994, pp.2627). Note that to achieve concentration the target has to be smaller than the source which, in geometrical terms, means that the entrance area (or entrance aperture) of the concentration system has to be larger than the receiver area, or receiver/exit aperture (Welford and Winston, 1978; Timinger et al, 2000).

Miñano and Gonzalez (1992) define a nonimaging concentrator as "*an optical device designed to transfer the incoherent radiation from a source to a receiver*" (Miñano and Gonzalez, 1992, pp.3051).

In nonimaging optics the conservation of phase-space volume and the Second Law of Thermodynamics will define the upper limit on concentration C_{max} and transmission efficiency T_E of the optical system (Ries et al, 1997, pp.2855; Ries, 1982). Nonimaging concentrators are usually described with respect to the phase-space volume conservation (étendue) - (Welford and Winston, 1978). Winston et al (2005) uses fluid dynamics as an analogy to describe the concept of phase-space volume (étendue) conservation. They borrow the term "*phase space*" and apply it in the analysis of optical systems, concluding that the étendue in an ideal system can only remain constant or decrease (Winston et al, 2005, pp.46; Welford and Winston, 1978).

The luminous flux Φ of light cannot increase as it travels through an optical system. If it did so, it would violate the Second Law of Thermodynamics (Welford and Winston, 1978; Luque, 1986). This means that the maximum transmitted luminous flux possible is $\Phi_{out} \leq \Phi_{in}$. In a theoretical ideal loss-less system the luminous flux Φ remains constant. However, for most practical applications, the transmitted luminous flux Φ will be significantly reduced due to interactions between light and matter (Welford and Winston, 1978; Hecht, 1998).

"*In geometrical optics a ray can be described by its intersection with a reference surface (x, y) and the direction sine of its path (kx, ky)*" (Ries and Rabl, 1994, pp.2627). From this definition one can derive the concept of phase space – which represents a point in a four dimensional manifold (Ries and Rabl, 1994, pp.2627; Luque, 1986). According to Luque (1986, pp.120) the propagation of a ray of light inside a nonimaging concentrator can be described by the vector differential equation:

$$dE = dxdydpdq = dx'dy'dp'dq' \qquad [2.16]$$

In the literature the invariant dE is usually called *étendue*, or density of flux conservation (Luque, 1986, pp.120). In equation 2.16 the entrance ray spatial coordinates are represented by (x, y, p, q), whereas the vector representation of the exiting ray is defined by the spatial coordinates (x', y', p', q'). Theoretically, considering that there is no attenuation, the étendue of a ray of light travelling through an ideal optical system remains constant. In other words, the étendue is conserved (Ries, 1982). However, this will be only true in ideal systems. In practice the étendue is not conserved due to absorption, attenuation and scattering (Ries, 1982; Welford and Winston, 1978).

The étendue for an ideal system can be estimated by applying the equation:

$$\textit{Étendue} = n^2 a^2 \Theta_{max}^2 \qquad [2.17]$$

Where,

n is the refractive index of the concentrator;

a is the area of the receiver;

Θ_{max} is the maximum acceptance angle of the concentrator.

The design of nonimaging optical devices is often based on the edge-ray principle, also known as extreme-rays principle (Welford and Winston, 1978, pp.48; Luque, 1986, pp.122). A more accurate definition of edge-rays is given by Ries and Rabl (1994), which define them as the "*rays that passes through the edge of a surface or are tangential to it*" (Ries and Rabl, 1994, pp.2627).

In general terms the edge-ray principle states that, in order to achieve maximum transmission efficiency, the incident rays that reach the edges of the entrance aperture of the concentrator must be the same rays that reaches the edges of the exit aperture of the concentrator (Welford and Winston, 1978, pp.48; Ries and Rabl, 1994; Luque, 1986, pp.122). If this condition is satisfied, it is expected that all other rays that fill the space between the edge rays will also be transmitted from the entrance to the exit aperture (Welford and Winston, 1978; Rabl, 1994; Ries and Rabl, 1994). A nonimaging concentrator is considered ideal when the edge-rays (or extreme rays) at the entrance aperture are the same edge-rays at the exit aperture (Welford and Winston, 1978, pp.48; Luque, 1986, pp.122; Ries and Rabl, 1994).

It is important to note that although the concept of edge-rays has been widely applied in the field of nonimaging optics, resulting in a variety of practical devices, so far no rigorous proof has been presented for its validation (Luque, 1986, pp.122; Ries and Rabl, 1994, pp.2627). However, according to Welford and Winston (1978, pp.48) the application of the edge-ray principle has resulted in solar collectors with higher concentration ratio and transmission efficiency.

2.11.2 Nonimaging solar concentrators

2.11.2.1 The Compound Parabolic Concentrator (CPC)

Compound parabolic concentrators (CPC) are well known optical devices used in the solar energy related areas and also in other applications where radiant energy concentration is needed, being defined as one of the first devices that resulted from the practical application of nonimaging optics (Welford and Winston, 1978). The device was developed almost simultaneously in the United States, United Kingdom and Germany, during the 1960's (Welford and Winston, 1978, pp.49; Winston et al, 2005).

Theoretically the CPC achieves maximum optical concentration by collecting all incident rays within its acceptance angle θ_{accept} (Welford and Winston, 1978). It has been argued that the concentration ratio of the CPC comes very close to the ideal theoretical concentration limit (Gordon and Rabl, 1992; Welford and Winston, 1978). There are several types of variations of the original CPC design (Welford and Winston, 1978; Garcia-Botella et al, 2006; Hatwaambo et al, 2008; Kiatgamolchai and Chamni, 2008). The CPC has been widely investigated and used for several applications where concentrated radiant energy is needed (Welford and Winston, 1978). For example, Kim et al (2008) analysed the thermal performance of a CPC-type collector designed for solar-thermal application, whereas Hatwaambo et al (2008) used a trough-like low cost CPC system for solar-photovoltaic application.

The CPC has an axis of symmetry which determines its overall length (Winston et al, 2005, pp.50). The internal reflexive surface of the CPC is obtained by rotating the parabola around the concentrator axis, not the axis of the parabola, as explained by Winston et al (2005, pp.50). There are also some practical advantages of CPC systems. For example, they are relatively simple to design and manufacture, not requiring extreme material properties (Welford and Winston, 1978; Timinger et al, 2000; Winston et al, 2005).

Schmidt-Kloiber and Schoeffmann (1986) investigated the propagation of light through hollow cones with highly reflective metallic internal surfaces. The angle of incidence θ_i of incoming light and the number of internal reflections will define the optical efficiency of the CPC-type device (Schmidt-Kloiber and Schoeffmann, 1986; Kiatgamolchai and Chamni, 2008).

One of the main problems with current CPC systems is that only moderate concentration is achievable due to physical limitations (Chaves and Collares-Pereira, 2000; Luque, 1986, pp.119). In fact most CPC designs achieve concentration below C_R

= 5X (Chaves and Collares-Pereira, 2000, pp.270). Higher concentrations can be achieved with CPCs with longer extension (height), which in most situations, lead to unpractical designs (Chaves and Collares-Pereira, 2000, pp.270). According to the Second Law of Thermodynamics, the radiance power of a light beam cannot increase along the passage through a concentrator (Welford and Winston, 1978, Luque, 1986). In a theoretical ideal CPC design this means that it can only remain constant, if it goes directly through the entrance aperture to the exit aperture, or decrease, if it is reflected by the mirror walls of concentrator (Ries, 1982, pp.380; Welford and Winston, 1978).

Attenuation losses in reflective CPC-type devices are qualitatively proportional to its height (Kiatgamolchai and Chamni, 2008). The higher the device, the higher is the number of internal reflections, resulting in higher attenuation (Welford and Winston, 1978; Chaves and Collares-Pereira, 2000; Kiatgamolchai and Chamni, 2008).

Rays entering a CPC system can be rejected (bouncing back to the entrance) if they reach the system at an incidence angle θ_i larger than the systems acceptance angle θ_{accept}. This happens after a number of reflections inside the system and the ray bounces back towards the entrance from which it first came from (Welford and Winston, 1978; Luque, 1986; Kiatgamolchai and Chamni, 2008).

Kiatgamolchai and Chamni (2008, pp.113) calculated that the maximum number of reflections (i_{max}) of ray inside a CPC or CPC-type device can be defined by:

$$i_{max} = 45°/\ 90° - \theta_i \qquad [2.18]$$

where θ_i is the ray incidence angle. For most situations, the closer the incidence ray is to the systems optics axis, the fewer reflections will be necessary to reach the exit aperture (Kiatgamolchai and Chamni, 2008, pp.114).

2.11.2.2 Solid dielectric nonimaging concentrators

Solid-dielectric nonimaging concentrators were firstly derived from the CPC-type concentrators (Goodman et al, 1976; Scharlack, 1977). The main difference is that they are made of solid transparent dielectric material, such as PMMA or glass. In general, they are efficient devices used to concentrate radiant energy for a variety of applications. They can be easily manufactured from a single material at relative low costs. The optical phenomenon of total internal reflection (TIR) is the main physical principle on which these devices are based on (Goodman et al, 1976; Scharlack, 1977; Welford and Winston, 1978; Ning et al, 1987a).

The dielectric totally internally reflecting concentrator (DTIRC), initially proposed by Ning et al (1987a), is basically a compound parabolic concentrator (or a CPC-type) filled with a solid-dielectric material (e.g. PMMA or glass) with a refractive index n greater than one (n>1). The higher refractive index n medium of the DTIRC increases the concentration ratio C_R and also takes advantage of the optical effect of total TIR (Welford and Winston, 1978; Ning et al 1987a).

The central idea of a DTIRC is to "*combine the front surface refraction with total internal reflection from the sidewall to achieve concentrations close to the theoretical maximum limits, the thermodynamic limit*" (Ning et al, 1987a, pp.).

Goodman et al (1976) investigated the use of solid-dielectric CPC-type devices to concentrate solar radiation for photovoltaic applications. Welford and Winston (1978, pp.136) presented a prototype (made of PMMA) of a solid-dielectric CPC-type array designed to concentrate sunlight on photovoltaic cells attached to the exit apertures.

The main advantage of TIR is that it is almost loss-free (Welford and Winston, 1978; Ning et al, 1987a). Another advantage is that the concentration ratio is multiplied by the refractive index n of the dielectric material, resulting in higher values of concentration (Chaves and Collares-Pereira, 2000). Due to its larger refractive index n and a curved front surface it is argued that the DTIRCs can achieve higher concentration than the CPCs (Ning et al, 1987a). For this reason the solid-dielectric CPC-type concentrators are usually more compact, with shorter length, than their reflective-type CPCs counterparts (Welford and Winston, 1978; Ning et al, 1987a; Nilsson, 2005; Chien et al, 2009).

According to Winston et al (2005) and Welford and Winston (1978, pp.70) the condition for TIR to occur inside a solid-dielectric CPC-type concentrator surrounded by air (n = 1,0) is given by the equation:

$$\sin \theta_i < n - (2/n) \qquad [2.19]$$

where θ_i is the incident angle of radiant energy at the air-dielectric interface and n is the refractive index of the solid-dielectric material (Welford and Winston, 1978, pp.70).

Gao et al (2006) described a device which they named "nonimaging beam expander" that is also based on the principle TIR. The geometry of the device resembles a CPC-type nonimaging concentrator. Depending on where it is located, such geometry could also potentially be used as an extractor device to extract light from a dielectric concentrator system or a dielectric light guide (Gao et al, 2006).

Zacharopoulos et al (2000) presented two variations of linear solid-dielectric nonimaging concentrators for solar-photovoltaic application that can be integrated into

a building façade. Their systems are made from of low-iron glass (refractive index n=1.523). They resemble a flat panel-type frontal surface with a side-profile cut-section formed by an array of linear trough-like CPC-type concentrators, with a depth of only 55mm. A series of photovoltaic cells are positioned at the exit aperture of each linear CPC-type. They claim that the system optical efficiency η_0 is over 90%, under a wide range of incidence angles θ_i (Zacharopoulos et al, 2000). Only about 10% of incidence solar radiation is lost due to absorption by the iron-glass or rejection by being reflected back to the outside environment (Zacharopoulos et al, 2000).

One of the main problems of solid-dielectric optical systems relates to the extraction of radiant energy that remains trapped inside the system by total internal reflection (Ries et al, 1997a; Masui et al, 2008). The higher the refractive index n of the material the more difficult it becomes to extract light from the system (Ries et al, 1997). The geometry of the exit aperture and its surface finishing quality also has an important contribution in allowing radiant energy to be extracted from the system (Ries et al, 1997a; Ning et al, 1987a).

According to Ries et al (1997a) the extraction of radiant energy from a high-refractive index medium to a low-refractive medium is limited by the conservation of the phase space (étendue). The authors calculated that the amount of light that can be extracted from a dielectric concentrator or a dielectric light guide, with a refractive index n higher that the refractive index n' of the surrounding medium, "*decreases continuously to zero with the increasing of the refractive index n*" (Ries et al, 1997a, pp.2872). The reason for this is that the increase of the refractive index n leads to a decrease of the critical angle θ_c inside the solid-dielectric medium. As a result the "angular window" for light to escape from the denser medium becomes smaller, meaning that more light is trapped inside the solid-dielectric medium by TIR (Welford and Winston, 1978; Freeman, 1990; Ries et al, 1997a; Hecht, 1998).

Ries et al (1997a) demonstrated that triangular and hexagonal shaped extractors approach maximum extraction efficiency for light in solid-dielectric light guides. They suggested that the diameter of the polygonal cross-section extractor should decrease gradually along the optical axis of the system in order to extract as much light as possible from the solid-dielectric light guide (Ries et al, 1997a, pp 2873-2874).

2.12 Combined imaging-nonimaging solar concentrators

More recently, solar concentrators are being developed by applying a combination of different optical configurations, such as: (1) combination of Fresnel lenses with non-imaging type mirrors; (2) the use of focusing optics for a first stage of concentration together with non-imaging optics as a second stage of concentration; and (3) double tailored devices among other solutions (Chaves and Collares-Pereira, 2000, pp.270; Welford and Winston, 1978; Ning et al, 1987b).

The combination of CPC and lens systems has already been investigated by some authors. Miñano and Gonzalez (1992) presented a methodological approach to the design of nonimaging systems in which nonimaging lens-CPC devices are presented and analysed. In a prior work, Collares-Pereira et al (1977) analysed the propagation and concentration of light through several different embodiments for possible CPC-lens-systems configurations.

2.13 Luminescent solar concentrators (LSC)

Luminescent solar concentrators (LSC) can be described as transparent sheets (or slabs) of dielectric material, usually glass or PMMA, doped with fluorescent particles (Lifante et al, 1983, pp.3966). The basic concept of LSC has been around since the mid 1970's. The invention of the LSC is attributed to Weber and Lambe (1976). In the mid 1980's, reported optical efficiencies of LSC were around 2.5% for single dye systems and 4% for "stacked" LSC systems during outdoor experimental tests (De Cardona et al, 1985; Sanderson, 2008; Rowan et al, 2008).

During the next two decades, progress in this area apparently came to a halt. However, recent publications reporting advances in efficiency ranging from 4.8% to 7.1% are regaining research attention to the area (Earp et al, 2004; Slooff et al, 2008; Sanderson, 2008). Sanderson (2008) reported on the development of an LSC with power conversion efficiency of 7.1%. This efficiency was achieved by a research team at the Imperial College of London. According to Sanderson (2008), the previous record was about 2.4%. The term power conversion efficiency relates to the amount of power generated by the LSC solar cells as a fraction of the incident light power that falls over the LSC frontal surface (Sanderson, 2008).

Incident light intercepts the LSC frontal surface and enters the dielectric medium with a refractive index n higher than its surroundings. Inside the LSC, the dye absorbs part of the light and re-emits the wavelength related to its colour pigmentation. This wavelength remains trapped inside the PMMA sheet by TIR. Light that is absorbed

and re-emitted by the dye is emitted in random directions Eventually, part of this trapped radiant energy reaches the side-edges of the sheet, where part of it can be absorbed by photovoltaic cells or redirected for other applications, such as daylighting or solar-thermal (Earp et al, 2004; Slooff et al, 2008; Sanderson, 2008; Lifante et al, 1983, pp.3966).

A reported advantage of the LSC is that it has a large acceptance angle. Some authors argue that an LSC has an acceptance angle of up to 180° (Lifante et al 1983; Smestad and Hamill, 1984). Another advantage is that LSC systems are compact static devices, not requiring expensive active-tracking systems (Rowan et al, 2008).

Earp et al (2004a) report on the application of luminescent concentrator technology for natural illumination. The authors developed a LSC composed by a stack of three clear PMMA sheets (2mm thick), each doped with a coloured fluorescent dye. The first PMMA sheet is doped with a violet coloured fluorescent dye; the second PMMA sheet is doped with a green coloured fluorescent dye; and the third PMMA sheet is doped with a pink coloured fluorescent dye. Three of the lateral sides and also the back side of the stack are covered with reflective mirror sheets to increase efficiency. Only one lateral side is left “open”. They tested their three-colour stack LSC (with frontal area of 1200mm x 135mm). They reported that their system, under a direct solar illuminance of 100,000lx, yields a luminous output of 995 lm, which represents an efficiency of 6.1% (light-to-light efficiency). However they do not mention the angular variation of incident direct sunlight, nor the orientation and positioning of the LSC (Earp et al, 2004a).

Swift and Smith (2003) also analysed the performance of a three-colour LSC. They selected a series of dyes from BASF (Lumogen®) with high quantum efficiencies.

The efficiency of a LSC is limited by three main factors:

- Transmission losses of radiant energy of the re-emitted wavelength along its path towards the edge of the sheet. This can be significant due to its random direction inside the LSC sheet (Lifante et al, 1983; Earp et al, 2004a; 2004b; Rowan et al, 2008).
- Partial absorption of radiant energy by the material sheet denser medium. (Sanderson, 2008; Rowan et al, 2008).
- Dye degrading. Another problem relating LSC is that most organic dyes, used to produce the fluorescence effect, tend to degrade overtime (Sanderson, 2008). In fact, the stability of the dye is of major importance for the efficiency a LSC over time (Mansour, 1998; Goldschmidt et al, 2009). Some dyes tend to degrade faster than others. For example, according Earp et al (2004) violet coloured dyes tend to degrade after only a few months. Applying an ultraviolet

(UV) blockage-coating on the frontal surface of the LSC may extend its lifetime (Rowan et al, 2008; Earp et al, 2004a; 2004b; van Sark et al, 2008).

A recent study conducted by van Sark et al (2008) tested the stability of dyes over a period of two years. However, despite reported advances no LSC system has already being commercialized in large scale. Van Sark et al (2008) highlighted the need for cost-economical studies to investigate the commercial viability of this technology. Some researchers even argue that it may take around ten more years for the LSC technology to reach the market at a competitive cost (Sanderson, 2008).

2.14 Discussion on the literature and research justification

Based on this literature review, it could be argued that the development and implementation of core-daylighting systems and solar-daylighting-collectors has proven to be an elusive solution to the challenge of increasing natural illumination in buildings (Selkowitz, 1998; Reinhart and Selkowitz, 2006; Rosemann et al, 2008). Indeed, despite decades of research most of the technologies designed to harvest and deliver natural illumination in core-building areas have not moved far beyond the prototyping stage (Selkowitz, 1998; Swanson, 2000). The few systems that enter the market are usually too expensive and/or directed to a restricted market-share (IEA, 2000; Reinhart and Selkowitz, 2006; Rosemann et al, 2008). Considering that most solar-daylighting technologies have been under intense research during the last 30 to 50 years (at least), and yet none of them has delivered a solution with significant market potential, it is reasonable to question if they will ever do. A similar opinion is expressed by several authors in the literature (Selkowitz, 1998; Swanson, 2000; Antón et al, 2003; Reinhart and Selkowitz, 2006).

This is not to say that solar-daylighting is not a desirable option. As seen, solar-daylighting can potentially lead to significant direct and indirect benefits, including:

- Direct reduction in electric energy consumption in 30% to 77% with a proportional reduction in building CO_2 emissions (Chen et al, 2004; Ihm et al, 2009; Jenkins and Newborough, 2007);
- Increase in buildings occupants health, satisfaction and productivity (Fontoynont, 2002; Galasiu and Veitch, 2006; Webb, 2006);
- Improve the building owner image and “green-credentials” (Omer, 2008; Thormark, 2002; de Vries et al, 2007);
- Environmental and economic benefits (Perez-Lombard et al, 2008).

Furthermore, the continuous increase in energy demand due to population and economic growth, the predicted end of cheap oil, scarce natural resources and climate

change are pressing governments and business around the world to find sustainable solutions (Ihm et al, 2009; Perez-Lombard et al, 2008; Jentsch et al, 2009; EIA, 2009). In this context, the investment in the development and implementation of sustainable building technologies, including solar-daylighting-technologies, should be compensated by the range of benefits that they bring over a long period of time (Omer, 2008; Reinhart and Selkowitz, 2006; Jentsch et al, 2009). For example, less energy-intense buildings means less energy-intense cities, resulting in a reduction in energy demand and less environmental impact (Perez-Lombard et al, 2008). Also, the increase of indoors natural illumination leads to an increase in human health and satisfaction, resulting in an increase in work / study productivity, and consequently, in the long-term, a decrease in public health costs (Olders, 2003; Pauley, 2004; Webb, 2006).

It is argued that the development of sustainable buildings and renewable-energy technologies should be bound together through a long-term perspective (Omer, 2008; Jentsch et al, 2009). Building standards and regulations already recommend the implementation of sustainable building practices (British Standard BS ISO 15392:2008; British Standard BS ISO 156686-5:2008). Energy policies of several countries are starting to address the importance and urgency of developing sustainable buildings and renewable energy technologies (Goldemberg, 2006; Block, 2006; Mancisidor et al, 2009). Tax incentives and support mechanisms are being applied in order to stimulate the development and implementation of renewable energy and low-carbon technologies (Ruiz et al, 2007; Diaz-Rainey and Ashton, 2008). It is very plausible that in the coming decades new buildings will only be approved if they are low-energy-demanding and equipped with renewable energy technologies to produce most part of their own electricity (Diaz-Rainey and Ashton, 2008).

Hence, in the present context, the development of solar-daylighting technologies is not only desirable but necessary. And considering the prospects for the near future, the need and demand for sustainable building technologies tends to grow significantly (Perez-Lombard et al, 2008; Jentsch et al, 2009; Andrews and Krogmann, 2009; EIA, 2009). The fundamental problem is how to harvest and distribute sunlight at an acceptable cost, with low-environmental impact and without compromising the building architectural composition (Nicoletti, 1998; Hestnes, 1999; Reinhart and Selkowitz, 2006; Rosemann et al, 2008; IEA, 2000; Probst and Roecker, 2007).

2.15 Gap in the literature and research opportunity

The problems relating to the design and implementation of solar-daylighting-collectors are complex and interdependent. A fundamental issue for high building integration potential relates to the compactness of the collector/concentrator. The quest for compact optical concentrators has been a main issue in the design of solar collector/concentrators systems (Winston, 1970; Welford and Winston, 1978; Ning et al, 1987a; Chaves and Collares-Pereira, 2000; Chien et al, 2009). The compactness of a concentrator device is geometrically defined by its aspect ratio (height divided by width) – (Welford and Winston, 1978; Chaves and Collares-Pereira, 2000). The higher the aspect ratio the more compact is the optical system. It is argued that compact solar collector systems, that is, systems that have a small depth compared to its frontal area, may find wider market acceptance since it can be more easily integrated into a buildings façade and/or roof (Chaves and Collares-Pereira, 2000; Chien et al, 2009). In terms of building integration, compact optics present several advantages over more massive and bulky systems such as the Himawari® systems and parabolic-dish concentrators, for example (Hestnes, 1999; IEA, 2000; Chien et al, 2009).

The geometric concentration ratio C_R of a solar collector/concentrator system is defined by their optical configuration (Welford and Winston, 1978; Chaves and Collares-Pereira, 2000). Most solar collectors/concentrators are constructed in such a way that the entrance aperture and the exit aperture are located in parallel planes separated by a distance d. For example: (A) in an imaging concentrator (e.g. Fresnel lens), the focal point plane is parallel to the lens surface plane (Sierra and Vazquez, 2005); and (B) in an nonimaging concentrator, such as the CPC device, the entrance aperture and exit aperture are also located in parallel planes (Welford and Winston, 1978; Hatwaambo et al, 2008). A negative consequence of this type of optical arrangement is that the final system configuration is usually not compact. According to Chaves and Collares-Pereira (2000, pp.270) the classic CPC nonimaging concentrator is limited to a geometric concentration ratio C_R between 3 and 5. CPC-type devices with a geometric concentration ratio $C_R > 5$ are unpractical because they become too tall with the increase of the concentration ratio (Welford and Winston, 1978; Chaves and Collares-Pereira, 2000, pp.270; Chien et al, 2009).

Alternative nonimaging optics constructions indicate the possibility of locating the exit aperture in a perpendicular plane or in an oblique plane in relation to the entrance aperture plane (Maruyama and Osako, 1999; Chaves and Collares-Pereira, 2000; Mallick et al, 2006; Chien et al, 2009). By doing so it is possible to develop compact systems. However, current systems with such optical arrangements also have

limited geometric concentration ratio C_R. For example, the asymmetric CPC for building façade integration developed by Mallick et al (2006) has a geometric concentration ratio C_R of 2.32. Solid-dielectric wedge-type concentrators, with the exit aperture perpendicular or oblique to the entrance aperture, present a geometric concentration ratio C_R between 2.5 and 5 (Maruyama and Osako, 1999; Chien et al, 2009).

Other systems, such as the "ultra-flat ideal concentrator" concept proposed by Chaves and Collares-Pereira (2000), with a geometric concentration ratio C_R of 15.8 (for an acceptance angle θ_{accept} = 10°) and the luminescent solar concentrator (Lifante et al, 1983; Mansour, 1998; Earp et al, 2004a), also present an optical arrangement in which the exit aperture is perpendicular to the entrance aperture. As a result they have a compact configuration with a relatively high concentration ratio C_R. However, problems in other areas such as manufacturing costs, durability and recycle/disposal costs may restrict their commercial potential (Swanson, 2000; British Standard BS 8887-1:2006; Rosemann et al, 2008).

The issue of "cost" should be seen in a broader perspective, encompassing: manufacturing/material costs, acquisition costs, installation costs, maintenance costs, use costs, recycling and/or disposal costs (British Standard BS 8887-1:2006; O'Driscoll, 2002; Ashby et al, 2007). For example, current luminescent solar concentrator (LSC) dyes have a limited life-span due to exposure to ultraviolet radiation (van Sark et al 2008; Sanderson, 2008; Rowan et al, 2008). LSC systems are also difficult to recycle due to the mixture of pigmented dyes inside the solid-dielectric bulk material, usually PMMA or glass (Sanderson, 2008; Rowan et al, 2008). This would make it very difficult for a LSC system to be approved by environmental standards. The British Standard BS 8887-1:2006, which relates to the design, manufacturing and recycling processes in the development of products with low environmental impact, recommends that a mixture of pigmented dyes and materials should be avoided because it makes it more difficult to recycle the product (British Standard BS 8887-1:2006, pp.34, 36).

Therefore, a research opportunity exists in the area of compact low-cost nonimaging solar collectors suitable for building integration. The main goal of this research is to develop a novel technology to harvest solar radiation for building applications, with emphasis on solar-daylighting application. The aim is to explore innovative optical configurations that allow the development of low-cost compact solar-daylighting-collectors suitable for building integration.

2.16 Summary and conclusions of Chapter 2

A review of solar collectors and solar concentrators, related technologies, optical design principles and theory has been presented and discussed. The main parameters involved in the development of solar-daylighting-collectors have been analysed. Advantages and disadvantages of daylighting in buildings have been outlined. A gap in the literature and a possible research opportunity to investigate has been identified and defined as the research area for this work.

It has been shown that the benefits of natural illumination extend far beyond the reduction of artificial lighting energy consumption, encompassing environmental and human health benefits (Reinhart and Selkowitz, 2006). Research indicates that the increase of natural illumination in buildings can contribute to a direct reduction of up to 40% of energy consumption and a proportional decrease in related CO_2 emissions (Jenkins and Newborough, 2007; Loe, 2003; Loe, 2009; Ihm et al, 2009). Recent studies are also linking the benefits of daylighting to several aspects of human health and indoors daily activities (Schanda et al, 2002; Pauley, 2004; Galasiu and Veitch, 2006; Nabil and Mardaljevic, 2006; Webb, 2006).

Current solar-daylighting-technologies, including solar-daylighting-collectors, are limited by a series of technical and cost constraints that have confined them to few applications and very restricted markets (Selkowitz, 1998; Swanson, 2000; Rosemann, 2008). Solar-daylighting-concentrators based on imaging optics and integrated to fibre optics are usually bulky expensive systems, requiring mechanical active-solar tracking support and maintenance (Tsangrassoulis et al, 2005; Kandilli et al, 2008; Maxey et al, 2008a; Maxey et al, 2008b). Most classic nonimaging concentrators such as the CPC are limited to a geometric concentration ratio $C_R < 5$ (Welford and Winston, 1978; Chaves and Collares-Pereira, 2000, pp.270). The luminescent solar concentrator (LSC) offers a compact system, however current luminescent dyes have a limited life-span due to UV-degrading (Mansour, 1998; Goldschmidt et al, 2009). The LSC is also more expensive to recycle due to the mixture of materials, making it difficult to attend the recommendations of sustainable design standards such as the British Standards BS 8887-1:2006 and BS ISO 15392:2008.

From this literature review it is possible to conclude that there is a clear need to develop novel concepts and design alternatives for low-cost compact solar-daylighting-collectors.

Chapter 3 - Research Methods and Optical Analysis Techniques

3.1 Introduction

The previous chapters have described the main issues and parameters regarding the development of solar collectors/concentrators and daylighting systems. It has been shown that despite decades of world-wide research there is still a great gap between what is expected from these technologies and what they currently provide (Selkowitz, 1998; IEA, 2000; Swanson, 2000; Matusiak, 2004; Reinhart and Selkowitz, 2006; Rosemann et al, 2008a).

This chapter describes the computer simulation tools, prototyping technique, optical methods and instrumentation applied in this research. The optical analysis techniques include a set of laboratory experimental test apparatus designed and manufactured in order to evaluate the performance of the demonstrations prototypes. The manufactured experimental apparatus to test the prototypes also included:

- Hollow cylindrical light pipes that were fabricated to function as light luminous flux integrating devices; and
- A novel device to analyse the spatial distribution of light emerging from the solar-collectors demonstration prototypes, named Angular Distribution Imaging Device (ADID).

3.2 OptiCAD® ray-tracing analysis and virtual simulation

OptiCAD® software provides a 3D environment for simulation and ray-tracing analysis of optical systems (OptiCAD Corporation, 2006). Computer ray-tracing analysis is a powerful tool applied in the development, optimisation and characterisation of optical systems and devices (Shannon, 1997; Smith, 2000; Geary, 2007). OptiCAD® software has been applied successfully by many researchers in the analysis of several optical applications, including lens design and solar concentrator systems (Chemisana et al, 2009; Canziani, et al. 2004; Andersen and de Boer, 2006). Screen shots of OptiCAD® software are displayed in Figure 3.1.

The solar-daylighting-collectors developed in this research were designed using CAD / SolidWorks® programme. To simulate their optical performance in the OptiCAD® programme, the files are converted into IGES (Initial Graphics Exchange Specification) CAD file format. OptiCAD imports the IGES file and converts them into a continuous (unfaceted) NURBS (Nonuniform Rational B-spline Surface) CAD model format. This process allows the CAD model designed in SolidWorks programme to be analysed in the OptiCAD environment, making it possible to perform ray-tracing analysis and other simulation tools (OptiCAD Corporation, 2006, pp. 6-2).

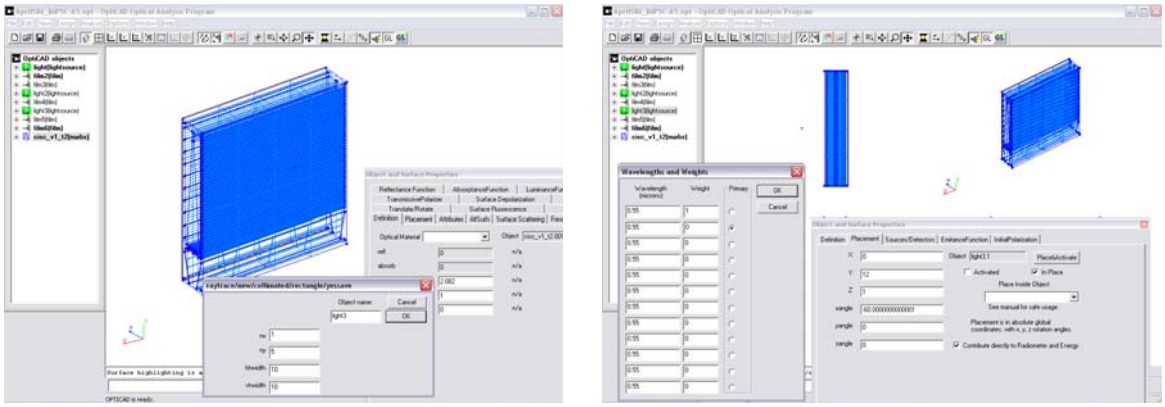

Figure 3.1 - OptiCAD® screenshots.

3.2.1 Ray-tracing analysis

Computer ray-tracing analyses are usually based on the vector form of the laws of reflection and refraction (Shannon, 1997; Geary, 2007). According to Welford and Winston (1978, pp.9) the Law of Reflection [$\theta_i = \theta_r$] is expressed by the vector equation:

$$\mathbf{r'} = \mathbf{r} - 2(\mathbf{n} \cdot \mathbf{r})\mathbf{n} \qquad [3.1]$$

where **r'** is the reflected ray, **r** is the incident ray and **n** is a unit vector positioned along the normal and pointing into the reflecting surface (Welford and Winston, 1978, pp.9). Also according to Welford and Winston (1978, pp.11) the vector notation of Snell's Law of Refraction [$n_1 \sin \theta_1 = n_2 \sin \theta_2$] becomes,

$$\mathbf{n'r'} = \mathbf{nr} + (\mathbf{n'r'} \cdot \mathbf{n} - \mathbf{nr} \cdot \mathbf{n})\mathbf{n} \qquad [3.2]$$

where, in this case, **r'** is the refracted ray, **r** is incident ray and **n** is a unit vector positioned along the normal and pointing into the reflecting surface (Welford and

Winston, 1978, pp.9). Note that both equations (Eq.3.1 and Eq.3.2) are defined as the dot product between the vectors **r'** and **r**, and the unit vector **n**. As a result the commutative operation in ray-tracing analysis is satisfied, meaning that the path of a ray is the same in both directions: reverse ray-tracing (Welford and Winston, 1978; Shannon, 1987; Geary, 2007; OptiCAD Corporation, 2006).

OptiCAD® initially considers the incidence angle spatial coordinates to find the point of intersection at the object/surface geometry. At the beginning of the ray-tracing simulations, the programme establishes an energy value of 1.0 (or 100%) for each ray. The corresponding unit (measured in Watts, W; or lumens, lm) can be defined by the user. The programme keeps track of each ray as it interacts with the optical system surface/geometry. Energy losses, scattering and attenuation can also be computed for each ray propagating through the optical system under analysis (OptiCAD Corporation, 2006). The optical properties of commercial grades of glazing glass (soda-lime), PMMA and polycarbonate (PC) are considered in the computer simulations. Refractive indices n presented by Nikolov and Ivanov (2000, pp.2069) served as references (Table 3.1).

Table 3.1 – Refractive indices for materials considered in OptiCAD® simulations according to wavelengths.

Material	**Wavelengths (nm)**				
	436	555	588	703	1052
PMMA	1.503	1.491	1.491	1.486	1.481
PC	1.617	1.587	1.592	1.582	1.572
Soda-lime (glass)		1.500			

3.2.2 Transmittance and absorption simulation

The transmittance of radiant energy through a bulk material is calculated in OptiCAD® by the equation:

$$E_{out} = E_{in} \times T_1 \times T_2 \, e^{-\alpha \cdot t} \qquad [3.3]$$

Where:

- E_{out} is the ray energy leaving the object;
- E_{in} is the ray energy entering the object;
- T1 is the surface transmittance at the object's entry surface;
- T2 is the surface transmittance at the object's exit surface;
- α is the bulk absorption coefficient (in m^{-1}); and
- t is the length of the ray path (different for each ray) through the object.

3.2.3 Surface scattering simulation

Surface scattering is simulated by OptiCAD® as a weighted random process in which an incident ray on a surface is perturbed about its specular component direction. This process, known as perturbed surface scattering modelling, treats surface scattering through a probabilistic approach, meaning that the results will vary slightly each time a ray-tracing analysis simulation is performed (OptiCAD Corporation, 2006). It is argued that this simulation model provides a more realistic approach for surface scattering. However, the downside is that it is a purely geometric approach. Variations of wavelength are not considered due to the complexities involved (OptiCAD Corporation, 2006, pp. 4-27 and pp. 10-43).

3.2.4 Volume scattering simulation

Volume scattering simulations are usually calculated by applying a series of probabilistic functions that considers both the distance between scattering sites and the change in direction after scattering for the ray path inside a dielectric material. According to the programme manual (OptiCAD Corporation, 2006, pp.10-3), the probability density function for the ray path between scatters is calculated by:

$$p(s) = \mu_t \cdot e^{-\mu_t \cdot s} \qquad [3.4]$$

Where:

- μ_t is the scattering coefficient (called scatter in OptiCAD®);
- s is the path between scatters.

To simplify the calculation process, the programme considers that the angular scattering for a ray propagating inside a dielectric medium with refractive index n is uniformly distributed around the z-axis, or vertical axis, of the optical system under analysis. The programme also considers multiple volume scattering inside solid dielectric medium (OptiCAD Corporation, 2006, pp.10-3).

3.2.5 Fresnel-reflection simulation

OptiCAD® programme calculates Fresnel reflections based on the average specular reflected/refracted component for each ray intersection with a dielectric surface (e.g. glass or optical plastic). The calculation considers the indices of refraction of the materials and the incidence angle θ_i formed between the incident ray and the local-surface-normal at the point of intersection. Fresnel reflection losses are

accounted at each interface as the ray propagates through the optical system (Hecht, 1998; OptiCAD Corporation, 2006, pp. 10-56).

3.2.6 Total internal reflection (TIR) simulation

Considering that scattering and absorption are not computed, the software estimates that all rays that undergo total internal reflection (TIR) are 100% loss-less. Evanescent waves, which represent the small portion of losses related to TIR in real-physical systems, are not considered by the programme (Hecht, 1998, pp.124). The critical angle θ_c for TIR is material related and depends on the refractive index n and the wavelength λ pre-defined by the user (OptiCAD Corporation, 2006).

3.2.7 Radiometer and spot diagrams

It is possible to measure the output efficiency of an optical system by applying a virtual radiometer inside OptiCAD® 3D environment. The radiometer can be attached to a film/detector surface that is positioned by the user at the desired location (x, y, z; θ_x , θ_y , θ_z). The programme calculates how many rays intercept the radiometer surface and measures the efficiency of the system by considering the initial ray energy value, attenuation losses through the system and the incident angle θ_i that the ray makes with the virtual radiometer surface normal (OptiCAD Corporation, 2006).

3.3 CAD-CAM-CAE design and analysis support tools

Injection moulding processes are well-known and widely used in several manufacturing industries (Nardin et al, 2002). It has also been successfully applied to manufacture high-quality optical components such as lenses and prisms (Weng et al, 2009; Smith, 2000).

Due to the high costs in tooling, it is useful to simulate the injection moulding process before committing to the necessary investment. A considerable amount of research in CAE (computer-aided engineering) has lead to the development of software able to simulate the injection moulding process with a high degree of certainty (Nardin et al, 2002).

Moldflow® (http://www.moldflow.com, accessed 03rd November 2008) is a CAD-CAE software used to simulate injection moulding processes. The software has been successfully applied in several industries and research-based applications. The intention of applying this simulation tool is to provide a preliminary study to verify the

feasibility of using injection moulding manufacturing processes to produce the solar collectors systems presented in this thesis (Nardin et al, 2002; Weng et al, 2009).

3.4 Laser-cutter rapid-prototyping process

The demonstration prototypes presented in this thesis were manufactured by using a laser-cutter rapid-prototyping process. The prototypes were made of a commercial grade of clear acrylic (PMMA) by using a laser-cutter rapid-prototyping manufacturing process. The choice of the material and the manufacturing process were defined by:

- The optical quality of PMMA, which presents high transitivity in the visible range of the spectrum (Dislich, 1979; Chien, 2009); and
- The low-cost, geometric precision and easy-to-use aspects of the laser-cutter rapid-prototyping process.

The thickness of the demonstration prototypes was defined by the technical limitation of the laser-cutter. The surface quality provided the laser-cutter process decays with the increase of the thickness of the PMMA sheet. Hence, the thickness of the PMMA sheets used to manufacture the prototypes was limited to 3mm and 5mm.

The technique of applying a laser to cut and drill materials, known as laser ablation, has bean successfully applied in many industries (Davim et al, 2008). Interactions between the laser and matter, and the effect of the laser cutting process on polymers have been investigated by a number of authors (Lippert at al, 2003; Yalukova and Sarady, 2006; Efthimiopoulos et al 2008).

The process of designing a CAD model on a computer and transforming it into a prototype using current laser cutter machines is straightforward. SolidWorks® software is used to design 3D CAD models of the solar-daylighting-collectors and related parts. Once the design is completed, the file is saved as a DXF file extension and exported to 2D graphic-design software Adobe Illustrator® to be converted into a vector-PDF file. The laser-cutter machine reads the vector-PDF file and cuts the exact geometry (with high precision) out of a clear PMMA sheet.

3.5 Surface analyses techniques

Two types of surface analysis techniques were applied in this research to evaluate the surface quality of the laser-cut demonstration prototypes: (A) the speckle-pattern surface analysis contrast technique (Lehmann, 1999; Dhanasekar et al, 2008); and (B) the scientific optical profiler Zygo® system (http://www.zygo.com, accessed 05th January 2009).

Lehmann (1999) considered the speckle-pattern illumination technique to characterize the surface-roughness of engineering surfaces. The contrast (dark and bright areas) generated by the speckle-pattern was used as a roughness parameter to estimate the finishing quality of the surface (Dhanasekar et al, 2008).

A CCD camera (EO USB 2.0 colour) with an optical zoom lens was used to provide images of the surface finishing quality provided by the laser-cutter machine. Two beams of white light (emerging from two fibre-optical cables) from illuminator MI-150 were applied to illuminate the surfaces and highlight possible defects. Both camera and illuminator were purchased from Edmond Optics (http://www.edmundoptics.com, accessed 10th Sept. 2009).

National Instruments LabVIEW® Vision Assistant® (http://www.ni.com, accessed 19th February 2008) software was used to assist in the surface analysis process. A series of optical profiles of the surface were used to evaluate the variations of surface roughness as a function of speckle-intensity fluctuations, measured in terms of pixel intensity (gray scale level, from 0 to 255). The software also recognises geometric patterns and shapes on an image, making it possible to estimate the total number sub-surface air-bubbles and other sub-surface defects generated by the laser ablation process.

3.6 Experimental optical analysis and characterisation methods

3.6.1 Photometry

The science that deals with the measurement of the electromagnetic spectrum can be divided in two branches: radiometry and photometry. Radiometry aims to measure all spectral regions, from x-ray to radio waves (DeCusatis et al, 1998). Photometry aims to measure only the visible region of the spectrum (380-780nm), having human vision as its reference (Ohno, 1998; Hovila, 2005). Photometric quantities are derived from radiometric quantities (DeCusatis et al, 1998). Photometry is used to evaluate several types of light sources in respect to the human eye

sensibility, being applied to measure both artificial and natural illumination (Ohno, 1998). Figure 3.2 displays the photopic luminous efficiency function V(λ) for the human eye adopted by the International Commission on Illumination (CIE) and used as an international reference standard (CIE, 1988; DeCusatis et al, 1998).

Most photometers, including commercial illuminance meters, are designed in order to present a response that resembles the daytime-response of the human eye, or photopic-vision, peaking at 555nm wavelength (green-yellow) which is normalized as 1,0 (Ohno, 1998; Schanda et al, 2002). This response is also described by the V(λ) function curve (Ohno, 1998; Hovila, 2005).

Both irradiance and illuminance (E_v) are considered to be instantaneous incident energies (Taylor, 2000; Zain-Ahmed, et al 2002). The photometric quantities that are more relevant for this research are described as follows:

- **Illuminance** (symbol: E or E_v ; unit: lm/m² = lux): measures the density of the luminous flux incident on a given surface or plane (NIST, 1997, pp.4; British Standard BS ISO 23539:2005, pp.2). Lux (lx) is the unit of illuminance (E). One *Lux* (lx) is one *lumen* (lm) per square meter. The orientation of the surface in relation to the incident light is essential to define the illuminance value that it receives (Ohno, 1998; Taylor, 2000).
- **Luminance** (symbol: L or L_v ; unit: cd/m²): defines the luminous intensity of a surface in a specific direction, divided by the projected area as viewed from that direction (NIST, 1997; British Standard BS ISO 23539:2005, pp.2).
- **Luminous flux** (symbol: Φ or Φ_v; unit: lumen, lm): measures the power of visible light. 1 lm is equal to 1cd radiation passing though 1 sr (solid angle) (NIST, 1997; Taylor, 2000; British Standard BS ISO 23539:2005, pp.1).

3.6.2 Transmission efficiency (or light-to-light efficiency)

The illuminance transmission efficiency T_E of a solar-daylighting-collector, also called light-to-light efficiency (Earp et al, 2004), can be defined in terms of the fraction of light that is intercepted by the collector at its entrance aperture and what percentage of it is transmitted through its exit aperture. The transmission efficiency T_E can be calculated in terms of a percentage (%) of the transmitted illuminance (lx) by the equation:

$$T_E = E_{out} / E_{in} \times 100\% \qquad [3.5]$$

Where:

- T_E is the illuminance transmission efficiency (or light-to-light efficiency);
- E_{out} is the illuminance (lx) measured at the exit aperture; and
- E_{in} is the illuminance (lx) measured at the entrance aperture (frontal surface).

It is important to note that the illuminance input E_{in} at the frontal surface (entrance aperture) of the solar collector varies in accordance to the Cosine Law of Illumination, also known as Lambert's law of intensity (Taylor, 2000; Smith, 2000, pp.221). According to Taylor (2000, pp.23) the Cosine Law of Illumination is given by:

$$E_\theta = E \cos\theta \qquad [3.6]$$

where E_θ is the illuminance measured at the illuminated surface, E is the illuminance measured at a perpendicular plane in relation to the direction of a isotropic collimated beam of light and θ is the angle of incidence in relation to the normal to the illuminated surface (Smith, 2000, pp.221; Taylor, 2000, pp.23). Considering this, the illuminance input E_{in} at the frontal surface (entrance aperture) of the solar collector is directly dependent on the incident angle θ_i of light. In other words: $E_{in} = E \cos\theta$.

3.7 Optical instrumentation

3.7.1 Photometers (lux-meters)

Photometers, also known as lux-meters or illuminance meters were used to evaluate the performance of the solar-daylighting-collectors prototypes manufactured in this research. Two commercial photometers, Extech E-31 and Extech E-33 (Figure 3.3) were used. Both are silicon-photodiodes detectors with cosine-correction diffuser dome (http://www.extech.com, accessed 08th June 2006).

Commercial diffuser-type photometers are suitable for illuminance, luminance and luminous-flux measurements of several types of light sources, including most artificial light, diffuse natural light and direct sunlight (Campos et al, 2003; Sametoglu, 2007; Hovila, 2005). The use of these devices to measure the illuminance distribution of daylighting is fairly common (IEA, 2000; Hovila, 2005).

The responsivity of photometers depends on two main functions: spatial response and spectral response (Doulos et al, 2008). Spatial response relates to the acceptance angle θ_{accept} (or acceptance cone) of the detector: the detector only

responds to rays that fall within its acceptance cone. Spectral response corresponds to the range of wavelengths that the detector can "read". This relates to the source of light that was used to calibrate the detector. Note that commercial silicon-photodiode photometers are defined "*in terms of power response or irradiance response over the wavelength range of 200 to 1100 nm"* (Schneider and Young, 1998, pp.254).

Most photometers are calibrated against a light source with a colour temperature that corresponds to the CIE Illuminant A, which represents a colour temperature of 2856 K (Plankian radiation) – (Ohno, 1998; Hovila, 2005; Sametoglu, 2007). This means that the spectral response of the photometer is "optimised" to measure light sources with similar colour temperature. An error might occur when it is exposed to light sources with different colour temperatures (Sametoglu, 2007). According to Hovila (2005) the response error can vary from 0.05% to 6% according to the colour temperature of the light source to which the photometer is exposed.

As noticed before, the CIE Standard Photometric Observer is based on the spectral efficiency function – the V(λ) function, which is defined in the range 360-830nm of the solar spectrum, peaking at 555nm (which is normalized as 1,0). This value represents the optimum photopic response of the human eye for the visible spectrum (Ohno, Ed. DeCusatis, 1998, pp.58). However, as noted by Ohno (1998) "*no photometer can be matched to the V(λ) function perfectly*" (Ohno, 1998, pp.143).

The photometers (illuminance meters) used in this research were already calibrated by the manufacturer (http://www.extech.com, accessed 08th June 2006) – (Figure 3.2).

(a)


(b)

Figure 3.2 – The commercial photometers (illuminance meters) used in this research (a). Picture (b) shows the dome-diffuser detector of the photometers exposed to direct sunlight.

3.7.2 Optical spectrum analyser (600nm to 1780nm)

The optical spectrum analyzer Ando AQ6317B, produced by Japanese scientific instrumentation manufacturer Ando Electric Co Ltd. (http://www.ando.co.jp, accessed 12th August 2008) was used to analyse the spectral composition of the light emerging from our solar-daylighting-collectors. The Ando AQ6317B optical spectrum analyzer uses a diffractive-grating monochromator (ruled grating) to separate the incoming spectrum and analyse each wavelenght. It measures the spectrum power distribution (SPD) of light in terms of power intensity (measured in nW) as a function of wavelength (λ, measure in nm).

Note that the optical spectrum analyser ANDO AQ6317B analysis range is limited to 600nm to 1780nm, corresponding to part of the mid-visible (mid-VIS) spectrum to part of the near-infrared (NIR).

3.7.3 Imaging analysis

A low-cost CMOS digital camera OpticStar® PL130M monochrome (available at: http://www.opticstar.com, accessed 2nd Sept. 2008) was used to help visualise the light flux uniformity and angular distribution. The camera has a wavelength response between 380nm to 1000nm.

The analysis of the images provided by the CMOS camera and the CCD camera were conducted with National Instruments® LabVIEW® Vision Assistant 8.0 software. This program offers up-to-date imaging acquisition and measuring tools. Valuable qualitative information is extracted from selected images and analysed in terms of RGB colours, uniformity distribution and pixel intensity. Data was exported to Excel® software for further analysis.

3.8 Hollow light pipes integrator tubes

A series of experimental hollow light pipes were manufactured to test the transmission efficiency of the solar collector prototypes and also to serve as an integrating device (to generate a uniform distribution of light over the photometer sensor). The light pipes were made out of Melinex® sheets (gloss white), semi-rigid polyester-aluminium sheets and commercial aluminium tube. The polyester-aluminium sheets presented a reflectivity of around 80-85% for the visible spectrum range. The sheets were folded in a tubular-shape. As seen in the literature review, aluminium is known to have a good reflectivity for most wavelengths of the spectrum (Serra, 1998).

It is important to note that the use of a hollow light pipe to function as a radiant energy integrating device for photometric measurements has been suggested as a practical alternative over the integrating sphere technique (Smith, 1997, pp.105; Greivenkamp, 2003). The distribution of radiant energy propagating through reflective hollow light pipes has been studied by a number of authors (Swift and Smith, 1995; Gupta et al, 2001; Cheng and Chern, 2006; Swift et al, 2006).

The following parameters of hollow light pipes are related to its irradiance transmission and uniform distribution qualities:

(1) Material and surface finishing: The material or coating should present high reflectivity of the wavelengths of the solar spectrum, or at least the range of wavelengths that are expected to be measured. For daylighting application the light pipe material should present high reflectance for wavelengths in the visible range (400nm to 780nm) of the spectrum (Ohno, 1998; Cheng and Chern, 2006).

(2) Geometry. A series of cylindrical reflective hollow light pipe with radius r and a cross-section area πr^2 were used. At the entrance aperture of the light pipe, the luminous flux Φ_0 can be calculated as a product of the transmitted illuminance E_T and the light pipe cross-section area $\pi.r^2$ (Swift and Smith, 1995; Gupta et al, 2001).

(3) Diameter. The diameter of the light pipe will have an influence on the number of reflections (bounces) that happens with off-axis rays (skew rays). Light pipes with smaller diameters will result in a larger number of reflections and vice-versa. In other words, light pipes with smaller diameter will result in high attenuation, whereas hollow light pipes with larger diameter will result in low attenuation due to internal reflections (Maxia et al, 1973; Swift and Smith, 1995).

(4) Length. The length of the light pipe will also influence on the number of reflections of the rays as they propagate through it. A longer light pipe will result in higher attenuation, while a shorter light pipe will result in less attenuation due to reflection (Swift and Smith, 1995; Gerchikov et al, 2005).

The internal surface of the light pipe should be smooth, preferably with optical finishing (Swift and Smith, 1995; Smith, 1997). In general terms, the reflectivity ρ of a hollow light pipe surface can be calculated by the equation:

$$\rho(\lambda) = 1 - \sigma(\lambda) \qquad [3.7]$$

where ρ is the surface reflectivity and σ is the surface absorption of the material (Swift and Smith, 1995; Schmidt-Kloiber and Schoeffmann, 1986). Note that both ρ (surface reflectivity) and σ (absorption) are wavelength λ dependent.

Figure 3.3 presents an imaging analysis done with the CMOS camera and the LabVIEW® Vision Assistant 8.0 software. The image on the left shows the distribution of light emerging from the "light-pipe-integrator". On the right, a 3D graph plots the pixel intensity (in RGB colours) of the light flux distribution emerging from the "light-pipe-integrator". Note that luminous distribution is quite even, especially at the central area.

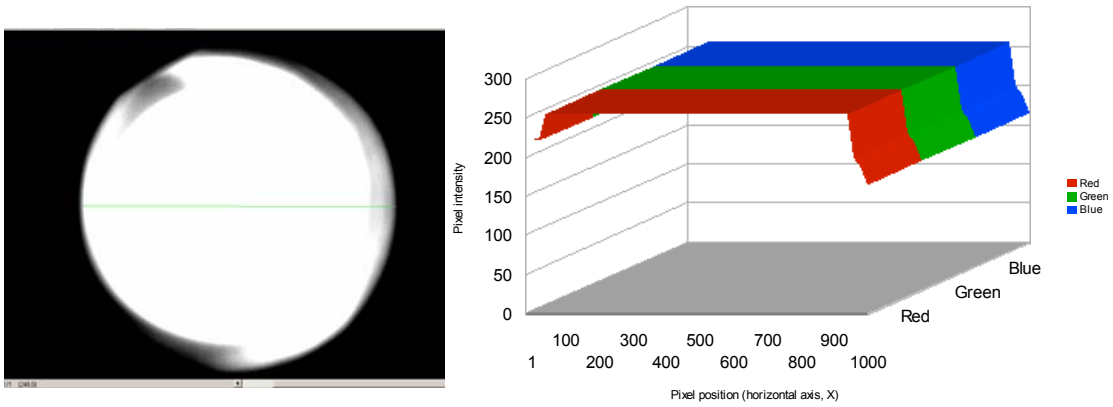

Figure 3.3 - Qualitative imaging analysis of transmitted luminous flux distribution emerging from the "light-pipe-integrator". Instrumentation: CMOS camera and the LabVIEW® Vision Assistant 8.0 software.

Considering that the light pipe presents mirror-reflective smooth surfaces, the angular distribution of outgoing rays as a function of the angular distribution of incoming rays remains constant. In other words, the angle of incidence θ_i remains unchanged at every reflection inside the light pipe (Maxia et al, 1973). According to Swift and Smith (1995) and Maxia et al (1973), the attenuation of radiant energy propagating inside a hollow reflective light pipe will be a product of:

- the incidence angle θ_i of light at the entrance of the light pipe;
- the length L of the light pipe;
- the diameter Ø of the light pipe;
- the reflectivity $\rho(\lambda)$ and surface-finishing of the light pipe material;
- the number of reflections N_R inside the light pipe.

It is important to stress that the measurements are directly influenced by the angular distribution $\Delta\theta$ of light propagating inside the light pipe. As a consequence, the value measured by a photodetector positioned at the end of the light pipe will be affected by the number of internal reflections and the length of the light pipe (Maxia et al, 1973; Swift and Smith, 1995; Gupta et al, 2001).

Figure 3.4 illustrates this possible situation. In Figure 3.4(a) only "ray 1" reaches the photodetector, while "ray 2" and "ray 3" don't. In Figure 3.4(b) all rays reach the photodetector. Hence, the photodetector reading will be higher in Figure 3.4(b) even if

it positioned at twice the distance from the solar collector exit aperture than in Figure 3.4(a). The variations in the photodetector reading can be considerably high at short distances from the light source (the solar collector exit aperture, in this case), but they tend to attenuate with longer light pipes.

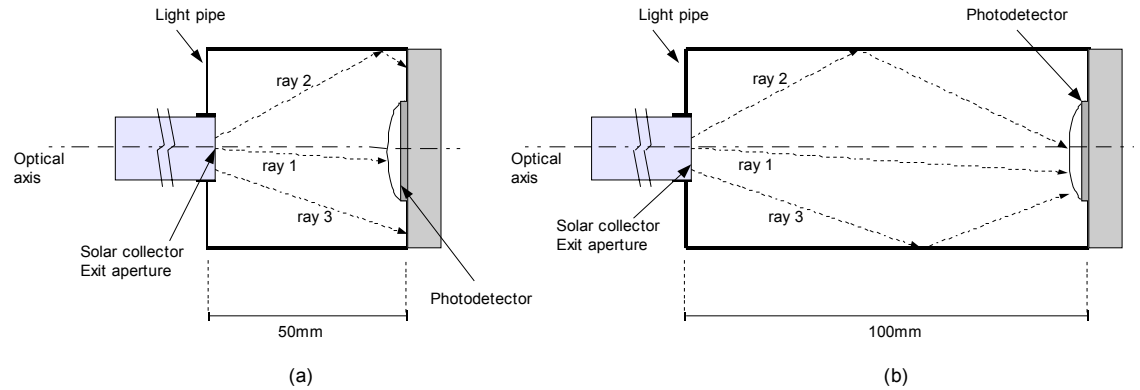

Figure 3.4 – Schematic diagram illustrating the variation of the angular distribution of the light inside the light pipe according to its length (mm).

3.9 Artificial light source for laboratory tests

A halogen light source Solux® 50W (available at: http://solux.net, accessed 28th July 2008) with spectral composition varying from 300nm to 1100nm was used as an "artificial sun" in the laboratory experimental tests. The light source has a colour temperature of 4700K, which approaches the standard CIE Illuminant B related to the colour temperature of direct sunlight (4874K) – (DeCusatis et al, 1998; Ohno, 1998).

A "partial collimator" tube was adapted to the light source in order to reduce beam divergence. A simplified version of a heliodon was designed and manufactured, allowing the light source to be positioned at different incidence angles θ_i while keeping a constant distance (90mm) in relation to the prototype entrance aperture (or entrance surface). The system was used to simulate the variations of the solar altitude angle h_s.

Figure 3.5 shows the results of illuminance measurements conducted to verify the illuminance output (lx) of the artificial light source (Solux® 50W) used in the laboratory experimental tests. The measurements were taken at a distance of 90mm from the exit of the collimator apparatus, which coincides with the distance to the frontal surface of the prototypes during the laboratory experimental tests.

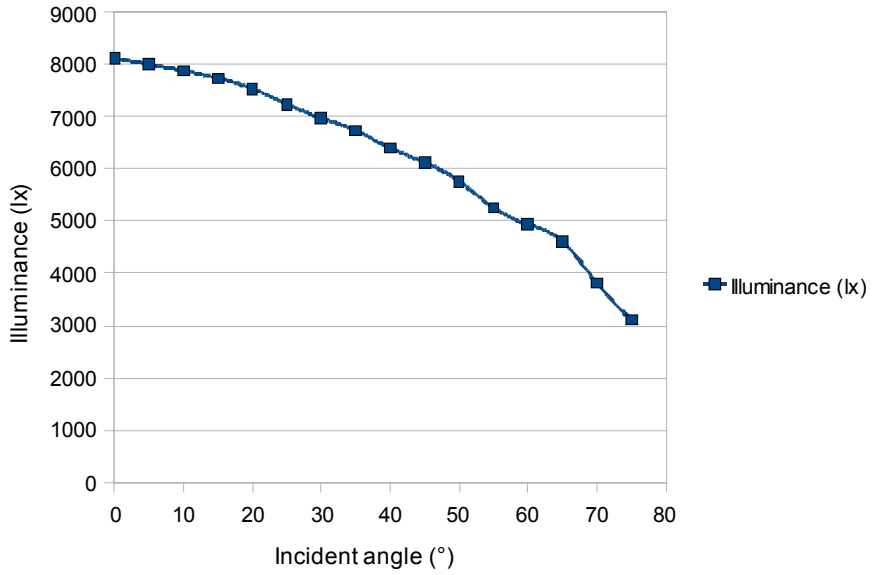

Figure 3.5 - Variations of illuminance measurement of Solux® 50W halogen light source at a distance d=90mm as a function of the incident angle θi.

3.10 Angular distribution imaging device (ADID)

A prototype for a novel type of luminous flux angular measuring device was designed and manufactured using a rapid-prototyping fluid deposition machine (FDM). The device was named Angular Distribution Imaging Device (ADID). The main function of the ADID apparatus (Figure 3.9), which also includes a CMOS camera, is to visualise the angular distribution Δθ of light emerging from the exit aperture of the RINSC prototypes.

The measurement of the angular distribution Δθ of a light source is important in optics because it gives valuable information about the spatial distribution and direction of the luminous flux Φ (Ohno, 1998; NIST, 1997). In the case of the solar-daylighting-collectors prototypes manufactured in this research, the measurements of the angular distribution Δθ of light emerging from the exit aperture provided useful information about the optical efficiency and utility of the systems.

The ADID consists of three main parts: (A) a dome-shaped collector with a series of holes symmetrically displaced along the semi-spherical surface; (B) a group of short-length fibre-optical cables; and (C) a flat-surface receiver with a series of holes symmetrically displaced along concentric circles. Parts (A) and (C) were designed on CAD programme SolidWorks® and manufactured by the FDM rapid-prototyping process. The FDM machine builds an exact 3D prototype model from ABS polymer. Each hole from the (A) dome-shaped part is connected to its “projected-counterpart-

hole" located on the (C) flat-surface receiver by a (B) fibre-optical cable. A total of forty one fibre-optical cables made of PMMA were used.

The device was assembled and installed over an optical bench in an optical laboratory at Brunel University. Magnetic-mounts and holders were used to support the structure. The final assembled apparatus can be seen in Figure 3.6. The ADID apparatus was used to access the distribution Δθ of light emerging from the exit aperture of a RINSC – IMPSC prototype (analysed in Chapter 7).

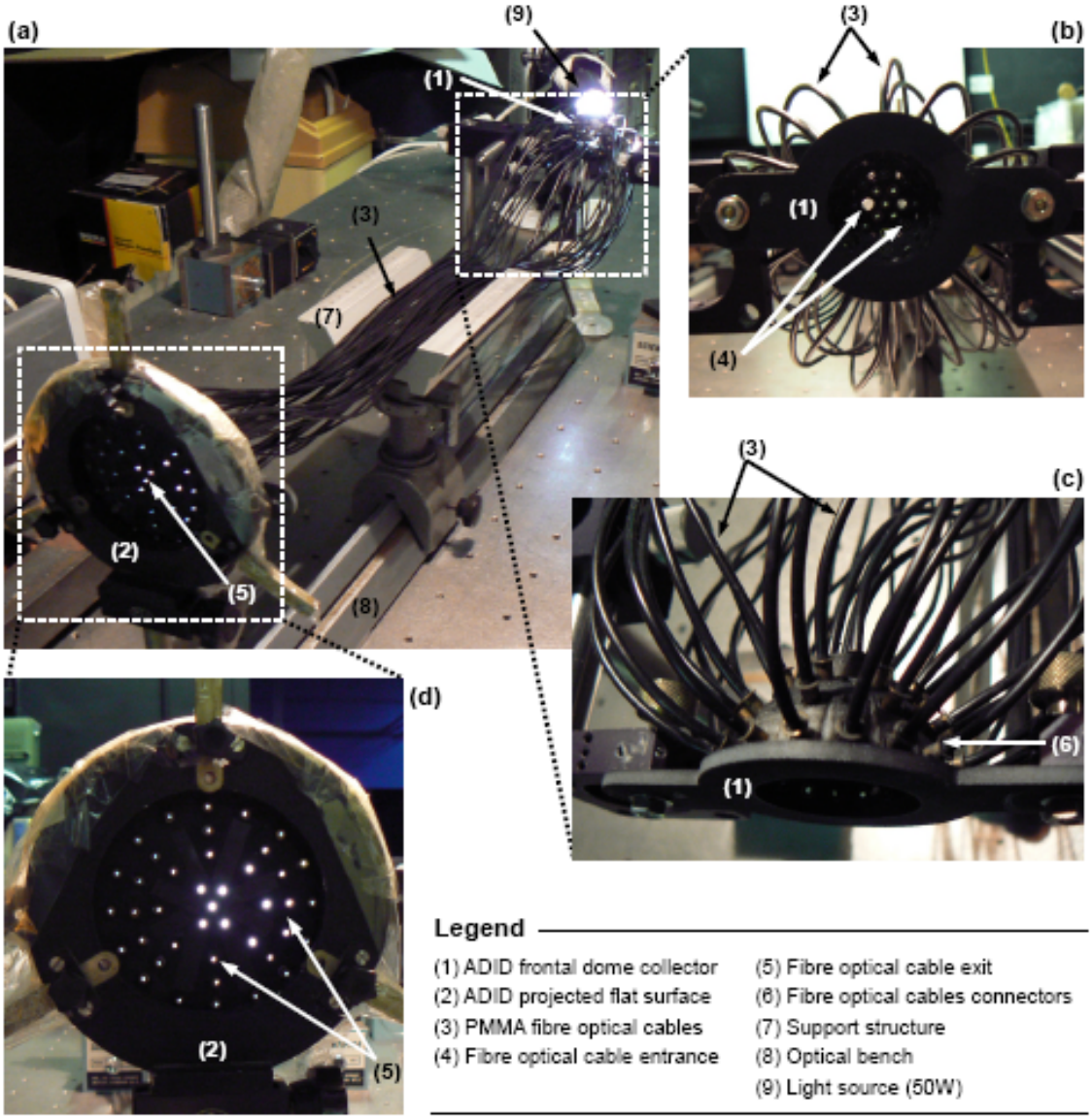

Figure 3.6 – The Angular Distribution Imaging Device (ADID) prototype.

3.11 Overview of experimental tests and measurements procedures

A fundamental issue in photometry and optical experimental tests is to define an optimum optical configuration, an experiment set-up, suitable for the proposed experiment (Ohno, in: Ed. DeCusatis, 1998). The experiment set-up also considered the limitations of the optical detectors and the geometric characteristics of the optical systems (in this case: solar-daylighting-collector prototypes) that were intended to be analysed and measured (Ohno, 1998; Hovila, 2005).

3.11.1 Sources of errors and uncertainties

Any scientific measurement has a related measurement uncertainty. According to Ohno (1998), Hovila (2005) and Sametoglu (2007), measurement uncertainties in photometry can be grouped in one of the two categories: (1) random measurement errors; (2) systematic measurement errors.

- Radom measurement errors (e.g. reading or positioning errors) can be reduced by repeating the number of measurements (Ohno, 1998; Hovila, 2005).
- Systematic measurement errors are often related with the instrumentations errors, making them more difficult to quantify (Ohno, 1998; Hovila, 2005).

According to Ohno (1998), Hovila (2005) and Sametoglu (2007), typical sources of errors in photometry include:

- Spectral mismatch of detector: occurs when the light source to be measured has a different "*spectral power distribution (SPD) from the standard light source for which the photometer was calibrated*" (Ohno, 1998, pp.143).
- Photometer / photodiode temperature variation: changes in the temperature of the photodiode/detector may result in significant sources of errors and even damage the sensor if it gets too hot (Ohno, 1998, Sametoglu, 2007).
- Stray light errors: stray light relates to light not intended to be measured during the experimental tests. Basically it relates to scattered or reflected ambient light coming from "sources" other than the expected "light source" Ohno (1998), Hovila (2005) and Sametoglu (2007).

3.11.2 Measurement procedures

The works of Walker (1972), Ohno (1998), Schanda (1998) and Hovila (2005) were considered to establish some important general requirements for the photometric experimental tests setup and measurement procedures.

- Unambiguity of measuring field: a fundamental factor that must be observed is that the measuring field of the photometer (or any other kind of photodetector device) should be limited. The optical detector should only "see" the light source expected to be measured (Walker, 1972, Ohno, 1998).
- Reference planes: a set of reference planes should be considered to plan the positioning of the optical detectors, the object to be measured and light source.
- Alignment: the alignment and angular displacement between the measured components and the measuring instrumentation is of extreme importance to collect reliable data and also to reproducibility of the photometric measurements (Schanda, 1998, pp.413). A level device was used to level the photometers, mounts and collectors in relation to the predefined reference planes.
- Limited movements: To reduce sources of errors it is also necessary to limit the possible range of movements for detectors and testing devices.
- Maximum transmittance and receiving efficiency: this means that the total optical path from the solar-daylighting-collector exit aperture to the photometer receiver should allow the maximum transmission of radiant energy.
- Repeat measurement: laboratory experimental tests were repeated up to 4 times in order to reduce reading errors.

3.11.3 Laboratory experimental tests set-up

Indoor experimental tests were conducted in an optical laboratory. The laboratory was a standard optical laboratory with flat black painted walls, equipped with a professional optical table with pneumatic vibration isolation, optical benches and magnetic mounts (Geary, 1993; Smith, 1997; Ohno, 1998).

The experiments were set-up on the optical table and aligned along optical benches. A series of aperture screens were positioned to isolate the "measurement area" (with the optical detectors) from the "experiment area" (with the light source).

The demonstration prototypes are characterised in respect to incident light θ_i at the meridional plane. Figure 3.7 presents a schematic view of the basic laboratory experiment set-up configuration.

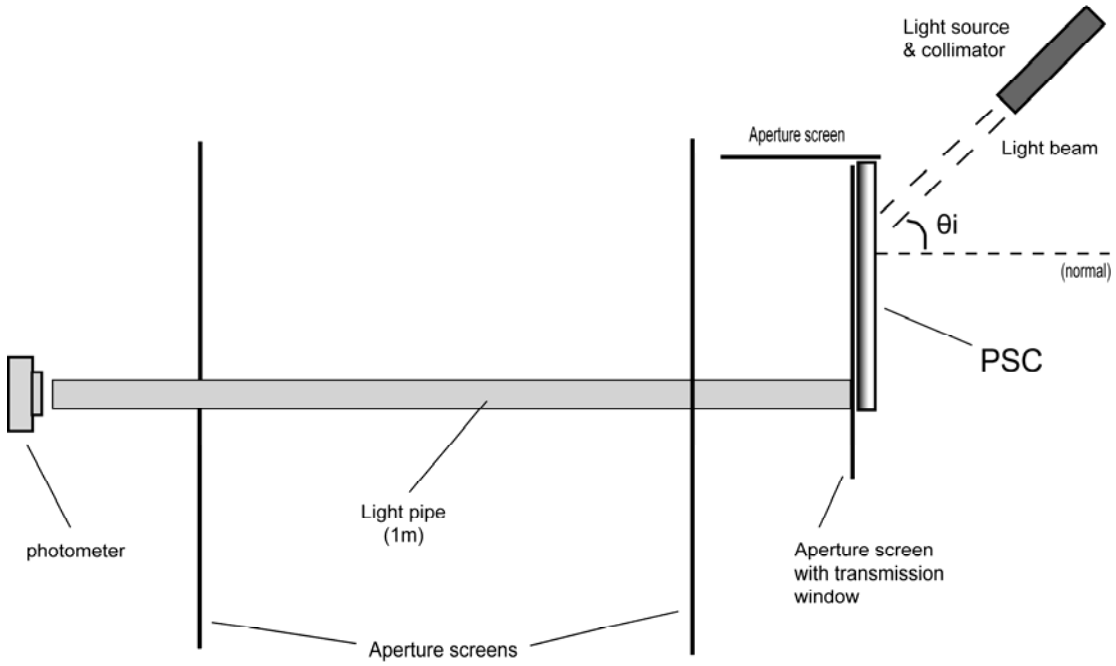

Figure 3.7 – Schematic view of the basic layout of laboratory experiment set-up configuration.

The artificial light source was attached to a partial collimator device in order to restrict the light beam angular divergence. The movement of the light source with collimator was limited to the meridional plane of the solar collector device under test. The movement represented the displacement of the solar altitude angle h_S. Hence, the apparatus provided a simplified way to simulate the performance of the solar collector demonstration prototypes in respect to the variation of the incident angle θ_i of direct light at their meridional plane (i.e., the plane which contains the main optical axis of the system).

3.11.4 Outdoors experimental test set-up

The outdoor experimental tests set-up was assembled in a similar configuration as the laboratory experimental tests set-up. All outdoors experimental tests were conducted at Brunel University campus, Uxbridge, London, United Kingdom. Geographic coordinates: 51° 33' 0" North, 0° 29' 0" West. The site of the experiment is located approximately 6 Km North from Heathrow Airport. Since Heathrow is one of the busiest airports, the emission of air-pollutants from airplanes could potentially have an influence on the absorption and scattering of solar radiation in the local atmosphere, resulting in an influence on the outdoor experimental tests measurements.

According to the BAA Heathrow Local Air Quality Action Plan 2007-2011 (2007, pp.4-5) the main air-pollutants in the local area are: nitrogen oxide (NO_2), nitric oxide

(NO), carbon dioxide (CO_2) and particles PM_{10} and $PM_{2.5}$. As seen in the literature review, the presence of these molecules and pollutant particles in the atmosphere has been associated with a decrease of the global solar radiation that reaches the ground (Jacovides et al, 2000). Of particular concern is the NO_2 absorption band (250nm to 700nm), which includes part of the ultraviolet and most of the visible part of the spectrum (Jacovides et al, 2000, pp.217). However, for the practical application of this research the influence of local air pollutants are considered negligible.

3.12 Summary and conclusions of Chapter 3

The main methods, optical analysis techniques and instrumentation applied in this research have been presented and discussed. The experimental tests limitations and major concerns have been outlined. Prototyping manufacturing techniques and considerations on the laser ablation process were made. The experimental tests set-up and measurement procedures have been presented.

A novel device conceived to analyse the spatial distribution of light emerging from the exit aperture of the solar-daylighting-collectors demonstration prototypes has also been introduced. The device, named angular distribution imaging device (ADID), applied a series of fibre optical cables connected to a dome-shaped component. A digital camera (CMOS) and image analysis software (NI LabVIEW® Vision Assistant 8.0) were also used to analyse the spatial distribution of the beams of light emerging from the exit aperture of the demonstration prototypes.

Chapter 4 - Refractive Integrated Nonimaging Solar Collectors

4.1 Introduction

This chapter introduces the basic conceptual design model of a novel category of nonimaging solar collectors, named Refractive Integrated Nonimaging Solar Collectors (RINSC). Related theory and technical issues regarding the characterisation and general working principle of the RINSC category are presented and discussed. The RINSC category, as presented in this work, is further divided into four distinct sub-categories and related sub-systems. The four sub-categories are: the Prismatic Solar Collectors (PSC), the Multi-Prismatic Solar Collectors (MPSC), the Integrated Multi-Prismatic Solar Collectors (IMPSC) and the Vertically Integrated Nonimaging Solar Collectors (VINSC). For better convenience each of these sub-categories are introduced and analysed in detail in Chapters 5, 6, 7 and 8, respectively.

Figure 4.1 presents a schematic diagram showing the RINSC category and its sub-categories introduced and analysed in this thesis.

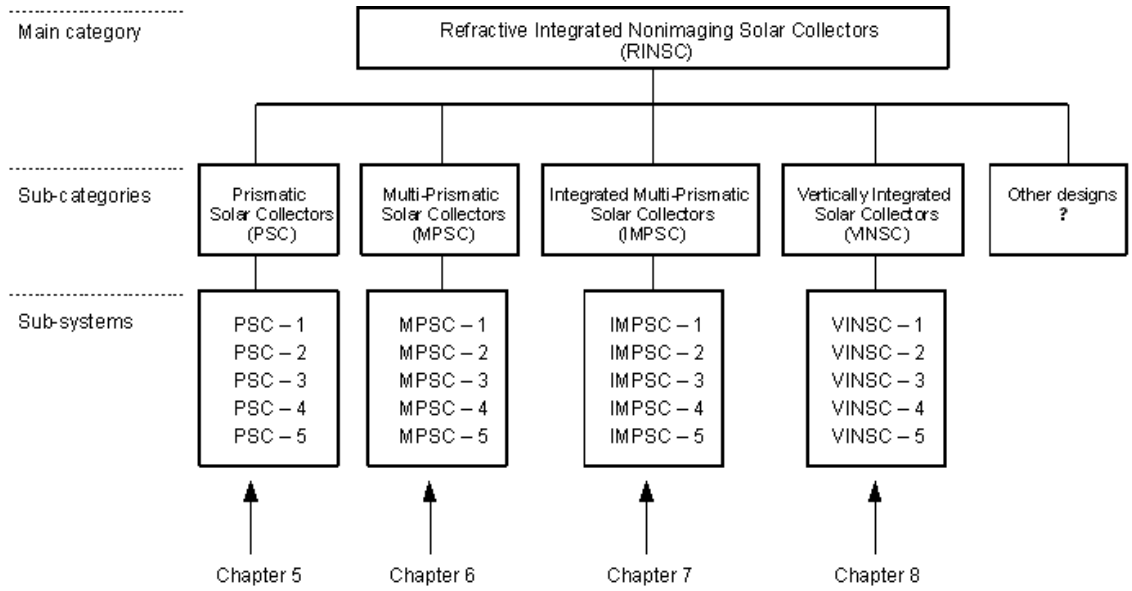

Figure 4.1 - Schematic representation of the RINSC category and related sub-categories and sub-systems introduced and analysed in this research. Related chapters are also indicated.

4.2 The Refractive Integrated Nonimaging Solar Collectors (RINSC) concept

A novel category of static nonimaging solar-daylighting-collectors named Refractive Integrated Nonimaging Solar Collectors (RINSC)[4] is introduced. The RINSC systems (and sub-categories) can be defined as compact solid-dielectric nonimaging optical systems that integrate several optical elements into a single-structure embodiment. They are based on refractive-optics and total internal reflection (TIR) and can be manufactured by mass-manufacturing processes such as injection moulding or casting. Its basic optical configuration provides a compact optical system in which the exit aperture is perpendicular to the entrance aperture.

The basic idea for the RINSC category is inspired by the concept of integrated optics currently used in the integration of optical features (such as light wave guides) directly into electronic devices (Hunsperger, 1995; Shannon, 1997).

The basic design goals for the RINSC category and its sub-systems can be summarised as:

- To provide a compact static solar collector that can be easily integrated into a building external surface, more specifically into a building façade system.
- To provide a concept for a low-cost system that can cover large areas in a building façade with minimum intervention;

Figure 4.2 displays a schematic representation for the conceptual model of the RINSC system. The reason for the question mark in Figure 4.2(b) is to suggest the question: What possible geometric configurations for the RIINSC optical profile section (ROPS) can be designed in order to collect incident light ($\Delta\theta_i$) at the entrance aperture and direct it towards the exit aperture?

In this conceptual model the following terms are defined:

- The RINSC Volumetric Space (RVS) is defined as the total volume occupied by the system;
- The RINSC Optical Profile Section (ROPS) is defined as the geometric optical profile inscribed into the vertical-section area of the volume. The vertical section area is defined in Figure 4.2(b) by the line segments: AB, BC, CD, DA.

[4] Note that in this thesis the RINSC category may also by referred as RINSC concept, RINSC system(s) or solely as RINSC.

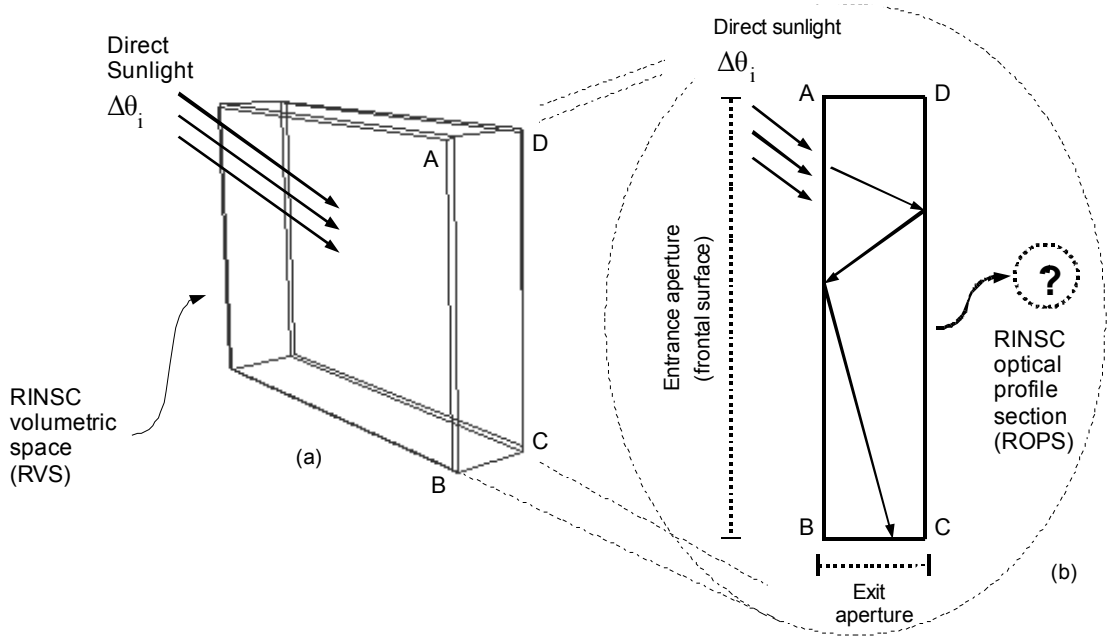

Figure 4.2 – Schematic representation of the RINSC conceptual model. In (a), the RINSC volumetric space (RVS) defines the expected 3D space-volume occupied by the system. In (b), the RINSC optical profile section (ROPS) represents the 2D vertical space-section of the integrated optical system.

As mentioned in the beginning of this chapter, the RINSC category, as presented in this work, is sub-divided into four distinct sub-categories of solar-daylighting-collector systems: Prismatic Solar Collectors (PSC), the Multi-Prismatic Solar Collectors (MPSC), the Integrated Multi-Prismatic Solar Collectors (IMPSC) and the Vertically Integrated Nonimaging Solar Collectors (VINSC).

The basic optical layout construction of the RINSC concept is significantly different from current optical configurations designed for capturing sunlight. Figure 4.3 shows a schematic comparison between the optical lay-out of the conceptual model for the RINSC systems and other solar concentrators described in the literature.

Note in Figure 4.3 that the only system that has a similar lay-out configuration is the luminescent solar concentrator (LSC) system displayed in Figure 4.3(b). However, the optical function of the LSC is based on a photo-luminescent material, while the RINSC system is based on a geometrical optical layout.

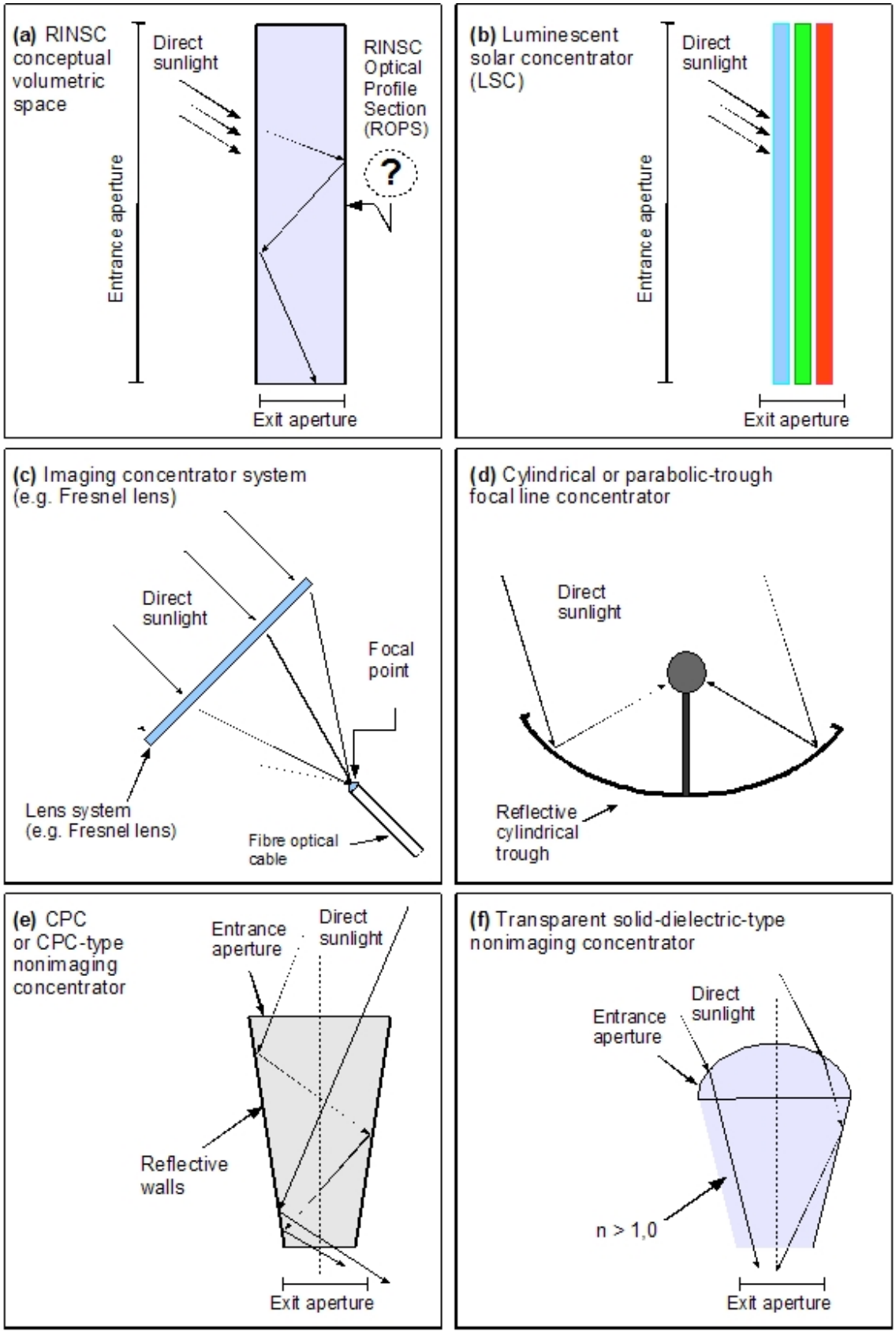

Figure 4.3 – Schematic comparison between the RINSC concept (a) and other solar concentrator systems optical lay-out configurations (b to f). Authors considered as references for the systems illustrated in (b) to (f): Earp et al, 2004; Fraas et al, 1983; Durán and Nicolás, 1987; Welford and Winston, 1978; and Ning et al, 1987.

4.3 General design considerations for the RINSC category

Considering the literature review on solar collectors, solar concentrators and daylighting systems, some preliminary requirements were established for the design and development of the RINSC systems. The main design requirements are presented as follows:

- "Single-integrated-optical-elements" design approach;
- Possible to integrate into building architecture with low interference;
- Able to cover large areas and deliver an acceptable level of illuminance;
- Use commercially available materials already used in the building industry with optical quality;
- Passive (non-tracking) solar collector modular array;
- Based on nonimaging optics;
- Easy to recycle or dispose of, considering the British Standard BS 8887-1:2006;
- Low-costs: low manufacturing costs; low-maintenance costs; low recycling costs.

4.3.1 Building integration considerations

One of the most important aspects of daylighting systems, besides its optical efficiency, is its integration with the building architecture and structure. As seen in Chapter 2, it has been reported that architects tend to give more value to the aesthetic impact of the daylighting systems on the overall building design rather than to its performance and efficiency (Hestnes, 1999; IEA, 2000; Mansy, 2004, pp.374).

Therefore, increasing the aesthetic value of the parts of the system that appears from the inside and the outside of the building is a promising strategy. This approach will contribute to a better cost-benefit relation for the final products. For example, when installed into the façade of a building the system should be regarded as an element with some aesthetic relation with the façade or be less intrusive as possible (Hestnes, 1999; Reijenga, 2003; Wustenhagen et al, 2007).

It is also important to consider in the design process a system feasible to be integrated into already existing building without significant costs and intervention. In other words, it is expected that the system should be adapted into the building and not the other way around. An interesting possibility is to explore design concepts that are

suitable to be integrated as part of a building façade or façade-curtain-walling system (British Standard BS EN 13119:2007).

The following possibility for the location of the RINSC systems on a building envelope are considered: (1) facade location (above window "viewing" area); and (2) flat roof-top location.

Figure 4.4 depicts a CAD model of a building (Tower A, Brunel University) where potential locations for the RINSC systems on the building façade are indicated.

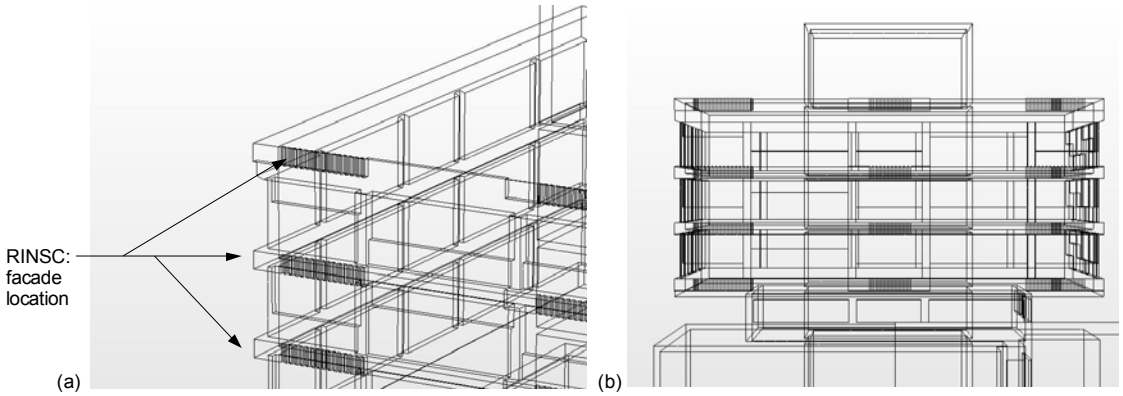

Figure 4.4 – CAD drawings demonstrating façade location of RINSC systems on a building envelope.

4.3.2 One-component-one-material-one-manufacturing-process concept

A recognised effective design strategy to reduce costs is to simplify the design of the product/system and reduce the number of stages in the manufacturing process (Edwards, 1998; O'Driscoll, 2002; Ashby et al, 2007). Limiting the use of materials will also have a contribution in reducing manufacturing cost, supplier management costs and recycling costs (O'Driscoll, 2002; British Standard BS 8887-1:2006). To achieve these goals, it was established for this research the design requirement of *one-component-one-material-one-manufacturing-process* concept, meaning that the RINSC category systems are defined by being made of a single component, made of a single material and using a single manufacturing process.

These requirements also aim to achieve the recommendations of the British Standard BS 8887-1:2006. Product life-cycle recommendations of British Standard BS 8887-1:2006 most relevant to this thesis are presented below:

- *"Use materials which are as ubiquitous and abundant as possible"* (British Standard BS 8887-1:2006, pp.34);
- *"Use recyclable materials and components for which collection for recycling is well established for the product customer group"* (British Standard BS 8887-1:2006, pp.34);

- *"Avoid pigmented plastics (for easier recycling) where possible"* (British Standard BS 8887-1:2006, pp.34);
- *"Avoid mixing as far as possible of component piece part materials which reduce the efficiency of recycling"* (British Standard BS 8887-1:2006, pp.36);
- *"Minimize the number of piece parts"* (British Standard BS 8887-1:2006, pp.36).

Due to its integral design – made out of a single material component - and relative simple geometry, the solar-daylighting-collectors of the RINSC category are expected to be manufactured by mass-manufacturing processes such as injection moulding or casting.

4.3.3 Trade-offs between building integration and optical design

The optical configuration layout (geometric design) of the RINSC categories is the cornerstone of their development process. All other design issues (e.g. building integration, life-cycle, costs, etc) are considered with regard to their main optical parameters.

The central idea is to design flat-compact solar-daylighting-collector systems that can be easily integrated into a buildings façade system or installed on a roof top. Therefore, the design of an optical geometry to serve both as a solar-collecting device and a building element may provide a strategy to achieve a system with high building integration potential. Ultimately, this design strategy could lead to embedding optical technology directly integrated into a building material / construction element, such as building curtain walling systems (British Standard BS EN 13119:2007).

As mentioned earlier in this chapter, the optics of the RINSC category is based on nonimaging optics. Also, in order to reduce costs it is necessary that the RINSC systems are all static solar collector systems, with no moving parts at all. Therefore, two important considerations should be highlighted here:

- Static solar-daylighting-collector systems will inevitably have a relative lower-efficiency than active-solar-tracking systems (heliostats) due to the constant variation of solar incident angles;
- A possible strategy to overcome the problem of relative lower efficiency of static solar-daylighting-collectors is to increase the collector area so that more light can be collected and efficiency losses can be accounted without compromising the overall utility of the system.

4.4 General theory and design principles for RINSC systems

As mentioned earlier, the design of the RINSC category and its sub-categories and sub-systems are based on refractive optics, TIR and nonimaging optics. Two important issues that were considered in the design of the RINSC systems are:

- The condition for total internal reflection TIR to happen;
- The extraction of light trapped by TIR from the solid-dielectric medium.

4.4.1 Basic theory related to the design of prismatic array systems

The RINSC systems introduced and analysed in this thesis apply a series of prismatic arrays as a means to divert incoming direct solar radiation and couple it into solid-dielectric light guides.

As a direct result of Snell's Law of Refraction, a ray of light entering a transparent denser medium (with higher refractive index n) will approach the normal to the incident surface (Freeman, 1990; Hecht, 1998). When leaving the denser medium to a less dense medium it will move away from the normal to the exit surface (Hecht, 1998; Freeman, 1990; Mouroulis and Macdonald, 1997).

In a prismatic array, the first refraction occurs at the entrance surface of the prism (Hecht, 1998, pp.190). The incidence ray is deflected from its original direction by the angular quantity $(\theta_{i1} - \theta_{t1})$, where θ_{i1} is the angle between the incidence ray and the normal of the prism entrance surface and θ_{t1} is the angle between the transmitted ray and the normal of the same surface. Inside the prism the direction of the transmitted ray remains the same, considering that the medium is homogenous (Hecht, 1990, pp 190). The second refraction occurs when the ray intercepts the exit interface surface and is deflected again, this time by the angular quantity $(\theta_{t2} - \theta_{i2})$, where θ_{t2} is the angle between the transmitted ray and the normal to the prism exit surface and θ_{i2} is the angle between the emerging ray and the normal to the same exiting surface (Hecht, 1990, pp 190). Hence, according to Hecht (1998, pp.190), the total angular deviation δ of a light ray as it passes through a prism is given by the equation:

$$\delta = (\theta_{i1} - \theta_{t1}) + (\theta_{t2} - \theta_{i2}) \qquad [4.1]$$

where, as described above, $(\theta_{i1} - \theta_{t1})$ corresponds to the angular displacement resulted from the refraction at the entrance surface, or entrance refraction, and $(\theta_{t2} - \theta_{i2})$ corresponds to the angular displacement resulted from refraction at the exit surface, or exit refraction (Hecht, 1998, pp.189-190).

The most important angle of a prism is the apex angle α. Prisms with small apex angle α will deviate light through small angles, while prisms with large apex angle α will deviate light through large angles. In a prismatic structure the second most important angle is the base angle β.

Hecht (1998) derives an equation that relates the total angular deviation δ to the apex angle α. The equation is presented as follows:

$$\delta = \theta_{i1} + \sin^{-1}\left[(\sin\alpha)\left[n^2 - \sin^2\theta_{i1}\right]^{1/2} - \sin\theta_{i1}\cos\alpha\right] - \alpha \qquad [4.2]$$

where, δ is the total angular deviation, θ_{i1} is the angle between the incidence ray and the normal of the prism entrance surface, α is the prism apex angle, and n is the refractive index of the prism material (Hecht, 1998, pp.190). Note that according to Equation 4.2, the total angular deviation δ increases as the refractive index n increases and/or the apex angle α increase (Hecht, 1998; Freeman, 1990).

Figure 4.5 displays a section-view of a prismatic element profile. Note that, for the practical applications in this research, the ray original incident angle θ_i was measured in relation to the normal of the vertical section of the prism, named as reference normal.

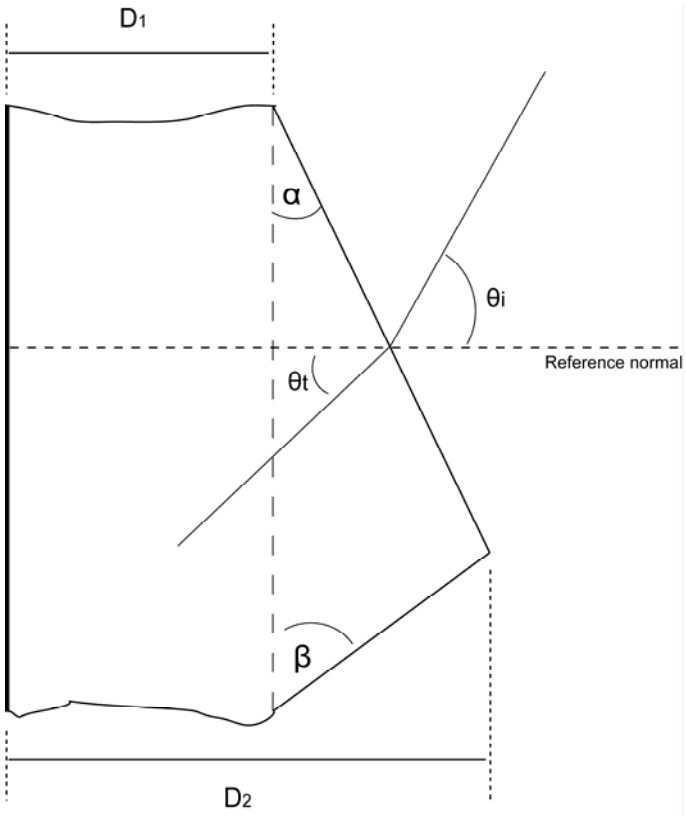

Figure 4.5 - Prismatic structure section-view, showing important angles and dimensions.

4.4.2 Condition for total internal reflection (TIR) and light collection

As seen in the literature review, total internal reflection (TIR) is a loss-free optical phenomenon that allows a ray of light to be totally reflected inside a denser dielectric media (Welford and Winston, 1978; Hecht, 1998).

To achieve total internal reflection (TIR) inside a RINSC system, the angular distribution $\Delta\theta$ of a ray of light travelling inside the device should be larger than the critical angle θ_c of the material at the moment when it intercepts one of the internal walls of the device. If this condition is satisfied the ray will remain trapped internally by TIR (Welford and Winston, 1978; Ning et al, 1987; Ries et al, 1997a; Hecht, 1998).

4.4.3 Light extraction at the exit aperture

Total internal reflection (TIR) at the final exit aperture surface can play against the transmission efficiency T_E of the system. Light that hits this interface at an angle larger than the critical angle θ_c of the material in relation to the surface normal will remain trapped inside the system. Therefore the geometry of this area/surface is essential for the overall transmission efficiency.

As seen in the literature review, the amount of light that can be extracted from a dielectric concentrator or a dielectric light guide, with a refractive index higher that the refractive index of the surrounding medium, "*decreases continuously to zero with the increasing of the refractive index n*" (Ries et al 1997a, pp.2872). The reason for this is that the increase of the refractive index n leads to the decrease of the critical angle θ_c inside the medium. In other words, the "window" for light to escape from the denser medium becomes smaller, meaning that more light is trapped inside by total internal reflection (TIR).

As noted in the literature review, the angular distribution of the output flux $\delta\theta_{out}$ emerging from the exit aperture of a nonimaging solar concentrator can have a significant impact on the transmission (deliver) efficiency of solar radiation. For refractive systems the angular distribution of the output flux $\delta\theta_{out}$ is limited by:

- The refractive index n of the material;
- The critical angle θ_c
- The exit aperture interface geometry; and
- The incident angle θ_i of the ray at the exit aperture interface.

These relations will define the potential of extracting light from the collector and coupling it into a light-transport system, such as a reflective hollow light guide, for example. Hence, the condition to extract light will be defined by the relation:

$$\delta\theta_{out} < \theta_c \quad [4.3]$$

where $\delta\theta_{out}$ is the angular distribution of rays emerging from the collector exit aperture, and θc is the critical angle for total internal reflection of the dielectric material (Ries et al, 1997a; Hecht, 1998; Masui et al, 2008). Denser solid dielectric materials with higher refractive index n have a smaller critical angle θ_c, meaning that it becomes more difficult to extract light from the collector medium (Ries et al, 1997a).

There are three possible fates for a beam of light that hits the interface of the exit aperture at an angle equal or larger than the critical angle θc of the collector material:

- It is reflected backwards by TIR into the collector and absorbed completely by the material after numerous internal reflections;
- It is reflected backwards by TIR and rejected to the outside environment after several internal reflections inside the collector;
- It is reflected backwards by TIR and after several internal reflections inside the collector it returns to the exit aperture at an angle smaller than the critical angle θ_c and is extracted from the collector with lower energy power due to attenuation inside the collector medium.

Note that in all situations mentioned above, most of the light beam will lose energy power along its path inside the collector. Absorption and attenuation by the solid-dielectric material can result in significant losses (Ashby et al, 2007, pp.377-379). Fresnel reflections and scattering losses at the interfaces will also occur (Hunsperger, 1995; Hecht, 1998).

4.4.4 Design constraints and contradictions

Using dielectric materials with higher refractive index n has both positive and negative implications. The positive implication is that it increases the potential to trap and transmit more light by TIR due to the fact that materials with higher refractive index n have a lower critical angle θ_c for TIR. Negative implications include that it will be more difficult to extract light from the dielectric light guide since the value of the critical angle θ_c for TIR will be smaller (Ries et al, 1997a).

The geometry of the RINSC system is expected to be simultaneously “open”, to harvest more light as possible, and also “closed”, to trap and transmit light by TIR. This means that the system needs to have large entrance area and acceptance angle θ_{accept}, while at the same time provide the means for the collected light to stay trapped inside

the system by TIR till it reaches the exit aperture. Note that this is very difficult to achieve this for all possible incidence angles θ_i at the entrance aperture since rays that are not trapped by TIR will escape from the system before it reaches the exit aperture.

4.5 Summary of Chapter 4

The conceptual model and the basic theory related to the design of the RINSC systems have been presented and discussed. The basic schematic design concept for the RINSC category comprises compact solid-dielectric nonimaging optical systems that integrate several optical elements into a single-structure embodiment. The RINSC optical working principle is based on refractive-optics, TIR and nonimaging optics. The concepts of the RINSC Optical Profile Section (ROPS) and the RINSC Volumetric Space (RVS) have been introduced.

Chapter 5 - Prismatic Solar Collectors

5.1 Introduction

This chapter introduces and analyses the Prismatic Solar Collector (PSC) concept. As mentioned in Chapter 4, the PSC is a sub-category of the RINSC category.

The basic idea for the PSC systems is derived from the prismatic panel concept described in the literature review (Chapter 2). However it is important to note that, although the idea of applying prismatic elements as a means to divert and/or redirect incident sunlight has been around for more than a century (Ewen, 1897; Wadsworth, 1903; Cutler et al, 2008), no work was found in the literature that describes their application to harvest and trap light inside prismatic panels by means of TIR.

The PSC concept was designed in order to analyse the potential to harvest and trap light by means of TIR inside a prismatic array system with combined light guide.

The PSC systems described in this chapter has resulted in an accepted journal paper (Pelegrini et al, 2009a).

5.2 The Prismatic Solar Collectors (PSC) concept

As the name suggests, the prismatic solar collector (PSC) has an array of prism-like geometries (prismatic elements) displaced along its entrance/frontal surface, or entrance aperture. The PSC system is the most simple and straightforward geometric configuration analysed in this thesis.

Some fundamental differences between the conventional prismatic panel and the PSC system are:

- The prismatic panel basic function is to divert and redirect incoming sunlight in such way that parts of the rays reaches deeper inside a building, therefore serving as a relative efficient daylighting system.
- The PSC harvest part of incident solar radiation by TIR. Light is then guided by the TIR light guide to the exit aperture, located at the low-end section of the system.

5.2.1 Design studies and initial configuration

A possible geometric configuration for the PSC system is presented in Figure 5.1 and Figure 5.2. This configuration is named here as PSC-A1. The basic concept of the PSC system can be divided into five stages, as briefly described below:

- 1st stage: the prismatic array corresponds to the entrance aperture. Incoming light is bent by the tilted walls of the prisms and coupled into the parallel light guide.
- 2nd stage: the total internal reflection (TIR) combined light guide. Both light guide and prismatic array are part of the same structure. When light hits the back surface of the light guide at an angle larger than the critical angle it is trapped inside by total internal reflection. In one possible alternative design version the back surface of the light guide coated by a high reflective coating or using reflective films. However, this increases the final costs of the system.
- 3rd stage: the compound-parabolic-concentrator type (CPC-type) and inverted CPC-type concentrator section. The intention of this stage of the PSC is to function as nonimaging optics concentrator-collimator device, correcting the angular distribution of the light trapped inside the device by total internal reflection in order that part of it is guided towards the next stage at an optimum angle.
- 4th stage: the 45°-TIR surface. After light passes through the 3rd stage it is reflected on the 45°-TIR surface and directed towards the exit aperture of the system.
- 5th stage: exit aperture. Light that emerges from the exit aperture is directed into a hollow reflective light guide towards its final application.

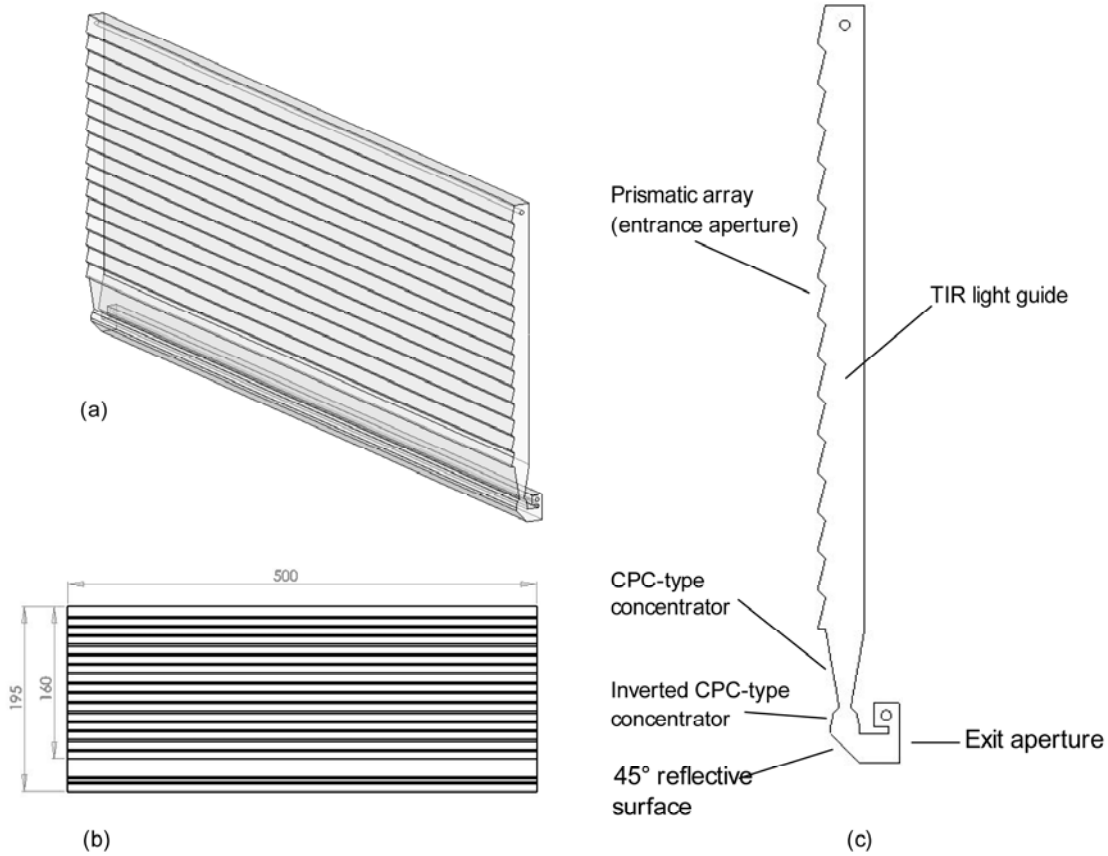

Figure 5.1 - The PSC-A1 system: (a) perspective view; (b) front-view; (c) section-profile view.

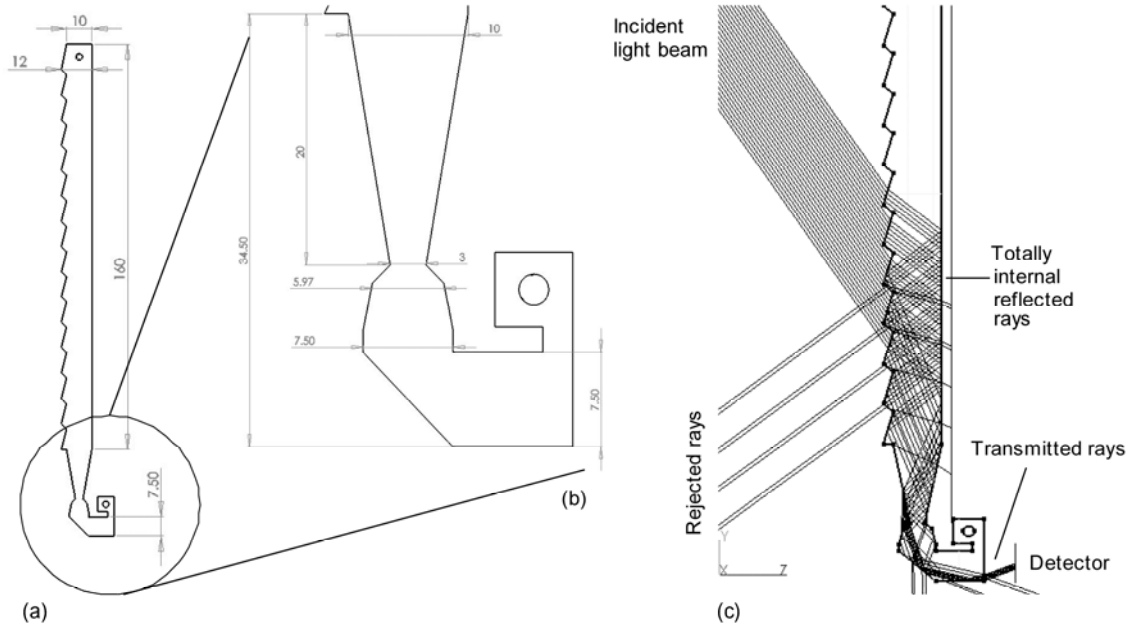

Figure 5.2 - General dimensions of the PSC-A1 system: (a) section-profile view; (b) detail view; (c) ray-tracing simulation.

The diagram in Figure 5.3 is a schematic representation for the expected optical path of light inside the PSC system. The diagram represents the ideal optical path for light collected and transmitted by the system.

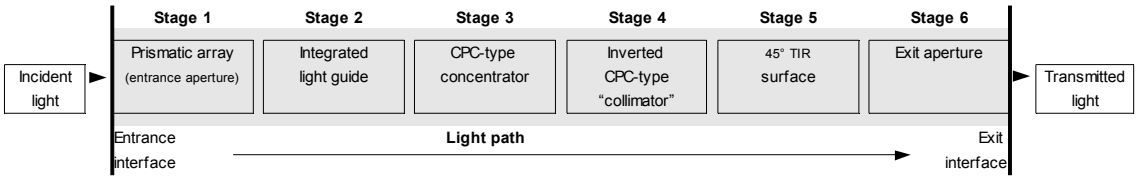

Figure 5.3 – Ideal optical light path diagram for the PSC systems. The gray colour area represents the continuum medium of solid-dielectric material that constitutes the PSC system.

5.2.2 PSC systems working principle

The PSC operates by deflecting the incidence angle θi of incident direct sunlight and trapping part of it inside a combined planar light guide by total internal reflection (TIR). In Figure 5.4, images (a) to (e) demonstrates how light is bent as it passes through the prismatic element at the entrance surface of a PSC device, with an apex angle α = 14°and refractive index n = 1.491. In all pictures incident light is coming from left to right. In each of these pictures the incidence angle θ_i is increasing.

In Figure 5.4(f), the light beam incident angle θ_i reaches θ_i = 58.65° and total internal reflection (TIR) occurs (for n = 1.491; λ = 555nm). Note that due to the prismatic array geometry, part of the light may still be transmitted through the system and/or reflected back to the environment.

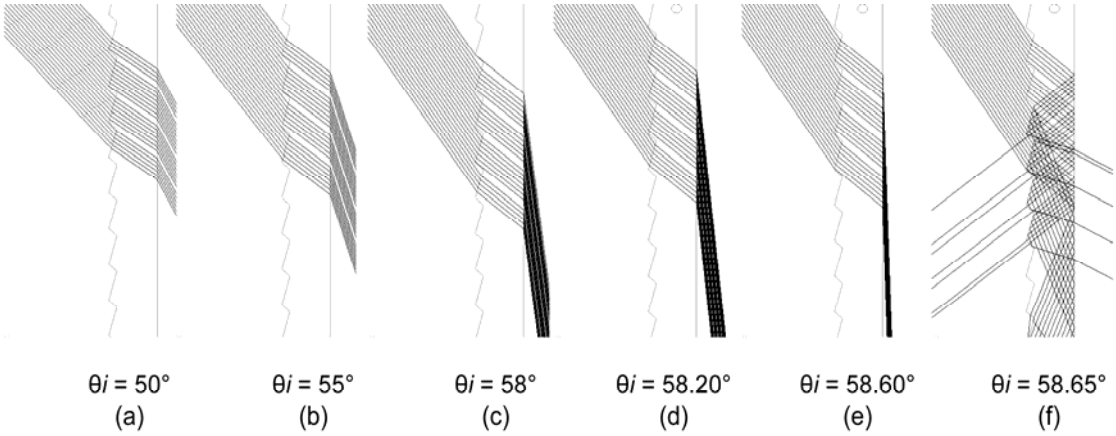

Figure 5.4 - Ray-tracing analysis sequence through the prismatic array section of a PSC system. Parameters: apex angle α = 14° and refractive index n=1.49 (PMMA).

By observing a series of ray-trace analysis executed with OptiCAD® programme it was noted that the amount of rejected light varies according to the value of the base angle β of the prismatic elements. Larger base angle β will lead to more rejected light

for most incidence angles θ_i and vice-versa. The reason for this relates to the angular propagation of light inside the PSC light guide. However, a portion of the light continues to be trapped inside the light guide by TIR and eventually reaches the exit aperture. With ray-trace simulations it was possible to notice that the amount of rejected light due to the geometric construction of the PSC system decreases as the incidence angle θ_i of direct light increased. However, the amount of light rejected due to Fresnel reflection losses at the entrance aperture surface increases with increasing incident angle.

Figure 5.5 illustrates how a PSC system can be integrated into a building façade and how it transmits light to increase natural illumination in deeper areas of a building. The exit aperture of the PSC system is connected to a hollow internally reflective light guide. The fact that the exit aperture of the PSC is very small results in a small output flux area that is coupled into the reflective light guide. This leads to the possibility of a very compact light guide that can be integrated or mounted along the ceiling. This configuration saves space and at the same time allows collected sunlight to be transmitted through hollow reflective light guides to core areas of the building.

Note that the rejected light shown in Figure 5.5 corresponds to rejected light due to the geometric construction of the PSC system under analysis. The simulation parameters were: incident angle $\theta_i = 60°$; apex angle $\alpha = 14°$; refractive index $n = 1.49$; wavelength λ=555nm; number of rays = 1000. Fresnel-reflections and surface scattering were not considered in this simulation.

Figure 5.6 presents a close-view of one of the low-end sections for the PSC-A1 system. The main function of this section is to redirect incoming light to change its propagation axis from the “vertical optical axis orientation” to the “horizontal optical axis orientation”. This is a necessary condition to redirect light indoors, as demonstrated previously in Figure 5.5.

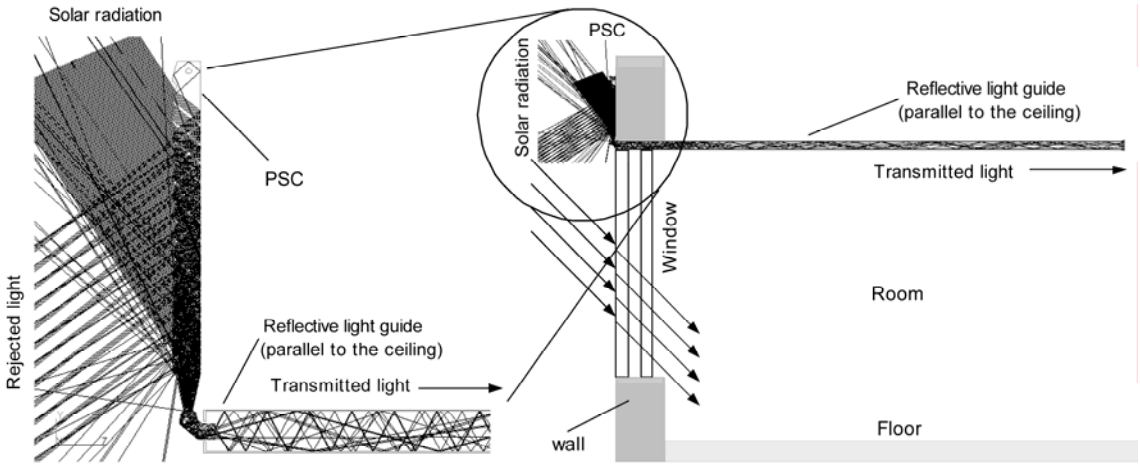

Figure 5.5 - Ray-tracing simulations showing a section-profile view of a PSC system transmitting light into a hollow light guide.

A critical area is the transition part between the light guide and the 45°-TIR reflective corner. It is expected that part of the incoming light flux that is transmitted through the light guide should be redirected indoors by TIR at the 45°-TIR corner.

In general terms, the efficiency of this section (the 45°-TIR reflective corner) is directly dependent on the angular distribution Δθ of light propagating inside the light guide, the refractive index n of the material of the guide, and the geometry of the corner. Using ray-trace simulations it was observed that the angular distribution Δθ of light inside the light guide varies in accordance to the incidence angle θ_i. This makes it very difficult to optimise the geometry of the 45°-TIR reflective corner for a specific acceptance angle θ_{accept} without compromising other possible incident angles θ_i.

Figure 5.7 and Figure 5.8 presents two sequences of ray-trace analysis considering prismatic arrays with different apex angles: α = 14° (Figure 5.7) and α = 28° (Figure 5.8). Both figures illustrate how an incident beam of monochromatic light (λ = 555nm) is deflected by the prismatic arrays and trapped inside the light guide by TIR. In Figure 5.7 the incident beam starts at θ_i = 0° (Figure 5.7a) and gradually increases till TIR occurs at θ_i = 65.08° (Figure 5.7g). The initial incident angle in Figure 5.8 is also θ_i = 0° (Figure 5.8a), however, TIR occurs at θ_i = 50.18° (Figure 5.8g) due to the larger apex angle (α = 28°) of the system. This demonstrates the influence of the apex angle α on the potential of the system to trap light by TIR. Hence, prismatic arrays with large apex angle α will lead to TIR at lower incidence angles θ_i, whereas prismatic arrays with small apex angle α will lead to TIR at higher incidence angles θ_i.

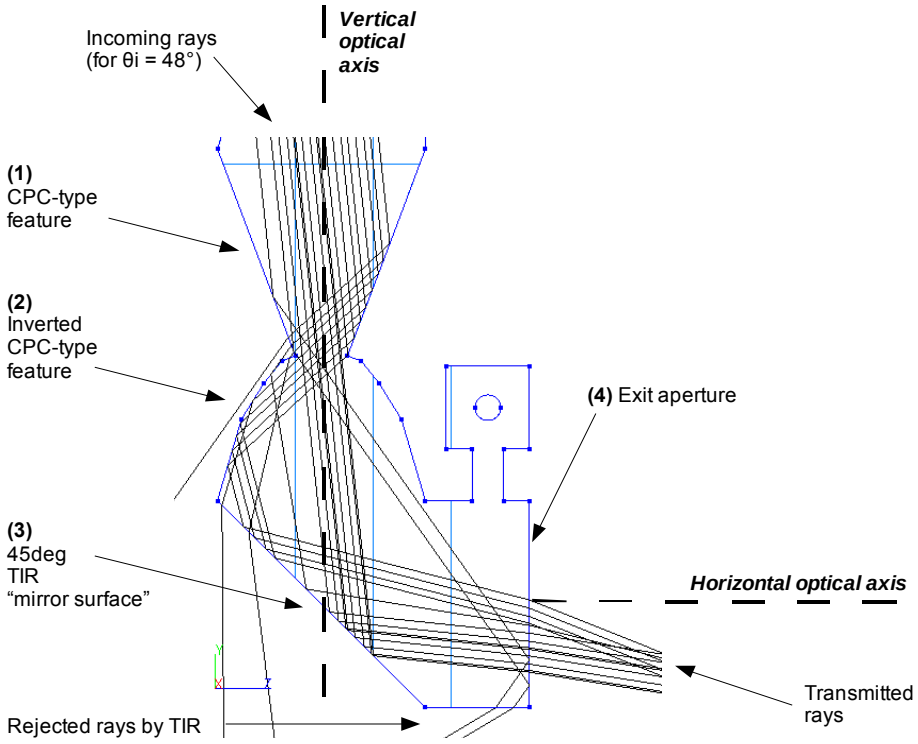

Figure 5.6 – Close-view of the PSC system low-section showing the 45°-TIR reflective corner.

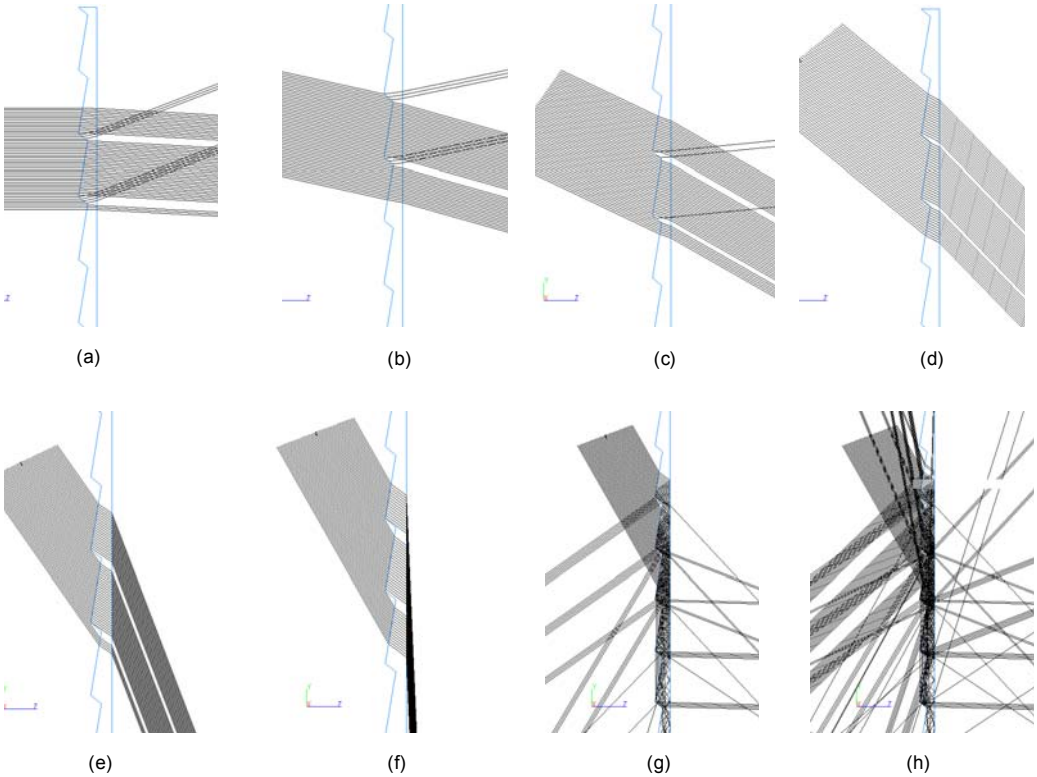

Figure 5.7 – Ray-trace analysis of collimated monochromatic light (λ = 555nm) passing through a prismatic panel (α = 14°). Incident angles (θ_i) are: 0° (a); 15° (b); 30° (c); 45° (d); 60° (e); 65° (f); 65.08° (g); 65.08° (h). Total internal reflection occurs around 65.08° (g and h). Fresnel-reflections are considered only in (h).

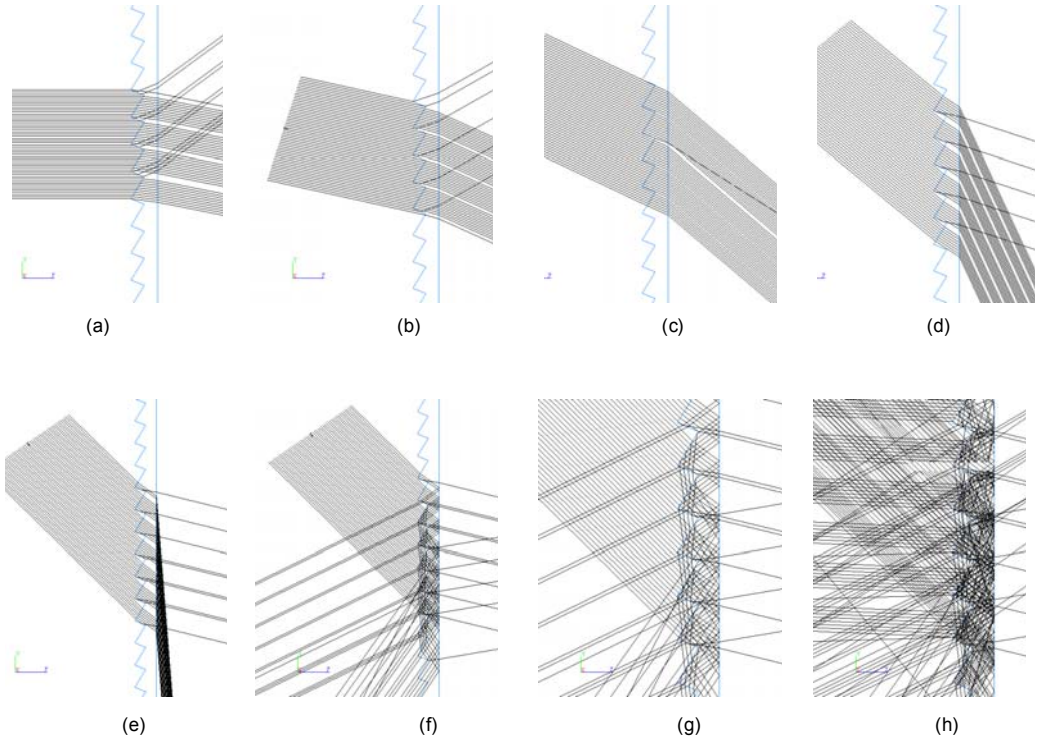

Figure 5.8 – Ray-trace analysis of collimated monochromatic light (λ = 555nm) passing through a prismatic panel (α = 28°). Incident angles (θ_i) are: 0° (a); 15° (b); 30° (c); 45° (d); 60° (e); 50° (f); 50.18° (g); 50.18° (h). Total internal reflection occurs around θ_i = 50.18° (g and h). Fresnel-reflections are considered only in (h).

5.3 PSC systems prototyping and surface analysis

A series of PSC-section demonstration prototypes was manufactured using a laser cutter machine. The prototypes were made out of a commercial grade of clear polymethyl-methacrylate (PMMA) with a refractive index n = 1.491 (for λ = 555 nm). The intention was to use the prototypes to prove the PSC concept.

Table 5.1 presents the general dimensions and values for the apex angle α and base angle β of the PSC laser-cut profile-section prototypes analysed in this thesis. The prototypes are displayed in Figure 5.9.

It is important to stress that each prototype constitutes a section-profile of the PSC geometry, only 5mm thick (width). The thickness is restricted by the laser cutter technical limitation to cut through PMMA sheets. As mentioned earlier in Chapter 3, the quality of the surface finishing provided by the laser cutter process decreases with the increase of the thickness of the PMMA sheet.

For comparative propose, a small rectangular section of PMMA (5mm thick), named “normal glazing” in Table 5.1, was also manufactured to serve as a reference standard to compare with the PSC-1 and the PSC-2 performances. The “normal glazing” has the same general dimensions as the PSC-1 and PSC-2. The basic difference is that it doesn’t have any prismatic features. The intention in using the PMMA “normal glazing” was to measure how much light could be trapped and transmitted internally by TIR through the vertical section of a window.

Table 5.1 - General dimensions and technical issues of manufactured PSC profile-section demonstration prototypes.

System	Material	General dimensions (mm)			Apex angle	Base angle	Entrance aperture (mm)	Exit aperture (mm)
		length	depth	width				
PSC-1	PMMA	200	12	5	28°	56°	160 x 5	7.5 x 5
PSC-2	PMMA	200	12	5	14°	45°	160 x 5	7.5 x 5
“Normal glazing”	PMMA	200	12	5	--	--	160 x 5	7.5 x 5

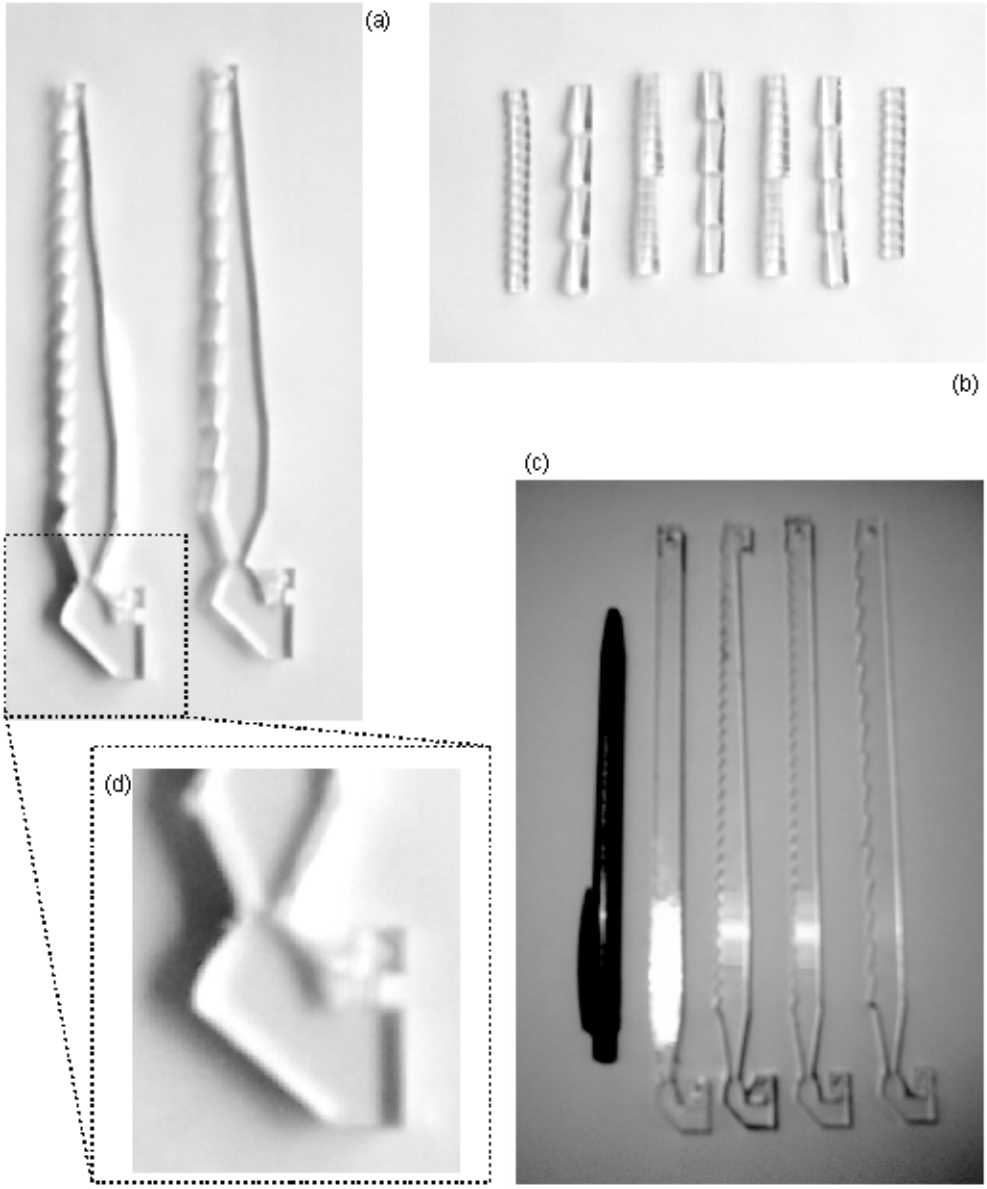

Figure 5.9 - Examples of PSC section-profile demonstration prototypes manufactured by laser-cutter process using clear PMMA (5mm). PSC systems displayed in (a) and (c); preliminary studies of linear prismatic arrays shown in (b); zoom view in (d).

5.3.1 PSC laser-cut prototypes surface analysis

A series of qualitative surface analysis with a CCD imaging camera and National Instruments LabVIEW® Vision Assistant 8.0 software was conducted in order to evaluate the surface quality provided by the laser ablation process. Partial results of this analysis are presented in Figure 5.10. Note that Figure 5.10a and Figure 5.10b images corresponds to an area of approximately 16mm^2 on the surface of the PSC prototypes. Figure 5.10c presents a 3D topographic visualisation of the image displayed in Figure 5.10b.

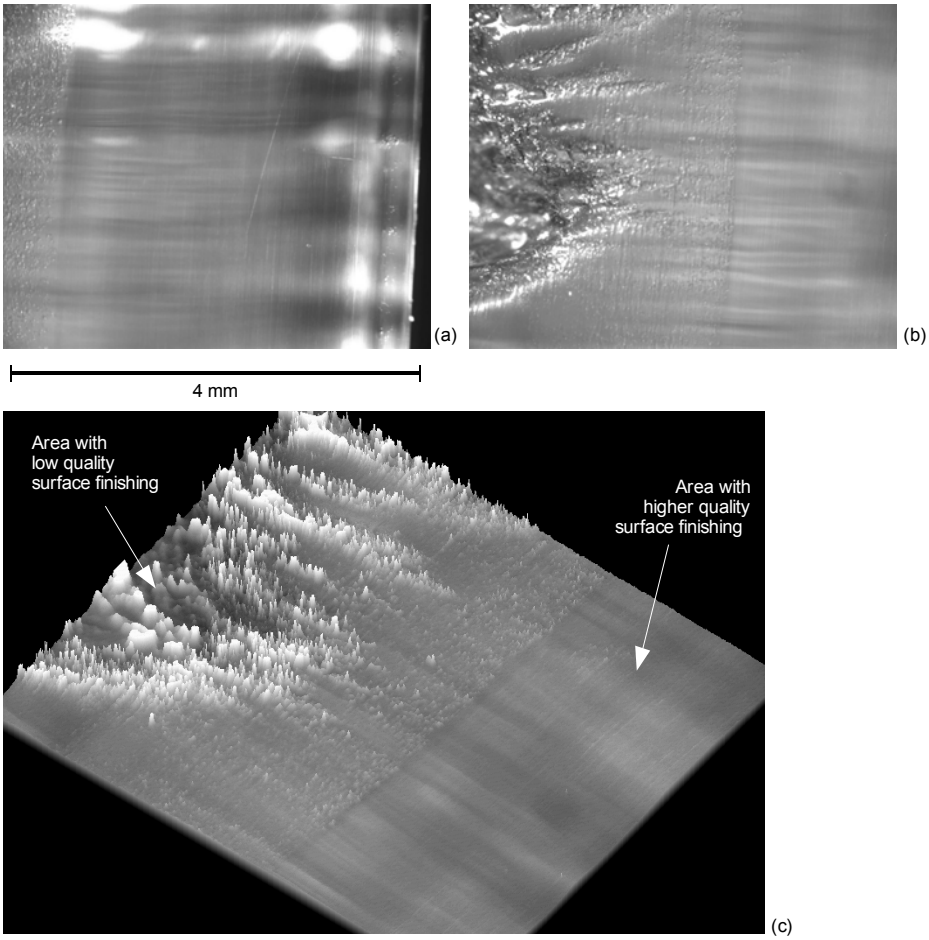

Figure 5.10 – Qualitative assessment of the surface quality provided by the laser ablation process in the manufacturing of the PSC prototypes. In (a) relative good surface quality; (b) defects due to the laser-cutter manufacturing process; (c) 3D topography analysis.

5.3.2 Vapour-deposition coating attempt

An attempt to coat the back surface and the low-section of the PSC laser-cut demonstration prototype (made of PMMA, 5mm thick) with reflective aluminium was conducted in order to reduce light losses and increase transmission efficiency. The vapour coating deposition system Cressington Coating System 308R was used. Due to the high temperature inside the vacuum chamber, it was necessary to apply the coating in the shortest time as possible. The coating materials used were: aluminium (Al) and silver (Ag). As seen in the literature review, both materials present high reflectivity efficiency (around 90%) in the visible range of the spectrum (Serra, 1998, pp.121). The disadvantage of applying a reflective coating directly to the external surface of the PSC system is that TIR would not happen anymore. The reflection at the coated surface will correspond to the reflectivity of the coating material and the quality (smoothness) of the coating surface.

Figure 5.11 presents a qualitative surface analysis of the results for 300nm of aluminium and 600nm of aluminium. In general, the results were not successful. The coating started to fall off the prototypes surface only a few hours after the coating application. The problem was that the coating didn't stick to the external surface of the prototype. This possibly happened due to impurities contained in the aluminium or, most probably, as a result of the limited time that the PSC prototype stayed inside the vapour-deposition chamber due to the high internal temperature (>60°C). None of the attempts was successful and the idea of coating was abandoned.

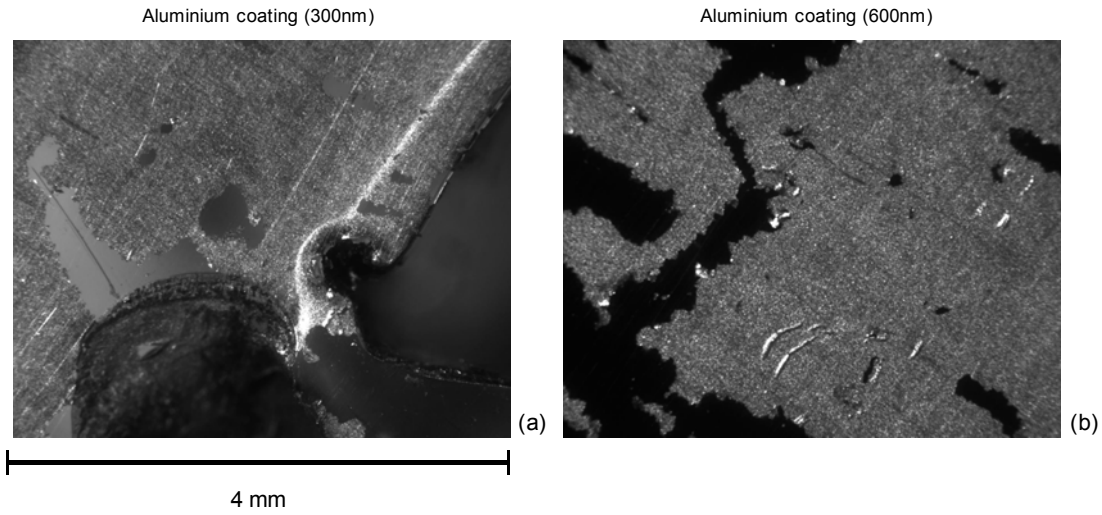

Figure 5.11 – Failed vapour deposition coating attempts.

5.4 PSC systems experimental tests

The selected PSC-section demonstration prototypes were tested during a series of laboratory tests and outdoor tests. The measurement procedures and results of the experimental tests for the developed PSC systems are presented as follows.

5.4.1 Laboratory tests of PSC systems

A series of experimental tests based on photometry measurement procedures, as described in Chapter 3, was conducted in order to evaluate the performance of the PSC demonstration prototypes. The first part of the photometric analysis experiment consisted of measuring the illuminance output E_{out}, measured in lux (lx), as a function of the incident angle θ_i of direct light at the meridional plane of the PSC prototypes. Experiments were conducted inside an optics laboratory. This allowed the repetition and comparison of measurements. The PSC demonstration prototypes, measuring devices and experimental apparatus were aligned along an optical bench. The basic

experiment set-up configuration has been explained in more detail in Chapter 3. Two PSC section profile designs with different apex angles α were tested: the PSC-1, with an apex angle α =28°; and the PSC-2, with an apex angle α = 14°.

Figure 5.12 presents the results of the transmitted illuminance by total internal reflection T_{TIR} (i.e. the illuminance output E_{out}) variation in relation to the incidence angle θ_i of direct light. Figure 5.12(a) plots the results for PSC-1, with apex angle α = 28°. Figure 5.12(b) plots the results for PSC-2, with apex angle α = 14°. Figure 5.12(c) shows the results for the "normal glazing" section, also manufactured by laser-cut process and made of PMMA, with no prismatic element. The intention was to use the "normal glazing" section as a reference standard to compare with PSC-1 and PSC-2. Figure 5.12(d) compares the three previous results. It is important to stress that the measured transmitted illuminance output E_{out} detected by the photometer actually corresponds to the overall transmission efficiency of the system PSC + 1m light pipe, rather than a direct measurement of the PSC output alone, due to the fact that the PSC exit aperture is directly connected to the aluminium hollow light pipe.

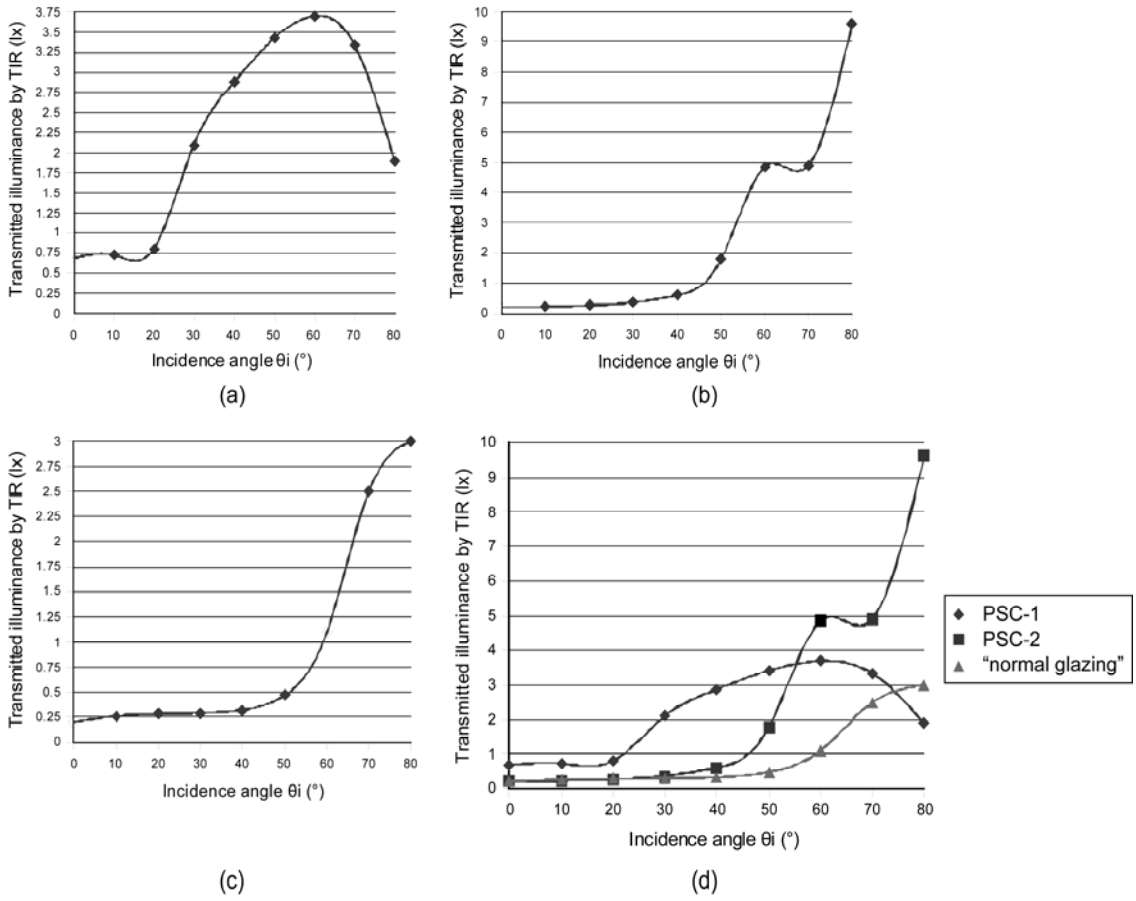

Figure 5.12 - Partial results of PSC laboratory tests. In (a) results of PSC-1 device, with an apex angle α = 14°; (b) results for PSC-2 device, with an apex angle α = 28°; (c) results for "normal glazing" section, with no prismatic array; (d) comparison of previous results. Values are measured considering the PSC + 1m hollow light pipe system.

5.5 Results and discussion on the PSC systems

Considering the basic PSC concept and working principle described in the beginning of this chapter, it was expected that:

- PSC-1 device, with an apex angle α = 28° would deliver better results for lower and medium incident angles θ_i of direct light (20°≤ θ_i ≥-45°);
- PSC-2 device, with a smaller apex angle α = 14°, was designed to operate better for higher incident angles (θ_i > 45°) of direct light at the meridional plane.

It was noticed that the measured results confirmed what was expected and also the basic theory described in Chapter 4. The best results were achieved with the PSC-2 device, with an apex angle α = 14° and base angle β = 45° (Figure 5.12-d). Peak illuminance output E_{out} ≈ 9.6lx was measured at the end of the 1m long hollow light pipe. Note that this corresponds to an illuminance output E_{out} approximately three times higher than the illuminance output E_{out} measured for the "normal glazing" device used as a comparative reference device (Figure 5.12d).

The overall transmission efficiency T_E is a direct result of the angular distribution Δθ of the light input flux, the refractive index n, the surface quality and the geometry of the PSC demonstration prototypes. As noticed, a critical area inside the PSC system is the transition part between the light guide and the 45°-TIR corner located at the low-end section of the system (see Figure 5.6). In these stages, the incoming light flux that is transmitted through the light guide must be directed indoors.

It is important to stress that that the PSC demonstrated and tested in this chapter corresponds to section-profiles of the PSC system. Each demonstration prototype entrance aperture has an area of only 160x5mm (A_1 = 800mm^2) and an exit aperture are of only 7.5x5mm (A_2 = 37.5 mm^2).

The prismatic solar collectors (PSC) concept demonstrates that it is possible to use a single solid-dielectric prismatic array panel with combined light guide to harvest and trap incident light by means of total internal reflection (TIR). The PSC systems geometries provides a high geometric concentration ratio C_R = 25X. However, the transmission efficiencies T_E of the PSC demonstration prototypes were very low: from T_E ≈ 0.12% (measured at a distance of 1000mm) to T_E ≈ 0.5% (measured at a distance of 50mm).

5.6 Summary and conclusions of Chapter 5

Basic theory, designs, ray-trace analysis and experimental tests of compact prismatic solar collectors (PSC) have been presented. Results indicate that such devices could provide an alternative low-cost solution to increase daylighting in deeper areas of buildings.

Due to its integral design (made out of a single material) and relative simple geometry, it is believed that the PSC system can be fabricated by mass-manufacturing processes, such as injection moulding or extrusion. This indicates that it could potentially be applied in large scale, to cover large extensions of a building façade.

The simplicity of the PSC design configuration also opens the possibility for it to be a built-in component in modular façades and glazing systems, usually manufactured by an off-site production process.

The PSC demonstration prototypes low performances are a consequence of a combination of the following limitation factors: (A) the low surface quality generated by the laser ablation prototyping process; (B) the limited acceptance angle θ_{accept} of the system; (C) the geometry of the low-end section of the device, which has a very small exit aperture area (only 5mm by 7.5mm); and (D) the configuration of the prismatic array which, due to its geometric constraints, allows that part of the light trapped by TIR escapes from the system.

Hence, it found was necessary to develop and analyse other optical geometric configurations that could potentially lead to better results. However, it is important to notice that, despite the poor results, the core idea of the PSC concept, that is, the idea of using prismatic arrays to deflect the incidence angle θ_i of direct light and trap part of it by TIR inside a combined light guide, was still evaluated positively because it provided a simple and low-cost solution to harvest incident light. The challenge was then to increase the potential of the system by increasing its acceptance angle θ_{accept} and transmission efficiency T_E. These issues are addressed in the next chapters.

Note that the PSC systems described in this chapter has resulted in an accepted journal paper (Pelegrini et al, 2009a).

Chapter 6 - Multi-Prismatic Solar Collectors

6.1 Introduction

This chapter introduces and analyses the multi-prismatic solar collectors (MPSC) concept. As explained in Chapter 4, the MPSC can be regarded as a sub-category of the RINSC category.

The basic idea of the MPSC derives from the prismatic solar collector (PSC) category introduced in Chapter 5. However, instead of having a single prismatic-array-light-guide structure, as does the PSC system, the MPSC consists of a series of parallel prismatic arrays. The MPSC basic optical layout provides a solution to increasing the acceptance angle θ_{accept} and the transmission efficiency T_E.

6.2 The Multi-Prismatic Solar Collector (MPSC) concept

The MPSC is also a refractive-type nonimaging solar collector made of transparent dielectric material, such as commercial glass, clear polycarbonate (PC) or clear acrylic (PMMA). A series of successive parallel prismatic arrays are used to divert and collect solar radiation. The prismatic arrays are positioned along parallel planes in such way that the angular displacement of incoming light is deflected as it passes through one prismatic array structure to another.

The condition for total internal reflection (TIR) to happen inside a MPSC system is the same as the condition described previously for the PSC and RINSC systems (Chapters 4 and 5). Since both systems are sub-categories of the RINSC category, the pre-condition for TIR is defined by the critical angle θ_c of the material. As seen earlier, in the literature review, the critical angle θ_c is wavelength λ dependent. Hence, the potential to trap light by TIR inside the parallel prismatic panels will also vary according to the wavelength λ and the refractive index n of the solid-dielectric material. Figure 6.1 shows a sequence of computer ray-tracing simulations for MPSC–X1 system. Simplified ray-tracing simulations, not including Fresnel-reflections and scattering, are presented in order to provide a clearer understanding of the optical light path and its interactions through the system. Incident angles θi, varying from 10° to 50° are

presented in each image. All images represent a vertical section-view of the MPSC system. The exit aperture is located at the bottom-end of the MPSC system, in a perpendicular plane to the entrance aperture. A back reflective mirror surface (90% reflectivity) is included in simulations (e), (f) and (g).

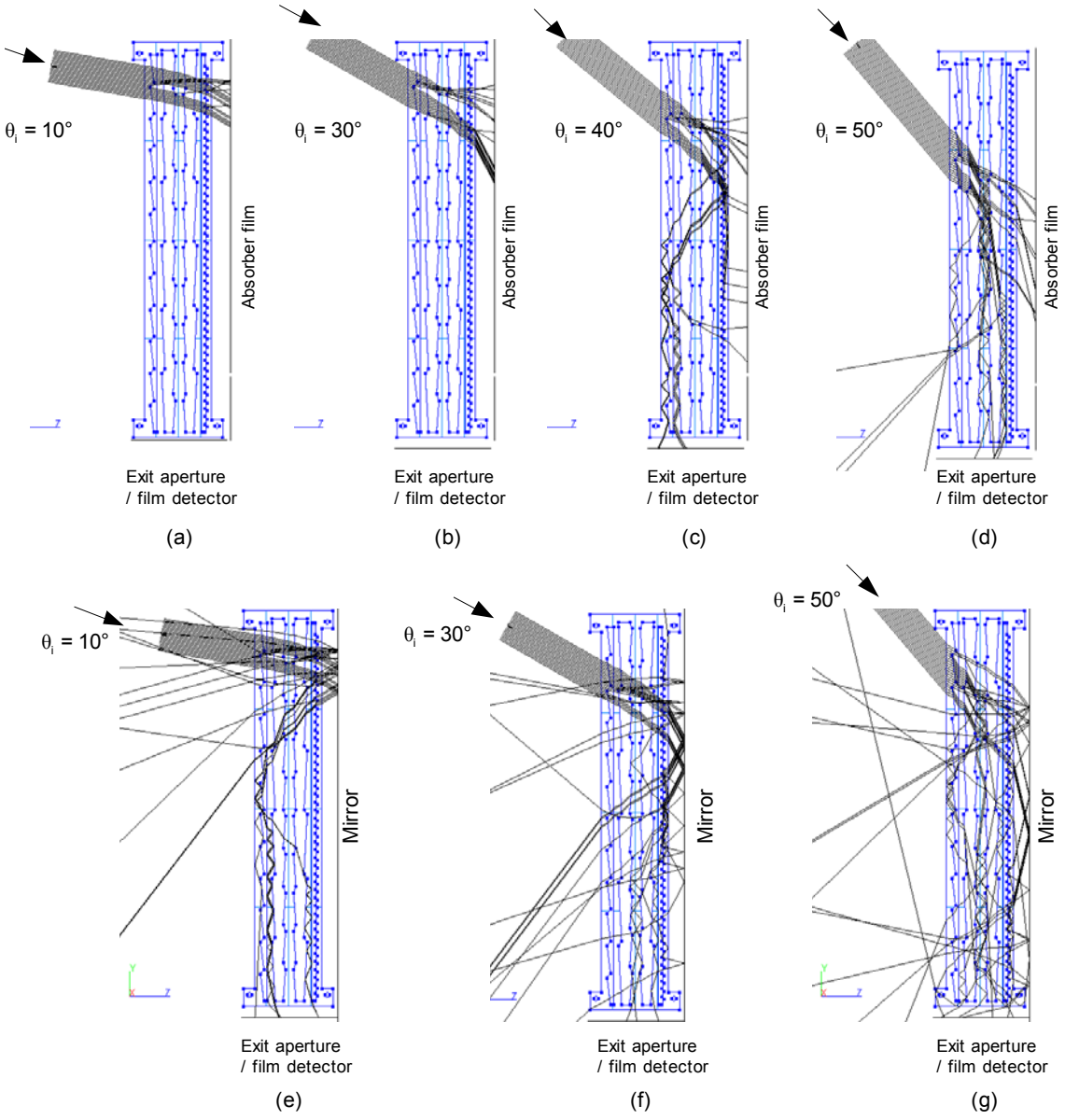

Figure 6.1 – Computer ray-tracing simulation sequence for different incident angles of direct light at the top-section of a MPSC system with five parallel prismatic-array-panels.

6.2.1 MPSC systems main geometric and optical features

The MPSC systems are more complex than the PSC systems (Chapter 5) due to the addition of optical surfaces and elements. Among the most important parameters of the MPSC systems, it is worth noticing:

- The apex angle α of the prismatic arrays, which can be specified in order for the system to be adapted for a particular incidence angle.
- The distance d between the parallel prismatic arrays panels;
- The order or sequence of the prismatic arrays apex angle α; and
- The orientation of the prismatic arrays: facing inwards or outwards.

The value of the apex angles α can be customised for a specific geographic location or building façade orientation. This can lead to commercial advantages by adapting the system for a specific or limited range of solar incidence angles. By doing so it is possible to optimise the system in order for it to yield higher transmission efficiencies T_E.

The distance d between the parallel prismatic arrays can also be considered as an interdependent parameter which plays an important role on the geometric concentration ratio C_R of the system. Prismatic array panels positioned at closer distance between each other will result in a more compact system with higher concentration ratio, whereas prismatic arrays panels positioned at larger distance will result in a less compact system with lower concentration ratio.

The order of the parallel prismatic arrays apex angle α is of fundamental importance for the acceptance angle θ_{accept} and the transmission efficiency T_E of the system. Computer ray-tracing analysis conducted with OptiCAD® indicated that the MPSC systems in which the value of the apex angle α increases from the outermost prismatic array panel (entrance aperture surface) to the innermost prismatic array panel can lead to system with wider acceptance angle θ_{accept}. This is due to the fact that the total angular deviation δ of a ray of light by the prismatic array tends to increase with the increase of the prisms apex angle α, as described previously in Chapter 4.

The inwards orientation of the prismatic arrays of the MPSC systems presents significant advantages over the outward orientation of the PSC systems prisms described in the previous chapter. Firstly, it increases the potential to “recycle” part of the light that otherwise would escape from the system. Second, it avoids the accumulation of dust and pollution particles over the prismatic arrays by confining them into a self-enclosed structure. This also can lead to the possibility of using “robotic-

manipulation"[5], which applies vacuum grippers to lift and install the MPSC panels on a building façade.

6.2.2 MPSC systems basic theory and working principle

Light travelling through a series of parallel transparent dielectric panels (such as a glass window, for example) will continue indefinitely or until it is completely absorbed by the panels (Freeman, 1990, pp.38-40). From Snell's Law of Refraction it's possible to verify that a ray normal to the surface of a glass plate crosses through the glass with no angular deviation (Freeman, 1990; Hecht, 1998). If a second glass plate is positioned behind the first one, the ray will continue to be transmitted through both glasses with no angular deviation at all. Losses will account as absorption and volume scattering through the denser medium and surface scattering at the entrance and exit interfaces (Freeman, 1990, pp.38-40; Hecht, 1998).

As explained in the literature review, Fresnel-reflection-losses are material dependent and incident angle θ_i dependent. Solid-dielectric materials with higher refractive index n will lead to more Fresnel-reflection-losses. The same is also observed with the increase of the incident angle θ_i of direct light (Hecht, 1998, pp. 111).

The idea of applying successive parallel prismatic panels as a means to change the light ray path leads to a complex optical system with many refractive interfaces. Figure 6.2 shows a sequence of computer ray-tracing simulations demonstrating the use of parallel prismatic panels to divert the direction of incoming beam of light. Fresnel-reflections are considered in Figures 6.2(a'), 6.2(b') and 6.2(c'). To simplify this simulation, only two parallel rays (λ = 555nm) are directed towards the sequence of prismatic panels. The prismatic panels refractive index was n = 1.50, the same as soda-lime glass. As seen in Figure 6.2, small changes in the distance between the panels can result in significant changes in the final direction of the incident rays.

[5] See, for example: O'Driscoll (2002) and Edwards (2002).

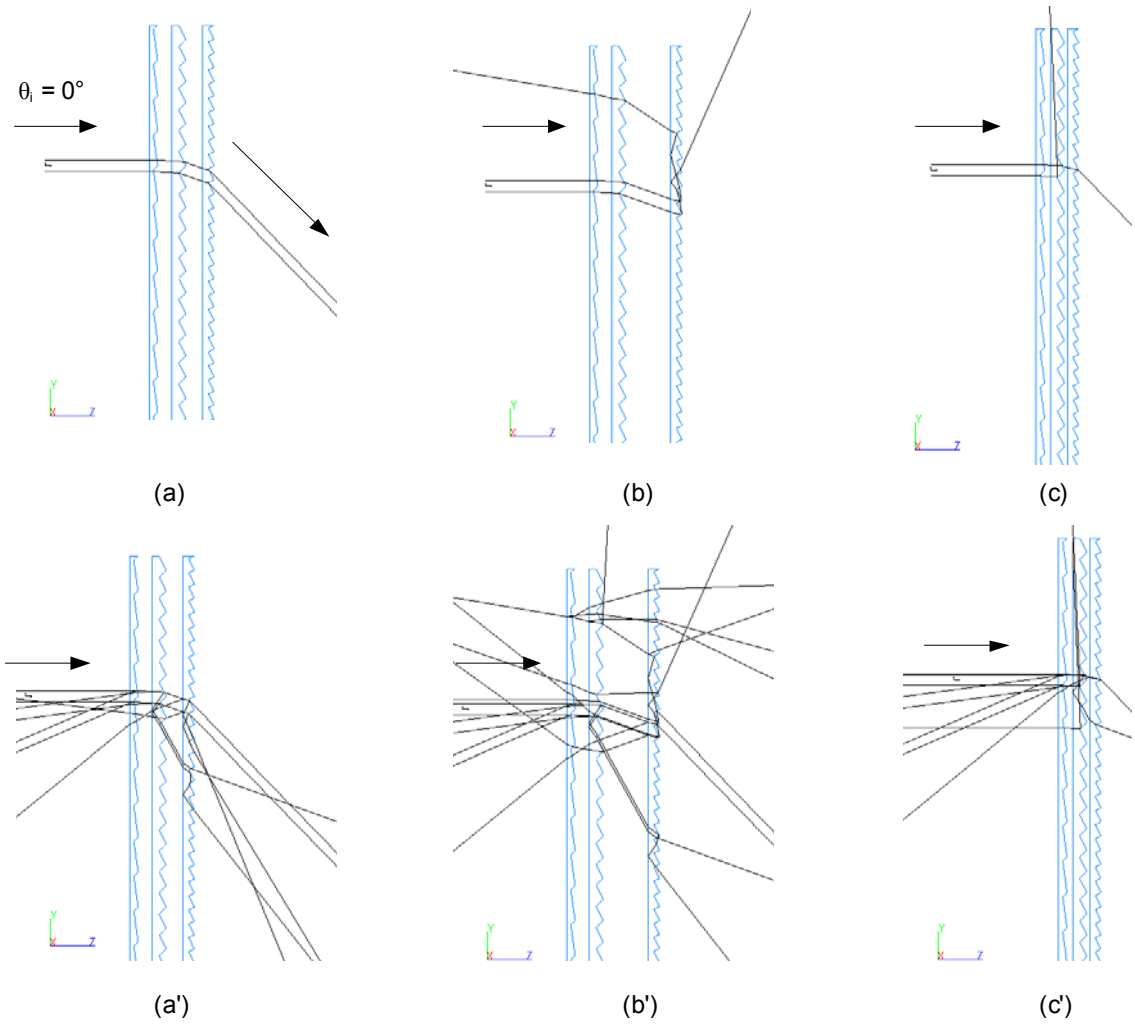

Figure 6.2 – Computer ray-tracing analysis using OptiCAD® programme demonstrating the effect of applying a set of parallel prismatic panels along the path of a ray of light.

6.3 Prototyping and surface analysis of MPSC systems

A series of MPSC laser-cutter prototypes are presented in Figure 6.3. It is important to note that the prototypes represent only a vertical section profile of the MPSC systems. Each section, made of clear PMMA, is only 5mm thick. However, they contain the meridional plane of the MPSC systems geometrical optics configuration.

A series of MPSC systems conceived to be manufactured by extrusion process are demonstrated in Figure 6.3(b). The geometric configuration of these prototype sections are structurally different than the MPSC systems presented in Figure 6.3(a).

Using a CCD camera (EO USB 2.0 colour) with a zoom-lens it was possible to observed the formation of air-bubbles and other sub-surface intrusions in the bulk of the PMMA material as a result of the application of the laser ablation process. This possibly happens due to compression and migration of material due to the pressures

generated by the thermal expansion caused by the laser heat. This has a series of negative consequence for light travelling through the material, resulting in significant losses due to scattering when a ray hits a microscopic air-bubble inside the material.

Figure 6.4 shows areas of the prototypes surfaces with extremely high concentration of air-bubbles. National Instruments LabVIEW® Vision Assistant 8.0 software provided a way for use to access the defects on a sub-surface level. The software "shape-recognition" tool was applied to measure and count the number of closed circular and elliptical shapes on a series of selected images. The software recognised 872 defects in the original image: Figure 6.4(a). These defects are highlighted in Figure 6.4(d), which presents a 3D view of the surface topography. These shapes are mainly air-bubbles trapped inside the material as a negative result of the laser ablation process used to manufacture the demonstration prototypes. This represents a defect concentration significantly higher than the limit recommended by the standard BS ISO 10110-3:1996. However, it is important to stress that not all the sections of the prototypes surface were in such bad condition. The image size in Figure 6.4(a) and Figure 6.4(c) corresponds to an area of approximately 14 mm^2. Figure 6.4(b) shows the optical profile of the surface in terms of pixel intensity (from 0 to 255).

Table 6.1 displays part of the results of surface and sub-surface shape-recognition analysis extracted from the NI LabVIEW® Vision Assistant 8.0 software.

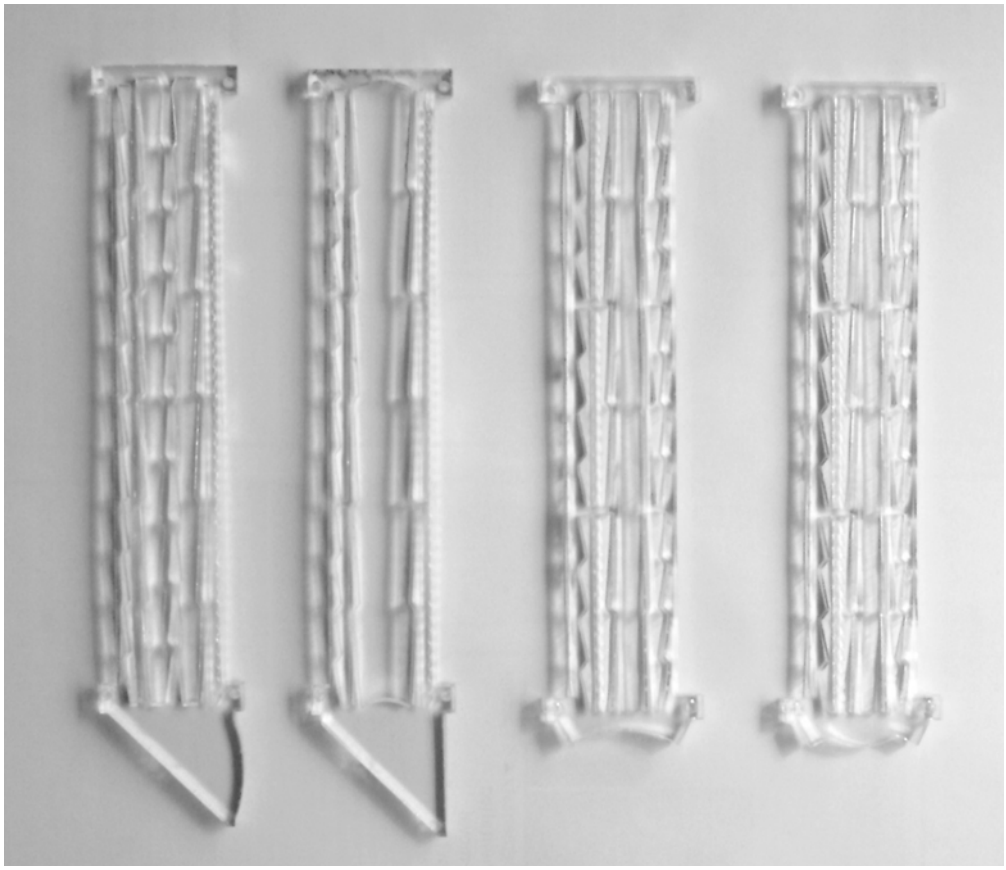

(a)

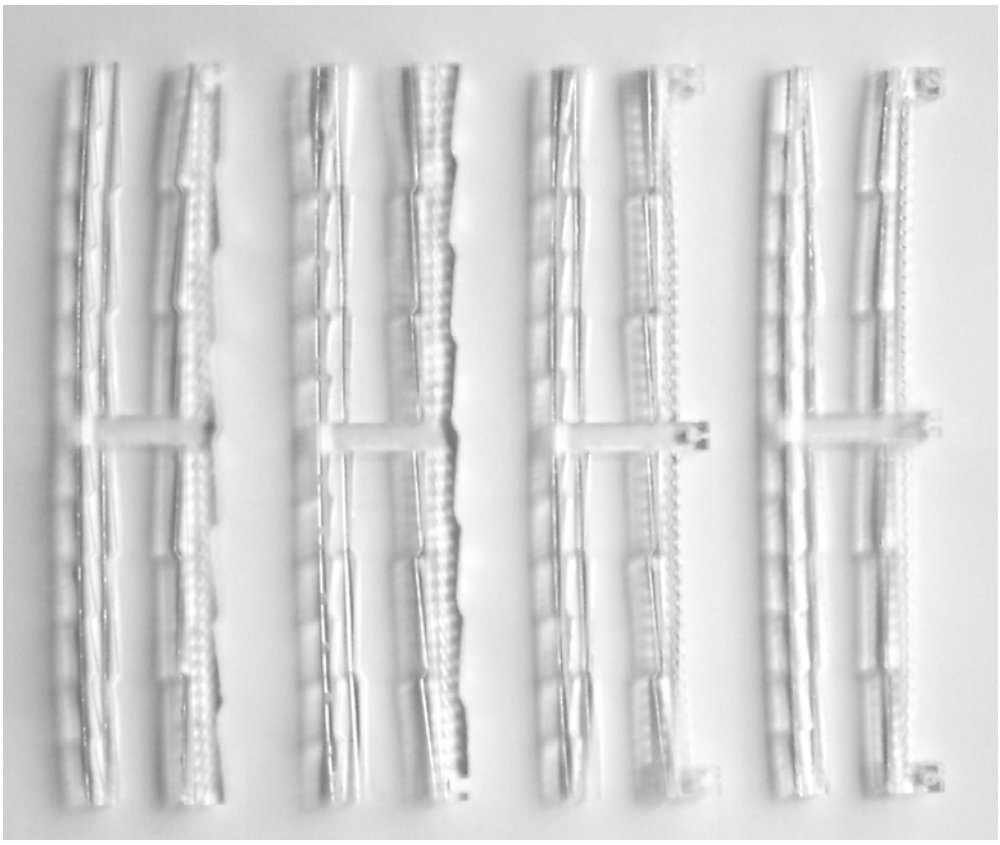

(b)

Figure 6.3 - MPSC laser-cut PMMA prototype-sections. Above (a), four MPSC prototypes with "closed geometry" conceived to be manufactured by injection moulding process. Below (b), four MPSC demonstration prototypes conceived for extrusion manufacturing process.

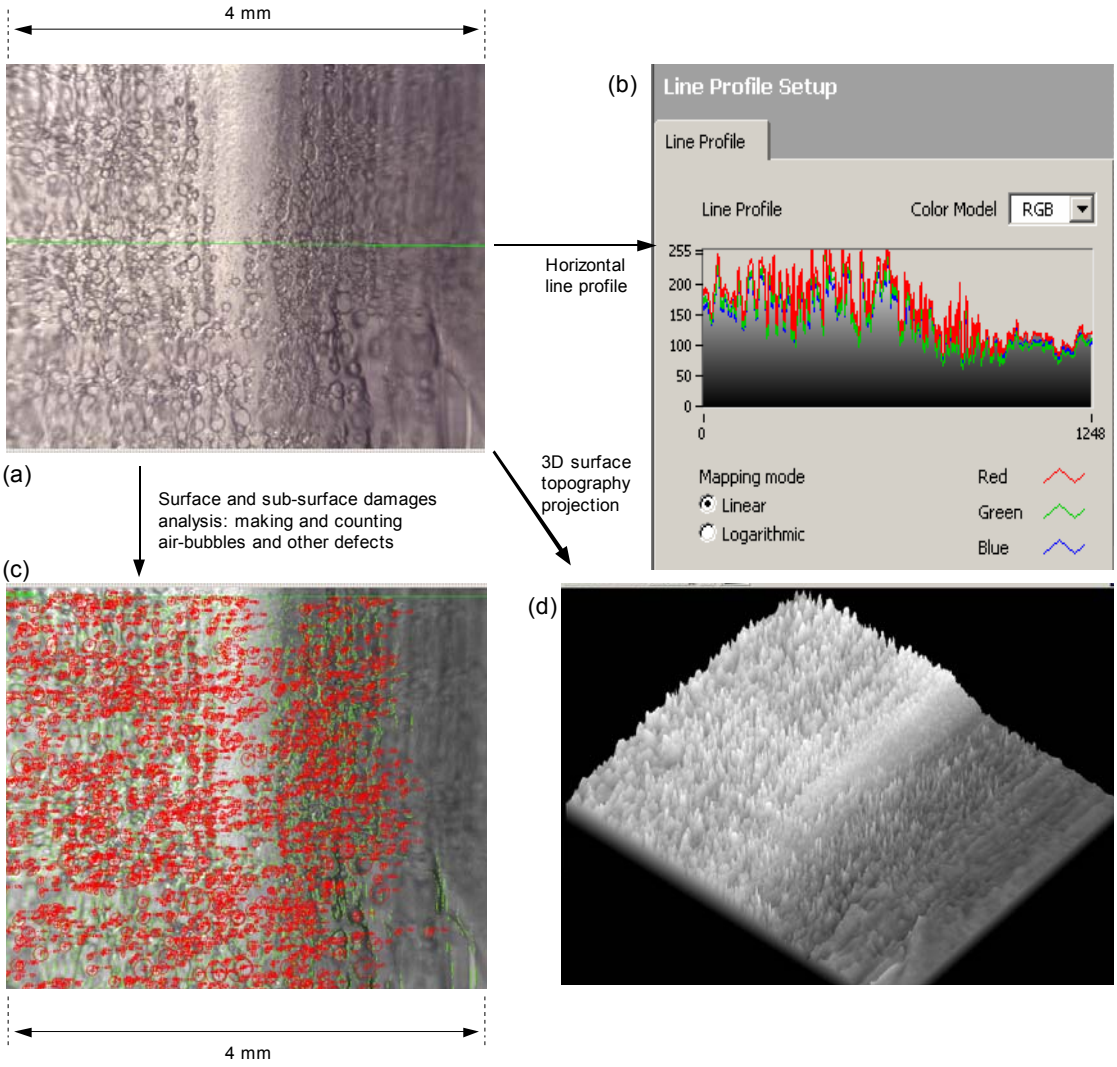

Figure 6.4 – Qualitative surface analysis of a section of a MPSC laser-cut demonstration prototype with extremely high concentration of surface and sub-surface defects.

Table 6.1 – Results for surface and sub-surface shape-recognition analysis related to the area shown in Figure 6.4(c).

Total number of recognised elliptical and circular shapes

Results ...	864	865	866	867	868	869	870	871	872
Score	314.29	311.11	310.34	309.09	307.69	307.69	307.69	304.35	304.35
Major Radius	6.98	6.11	11.13	11.13	10.77	16.66	4.69	9.31	7.94
Minor Radius	6.98	6.11	11.13	11.13	10.77	16.66	4.69	9.31	7.94

6.4 MPSC systems experimental tests

Both the laboratory and outdoors experimental tests were conducted in accordance to the basic measurement procedures and set-up configuration described initially in Chapter 3. Figure 6.5 presents a MPSC laser-cut PMMA prototype section positioned for the outdoor tests (Fig.6.5a) and for the laboratory tests (Fig.6.5b). Table 6.2 shows the main parameters of the manufactured MPSC demonstration prototypes used in the experimental tests.

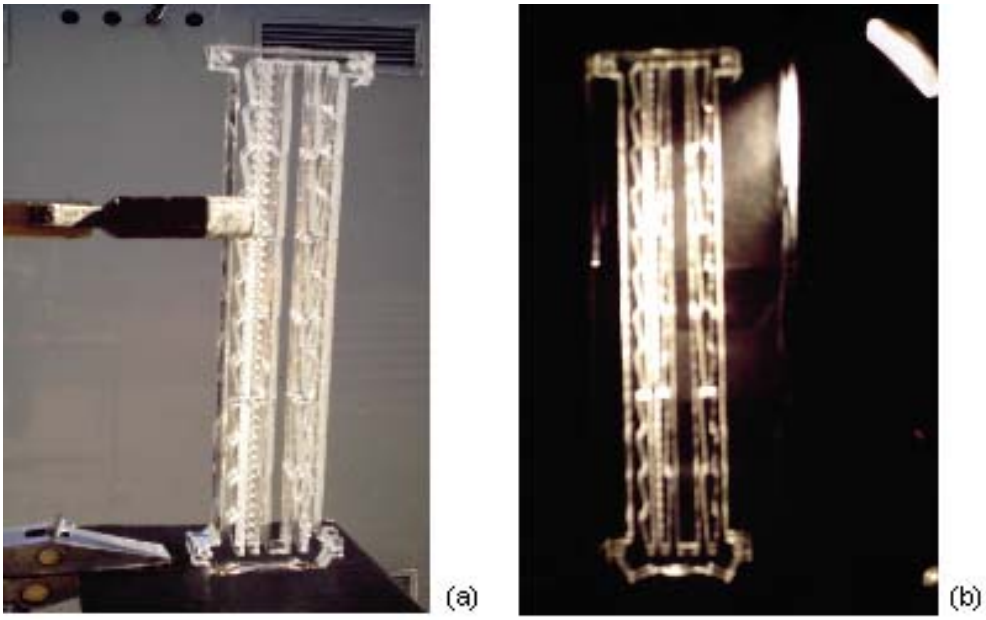

Figure 6.5 – Set-up for MPSC system experimental tests. Outdoor tests (a) and laboratory tests with artificial light source (b).

Table 6.2 – MPSC laser-cut manufactured demonstration prototypes main parameters and dimensions.

MPSC systems	**Parameters**							
	1st PA apex angle	2nd PA apex angle	3rd PA apex angle	4th PA apex angle	5th PA apex angle	Entrance area A1	Exit area A2	Geome. C_R (≈)
MPSC – X1 (2P)	24°	12.5°	6°	12.5°	24°	165x5	30x5	5.6
MPSC – X1 (3P)	8°	12.5°	6°	12.5°	24°	165x5	30x5	5.6
MPSC – X2 (2P)	24°	12°	4.8°	12°	24°	165x5	30x5	5.6
MPSC – X2 (3P)	8°	12°	4.8°	12°	24°	165x5	30x5	5.6
MPSC – S1 (SA)	8°	5.6°	5.6°	24°	-	165x5	22x5	7.5
MPSC – S1 (LA)	24°	5.6°	5.6°	8°	-	165x5	22x5	7.5
MPSC – L2	8°	12°	4.8°	12°	24°	165x5	30x5	5.6

6.4.1 Laboratory tests of MPSC systems demonstration prototypes

The goal of this series of laboratory experimental tests is:

- To measure the illuminance output E_{out} (in lux, lx) of the MPSC prototypes;
- To calculate the transmission efficiency T_E of the MPSC systems from the measurements of the illuminance output E_{out}, and considering the illuminance of the artificial light source (Solux® halogen 50W, 300-1100nm) varying in accordance to Cosine Law of Illuminance.

Figures 6.6 to 6.9 presents the results for the illuminance output E_{out} as a function of the incident angle θ_i of direct light (Solux® halogen 50W, λ = 300nm-1100nm) at the meridional plane of the MPSC systems laser cut demonstration prototypes (PMMA, 5mm thick).

Figures 6.10 to 6.15 plots the main laboratory results for the MPSC considering the Illuminance output E_{out} (lx)) and the respective transmission efficiency T_E. (%), both as a function of the light pipe length (mm). A series of polyester-aluminium (80-85% reflectance for the visible spectrum) hollow cylindrical light pipes with lengths varying from 50mm to 1500mm were used. All light pipes have a diameter of 50mm.

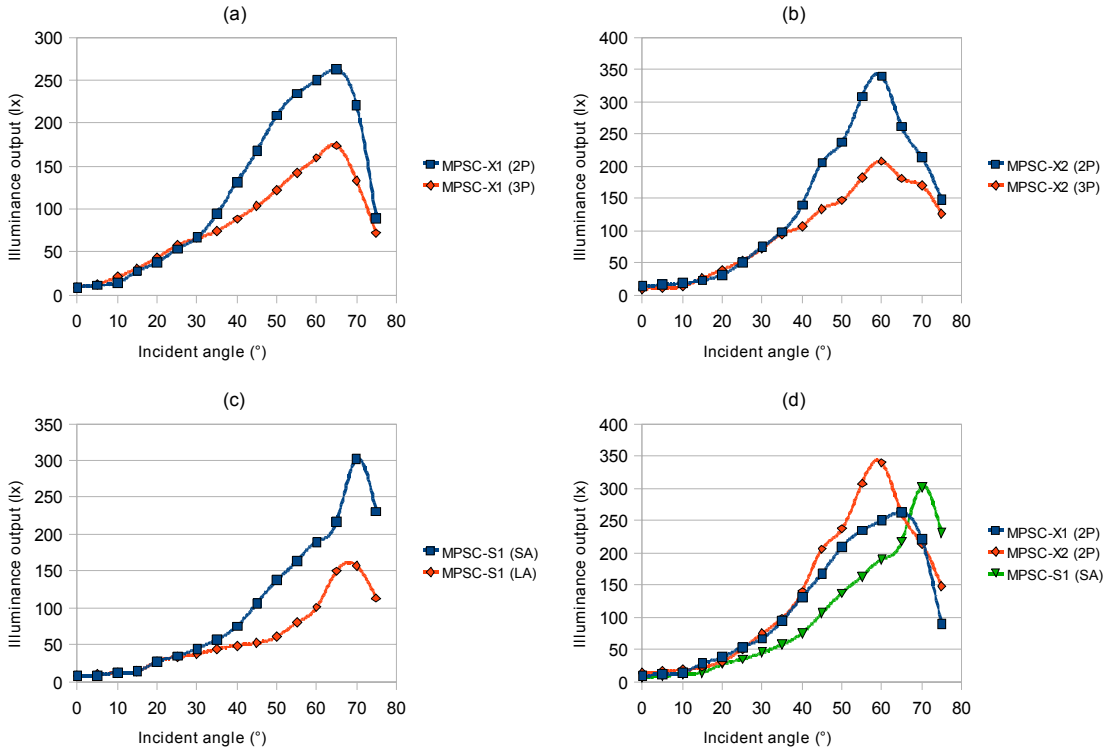

Figure 6.6 – Illuminance output E_{out} (lx) as a function of incident angle θ_i for six configurations of the MPSC systems demonstration prototypes (PMMA, 5mm thick). Measurements taken at end of a hollow light pipe 50/50mm made of a folded aluminium sheet.

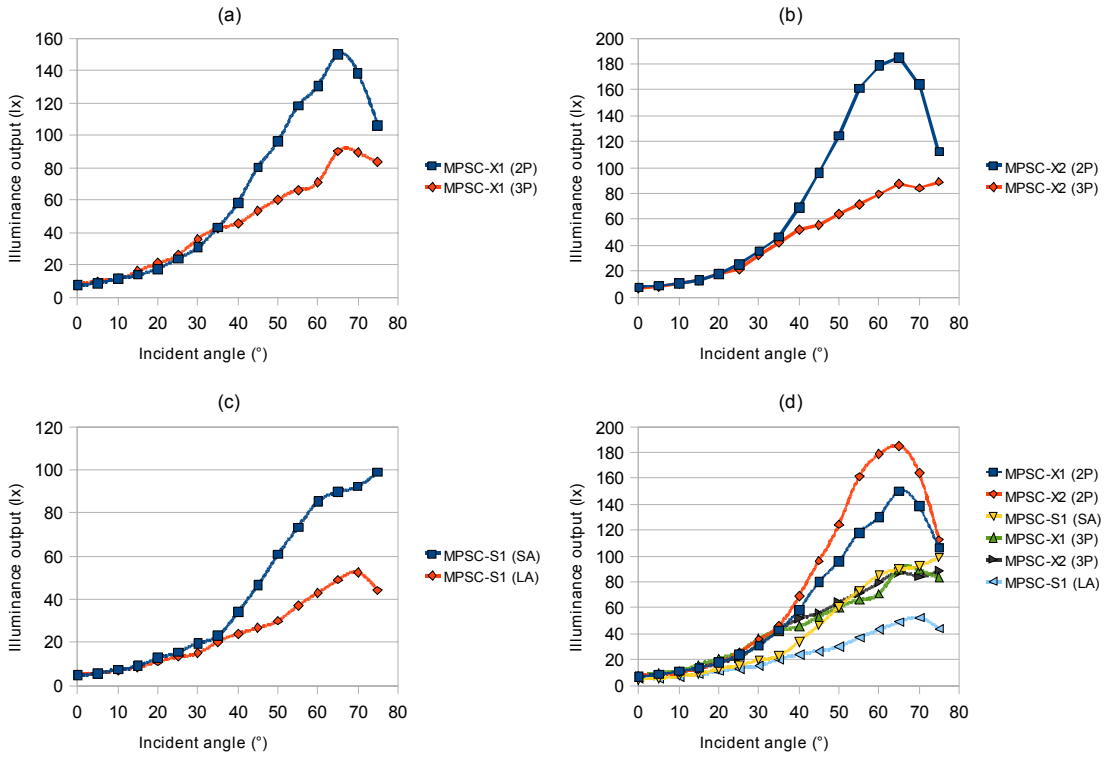

Figure 6.7– Illuminance output E_{out} (lx) as a function of incident angle θ_i for six configurations of the MPSC systems demonstration prototypes (PMMA, 5mm thick). Measurements taken at end of a hollow light pipe 100/50mm made of a folded aluminium sheet.

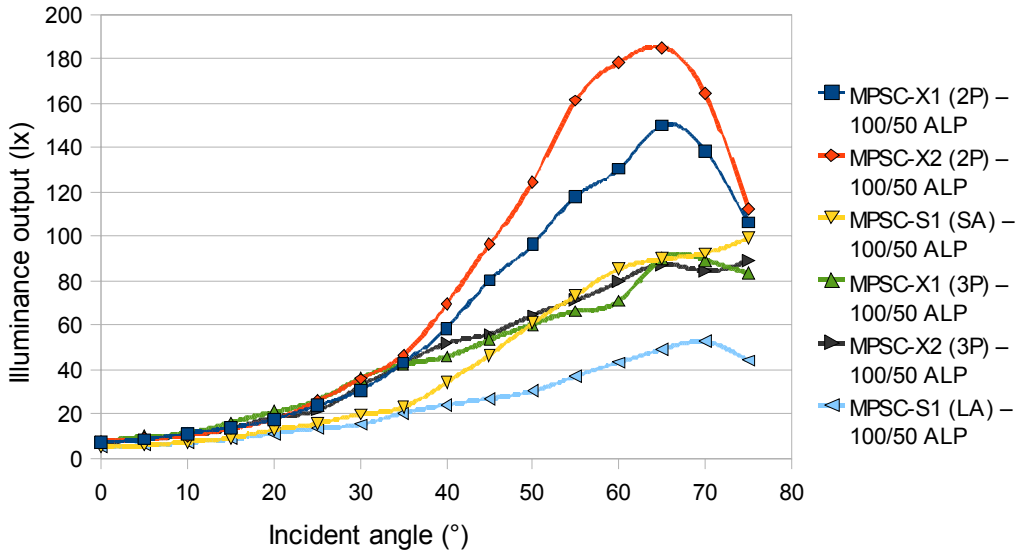

Figure 6.8 - Comparison of illuminance output E_{out} (lx) between six configurations the MPSC systems demonstration prototypes (PMMA, 5mm thick). Measurements taken at end of light pipe 100/50mm made of a folded polyester-aluminium sheet.

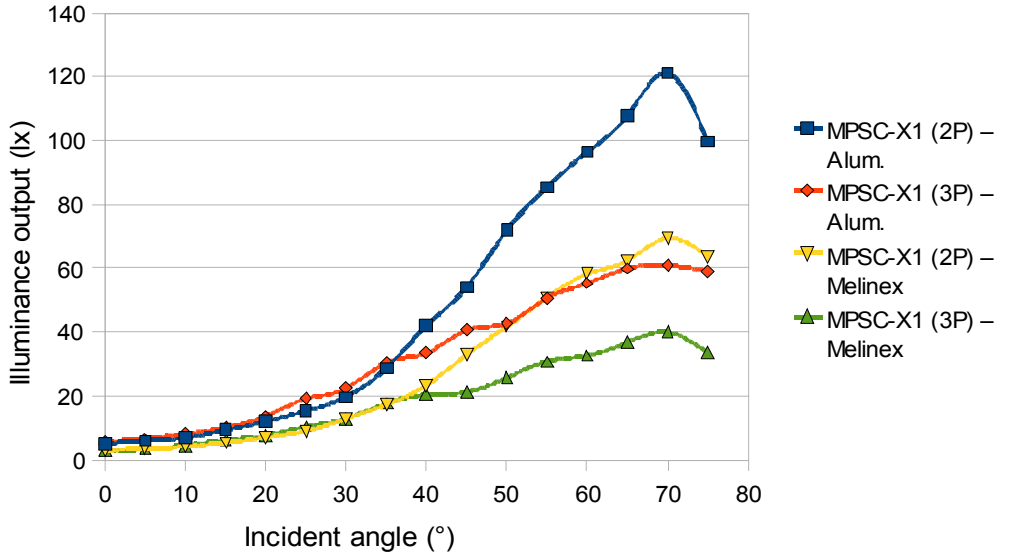

Figure 6.9 – Comparison between the illuminance output E_{out} (lx) of two MPSC systems coupled with two different light pipes: one made of folded polyester-aluminium sheet (Alum.) and one made of folded Melinex® gloss white sheet. Both light pipes have the same dimensions (200/50mm): length = 200 mm; diameter = 50 mm.

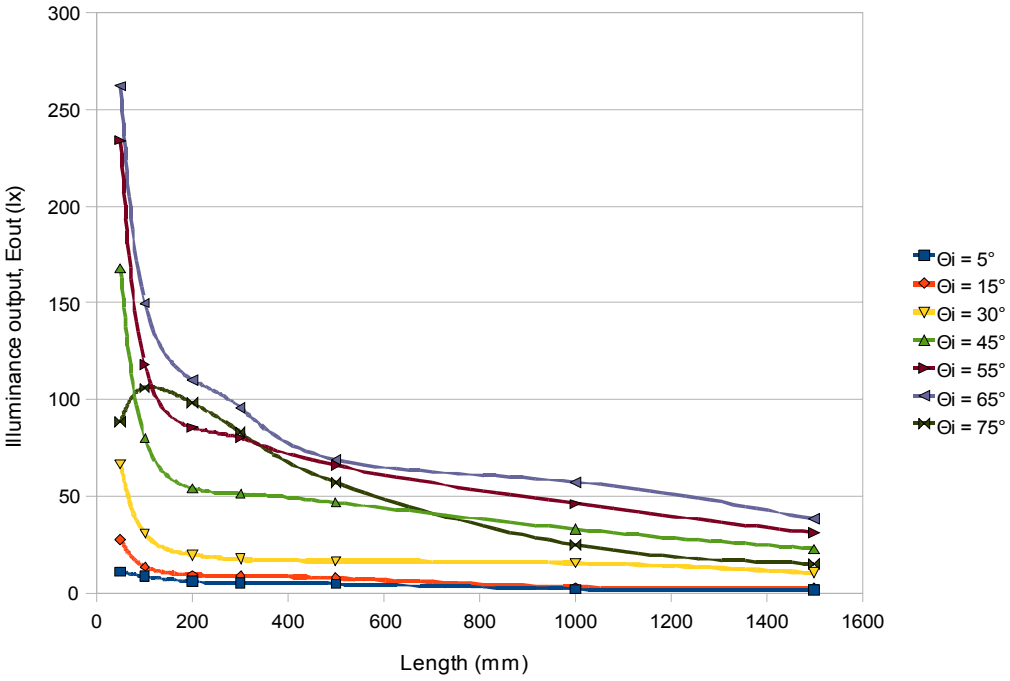

Figure 6.10 – Illuminance output E_{out} of the MPSC-X1(2P) system demonstration prototype. Measurements taken at the end of a series of hollow light pipes made of folded aluminium sheet, with Ø = 50mm and length varying from L = 50mm to 1500mm.

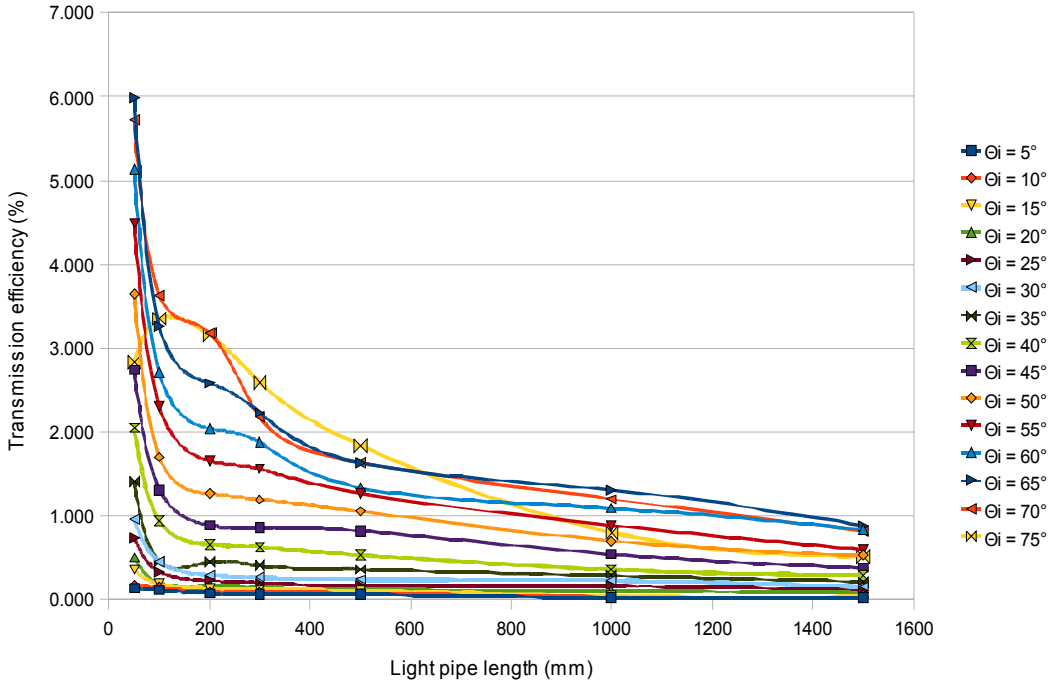

Figure 6.11 – Transmission efficiency T_E of the MPSC-X1(2P) system demonstration prototype. Measurements taken at the end of a series of hollow light pipes made of folded aluminium sheet, with Ø = 50mm and length varying from L = 50mm to 1500mm.

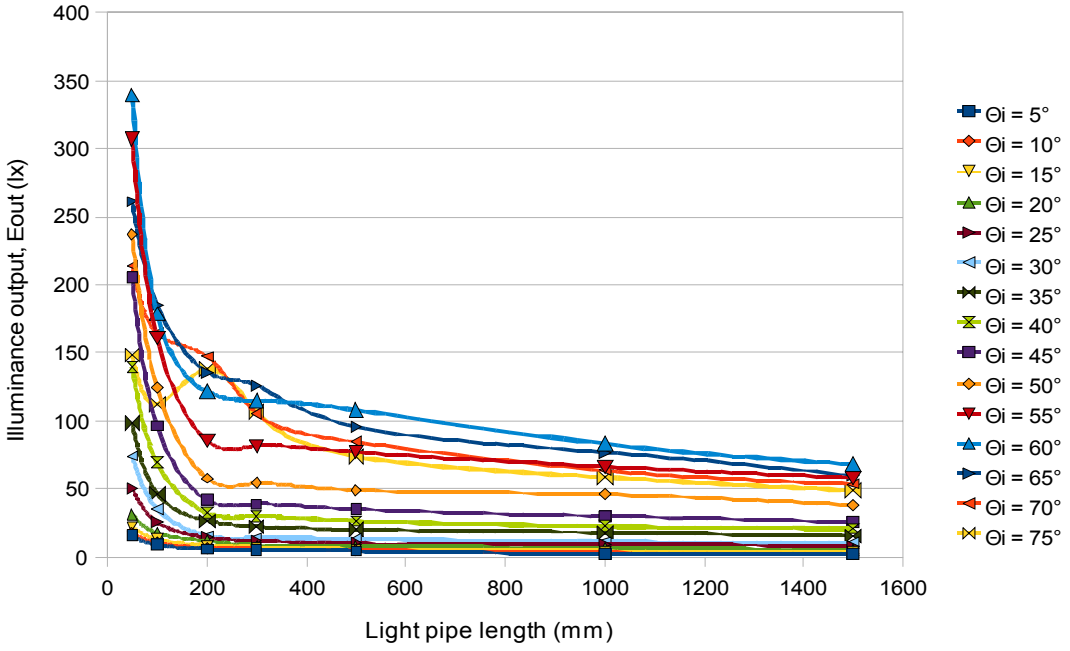

Figure 6.12 – Illuminance output E_{out} of the MPSC-X2(2P) system demonstration prototype. Measurements taken at the end of a series of hollow light pipes made of folded aluminium sheet, with Ø = 50mm and length varying from L = 50mm to 1500mm.

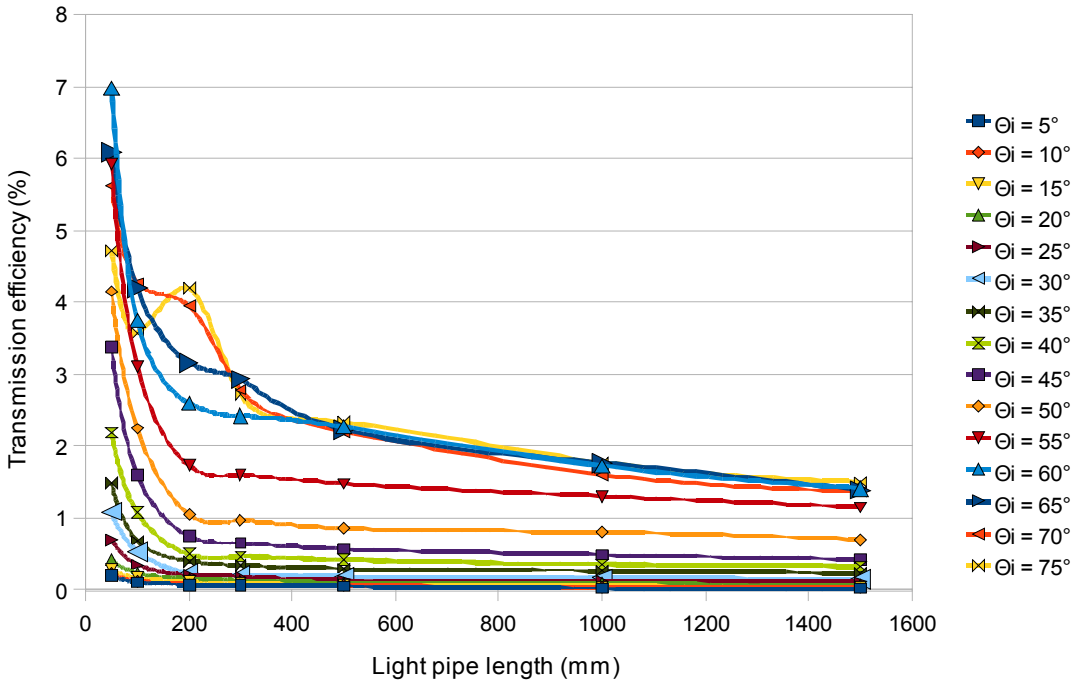

Figure 6.13 – Transmission efficiency T_E of the MPSC-X2(2P) system demonstration prototype. Measurements taken at the end of a series of hollow light pipes made of folded aluminium sheet, with Ø = 50mm and length varying from L = 50mm to 1500mm.

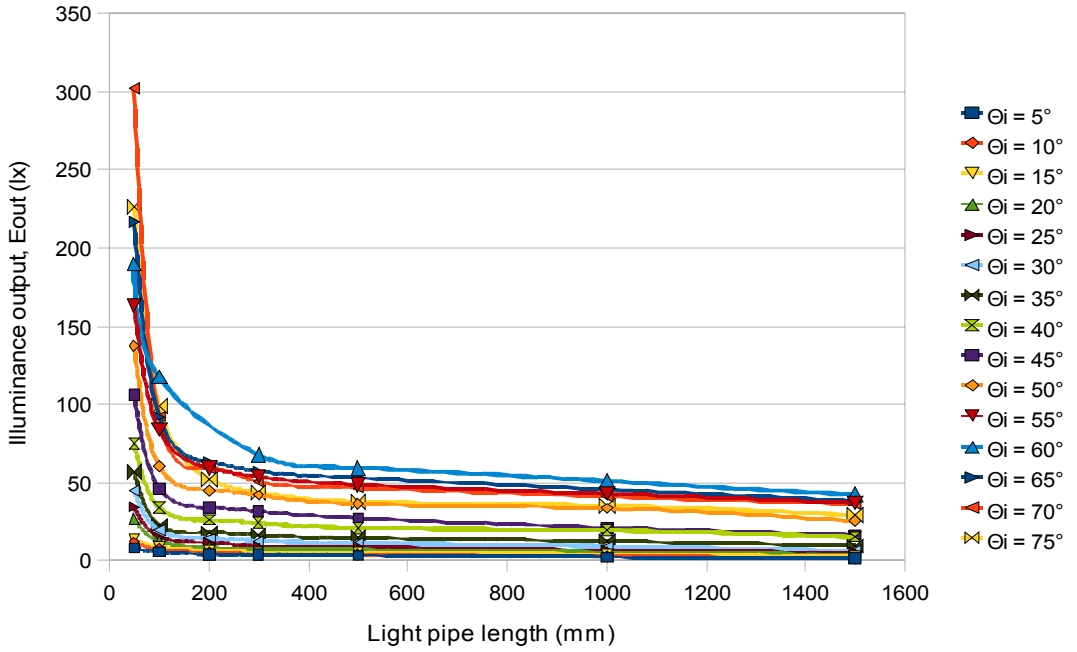

Figure 6.14 – Illuminance output E_{out} of the MPSC-S1(SA) system demonstration prototype. Measurements taken at the end of a series of hollow light pipes made of folded aluminium sheet, with Ø = 50mm and length varying from L = 50mm to 1500mm.

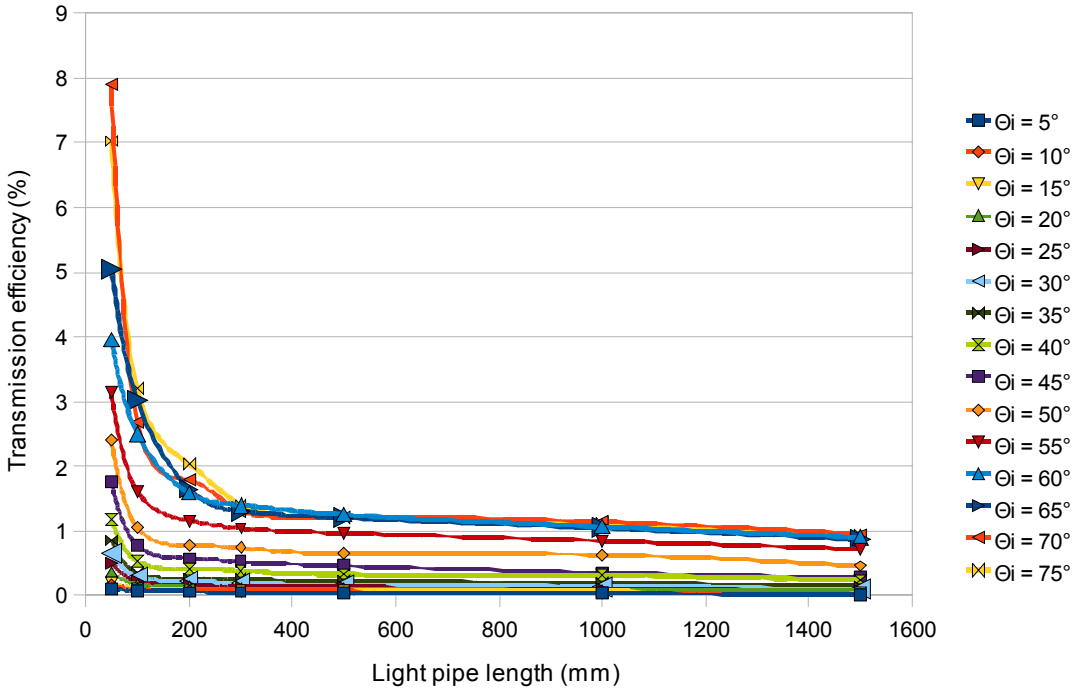

Figure 6.15 – Transmission efficiency T_E of the MPSC-S1(SA) system demonstration prototype. Measurements taken at the end of a series of hollow light pipes made of folded aluminium sheet, with Ø = 50mm and length varying from L = 50mm to 1500mm.

6.4.2 Outdoor tests of MPSC systems demonstration prototypes

A series of outdoors experimental tests were conducted to analyse the performance of the MPSC systems under real weather conditions and incident global solar radiation. The experiments were set at Brunel University campus in Uxbridge, west London - UK (geographic location: 51 38' N; 07' W). It is important to stress that the results are strictly dependent on the geographic location and weather conditions during the days they were taken.

As seen in Figure 6.16, a prototype-section of the MPSC system was positioned vertically with its exit aperture directed towards the entrance of a hollow light pipe integrator. A protective screen cap coated in matte black was used to block unwanted light to enter the hollow light pipe integrator. A "window" with the same dimensions as the exit aperture area of the MPSC was cut through the protective screen cap, allowing only light that emerges from the exit aperture of the MPSC to enter the hollow light pipe integrator (Ø = 50mm; L =300mm). A photometer (Extech EA-31 light meter) with cosine-corrector diffuser dome was positioned at the low-end section of the hollow light pipe integrator, aligned with the vertical optical axis of the system. To avoid stray light the photometer was positioned inside a protective box (not seen in the figure) covered with a black cloth.

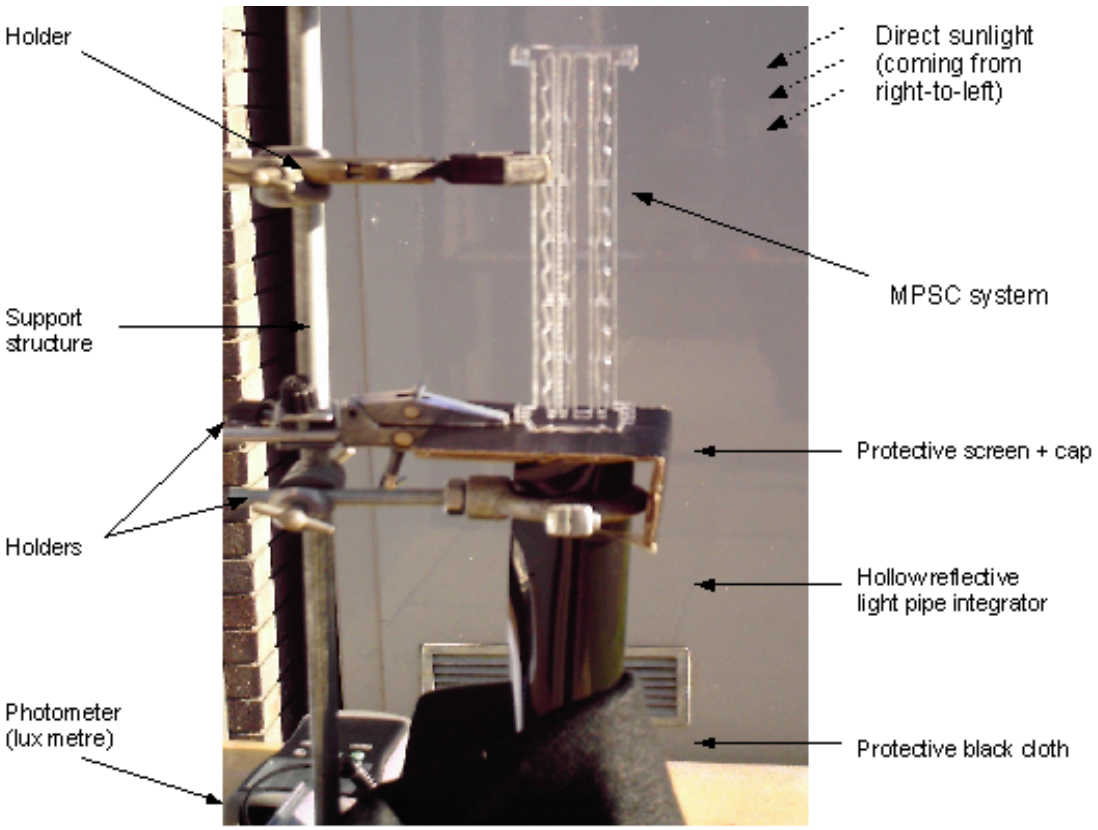

Figure 6.16 – Outdoor experimental test set-up configuration for the MPSC systems.

Figures 6.17 to 6.19 shows the results for the outdoor experimental tests with the MPSC-X1(2P) laser-cut demonstration prototype (PMMA; 5mm thick). The system was vertically positioned as shown in Figure 6.16 (above), facing south. A magnetic compass was used to verify the correct orientation.

Figure 6.17(a) plots the variation of the measured global illuminance falling on a vertical south-orientated façade. Figure 6.17(b) plots the illuminance output E_{out} (measured in lux, lx) emerging from the exit aperture of the MPSC-X1(2P) laser-cut prototype. Both measurements (vertical/façade illuminance and illuminance output) were taken simultaneously during a period of 3 hours (11:00 – 14:00hs, local GMT time) at 5 minutes intervals. Figure 6.17(c) presents the calculated results for the illuminance transmission efficiency T_E considering the illuminance output E_{out} as a percentage of the vertical/façade illuminance (illuminance input E_{in}).

(a)

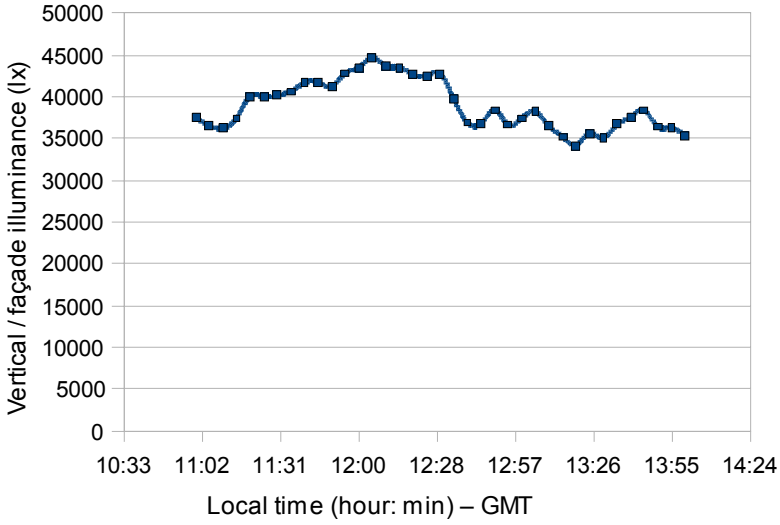

(b)

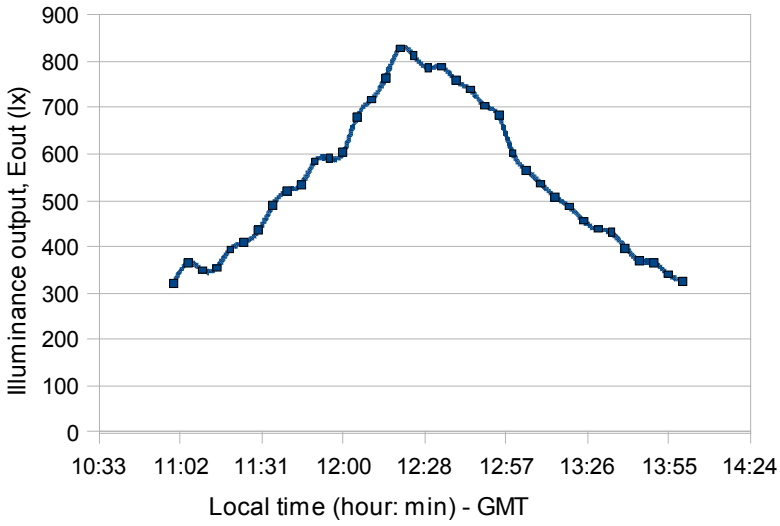

(c)

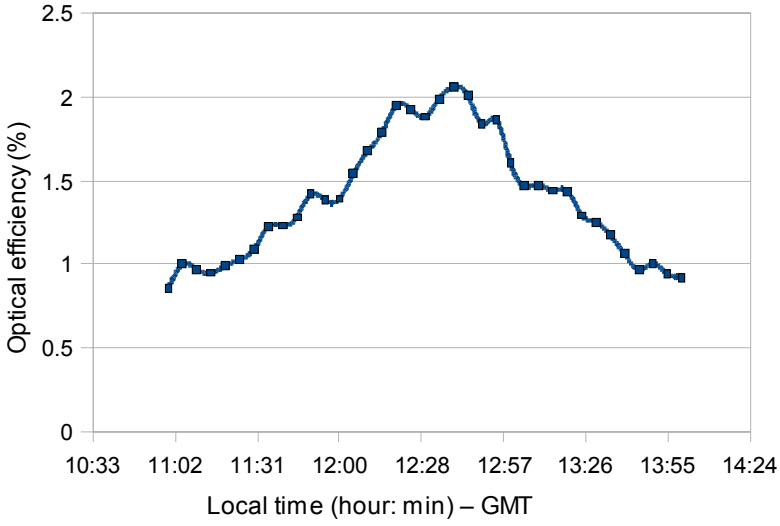

Figure 6.17 – Outdoor experimental tests results for the MPSC-X1 (2P) system. The graph in figure (a) shows the vertical/façade illuminance measured at the entrance aperture of the system; in (b) the illuminance output E_{out} of the system; and in (c) the optical transmission efficiency T_E. Set-up position: vertical. Orientation: south. Experiment date: 21/01/09.

Figures 6.18 and 6.19 display the combined illuminance output E_{out} (lx) for the MPSC-X1(2P) system considering five different orientations: east, south-east, south, south-west and west. The total sum of the results is displayed in Figure 6.19. Overlapping measurements displayed in Figure 6.18 were taken with a time difference of about 1min between them. In other words, the graph in Figure 6.19 shows an approximation of the total sum of the illuminance output E_{out} considering the situation where all the collected light coming from the MPSC-X1(2P) system demonstration prototype (PMMA, 5mm thick, laser-cut) orientated towards the five directions (E, SE, S, SW and W) is directed to the same receiving area. Experiments date: 24/01/09.

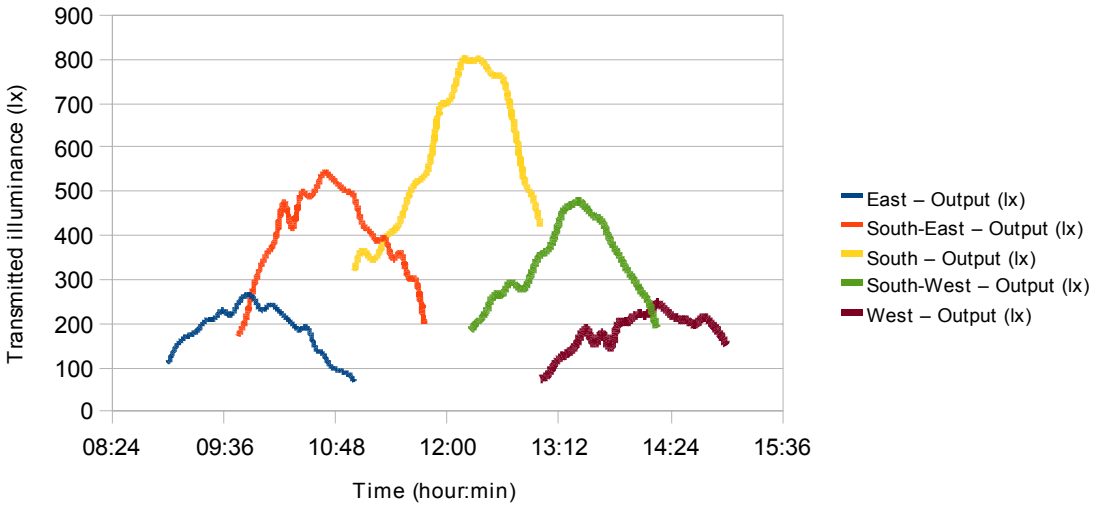

Figure 6.18 – Combination of five graphs plotting results of outdoors experimental tests considering five different orientations for the MPSC-X1(2P) system (PMMA; 5mm thick). Overlapping results represents measurements taken with a time difference of about 1min between them. Experiments date: 24/01/09.

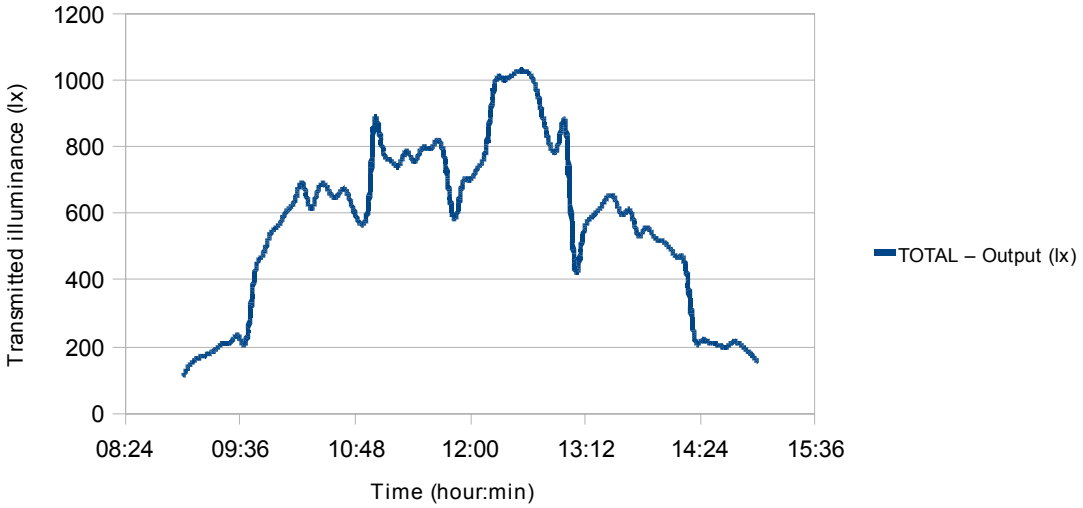

Figure 6.19 – Total sum (distributed over time) of the results displayed previously in Figure 6.18 (above). The sum relates to the overlapping of the previous graphs. System: MPSC-X1(2P) system (PMMA; 5mm thick). Experiments date: 24/01/09.

6.4.3 Partial spectral analysis (600nm – 1780nm)

Firstly it is important to stress that the spectrum analysis presented here is limited to the spectrum range (600nm to 1780nm) of the optical spectrum analyser Ando AQ6317B. Note that the results provide only a small sample of the total collected and transmitted radiant energy.

Measurements were taken in accordance to the procedures described in Chapter 3. The experiment set-up apparatus includes a commercial aluminium cylindrical tube (length = 1000mm; internal diameter = 25mm) used as a light pipe integrator. The MPSC-L2 prototype is coupled at the entrance of the light pipe and the measurements are taken at the end. Figure 6.20 shows the "measuring area" of the experiment set-up apparatus.

Figure 6.21 presents the results of a series of partial spectral analysis considering the spectral power distribution (measured in nW) as a function of the wavelength λ emerging from the exit aperture (5mm x 30mm) of a MPSC-L2 laser-cut prototype (PMMA, 5mm thick) exposed to direct solar radiation. Measurements, using the optical spectrum analyser Ando AQ6317B, were taken on the 21st of September 2008 between 12:00-14:00hs (local time, GMT).

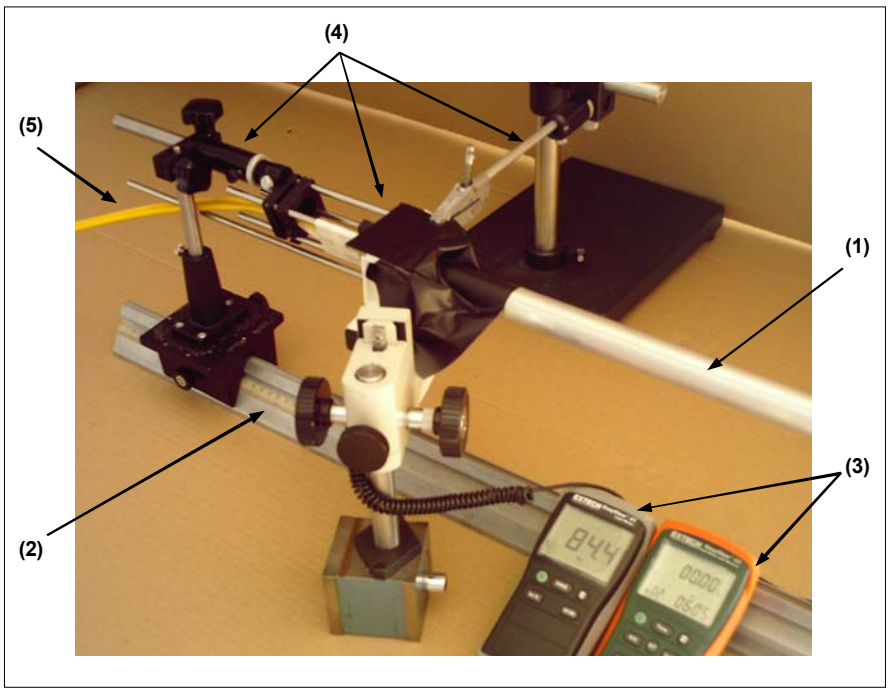

(1) Light pipe (1m long);

(2) Optical bench;

(3) Photometers;

(4) Supporting mounts

(5) Fibre optical cables (connected to optical spectrum analyser)

Figure 6.20 – Experiment set-up apparatus showing the "measuring area" for the partial optical spectral outdoor tests.

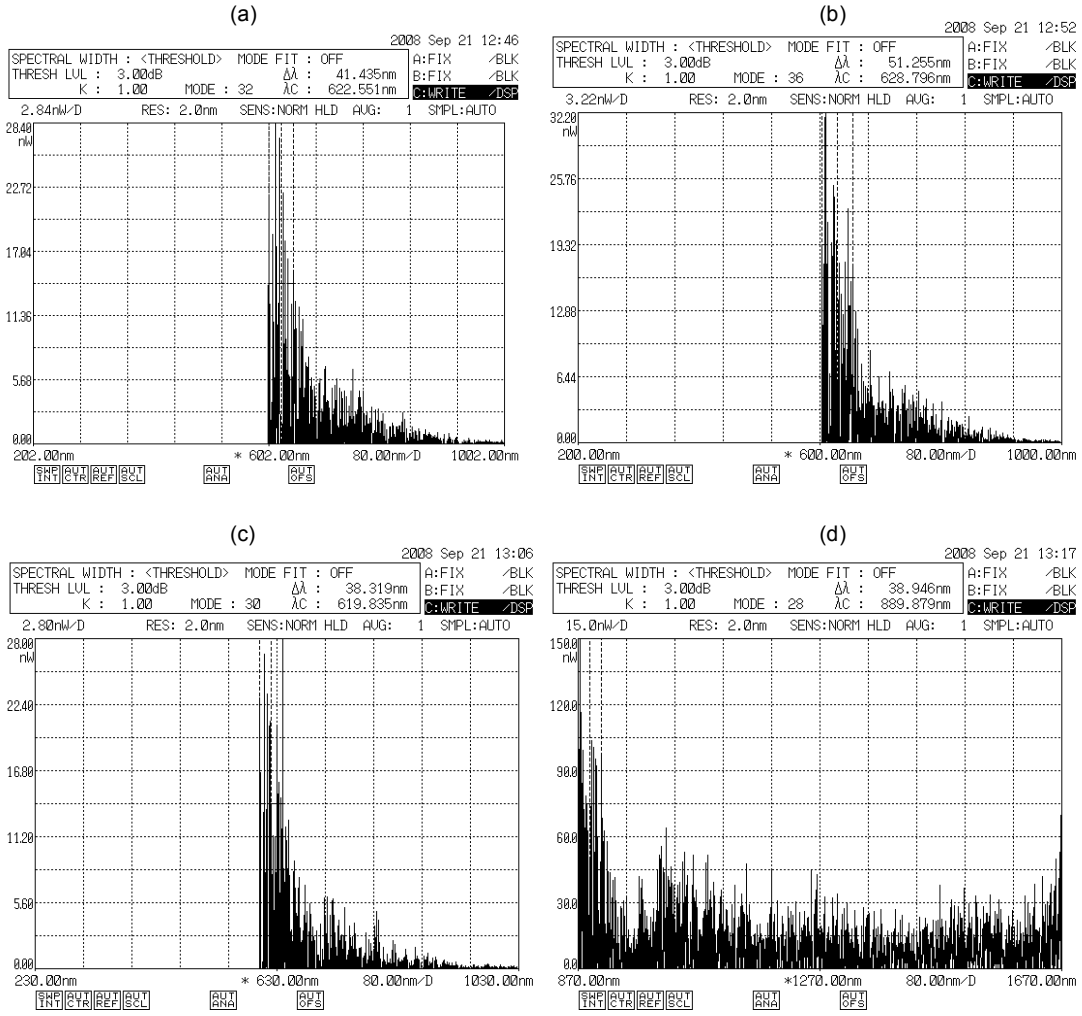

Figure 6.21 – Partial spectral analysis for the MPSC-X1(2P) system demonstration prototype under direct sunlight. Experiment set-up position: vertical. Orientation: south. Experiment date: 19/01/09.

In Figure 6.21, the graphs (a), (b) and (c) displays the results for the MPSC-X1(2P) system coupled to a light pipe integrator hollow cylindrical aluminium tube 300mm long, 50mm in diameter. Graph (d) plots results for direct sunlight (only). Instrumentation: optical spectrum analyser Ando AQ6317B (600nm to 1780nm).

Note that the spectrum output displayed in Figure 6.21 starts at 600nm (mid-visible light) and decays to almost zero after approximately 900nm. This indicates that the MPSC-L systems are good for transmitting visible-light (400-780nm) and not good for transmitting infra-red radiation (above 800nm).

This result is partially due to the transmittance range (300nm-1000nm) of the clear PMMA material used to manufacture prototypes. The geometry of the MPSC/RINSC systems also has an important influence on its capability of transmitting visible-light (VIS) and not much near-infrared radiation (NIR). According to the refractive optics theory presented in Chapter 2, shorter wavelengths refract most while

longer wavelengths refract least. As a result, part of the visible range of the spectrum is refracted and transmitted by the system without infrared radiation (longer wavelengths). This is a positive function for daylighting application, since only visible light is needed and infrared should be avoided to reduce solar-heat gain and overheating in indoors environment.

6.5 Results and discussion on the MPSC systems

The multi-prismatic solar collectors (MPSC) expanded the PSC concept by providing the original optical arrangements characterised by a series of parallel prismatic arrays with combined light guide integrated into a self-contained solid-dielectric optical system. It demonstrates that the introduction of parallel prismatic arrays can lead to larger acceptance angles θ_{accept} and higher transmission efficiencies T_E than the previous PSC systems. The basic design of the MPSC system provides a geometric concentration ratio of $C_R \approx 5.6X$. MPSC demonstration prototypes made of clear PMMA and manufactured by laser ablation process, yield peak transmission efficiencies T_E from $T_E \approx 6\%$ to $T_E \approx 8\%$ [for the MPSC-S1(SA) prototype] considering an incident radiant energy (λ = 300nm - 1100nm) at the entrance aperture meridional plane varying from $\theta_i = 5°$ to $\theta_i = 75°$.

The laboratory experimental tests in which a series of hollow cylindrical light pipes were coupled to the exit aperture of the MPSC prototypes demonstrate the potential of the system to transmit direct light for natural illumination application. It was noticed that the angular distribution $\Delta\theta$ of the luminous flux Φ emerging from the exit aperture of the MPSC prototypes has a significant impact on the systems efficiencies. This is clearly evident, for example, when comparing the results from Figures 6.12 and 6.13, both related to the MPSC-X2(2P) prototype, and Figures 6.14 and 6.15, related to the MPSC-S1(SA) prototype. Despite providing a higher transmission efficiency $T_E \approx 8\%$ (for $\theta_i = 70°$), measured at a distance of 50mm from its exit aperture, the MPSC-X2(2P) prototype luminous output angular distribution $\Delta\theta$ is too wide spread, resulting in a higher attenuation inside the hollow cylindrical light pipe. This explains the fast drop of its illuminance output E_{out} (Figure 6.14) and related transmission efficiency T_E (Figure 6.15). The MPSC-S1(SA) prototype provides a relatively lower transmission efficiency $T_E \approx 7\%$ (for $\theta_i = 60°$), however its luminous output angular distribution $\Delta\theta$ is less spread around the optical axis of the hollow cylindrical light pipe. Consequently the transmission efficiency T_E of the MPSC-X2(2P)+light pipe system measured at distances > 1000mm (light pipe length) is almost two times the transmission efficiency T_E of the MPSC-S1(SA)+light pipe system measured at the same distance. By

comparing Figures 6.13 and Figure 6.15 it is possible to notice that this holds true for almost all incidence angles θ_i of direct light at the entrance aperture meridional plane.

These results demonstrate that if a series of MPSC systems are installed into a building facade (east, south-east, south, south-west and west), the overall transmitted illuminance output (lx) emerging from the combined system can be satisfactory, approximating the natural illumination requirements described in the literature and required by most building standards (IEA, 2000; BS 8206-2:2008). A peak transmission efficiency of 2% was measured during outdoors experimental tests during the winter-period (experiment date: 21/01/09). However it is important to notice that the solar incidence angle (h_s; γ_s) on the date of the experiment was lower than the acceptance angle θ_{accept} of the MPSC demonstration prototype, which explains the lower result.

National Instruments LabVIEW® Vision Assistant 8.0 software provided a way to analyse the defects on a sub-surface level. The software "shape-recognition" tool was applied to measure and count the number of closed circular and elliptical shapes on a series of selected images. These shapes are mainly air-bubbles trapped inside the material as a negative result of the laser ablation process used to manufacture the MPSC demonstration prototypes. As seen, the concentration of surface and sub-surface damage in some areas of the prototypes was higher than the maximum recommendation by the standards BS ISO 10110-4:1997 and BS ISO 10110-8:1997.

Air-bubbles and other sub-surface intrusions in the bulk of the PMMA material are a result of the application of the laser ablation process. This possibly happens due to compression and migration of material due to the pressures generated by thermal expansion. This has a series of negative consequences for light travelling through the material, resulting in significant losses due to scattering when a ray hits a microscopic air-bubble inside the material. Surface defects and sub-surface as well also leads to a reduction in TIR of light propagating inside the solid-dielectric medium of the MPSC demonstration prototypes. Hence, the efficiency losses due to manufacturing errors are considerably high.

Spectral analysis conducted with the optical spectrum analyser Ando AQ6317B (600nm to 1780nm) indicates that most of the spectrum transmitted by an MPSC demonstration prototype was contained in the visible band range.

6.6 Summary and conclusions of Chapter 6

The Multi-Prismatic Solar Collector (MPSC) concept has been introduced and analysed. Computer ray-tracing analysis has been applied to characterise the systems. A series of MPSC demonstration prototypes manufactured by laser ablation process has been tested in laboratory and field/outdoors experimental tests.

The MPSC system can be customised for specific site/geographic locations and orientations (N, S, E, W, etc.) by specifying different values for the apex angles α for the group of parallel prismatic arrays.

The higher number of interfaces/surfaces in the MPSC systems results in higher surface scattering, attenuation and Fresnel reflection losses. It is argued that a portion of these losses is "recycled" by the MPSC system due to its geometric construction and optical layout (e.g.: the prismatic arrays are "facing inwards"). However, in the case of the MPSC demonstration prototypes, these losses are in fact increased due to manufacturing defects (e.g. air-bubbles and strains) caused by the laser ablation prototyping process.

The importance of the angular distribution Δθ of the output luminous flux Φ in the overall transmission efficiencies T_E of the MPSC + light pipe systems has been discussed. Laboratory experimental tests have shown that improvement in the output luminous flux Φ angular distributions Δθ (e.g. angular cone closer to the optical axis of the light pipe system) can lead to better results.

The main conclusions regarding the MPSC systems as presented here are:

- The inclusion of a series of parallel prismatic arrays with combined light guide increases the systems acceptance angle θ_{accept} and transmission efficiencies T_E;
- It is necessary to find design alternatives to reduce the number of interfaces/surfaces of the system in order to reduce and/or "recycle" surface scattering and Fresnel reflections losses;
- It is necessary to explore design alternatives to improve the total internal reflection (TIR) trapping and transmission efficiencies while at the same time increase the potential to extract light trapped inside the system by TIR when it reaches the exit aperture;
- Optical design configurations that lead to a possible improvement in the angular distributions Δθ of output luminous flux Φ emerging from the systems exit aperture are recommended.

Chapter 7 - Integrated Multi-Prismatic Solar Collectors

7.1 Introduction

In the last chapters, the analysis and experimental tests conducted with the PSC and MPSC demonstration prototypes has shown that it is possible to apply prismatic arrays with combined light guides to harvest and transport light by means of TIR. Both the PSC and MPSC systems presented compact optical configurations that are suitable for building integration. However, due to their geometric constructions (i.e. prismatic array with combined light guide) a significant portion of the light trapped by TIR inside the solid-dielectric structure may still escape from the system due to the non-continuum geometry of the prismatic arrays. Hence, it is necessary to explore other optical configurations that can offer potential solutions to this problem.

This chapter introduces and analyse the Integrated Multi-Prismatic Solar Collector (IMPSC). The IMPSC also applies a series of prismatic arrays as a means to change the direction of incoming solar radiation. However, the main difference between the IMPSC and the previous systems is that it comprises at least one "independent" solid-dielectric light guide that runs parallel to the prismatic arrays and has a continuous geometry. This solution increases the efficiency of the system to trap and transmit light by TIR and, consequently, also increases its acceptance angle θ_{accept}.

A paper related to the IMPSC system has been submitted to a scientific journal (Pelegrini et al, 2009b).

7.2 The Integrated Multi-Prismatic Solar Collector (IMPSC) concept

The IMPSC concept can be classified as a solid-dielectric nonimaging optical system that integrates several optical elements into a single-structure embodiment.

The basic configuration of the IMPSC, shown in Figure 7.1, is divided into the four main parts: (1) parallel prismatic arrays: (2) symmetrical integrated light guide (SILG); (3) light extractors section; and (4) concentrator section. The entrance aperture of the system is defined by the frontal prismatic array. The exit aperture is located at the low-end of the concentrator section.

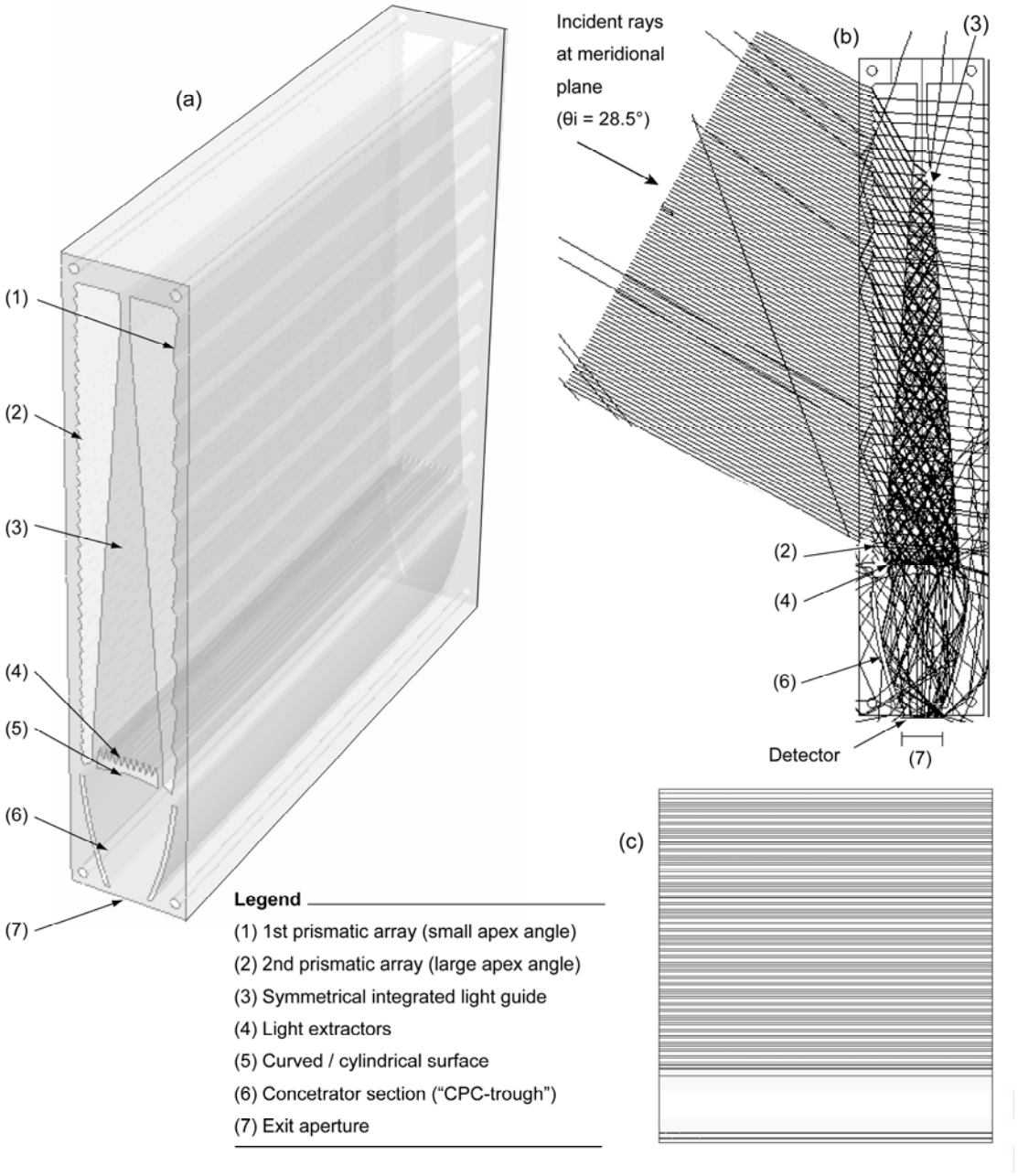

Figure 7.1 - CAD model views of the basic configuration for the IMPSC system. 3D perspective view shown in (a); ray-tracing analysis shown in (b), frontal view shown in (c). Fresnel reflections were not considered in the simulation (c). Views are not in scale.

The optical configuration of the IMPSC can be considered as a two dimensional (2D) nonimaging concentrator system. Given the precondition that the incident angle θ_i of direct light at the frontal entrance aperture is contained within the IMPSC acceptance angle θ_{accept}, the working principle of the IMPSC system can be briefly described as:

- Incident light ($\theta_i \approx \theta_{accept}$) enters the system through the entrance aperture and is diverted by the prismatic array;
- A fraction of this light is coupled into the SILG and transmitted TIR to the light extractors section;

- A fraction of the light trapped by TIR is extracted from the SILG at the extractors and directed towards the concentrator section to further reach the exit aperture.

Note that the basic IMPSC optical profile configuration is enclosed inside a rectangular frame. This “closed” geometric configuration provides the advantages:

- The main optical elements are kept protected inside the enclosed structure, avoiding possible damages due to manipulation during the manufacturing and installation process, and minimising weathering impact;
- The final configuration resembles a modular building-block component, suitable for building façade integration.

Figure 7.2 shows the IMPSC-A1 system configuration.

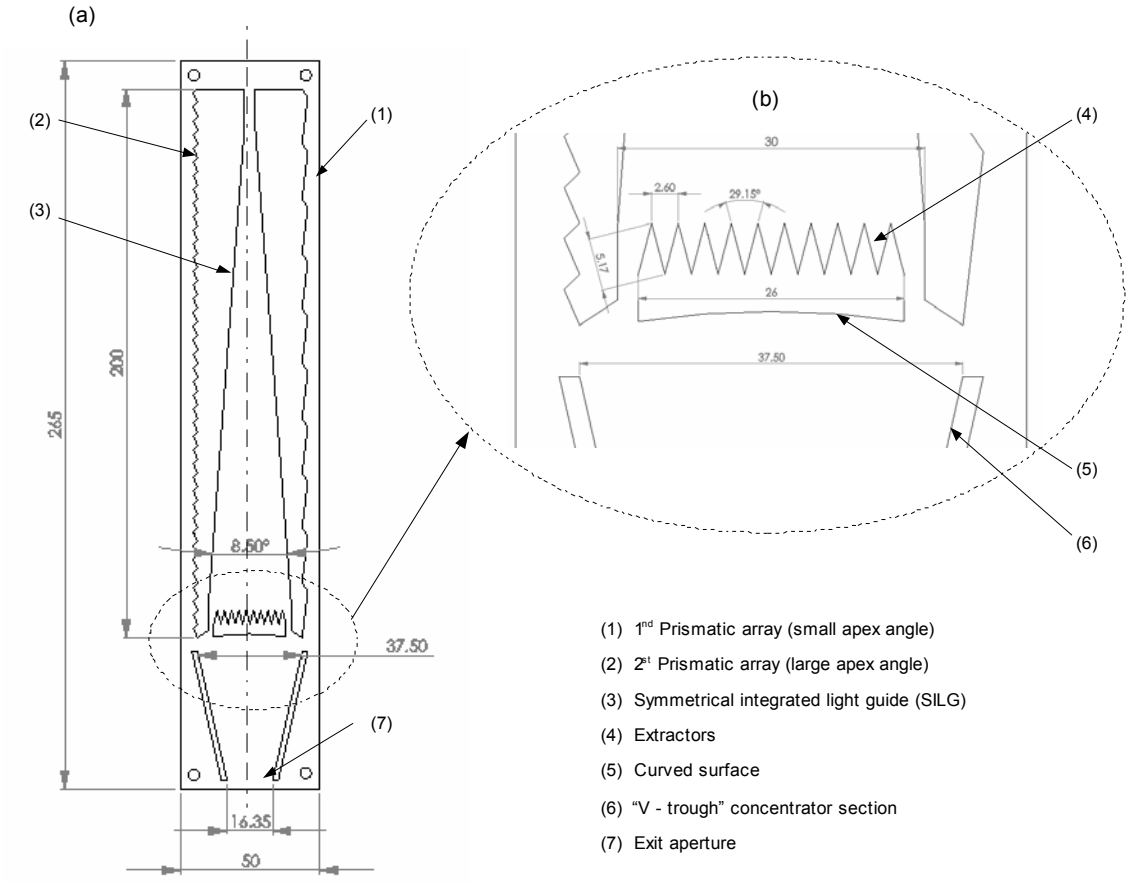

Figure 7.2 – CAD model 2D view of the vertical-section optical profile configuration for the IMPSC-A1 system.

7.3 IMPSC systems geometric features and working principle

7.3.1 Prismatic array panels (entrance aperture)

The IMPSC systems described in this chapter have two prismatic array panels, named here as 1st prismatic array panel (PA1) and 2nd prismatic array panel (PA2). The prismatic arrays correspond to the entrance aperture of the system. The acceptance angle θ_{accept} of each prismatic array is defined by their respective apex angles: α_{PA1} for PA1 and α_{PA2} for PA2. The entrance aperture of the IMPSC system is defined by which prismatic array (PA1 or PA2) is positioned towards the outside to receive incident sunlight. The construction of the prismatic arrays follows the same basic theory and design principles described in the previous chapters. In the configurations described in this chapter, both prismatic arrays (PA1 and PA2) have their prisms directed inwards.

In accordance to the value of the prismatic array apex angle α, we may distinguish the prismatic arrays of the IMPSC systems as:

- SA for a prismatic array with "small apex" angle ($\alpha < 20°$);
- LA for a prismatic array with "large apex" angle ($\alpha > 20°$).

Considering this, the system can be designed with two different acceptance angles θaccept by assigning different values for each prismatic array apex angle α, say for example, $\alpha_{PA1} = 8°$ and $\alpha_{PA2} = 24°$. Note in Figure 7.1 and Figure 7.2 that both prismatic arrays are directed "inwards". This has the advantage of providing a plain and smooth exterior surface and minimises the accumulation of dust and particles over the prismatic elements. It also aims to "recycle" part of the light rays that otherwise would escape from the system. A reflective surface or coating can be added to back side of the remaining prismatic array to increase the efficiency.

7.3.2 Symmetrical integrated light guide (SILG)

The symmetrical integrated light guide (SILG) is located in between the prismatic arrays (Figure 7.1 and Figure 7.2). The basic functions of the SILG can be defined as:

- To trap light by total internal reflection (TIR);
- To guide trapped light by TIR towards its exit aperture (or extractor section);
- To decrease the angular distribution Δθ of light trapped by TIR as it propagates towards the exit aperture/extractor.

As presented in Figures 7.1 and 7.2, the profile shape of the SILG resembles an “inverted V”. The geometric configuration of the SILG is defined by a continuous linear profile with interconnections (structural junctions) located only at its extreme ends. This provides a significant advantage to trap light by TIR if compared with the “light guide combined with prismatic array” solutions disclosed on the designs of the PSC systems (Chapter 5) and the MPSC systems (Chapter 6). Given an optical smooth surface, accepted light will remain trapped internally by TIR.

The apical angle formed between the light guide (SILG) walls is named here as the symmetrical integrated light guide (SILG) apex angle α_{SILG}. The half apex angle ½ α_{SILG} is the angle formed between one of the tilted walls of the light guide and the vertical optical axis of the system. The main conditions that define the “light trapping efficiency” of the light guide are:

- The first condition relates to the refractive index n of the solid-dielectric material of the light guide. Light will remain trapped inside the symmetric integrated light guide (SILG) as long as its incident angle θ_i at the light guide walls are equal or larger than the critical angle θ_c of the solid-dielectric material of the light guide in relation to its surrounding medium. The increase of the refractive index n leads to the decrease of the critical angle θ_c. Note that both the refractive index n and the critical angle θ_c are wavelength λ dependent.
- The second condition to trap light by total internal reflection (TIR) inside the symmetric integrated light guide (SILG) relates to its geometry.

Ray-tracing analysis is presented in Figure 7.3 to demonstrate how light propagates inside the symmetrical integrated light guide (SILG) by total internal reflection (TIR). A film/detector is positioned along the vertical optical axis of the system to measure variations in the density and distribution of light trapped inside the light guide (SILG). Spot diagrams serve to visualize these variations. Note that the distribution of intercepted rays on spot diagram (B) is more dispersed than in spot diagram (A), indicating that the density of radiant energy inside the light guide decreases as it propagates towards the exit aperture.

Figures 7.3, 7.4 and 7.5 demonstrate the process of coupling light into the symmetrical integrated light guide (SILG). It is possible to distinguish three possible ways to couple light into the symmetrical integrated light guide (SILG):

- Direct light coupling: happens when incident light is diverted by the frontal prismatic array and coupled directly into the light guide, as shown in Figure 7.3;

- Indirect light coupling: happens when incident light first undergoes total internal reflection (TIR) inside the frontal prismatic array panel, and only after escaping from the prismatic array panel (by intercepting the “negative section” of the prisms, defined by the prism base angle β) it is coupled into the light guide. See Figure 7.4.
- Random light coupling: relates to the coupling of scattered light or light originated from Fresnel reflections inside the system.

The computer simulation parameters specified in Figure 7.3 were: collimated monochromatic light λ = 555nm; solid-dielectric material refractive index n = 1.491; 1st prismatic array apex angle α_{PA1} = 24°; SILG apex angle α_{SILG} ≈ 8°. The parameters specified in Figure 7.4 are the same, except the apex angle α_{PA1} = 33°.

Figure 7.5 shows a sequence of ray-tracing simulations to illustrate how light is coupled at the top-end section of the light guide (SILG). The light guide has an apex angle α_{SILG} = 8°. The system is considered to be made of PMMA, with a refractive index of 1, 491 (for λ = 555nm). A beam of collimated monochromatic light (λ = 555nm) is directed towards the light guide (SILG) at an incident angle θ_i = 40° (Figures 7.5a and 7.5b) and θ_i = 60° (Figures 7.5c and 7.5d). To simplify the simulation, the beam is positioned after the 1st prismatic array, already inside the IMPSC system. Fresnel reflections are considered in Figures 7.5b and 7.5d.

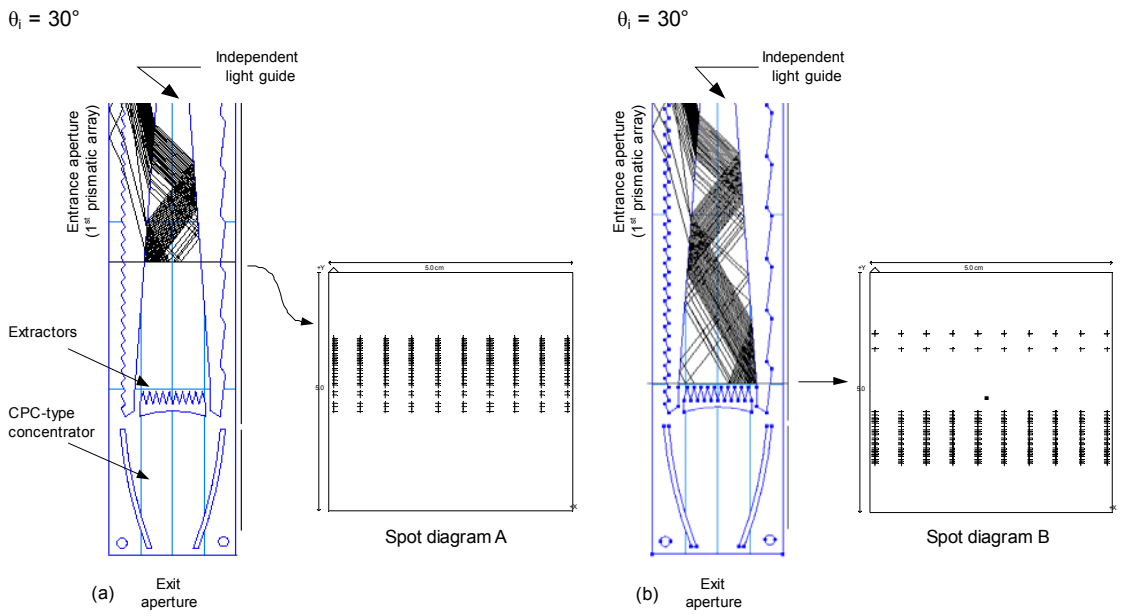

Figure 7.3 – Ray-tracing analysis showing light propagation inside the IMPSC-A2 system SILG. Spot diagrams demonstrate changes in the light path direction and (de)concentration inside the light guide.

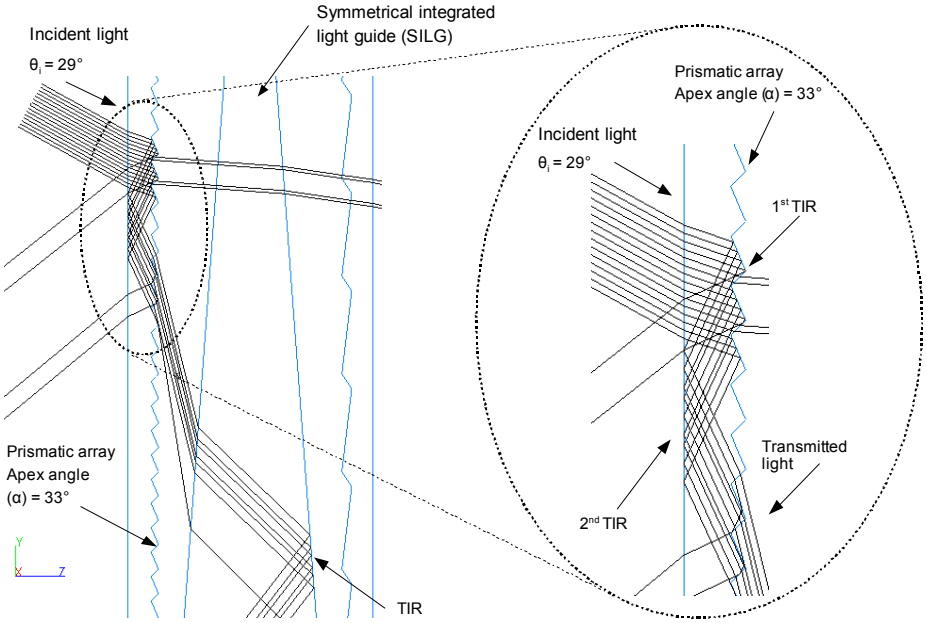

Figure 7.4 – Ray-tracing simulation demonstrating indirect light coupling into SILG at an initial incident angle $\theta_i = 29°$ at the meridional plane.

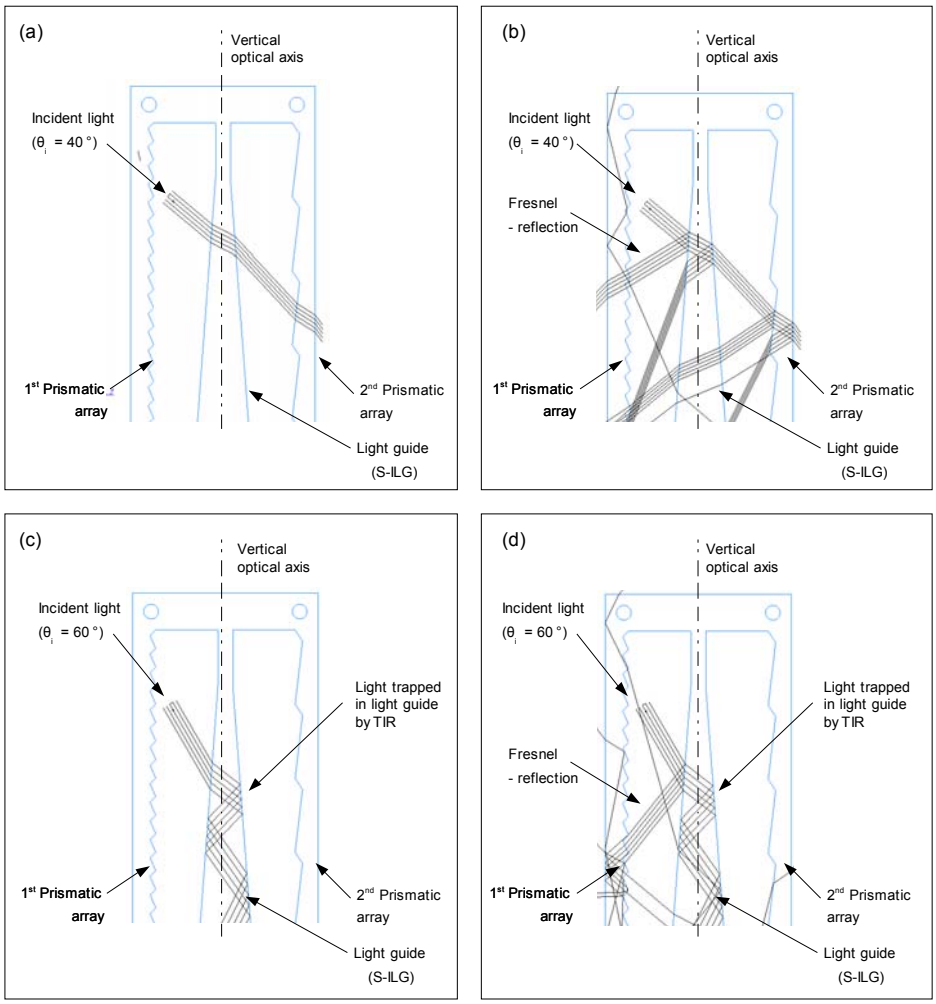

Figure 7.5 – Top section of IMPSC system showing propagation of light inside the SILG with apex angle $\alpha_{SILG} \approx 8°$. Fresnel reflections are only considered in (b) and (d).

7.3.2.1 Angular increment of light inside the SILG

The angular distribution Δθ of light propagating inside the light guide (SILG) tends to decrease in relation to the vertical optical axis of the system. The geometric concentration of radiant energy inside the light guide tends to decrease with the increase of its horizontal-section area. Larger apex angle α_{SILG} will result in more light trapped internally by TIR inside the symmetric integrated light guide (SILG). However, the continuous increment of the apex angle α_{SILG} is limited by geometric and dimensional constraints.

Light trapped inside the light guide (SILG) will increase its incident angle θ_i at the light guide surface as it propagates downwards towards the exit/extractor section of the light guide (Figure 7.6). This increase, named here as angular increment S_θ, is a direct result TIR and the geometry of the light guide, specifically of its apex angle α_{SILG}.

The sum of all angular increments TS_θ inside the light guide (SILG) can be estimated by the equation:

$$TS_\theta = T_{\theta 1} + [(\alpha_{SILG} / 2) \times N_{TIR}] \quad [7.1]$$

Where:

- TS_θ is the total angular increment;
- $T_{\theta 1}$ is the angular increment resulted from the first total internal reflection;
- $\alpha_{SILG} / 2$ corresponds to half of the light guide (SILG) apex angle (α_{SILG}); and
- N_{TIR} is the number of times that the ray of light undergoes total internal reflection (TIR).

The number of total internal reflections N_{TIR} inside the light guide varies both with the incident angle θ_i and the intersection point (or intersection section) where the ray first enters the light guide.

Figure 7.6 shows a vertical section-cut of the IMPSC-A2 system to demonstrate angular increment S_θ added to a light beam as it propagates through the light guide (SILG). The simulation parameters were: initial incident angle $\theta_i = 60°$ at the meridional plane; collimated monochromatic light $\lambda = 555nm$; solid-dielectric material refractive index n = 1.491.

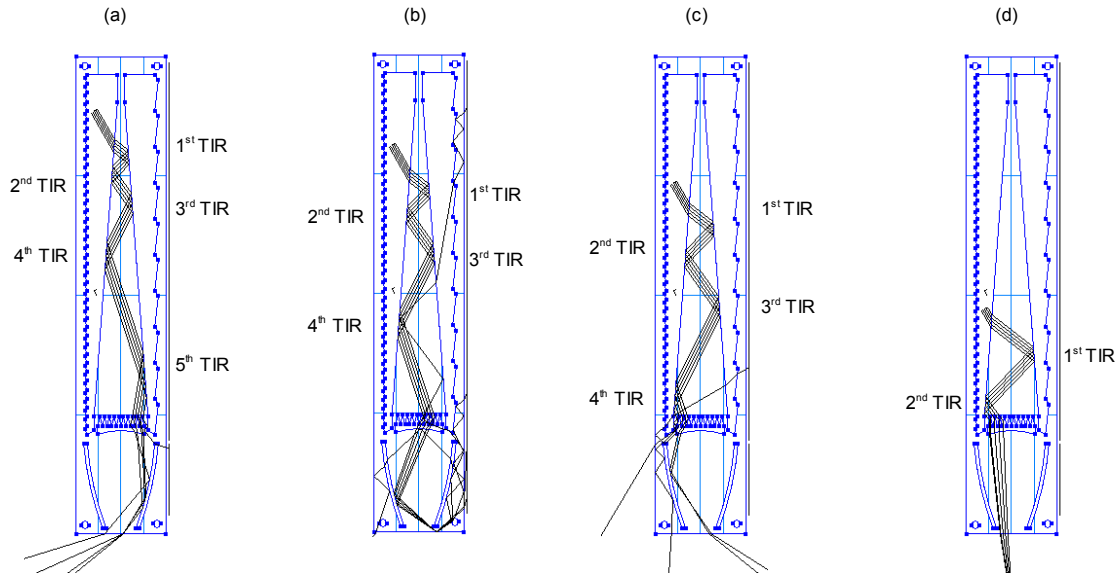

Figure 7.6 – Computer ray-tracing analysis demonstrating the angular increment S_θ added to a beam of light propagating inside the light guide (SILG) as a result of the number of total internal reflections (TIR).

Since the total angular increment TS_θ is a result of the total number of times that light is reflected internally by TIR, the rays that enters the light guide at its top-end section will reach the light guide exit/extractor section at a larger angular increment than a ray that enters its lower-end section (Figure 7.6).

The increase of the apex angle α_{SILG} leads to the decrease of Fresnel-reflection losses of incident light at the frontal surface of the light guide (SILG). At first sight this might be an effective design strategy to minimise Fresnel-reflection losses. However, the increase of the apex angle α_{SILG} also leads to a gradual decrease of the geometric concentration ratio of the light guide.

7.3.3 Light extractors

The term light extractor(s) is applied here to define a series of geometric optical features that have the function to increase the potential to extract light from the light guide (SILG).

The light extractors are polygonal-shaped elements located at the low-end section of the light guide SILG. The main function of the extractors is to “correct” the angular distribution $\Delta\theta$ of rays reaching the low-end section of the SILG. The incident angle θ_i of a ray at the inner interface of the extractor decreases as it propagates through the extractor section. The ray is extracted from the SILG-extractor section when the incident angle θ_i is lower than the critical angle θ_c.

As mentioned earlier, there are three main factors that influence the extraction of radiant energy from a medium of high refractive index n to a medium of lower refractive index n' are:

- The differences between the refractive indexes n (wavelength λ dependent);
- The geometry of the optical interface; and
- The incident angle θ_i of light at the optical interface.

Figure 7.7 shows a sequence of ray-tracing to highlight the function of the extractors. The simulation parameters were: incident angle θi = 60° at the meridional plane; collimated monochromatic light λ = 555nm; and refractive index n = 1.491. Fresnel reflections, scattering and absorption were not considered in the simulation.

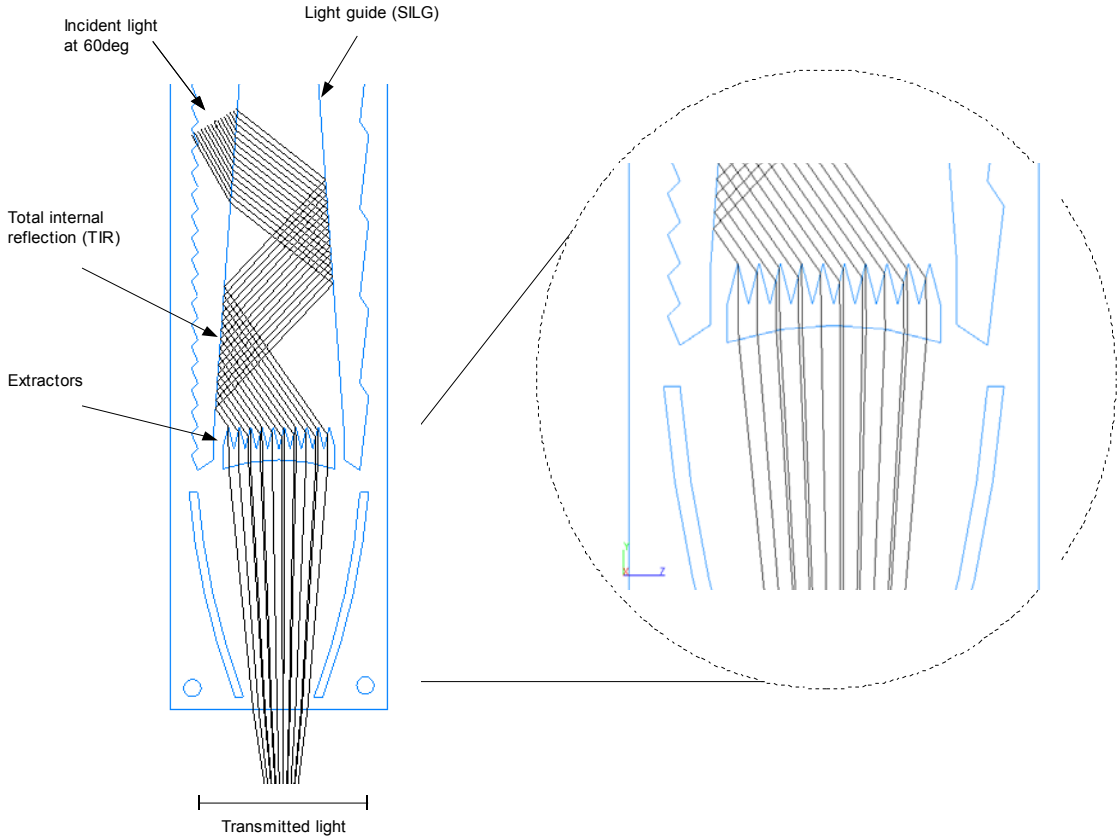

Figure 7.7 – Computer ray-tracing simulation of IMPSC-A2 system, vertical profile-section highlighting the function of the light extractors section.

7.3.4 Concentrator section: V-trough" or "CPC-type"

Light exiting from the extractors reaches the concentration section. The main function of this section is to increase the geometric concentration ratio CR of the system. The exit aperture of the IMPSC system is located at the low-end of the concentrator section. The geometric profile of the concentration section resembles a "CPC-type trough". Possible design variations include a "V-trough" and a "hyperbolic-trough" geometric profile. It is also possible to increase the final concentration ratio CR of the system by increasing the curvature of the entrance surface of the concentration section. This possibility may be interesting to concentrate sunlight on photovoltaic cells.

It is possible to increase the final concentration ratio of the system by increasing the curvature of the entrance surface of the concentration section, as demonstrated in Figure 7.8. This possibility may be interesting to apply these systems to concentrate light over photovoltaic cells. Although this was not the focus of this work, Figure 7.8c indicates possible locations for solar-photovoltaic cells.

Note that the IMPSC system with a "V-trough" concentration section is named here as IMPSC-A1. The variation with a "CPC-trough" concentration section is named as IMPSC-A2.

7.3.5 Final exit aperture

The location of the exit aperture in relation to the entrance aperture is an important issue in the design of the IMPSC systems and also in the design of the other RINSC systems (Chapters 5, 6 and 8).

The final exit aperture of the IMPSC can be located along its main vertical optical axis or, in an alternative design, at the low-end section of the device back side (parallel to the entrance aperture plane) – Figure 7.9. As mentioned earlier, if light hits the internal exit aperture interface/surface at an angle equal or larger than the critical angle θ_c of the solid-dielectric material it will undergo total internal reflection (TIR) and be reflected back into the system. The critical angle θ_c of PMMA for $\lambda = 555nm$ is $\theta_c \approx 42°$. Considering the entire visible spectrum, the critical angle θ_c of PMMA varies from $\theta_c \approx 41.7°$ (for $\lambda = 400nm$) to $\theta_c \approx 42.35°$ (for $\lambda = 780nm$).

Therefore the geometry and the surface finishing quality of the exit aperture interface have an important influence upon the optical efficiency of the system. Rough surfaces will lead to more losses due to scattering.

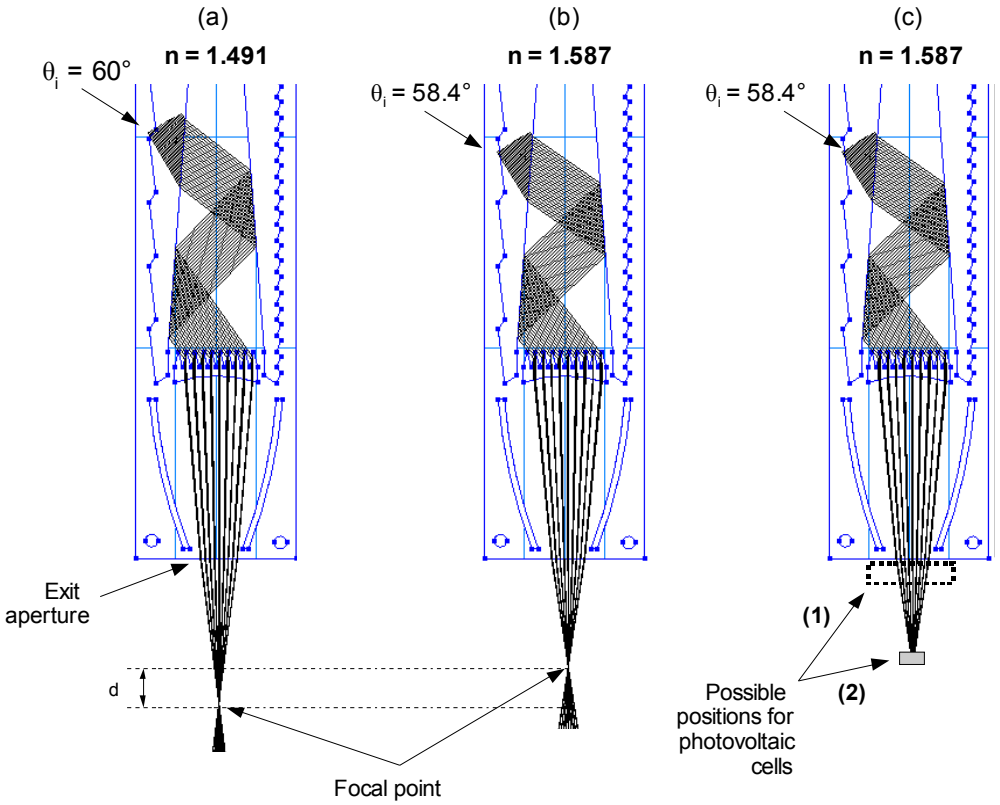

Figure 7.8 – Ray-tracing analysis showing the variation the distance of the focal point (or focal line) due to the refractive index (a) and (b). Two possible locations for photovoltaic cells are indicated in (c). System: IMPSC-A2.

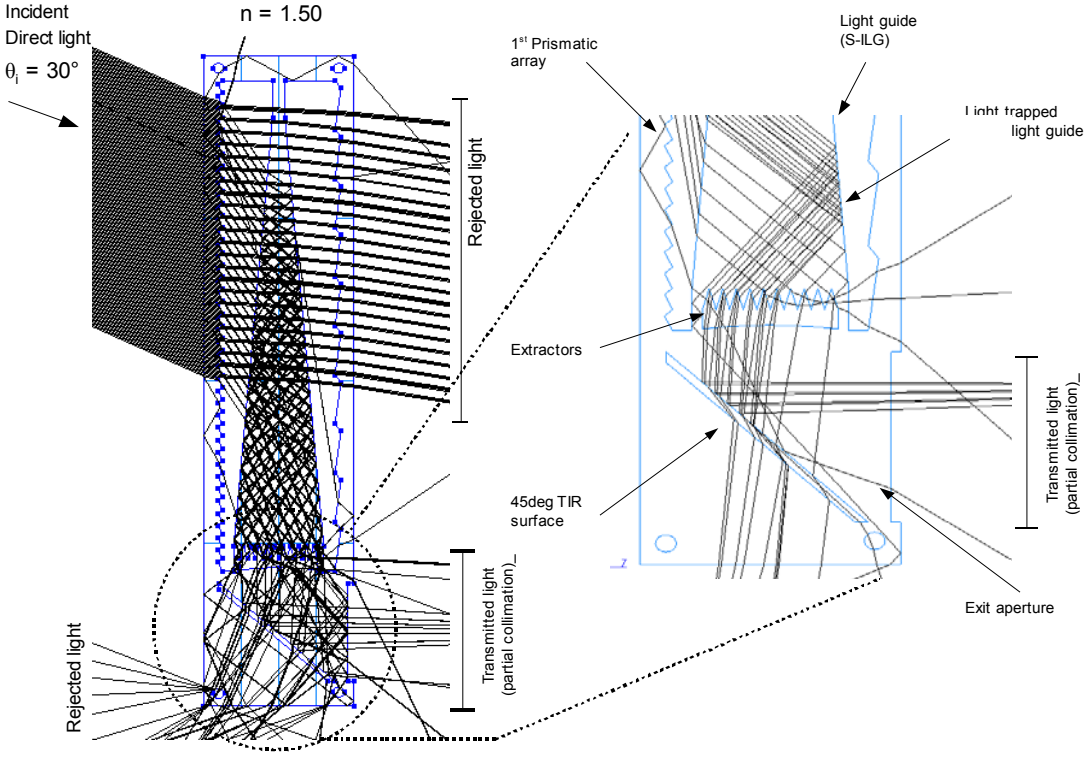

Figure 7.9 – Ray-tracing analysis showing the IMPSC-A3 concept with a 45° TIR surface and an exit aperture.

7.4 IMPSC with double symmetrical-integrated-light-guide (IMPSC-D)

A possible design variation of the IMPSC system considers the inclusion of a second light guide parallel to the first one. This variation is named IMPSC-D, with double symmetrical-integrated-light-guide (D-SILG). In the example presented here, both light guides D-SILG have apex angles $\alpha_{D\text{-}SILG}$ = 4°, corresponding to half of the apex angle α_{SILG} = 8°of the single light guide IMPSC systems described earlier.

Figure 7.10 shows a sequence of computer ray-tracing simulations for two design concepts for the IMPSC-D system. The working principle of the IMPSC-D systems is basically the same as previous IMPSC systems described previously.

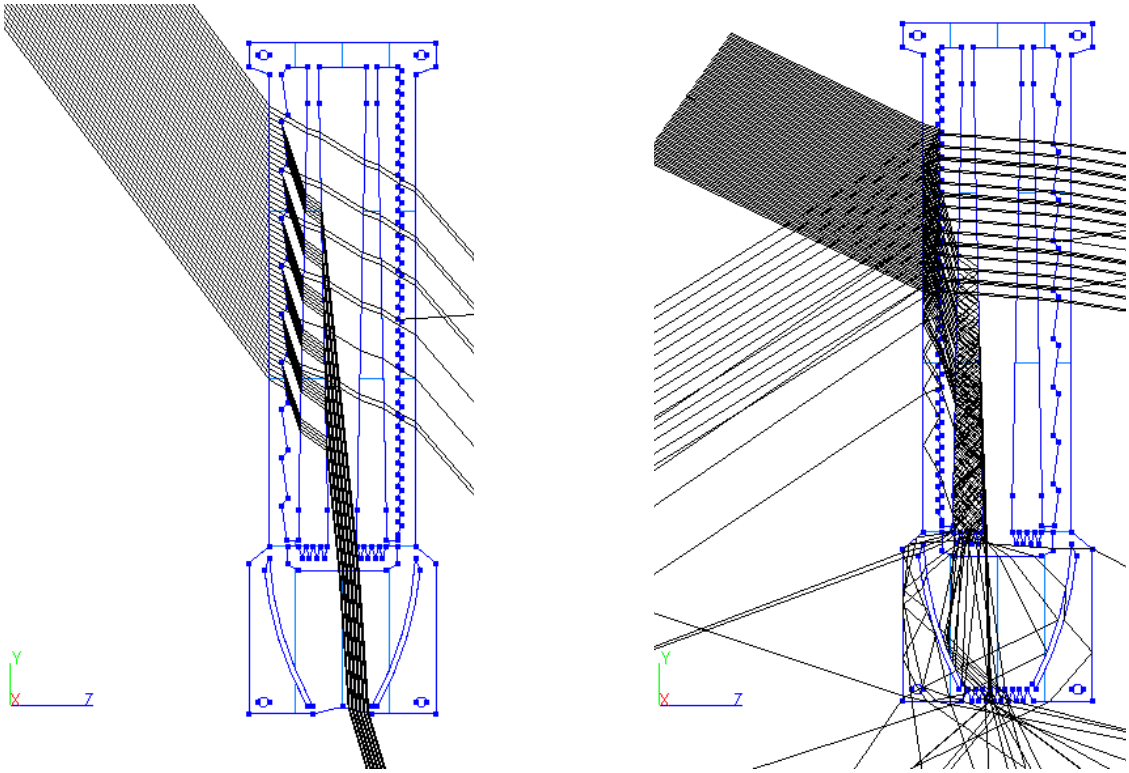

Figure 7.10 – IMPSC-D systems with double symmetrical-integrated-light-guide (D-SILG). System parameters: $\alpha_{D\text{-}SILG}$ = 4°.

7.5 Computer ray-trace analysis and simulations for IMPSC systems

A series of computer simulations was performed in order to analyse the performance of the IMPSC systems. OptiCAD® optical specialist programme was used.

Figure 7.11 presents the results for a series of ray-tracing simulations conducted with OptiCAD® programme for the IMPSC-A2-(LA) system. Note that "(LA)" refers to the side of the IMPSC-A2 system with "large apex angle", which in this case is

α ≈ 24°. Figure 7.12 presents the results for a series of ray-tracing simulations conducted with OptiCAD® programme for the IMPSC-A2-(SA) system. Note that "(SA)" refers to the side of the IMPSC-A2 system with "small apex angle", which in this case is α ≈ 8°. The simulation parameters adopted in this analysis are the same for all the simulations in Figure 7.11 and Figure 7.12.

In simulation 1 (Figures 7.11a and 7.12a) Fresnel reflection, scattering and absorption were not included in the analysis. Simulation 2 (Figure 7.11b and 7.12b) plots the results considering Fresnel reflections. Simulation 3 (Figures 7.11c and 7.12c) plots a more realistic simulation where Fresnel reflections, scattering and absorption are considered in the analysis. Figures 7.11d and 7.12d compare the previous respective simulations. The physical parameters considered in all simulations of Figure 7.11 and Figure 7.12 are: incident monochromatic light (λ=555nm) at meridional plane; solid-dielectric material with refractive index n=1,491.

Figure 7.13 compares the results of the computer ray-tracing analysis. A virtual radiometer is attached to the exit aperture of the IMPSC CAD model to measure its transmission efficiency TE. The simulation considered a beam (10.000 rays) of collimated monochromatic light (λ = 555nm) incident at the frontal entrance aperture of the IMPSC system. The incident angle θ_i, at the entrance aperture (meridional plane), varies from $\theta_i = 0°$ to $\theta_i = 80°$.

Note in Figure 7.13 that the difference between the two transmission efficiency T_E (%) curves plotted in the graph is a result of the apex angles α of the prismatic array that is facing the incident beam of direct light. This provides two different ranges of acceptance angles θ_{accept} for the system. The first curve (dashed line), peaking at $T_E \approx 21\%$ for $\theta i \approx 23°$, results from the situation where the second prismatic array (PA2) with an apex angle $\alpha_{PA2} = 24°$ is considered to be the entrance aperture of the system. The second curve (solid line), peaking at $T_E \approx 26.8\%$ for $\theta_i \approx 58°$, results from the situation where the first prismatic array (PA1) with an apex angle $\alpha_{PA1} = 8°$ is considered as the entrance aperture of the system. In both cases, the light guide (SILG) apex angle $\alpha_{SILG} = 8°$. Fresnel reflections and surface scattering were also computed in the simulation. Measurements are taken by attaching a virtual radiometer/detector at the exit aperture of the IMPSC computer model.

Note that in simulations Figure 7.11 to 7.13, the refractive index was specified as n = 1.491 (for λ = 555nm)

(a)

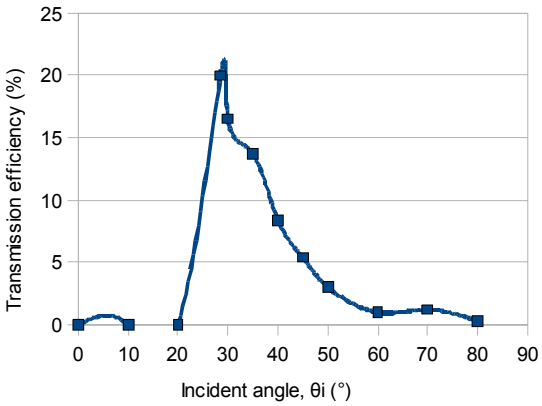

(c)

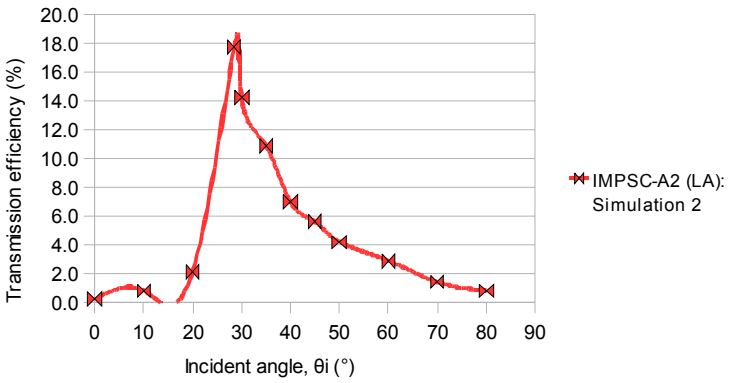

(b)

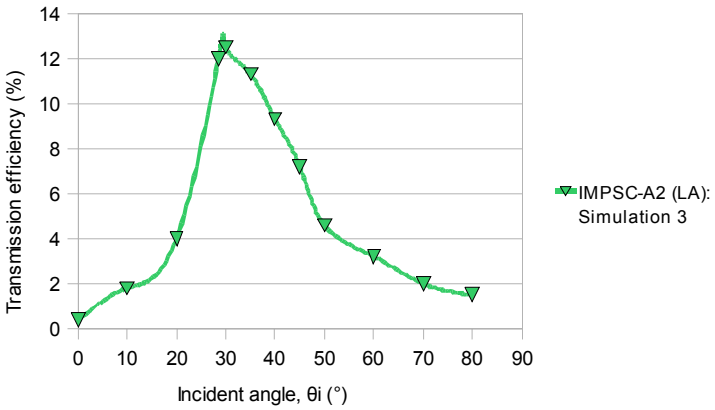

(d)

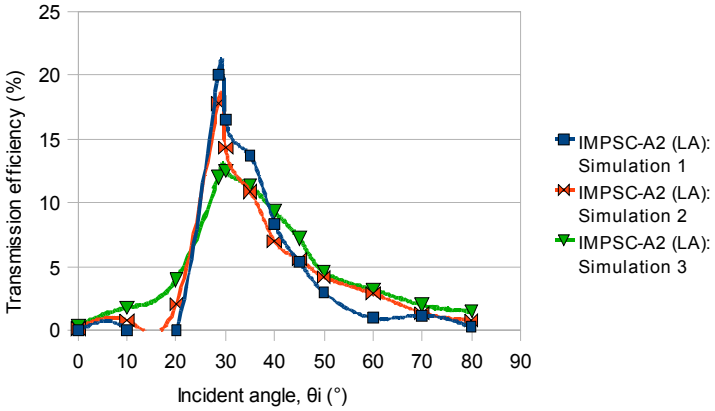

Figure 7.11 – Results of OptiCAD simulations for IMPSC-A2 (LA) system. (a) results for Simulation 1; (b) results for Simulation 2; (c) results for Simulation 3; (d) comparison between the previous simulations.

(a)

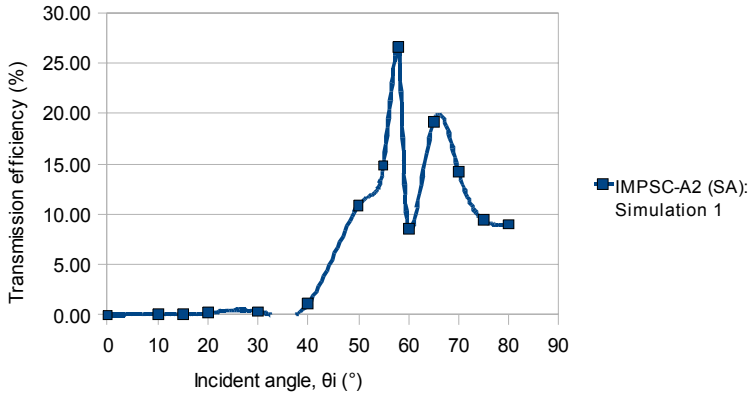

(c)

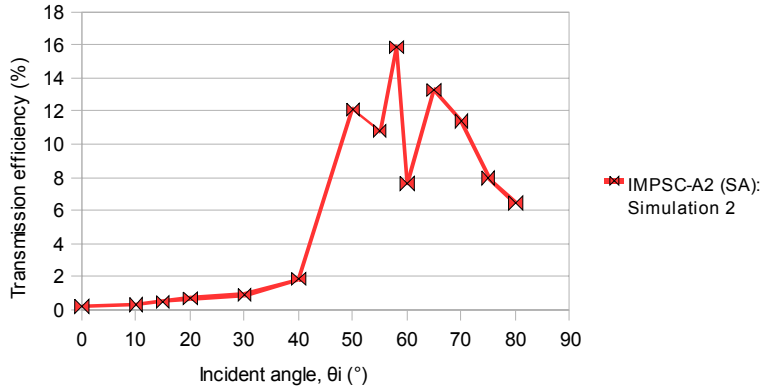

(b)

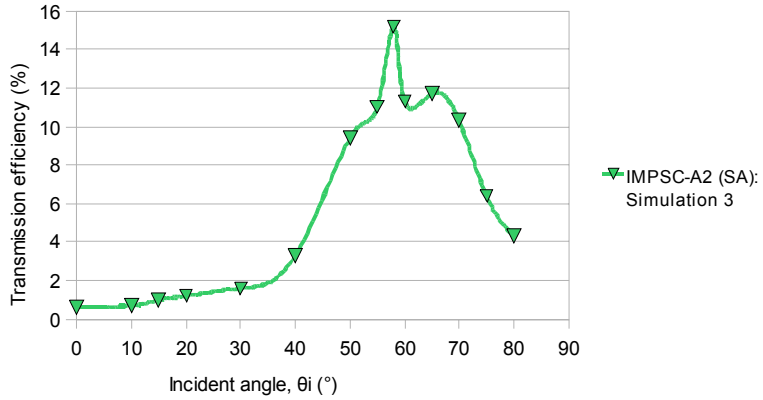

(d)

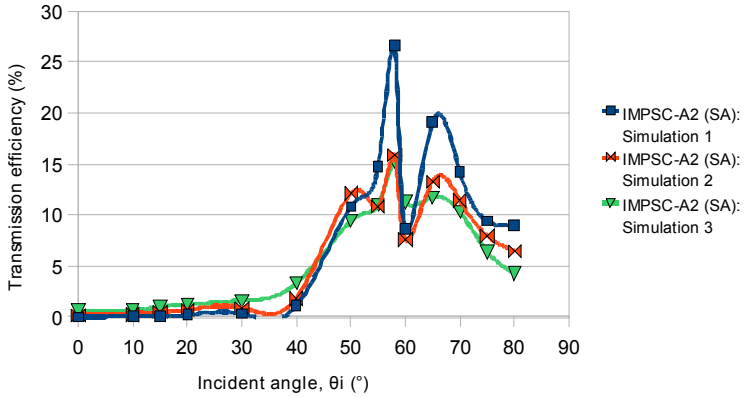

.

Figure 7.12 – Results of OptiCAD simulations for IMPSC-A2 (SA) system. (a) results for Simulation 1; (b) results for Simulation 2; (c) results for Simulation 3; (d) comparison between the previous simulations.

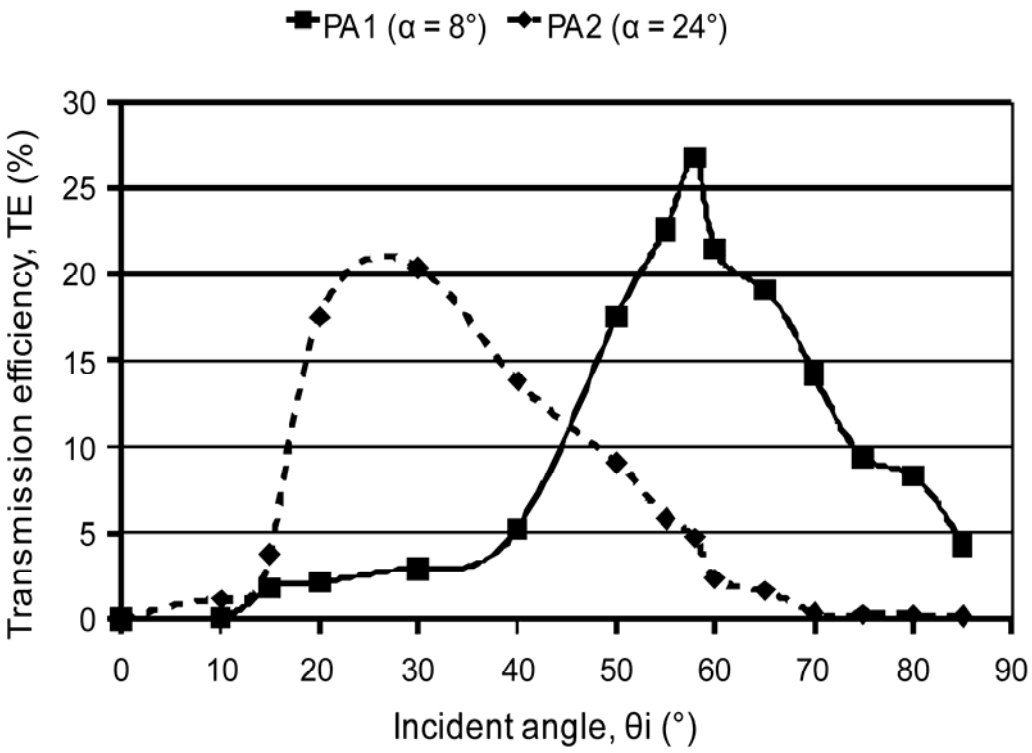

Figure 7.13 – Comparison between ray-tracing analysis results for the IMPSC-A2-(LA) system (PA2, α=24°), dashed line, and the IMPSC-A2-SA (PA2, α=8°), solid line.

7.6 Laser-cut prototyping and surface analysis of IMPSC systems

A series of IMPSC and IMPSC-D laser-cutter demonstration prototypes made of clear PMMA (5mm thick) are displayed in Figures 7.14 and 7.15. It is important to note that the prototypes represent only a vertical cross-section profile of the final systems.

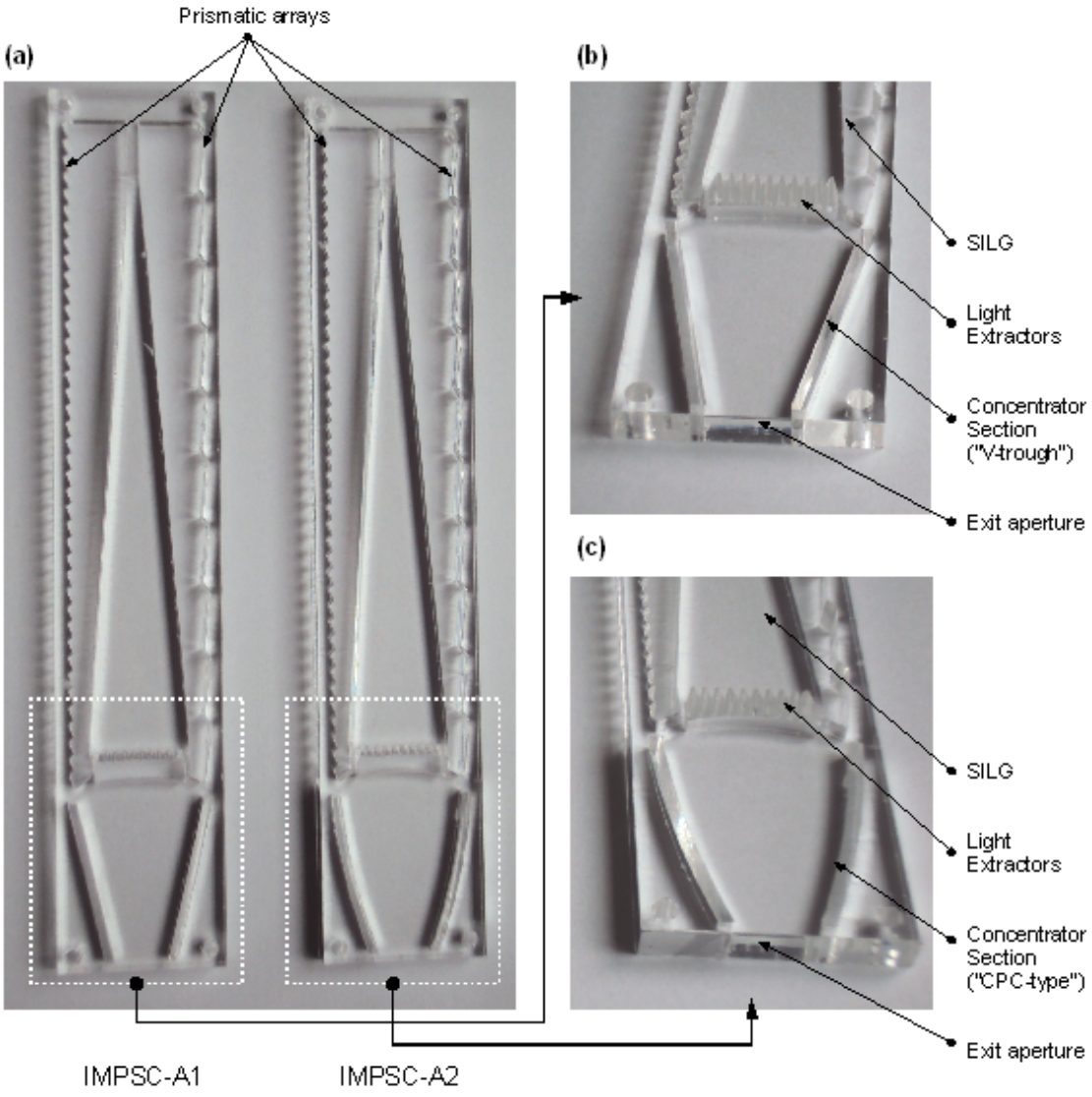

Figure 7.14 – IMPSC demonstration prototypes manufactured by laser ablation process.

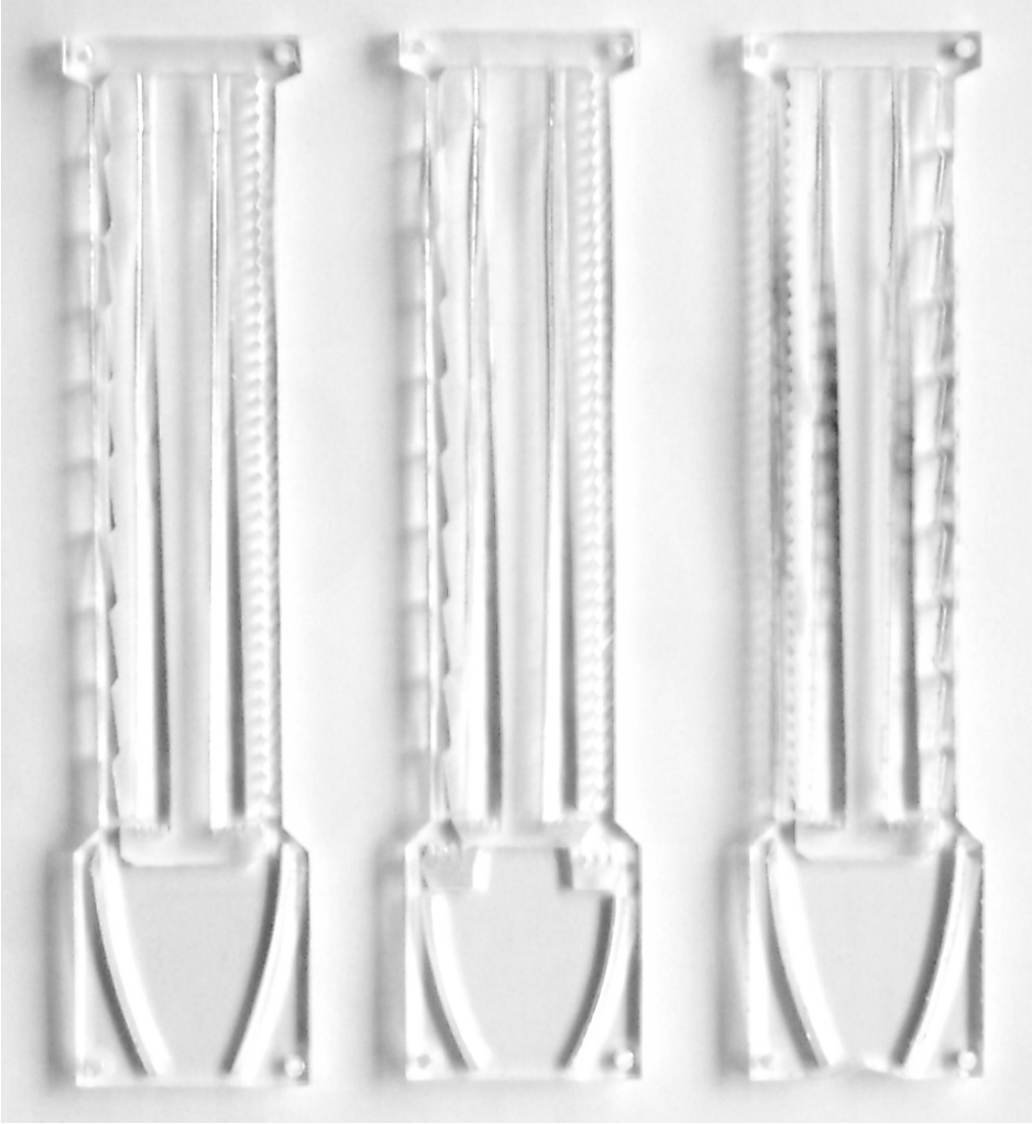

Figure 7.15 – IMPSC-D demonstration prototype sections (with double symmetrical integrated light guide, D-SILG).

Figure 7.16 displays the results of the surface quality assessment of the light guide surface of the IMPSC-D system. A close-up view of the surface of the light guide can be seen in Figure 7.16(a). A line profile is vertically applied across the centre of the light guide (Fig.7.16-b). The line profile measures the contrast of light and darkness reflected from the surface. Measured values are expressed in scale of pixel intensity, where 255 represents a white pixel (maximum intensity) and 0 (zero) represents a black pixel (zero intensity). The software (NI Lab-VIEW® Vision Assistant 8.0) uses this scale to plot the line profile shown in Figure 7.16(b). This analysis provides a qualitative assessment of the surface roughness along the line profile.

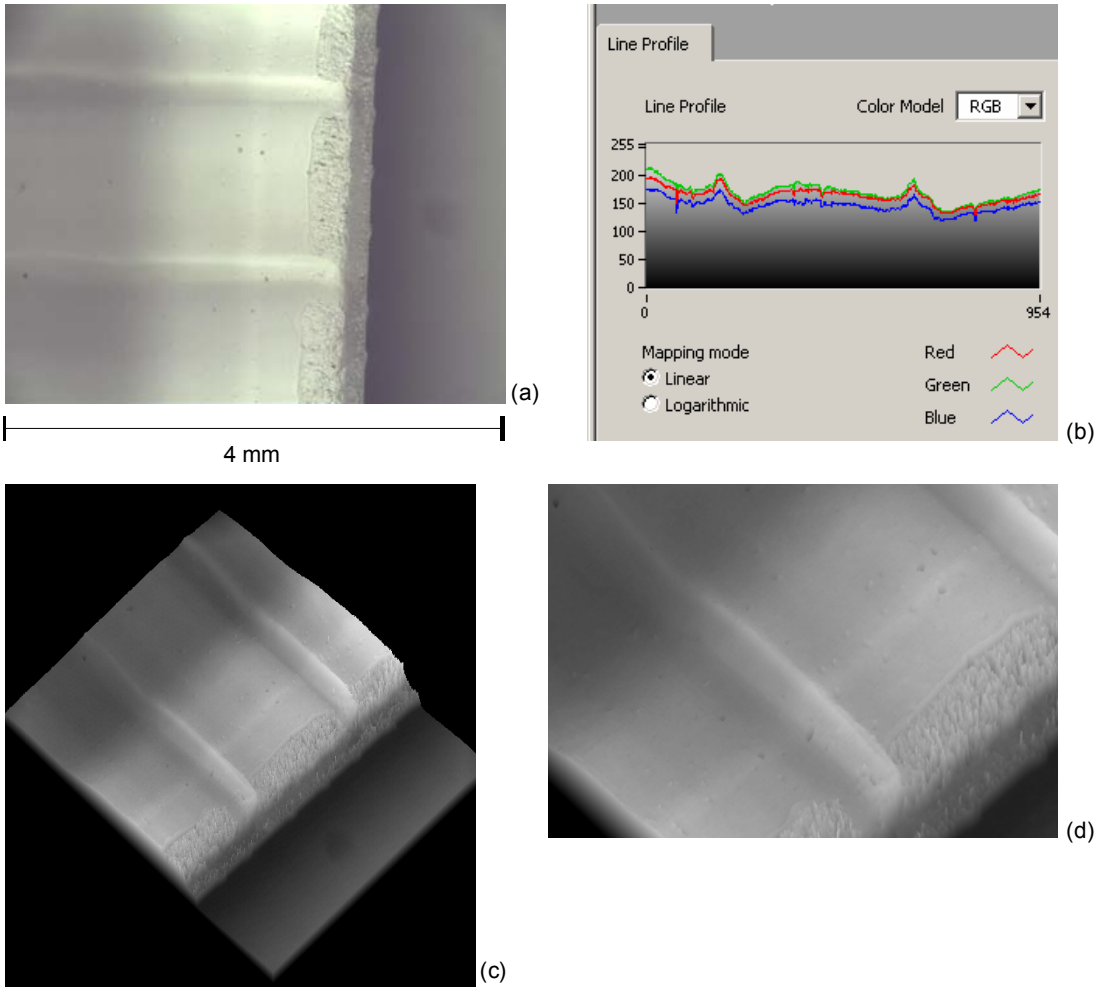

Figure 7.16 – Partial surface analysis of a section of the lateral side of the symmetrical integrated light guide (SILG) of the IMPSC-D prototype made of clear acrylic (PMMA) and manufactured by laser cutter process. A 3D topographic visualization is presented in (c) and (d).

Note that the horizontal depression lines shown in Figure 7.16(a), and in more detail in Figure 7.16(c) and Figure 7.16(d), are formed by the laser ablation process. These depressions are displaced about 2mm from each other. These manufacturing errors have negative consequences for the expected light path through the prototype. For example, light that is trapped by total internal reflection (TIR) may escape from the light guide when it encounters defects along the light guide surfaces. This also may lead to light losses due to leakage and backscattering for light propagating inside the light guide (SILG).

Figure 7.17 presents a zoom-view that details the surface quality around the extractors section at the lower-end of the light guide. Note the formation of “melted bubbles” at the borders of the extractors generated by melted polymer. The surface quality at the lateral side of the extractors also presents a rough finishing as a result of the laser ablation process.

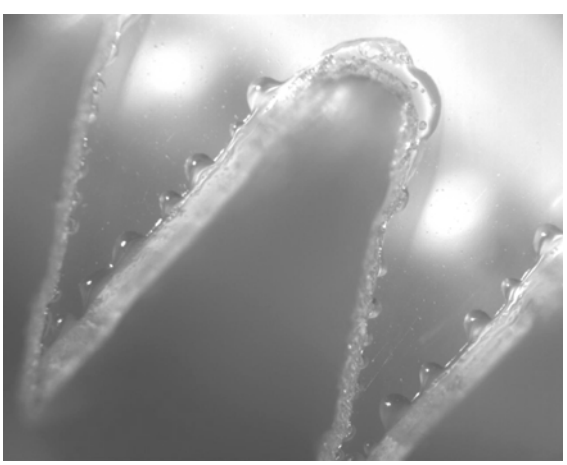
(a)
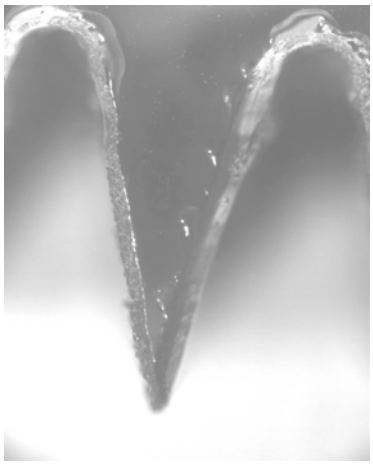
(b)

Figure 7.17 – PMMA laser-cut prototype. Details of light guide extractor geometry and surface quality. The width of image (a) corresponds to approximately to 4mm.

As discussed in the previous chapters, the consequence of the surface and sub-surface defects caused by the laser ablation process has a negative impact upon the optical transmittance efficiency of the system. A significant portion of the incident light will not follow the expected light path through the system due to surface scattering and volume scattering losses that are believed to be significant due the high concentration of air-bubbles trapped inside the bulk of the material.

It is important to stress that these defects are strictly related to the laser ablation manufacturing process used to fabricate the prototypes for this research. Other manufacturing techniques used to produce optical components, such as injection moulding, provide far better surface quality results.

Figure 7.18 displays the results for a qualitative/quantitative assessment of the surface quality of part of the extractor section of the IMPSC-A2 prototype. The analysis is conducted with the support of the NI LabVIEW® Vision Assistant software. The central image (Figure 7.18e) shows the polygonal section of the extractor. The main surface and sub-surface defects are highlighted and counted by the programme in Figures 7.18(b), 7.18(c) and 7.18(d). A linear profile of part the lateral side of the extractor is shown in Figure 7.18(a).

Figure 7.19 plots the results for a quantitative surface analysis of the IMPSC-A2 system conducted with the Zygo® optical profiler system. The average surface roughness measured with the Zygo® optical profiler was ≈ 2-3 micrometers.

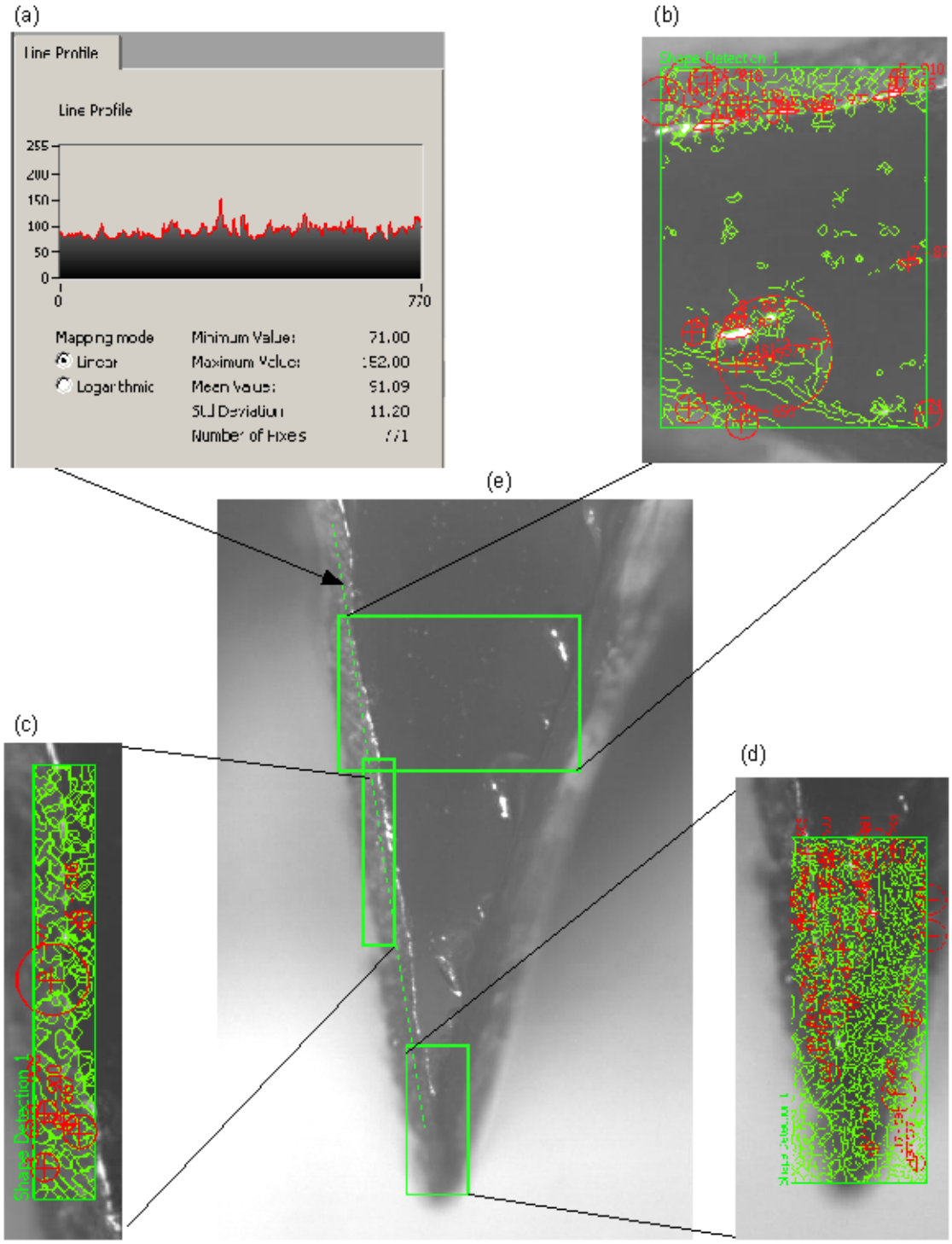

Figure 7.18 – Surface analysis of the extractor vertical profile-section of IMPSC-A2 laser-cut prototype.

(a)

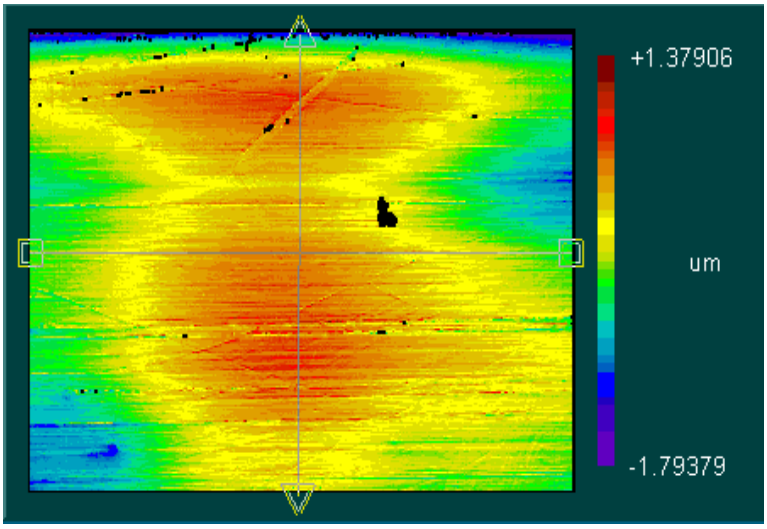

(b)

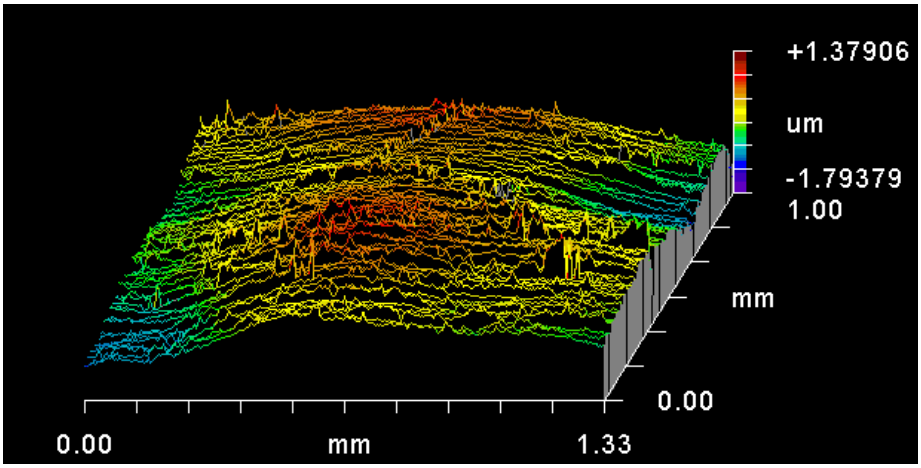

(c)

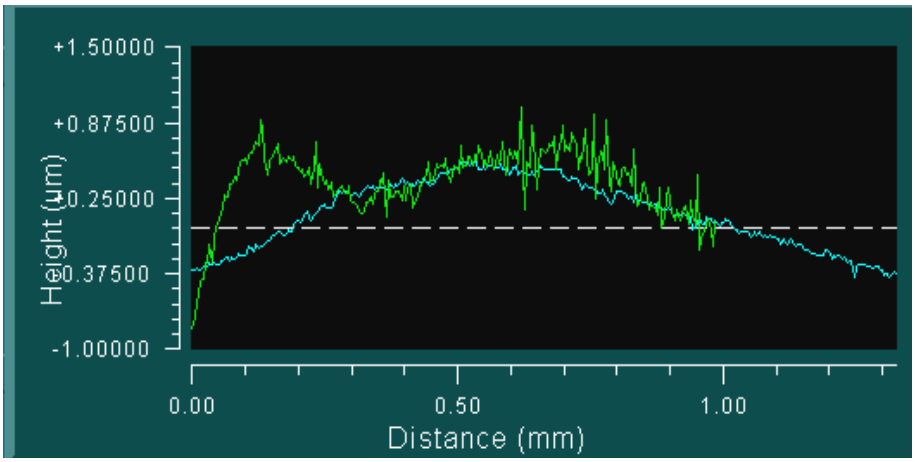

Figure 7.19 - Surface analysis of IMPSC laser-cut prototype (PMMA, 5mm thick) conducted with Zygo® surface profiler system. A 2D image of the surface is displayed in (a). A 3D view of the surface roughness is shown in (b). Graph in (c) plots the vertical line profile and the horizontal line profile of the surface roughness. Average surface roughness ≈ 2-3 micrometers.

7.7 Experimental tests of the IMPSC systems prototypes

It is important to stress that the results presented here corresponds to experimental tests done with PMMA laser-manufactured prototypes that are only 5mm thick. The prototypes serve to characterize the IMPSC systems considering incident rays at the system meridional plane. This type of characterisation is the standard procedure to define an optical system (Smith, 2000; Smith, 1997; Mouroulis and Macdonald, 1997).

7.7.1 Laboratory tests of IMPSC systems prototypes

Figure 7.20 presents three photographic images of part of the laboratory experimental tests set-up, installed over an optical table. The IMPSC section-prototype was positioned on a flat surface (matte black). In Figure 7.20 it can be seen that the light source with an attached collimator was directed towards the frontal prismatic array (entrance aperture) of the IMPSC section prototype. The exit aperture of the IMPSC section-prototype was aligned with an “entrance window”, which was connected to the light pipe integrator. A series of magnetic mounts and auxiliary support apparatus were also used in the experiment set-up. The final experiment setup configuration was similar to the setup proposed by Ohno (1998) and Smith (1997).

In Figure 7.20, the artificial light source and the collimator were mounted over a pivotal arm which can be moved around a centre point. A disc-shaped angular measurement device was used to measure the angular displacement of the light source.

Figure 7.21 shows three photographic images taken during the laboratory experimental tests with the IMPSC-A2 system. Note that the brightness of the extractor section (low-end of the light guide) increases with the increase in the incident angle, meaning that more light is reaching this area. Note that a significant increase in the brightness of the light extractor section can be seen in Figure 7.21(c), when the incident angle is $\theta_i = 40°$.

Table 7.1 describes the main parameters of the IMPSC systems demonstration prototypes that were manufactured and tested in the laboratory and outdoor experimental tests.

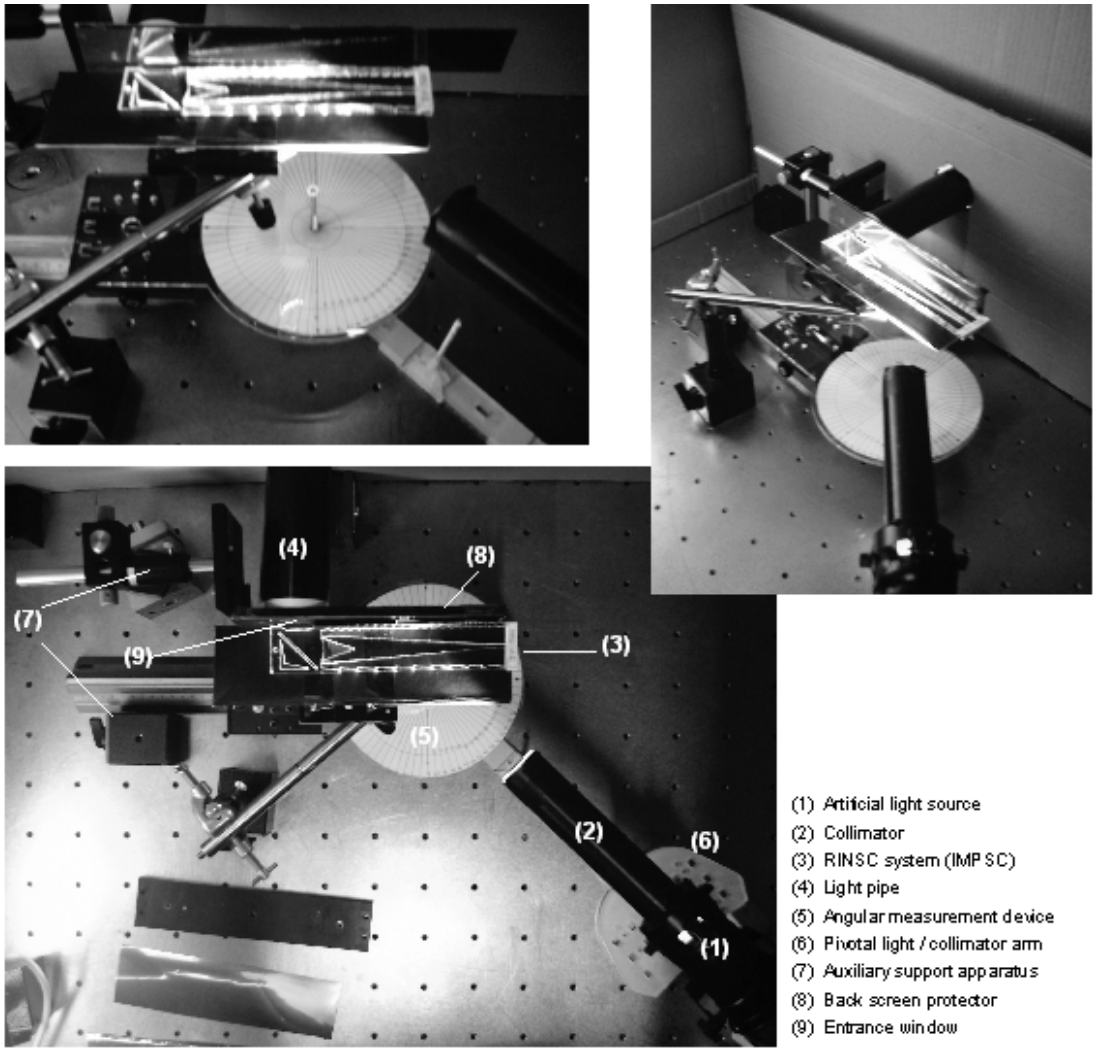

Figure 7.20 – Laboratory experiment basic set-up configuration for the IMPSC systems.

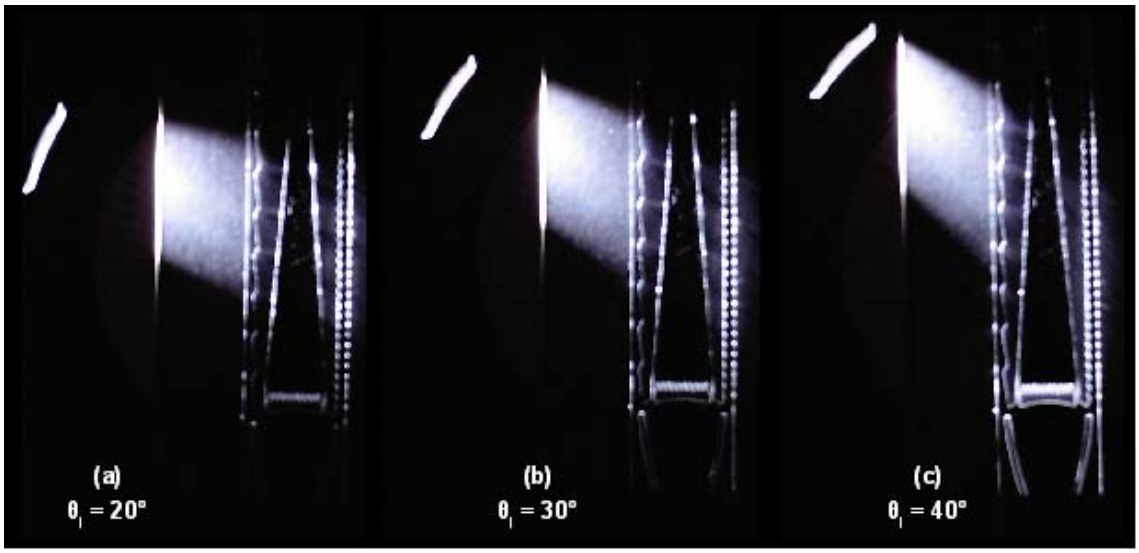

Figure 7.21 – Sequence of laboratory tests with IMPSC-A2 system. A beam of white light (wavelengths; power; colour temperature) at three different incident angles at 20°, 30°, and 40° is directed from left-to-right.

Table 7.1 – IMPSC systems demonstration prototypes main parameters and description.

IMPSC SYSTEMS	PARAMETERS (of demonstration prototypes)						Brief description / observations	SILG (light guide)
				(in mm)				
	1st PA apex angle	2nd PA apex angle	SILG apex angle	Entrance area A1	Exit area A2	Geome. Con. C_R		
IMPSC–A1 (SA)*	8°	24°	4°	150x5	12x5	12.5		single SILG
IMPSC–A1 (LA)**	24°	8°	8.5°	150x5	12x5	12.5		single SILG
IMPSC–A1 (SA)+BR-Alu	8°	24°	8.5°	150x5	12x5	12.5	includes back reflective surface	single SILG
IMPSC– A1 (SA)+BRA+DLC	8°	24°	8.5°	150x5	12x5	12.5	includes back reflective surface + DLC ***	single SILG
IMPSC–A2 (SA)	8°	24°	8.5°	150x5	12x5	12.5		single SILG
IMPSC–A2 (LA)	24°	8°	8.5°	150x5	12x5	12.5		single SILG
IMPSC–A2 (SA)+LGR	8°	24°	8.5°	150x5	12x5	12.5	includes reflective surface at light guide	single SILG
IMPSC–A2 (SA)+LGR+(DLC)	8°	24°	8.5°	150x5	12x5	12.5	includes reflective surface at light guide + DLC	single SILG
IMPSC–A3 (SA)	8°	24°	8.5°	150x5	21x5	7.14		single SILG
IMPSC–D1 (SA)	8°	24°	4°	150x5	14x5	10.7		double SILG
IMPSC–D1 (LA)	24°	8°	4°	150x5	14x5	10.7		double SILG
IMPSC–D1 (SA)+BR-Alu	8°	24°	4°	150x5	14x5	10.7	includes back reflective surface	double SILG
IMPSC–D2 (SA)	8°	24°	4°	150x5	14x5	10.7		double SILG
IMPSC–D2 (LA)	24°	8°	4°	150x5	14x5	10.7		double SILG

(*) SA = smaller apex angle α prismatic array facing direct light
(**) LA = larger apex angle α prismatic array facing direct light
(***) DLC = deconcentrator light cone

The results of laboratory measurements of illuminance output E_{out} (measured in lux, lx) as a function of the incident angle θ_i for the IMPSC-A1 and IMPSC-A2 systems are plotted in Figure 7.22 to Figure 7.25.

Figure 7.23 compares the illuminance output E_{out}, measured in lux (lx), for three possible configurations of the IMPSC-A2 system. The capital letters inside the brackets relates to “small apex” angle α, meaning that the frontal surface/entrance aperture corresponds to the prismatic array with small apex angle prisms. The IMPSC-A2 (SA) + LGR system corresponds to the IMPSC-A2 system with a reflective-mirror sheet (aluminium) positioned at the back of the light guide. This graph shows that an inclusion of a reflective surface at the back of the light guide surface has a significant impact on the efficiency of the IMPSC-A2 system. The illuminance output E_{out} is significantly higher for an incident angle θ_i between $\theta_i = 30°$ and $\theta_i = 50°$ at the system optical meridional plane.

Figures 7.24 and Figure 7.25 present the results of laboratory measurements of illuminance output E_{out} (measured in lux, lx) for the IMPSC-D1 and IMPSC-D2 systems.

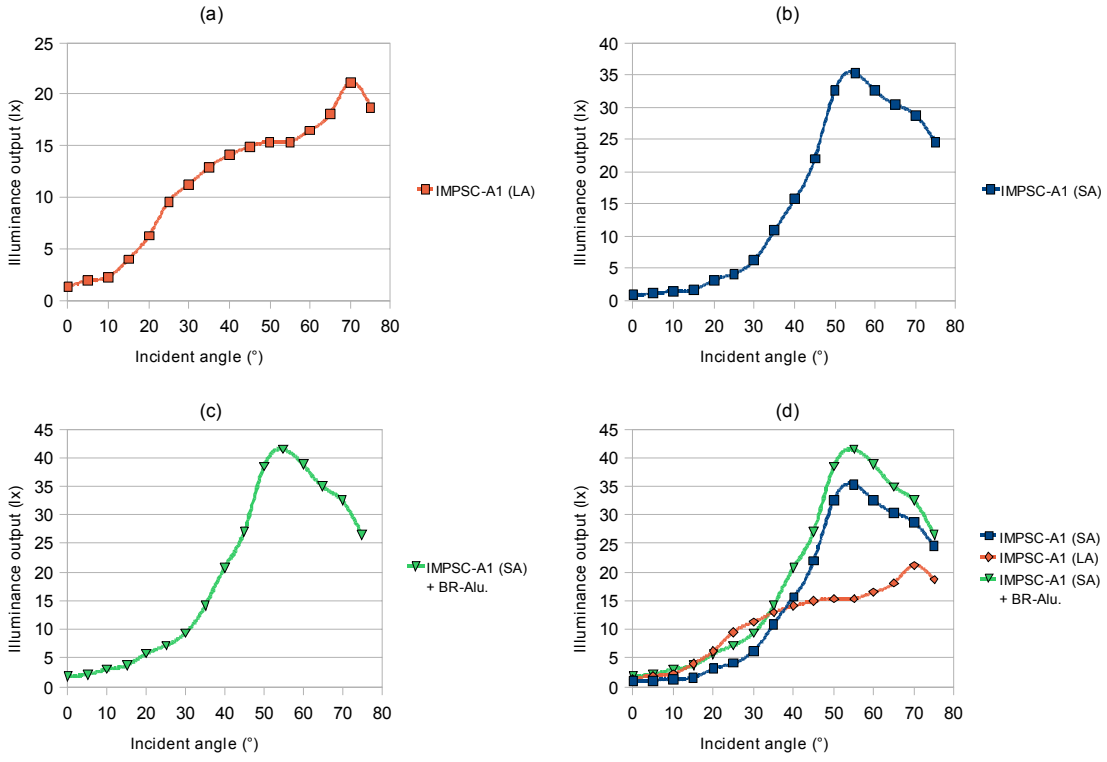

Figure 7.22 – Partial laboratory results for IMPSC-A1 systems, illuminance output (lx) as a function of incident angle (°) of direct light at the meridional plane. Light beam directed towards the centre-mid-section of system. Light pipe: hollow aluminium sheet-tube: length = 1000mm; diameter = 50mm.

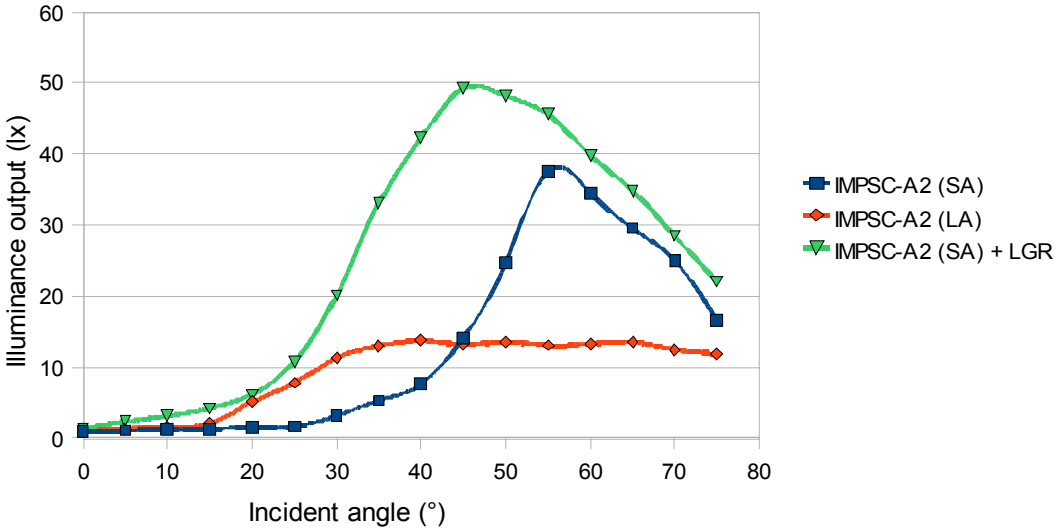

Figure 7.23 – Partial laboratory results for IMPSC-A2 systems, illuminance output (lx) as a function of incident angle (°) of direct light at the meridional plane. Light beam directed towards the centre-mid-section of system. Light pipe: hollow aluminium sheet-tube: length = 1000mm; diameter = 50mm.

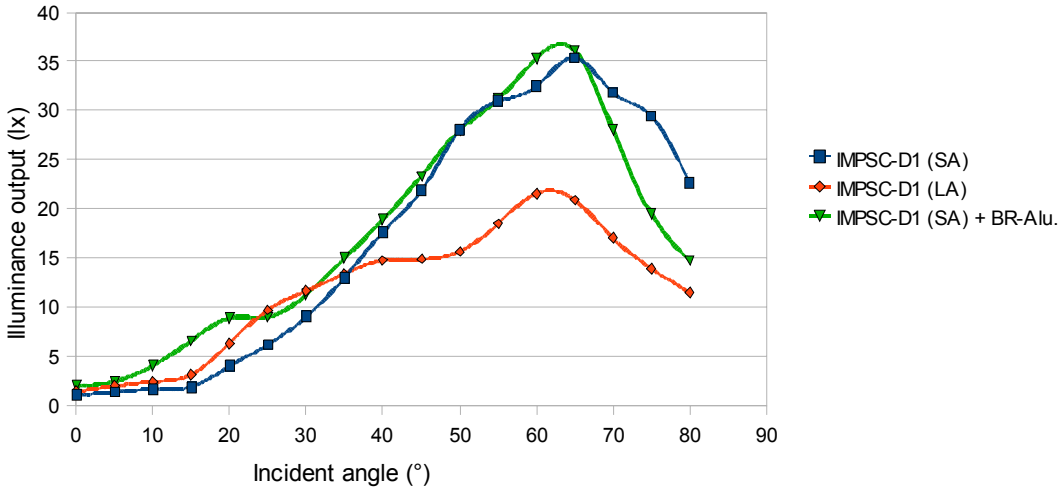

Figure 7.24 – Partial laboratory results for IMPSC-D1 systems, illuminance output (lx) as a function of incident angle (°) of direct light at the meridional plane. Light beam directed towards the centre-mid-section of system. Light pipe: hollow aluminium sheet-tube: length = 1000mm; diameter = 50mm.

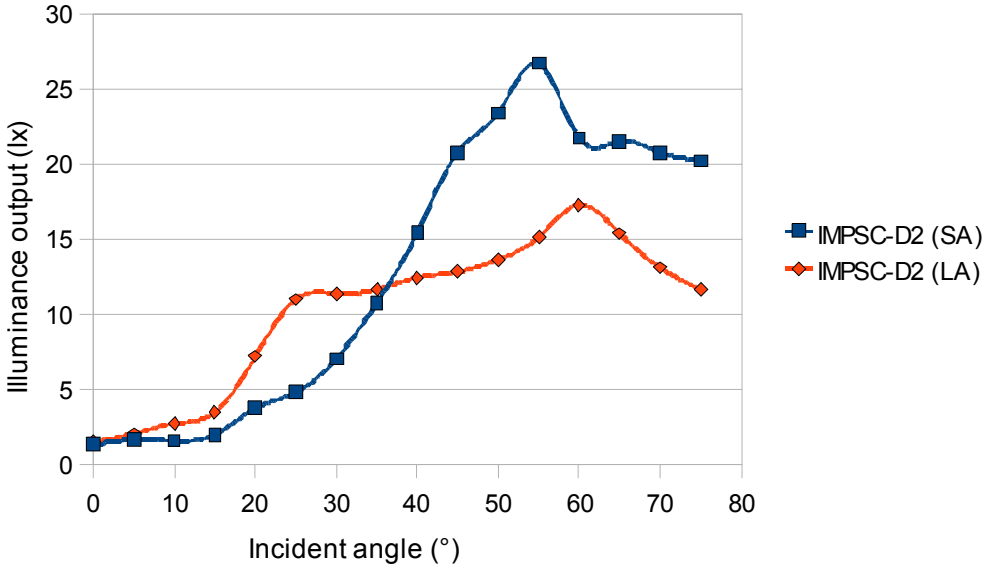

Figure 7.25 – Partial laboratory results for IMPSC-D2 systems illuminance output (lx) as a function of incident angle (°) of direct light at the meridional plane. Light beam directed towards the centre-mid-section of system. Light pipe: hollow aluminium sheet-tube: length = 1000mm; diameter = 50mm.

Figures 7.26 to 7.31 presents the results for the Illuminance output E_{out} (lx) and corresponding transmission efficiencies T_E for the IMPSC-A1(SA) and IMPSC-A1(LA) systems as a function of the length of the hollow light pipe (mm) coupled to their exit apertures. Measurements were taken considering the incident light on the meridional plane of the system varying from θ_i = 5° to θ_i = 75°. In Figure 7.26 the maximum illuminance output (lx) peaks at approximately 137lx for an incident angle θ_i = 55°, measured at a distance of 50mm from the exit aperture of the IMPSC-A1(SA) system. The measured peak transmission efficiency T_E for the IMPSC-A1(SA) laser-cut prototype (PMMA, 5mm thick) was $T_E \approx 3\%$ at a distance of 100mm.

Figure 7.32 and Figure 7.33 plot the laboratory results for illuminance output E_{out} (lx) and the transmission efficiency T_E for the IMPSC-D1(SA) laser-cut prototype (PMMA, 5mm thick).

The light pipes were made by folding flexible polyester-aluminium sheets. The lengths are: 50mm, 100mm, 200mm, 300mm, 500mm, 1000mm and 1500mm. All light pipes have the same diameter Ø = 50mm.

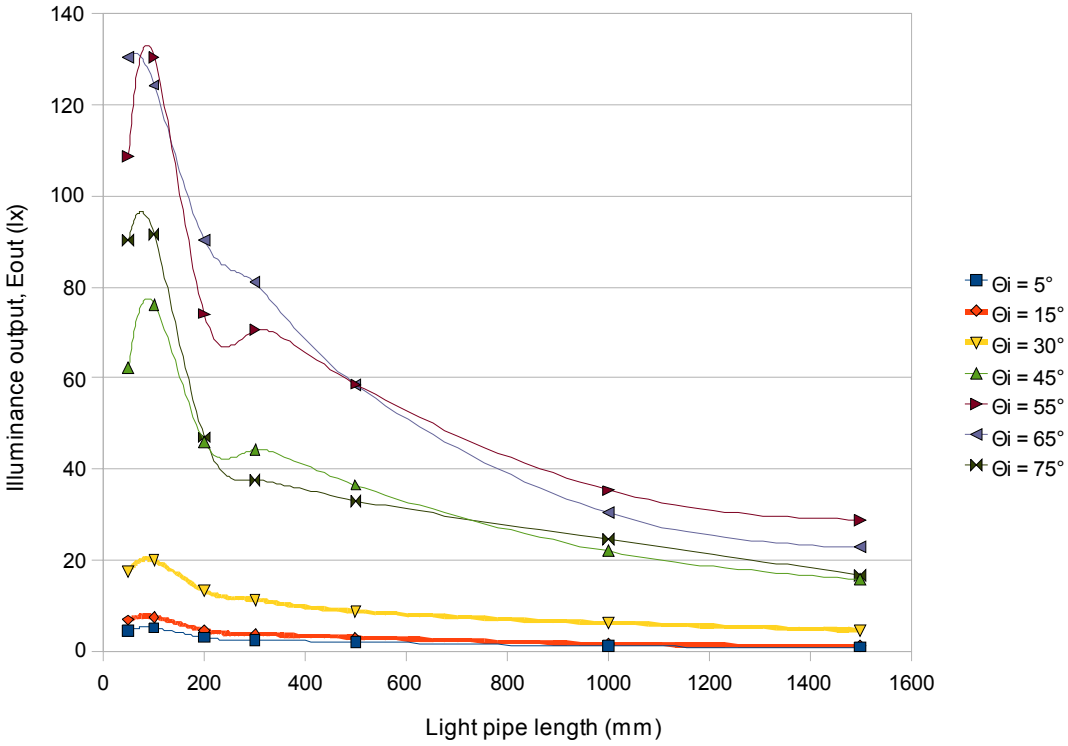

Figure 7.26 – Illuminance output E_{out} of the IMPSC-A1(SA) system demonstration prototype. Measurements taken at the end of a series of hollow light pipes made of folded aluminium sheet, with Ø = 50mm and length varying from L = 50mm to 1500mm.

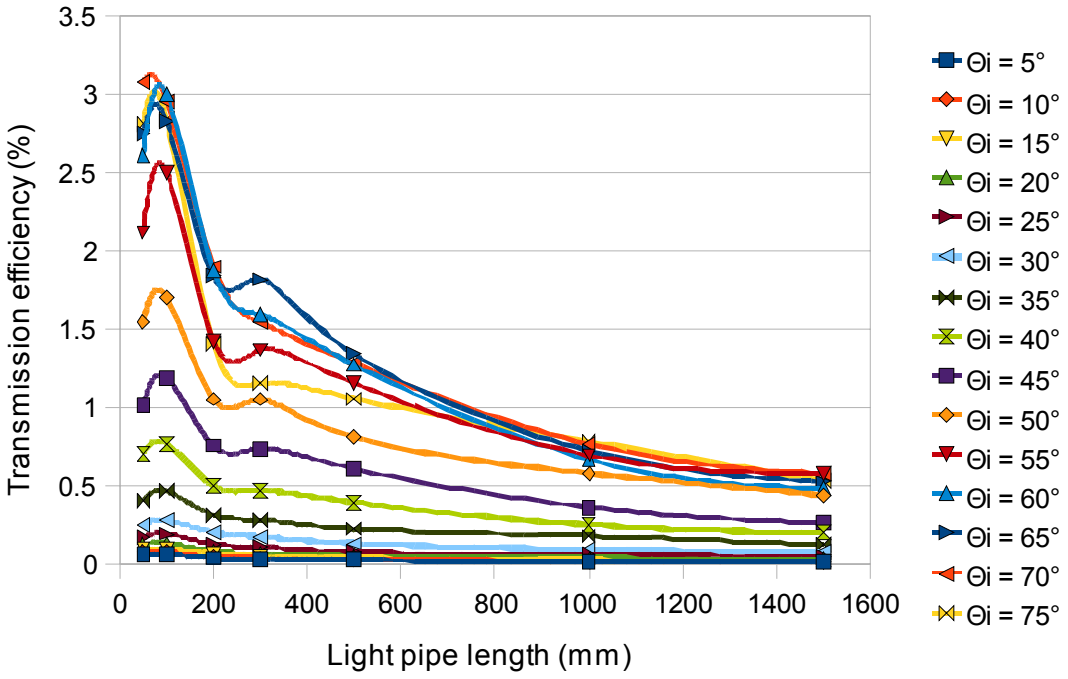

Figure 7.27– Transmission efficiency T_E of the IMPSC-A1(SA) system demonstration prototype. Measurements taken at the end of a series of hollow light pipes made of folded aluminium sheet, with Ø = 50mm and length varying from L = 50mm to 1500mm.

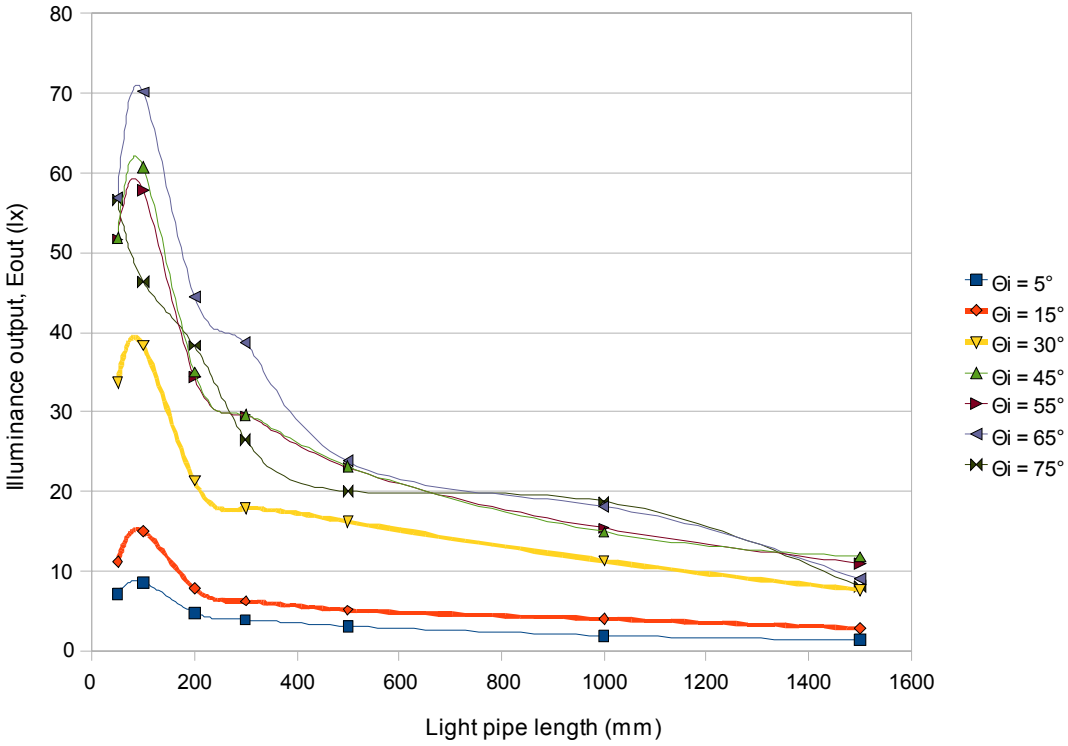

Figure 7.28 – Illuminance output E_{out} of the IMPSC-A1(LA) system demonstration prototype. Measurements taken at the end of a series of hollow light pipes made of folded aluminium sheet, with Ø = 50mm and length varying from L = 50mm to 1500mm.

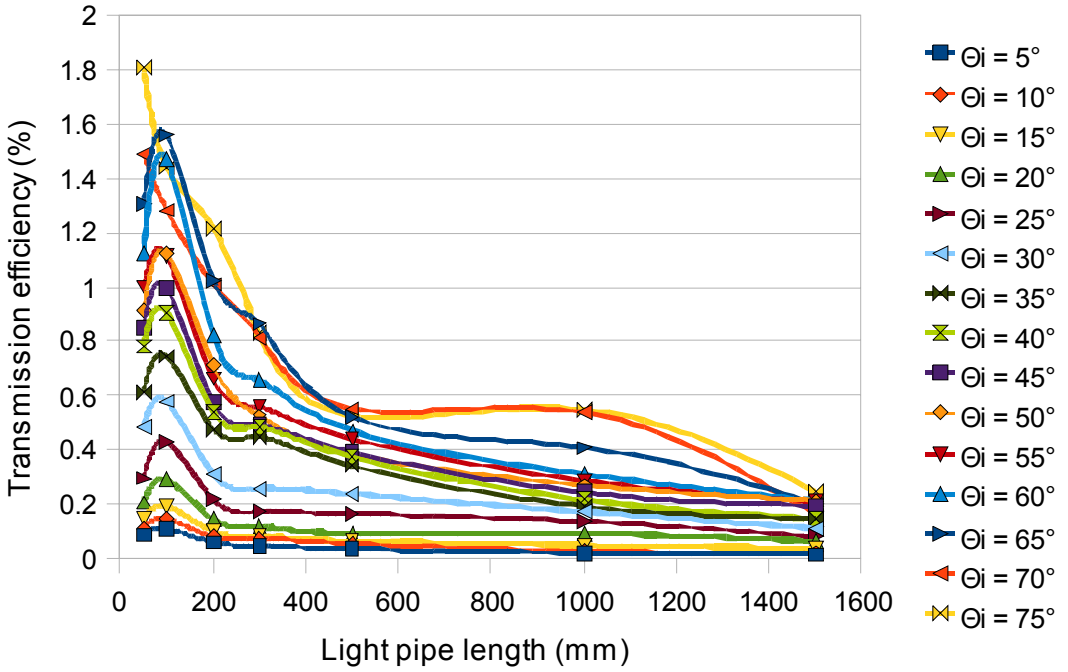

Figure 7.29 – Transmission efficiency T_E of the IMPSC-A1(LA) system demonstration prototype. Measurements taken at the end of a series of hollow light pipes made of folded aluminium sheet, with Ø = 50mm and length varying from L = 50mm to 1500mm.

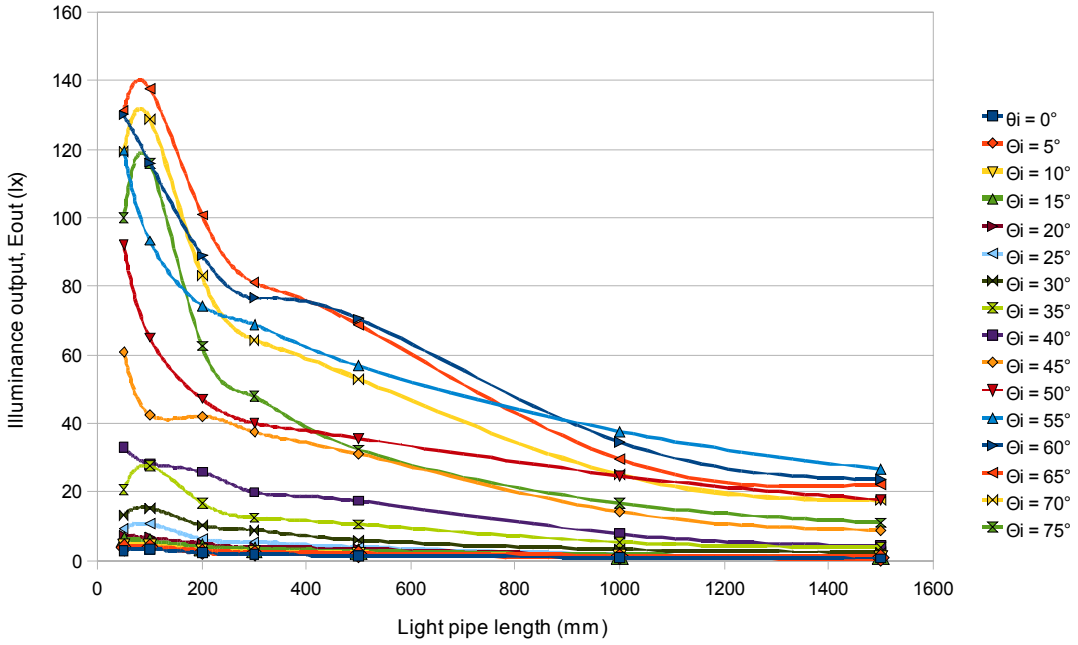

Figure 7.30 – Illuminance output E_{out} of the IMPSC-A2(SA) system demonstration prototype. Measurements taken at the end of a series of hollow light pipes made of folded aluminium sheet, with Ø = 50mm and length varying from L = 50mm to 1500mm.

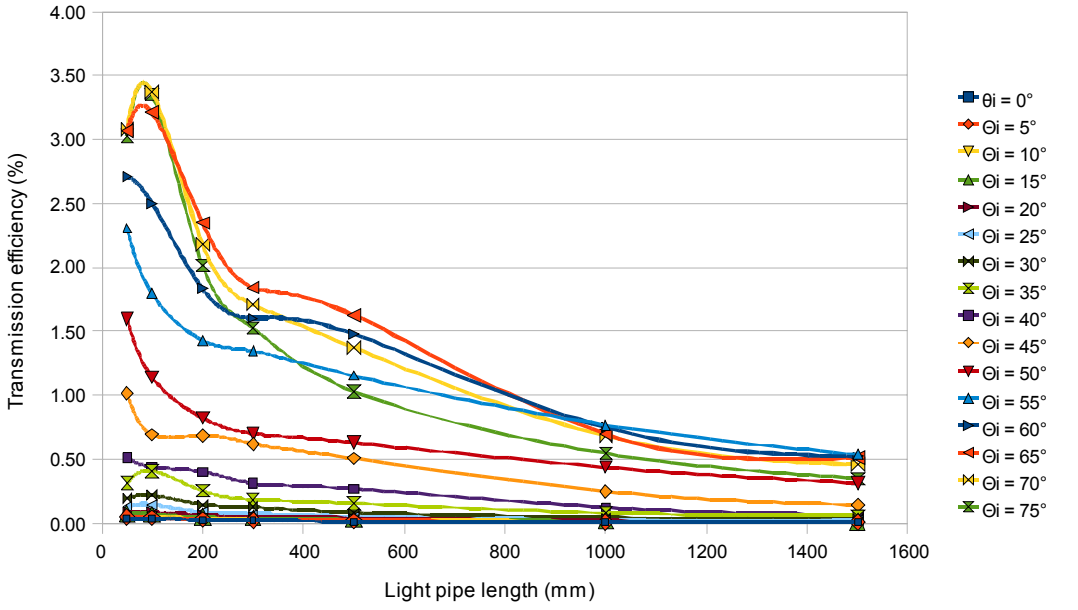

Figure 7.31 – Transmission efficiency T_E of the IMPSC-A2(LA) system demonstration prototype. Measurements taken at the end of a series of hollow light pipes made of folded aluminium sheet, with Ø = 50mm and length varying from L = 50mm to 1500mm.

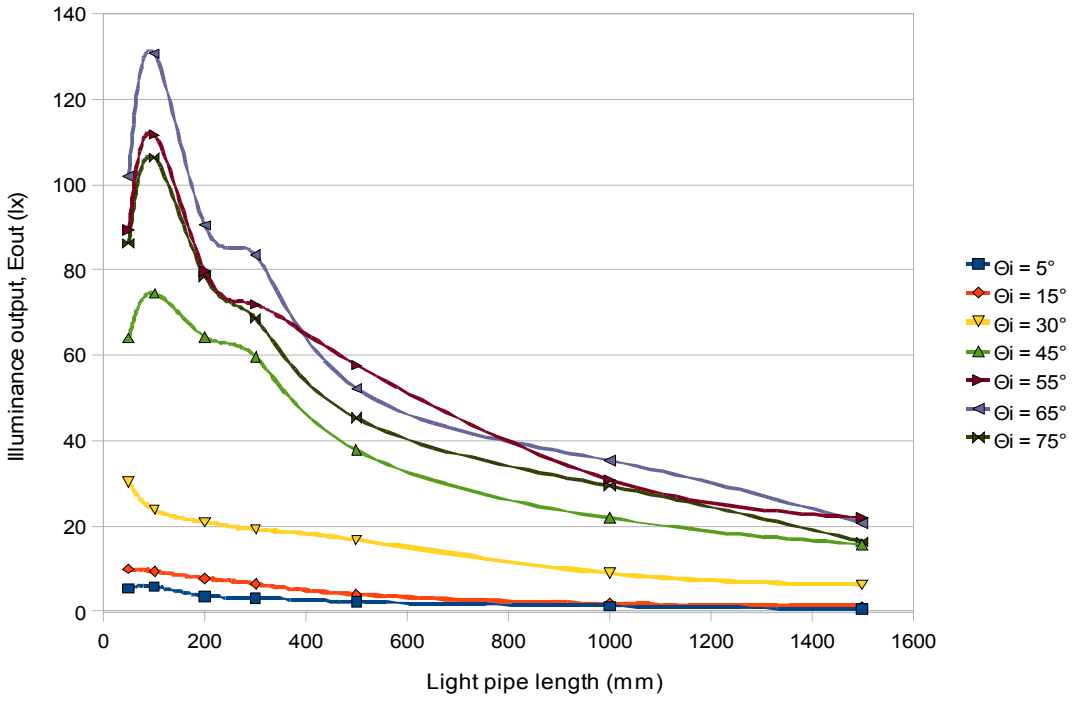

Figure 7.32 – Illuminance output E_{out} of the IMPSC-D1(SA) system demonstration prototype. Measurements taken at the end of a series of hollow light pipes made of folded aluminium sheet, with Ø = 50mm and length varying from L = 50mm to L=1500mm.

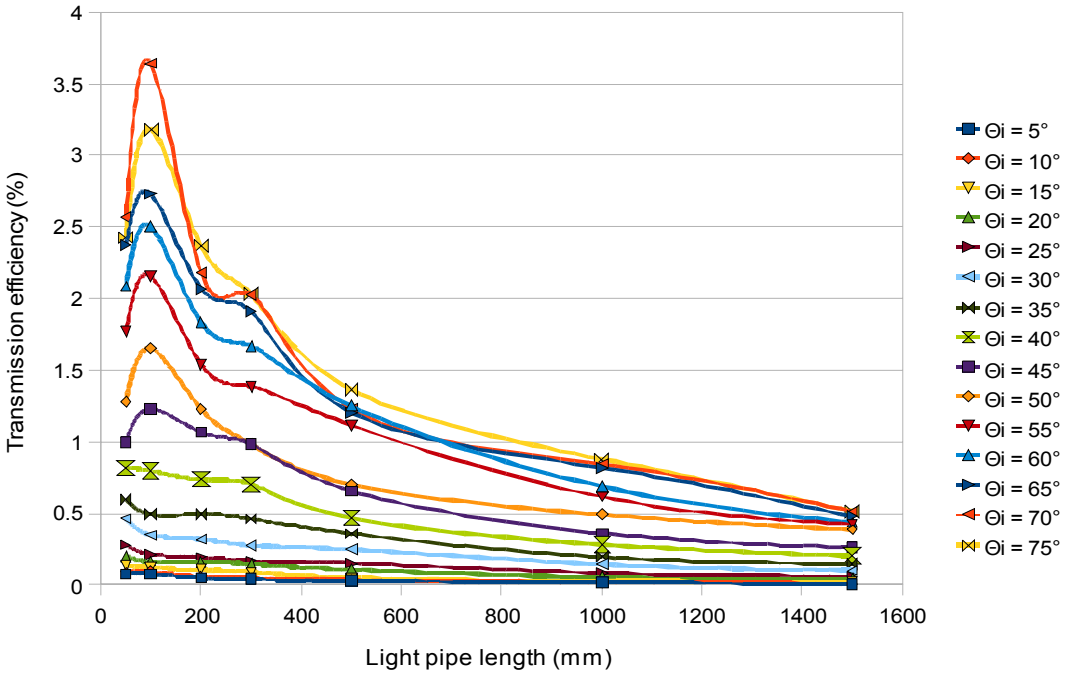

Figure 7.33 – Transmission efficiency T_E of the IMPSC-D1(SA) system demonstration prototype. Measurements taken at the end of a series of hollow light pipes made of folded aluminium sheet, with Ø = 50mm and length varying from L = 50mm to L=1500mm.

7.7.2 Improving angular distribution and transmission efficiency

The angular distribution Δθ of the luminous flux Φ emerging from the exit aperture of the IMPSC-A2 system was analysed by using the angular distribution imaging device (ADID), previously described in Chapter 3 (section 3.7.5).

The ADID provides a low-cost solution to visualise the spatial distribution of the luminous flux Φ. The spatial distribution of light emerging from the exit aperture of the IMPSC-A2 prototype increases with the increase of the incident angle θ_i.

The inclusion of a deconcentrator light cone (DLC) at the beginning of the light pipe provides a simple and efficient way to improve the angular distribution of light propagating inside the hollow light pipe. The DLC works like an inverted light-cone concentrator. Light emerging from the IMPSC demonstration prototype exit aperture is coupled into the DLC + hollow cylindrical light pipe system. The DLC was fabricated by folding polyester-aluminium sheets into a cone-like shape. The aluminium hollow light pipe provides 80% to 85% of specular reflectivity. The DLC was attached at the beginning of the hollow light pipe system assembled over an optical bench. Figure 7.34 presents a schematic diagram illustrating the set-up configuration including the DLC coupled to the hollow cylindrical light pipe.

Figure 7.35 displays the results of the angular distribution Δθ of the luminous flux Φ emerging from the IMPSC-A2-(SA) system analysed with the ADID apparatus. This result provides qualitative information about the relation between the incident angle θ_i of light (in this case: λ = 300-1100nm) at the IMPSC entrance aperture and the angular distribution $\delta\theta_{out}$ of light emerging from its exit aperture. Note that the spatial/angular distribution $\delta\theta_{out}$ of the luminous flux Φ spreads with the increase of the incident angle θ_i of direct collimated light at the meridional plane (Figure 7.35).

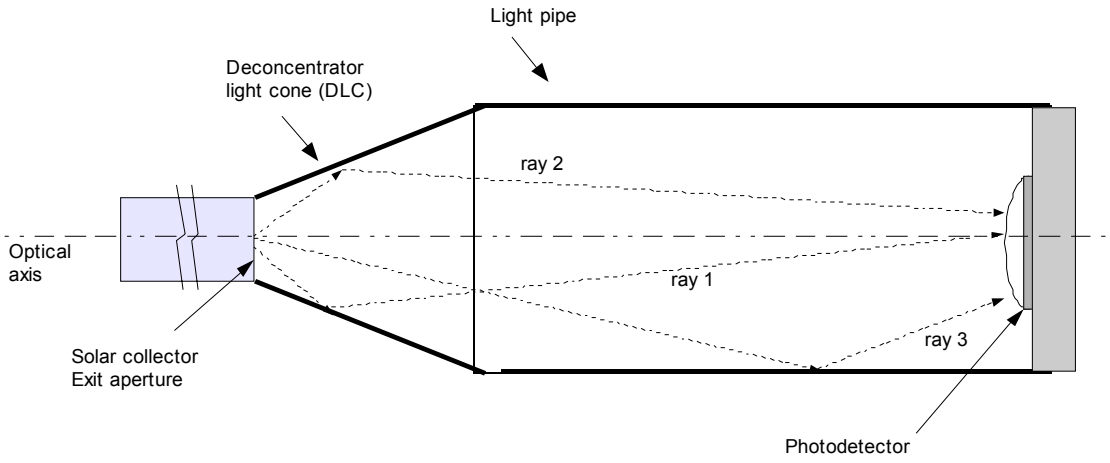

Figure 7.34 – Schematic diagram demonstrating the inclusion of a deconcentrator light cone (DLC) attached to the beginning of a hollow cylindrical light pipe.

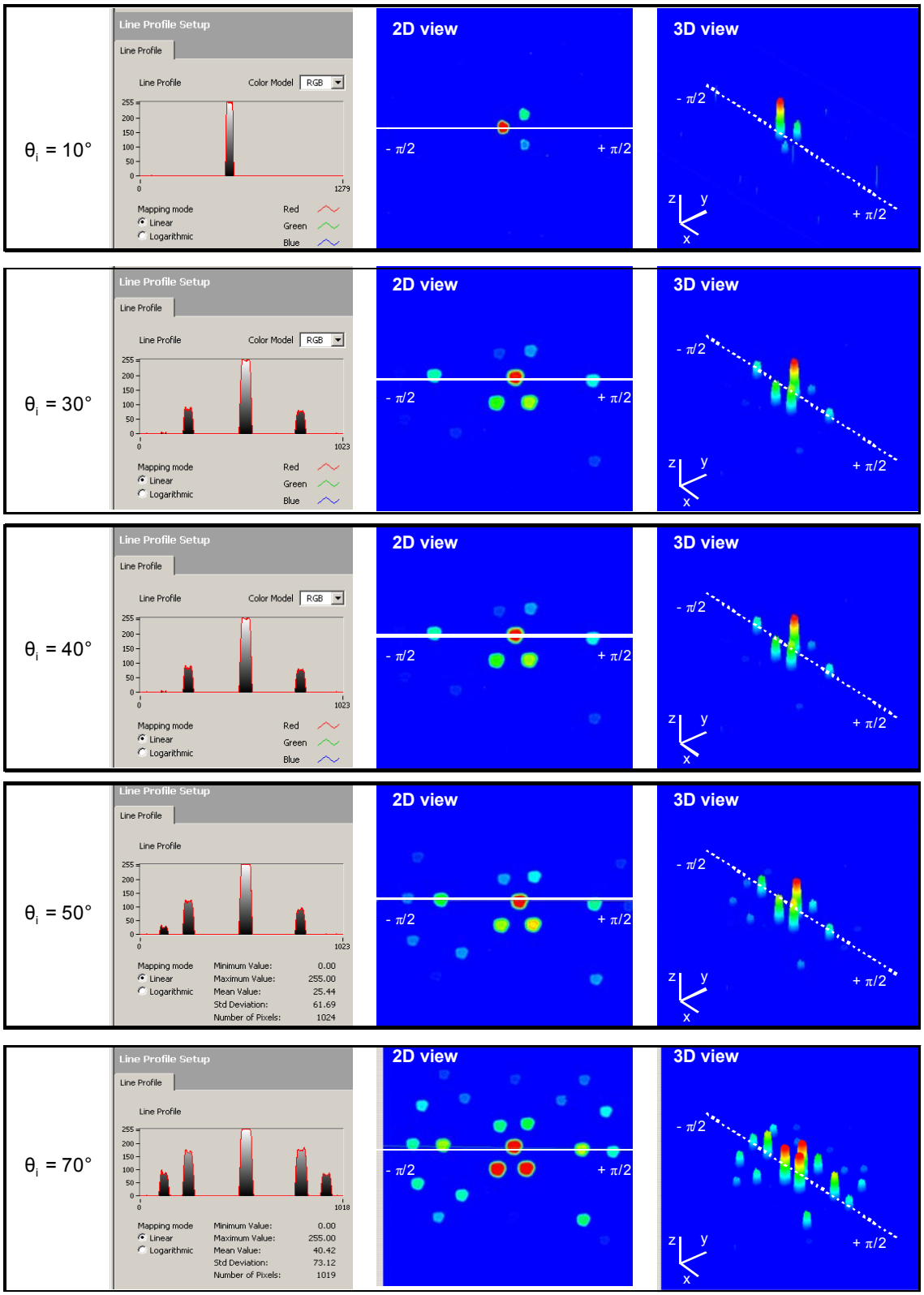

Figure 7.35 – ADID qualitative analysis of the angular distribution Δθ of the luminous output flux Φ emerging from the IMPSC-A2-(SA) demonstration prototype. Experiment instrumentation: ADID, CMOS camera and NI LabVIEW® Vision Assistant programme.

Figures 7.36 to 7.38 presents the results for the tests of the illuminance output E_{out} and the transmission efficiency T_E for a series of IMPSC systems considering the inclusion of the DLC attached to the beginning of the hollow light pipes. The tests follow the same set-up and measuring procedures described previously.

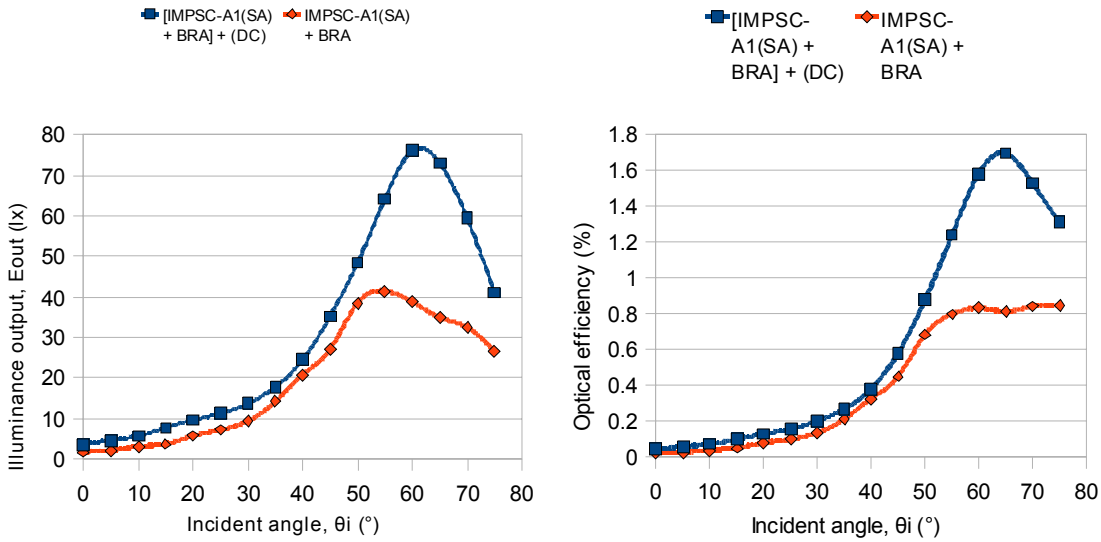

Figure 7.36 – Comparison between IMPSC-A1 systems with and without deconcentrator light cone (DLC). The DLC is coupled at the entrance of a 1m long folded aluminium sheet light pipe (Ø = 50mm).

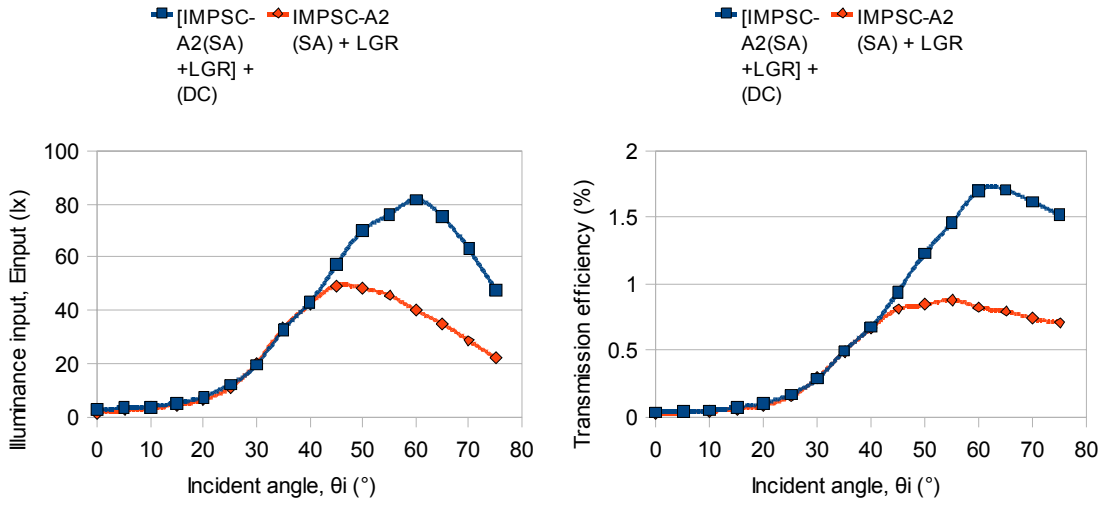

Figure 7.37 – Comparison between IMPSC-A2 systems with (higher values) and without (low values) a deconcentrator light cone (DLC). The DLC is coupled at the entrance of a 1m long folded aluminium sheet light pipe (Ø = 50mm).

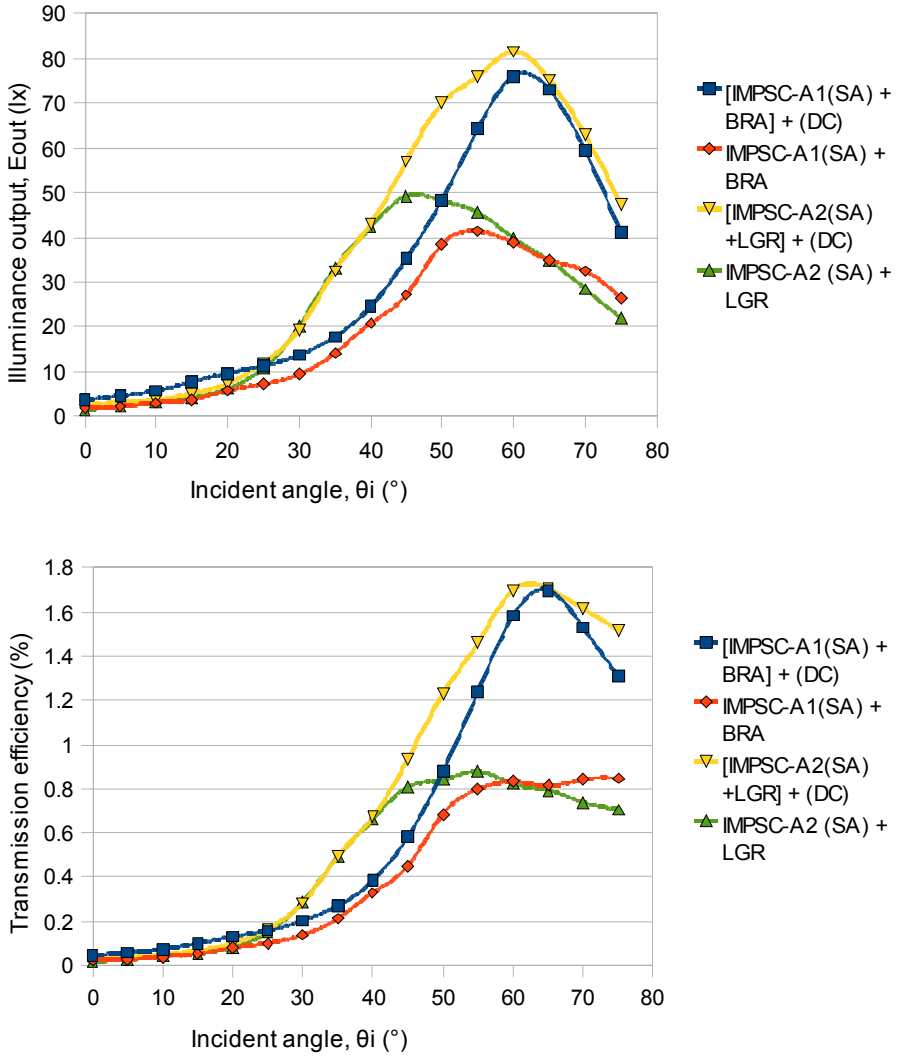

Figure 7.38 – Comparison between the previous IMPSC-A1 and IMPSC-A2 systems (Figs. 7.37 & 7.38) considering the inclusion of a deconcentrator light cone (DLC). Above, illuminance output E_{out} (lx) as a function of the incident angle θ_i. Below, transmission efficiency (%) as a function of the incident angle θ_i.

Figure 7.39 plots the results for the IMPSC-A1-SA (+BRA+DLC) system considering the inclusion of a back aluminium reflector (BRA) and deconcentrator light cones (DLC) coupled to the beginning of the light pipes. The lengths of the light pipes are: 50mm, 100mm, 200mm, 300mm, 500mm, 1000mm and 1500mm. All light pipes have the same diameter Ø = 50mm. The DLC main dimensions are: entrance aperture diameter $Ø_1$ = 20mm; exit aperture diameter $Ø_2$ = 50mm; length = 80mm.

Measurements of the illuminance output E_{out} (lx) and the illuminance transmission efficiency T_E, both as a function of the length of light pipe (mm) were taken.

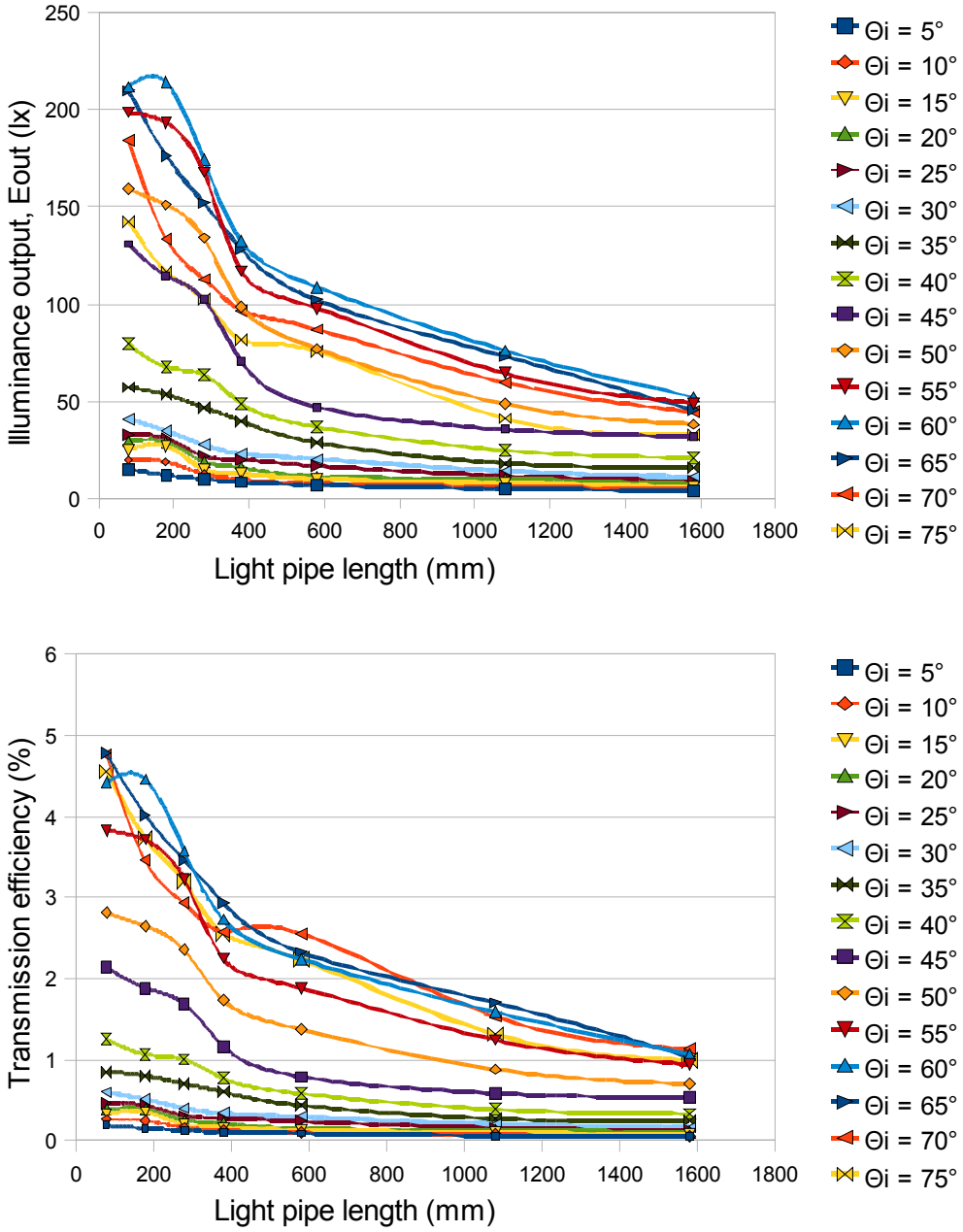

Figure 7.39 - Illuminance output E_{out} (above) and transmission efficiency T_E (below) of the IMPSC-A1-SA (+BRA+DCL1) system. Measurements taken at the end of a series of hollow light pipes made of folded aluminium sheet, with Ø = 50mm and length varying from L = 50mm to 1500mm.

Figure 7.40 compares the peak illuminance output E_{out} (lx) and the peak transmission efficiency T_E (%) of several IMPSC systems laser-cut prototypes (PMMA, 5mm thick).

Figure 7.41 compares the average illuminance output E_{out} (lx) and the average transmission efficiency T_E (%) of several IMPSC systems laser-cut prototypes.

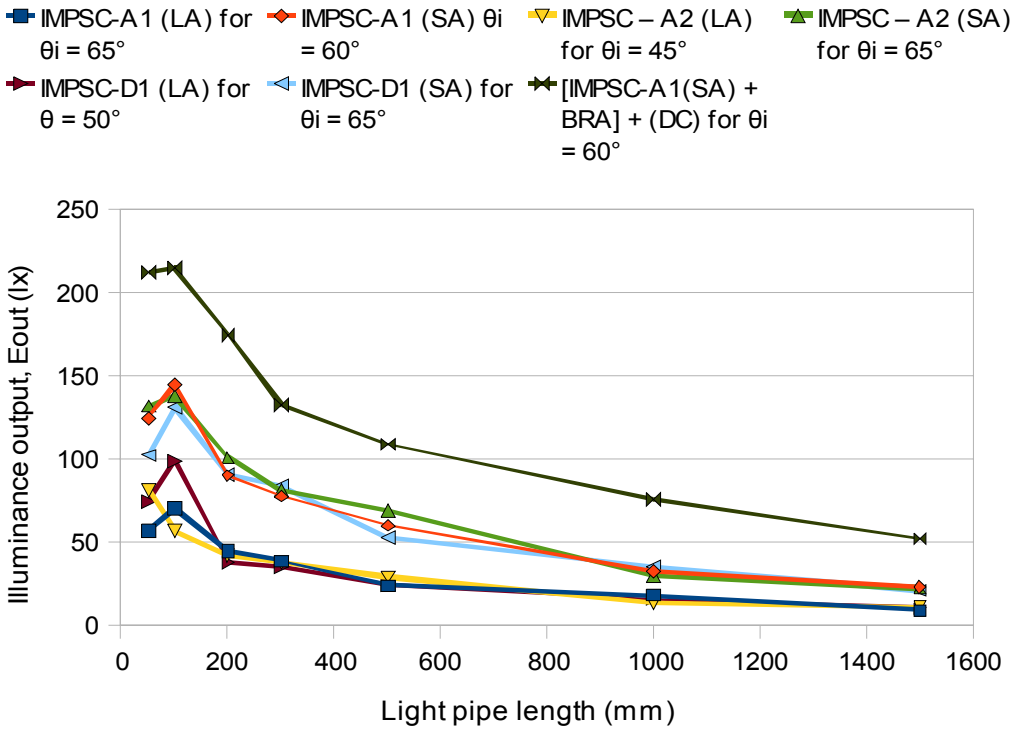

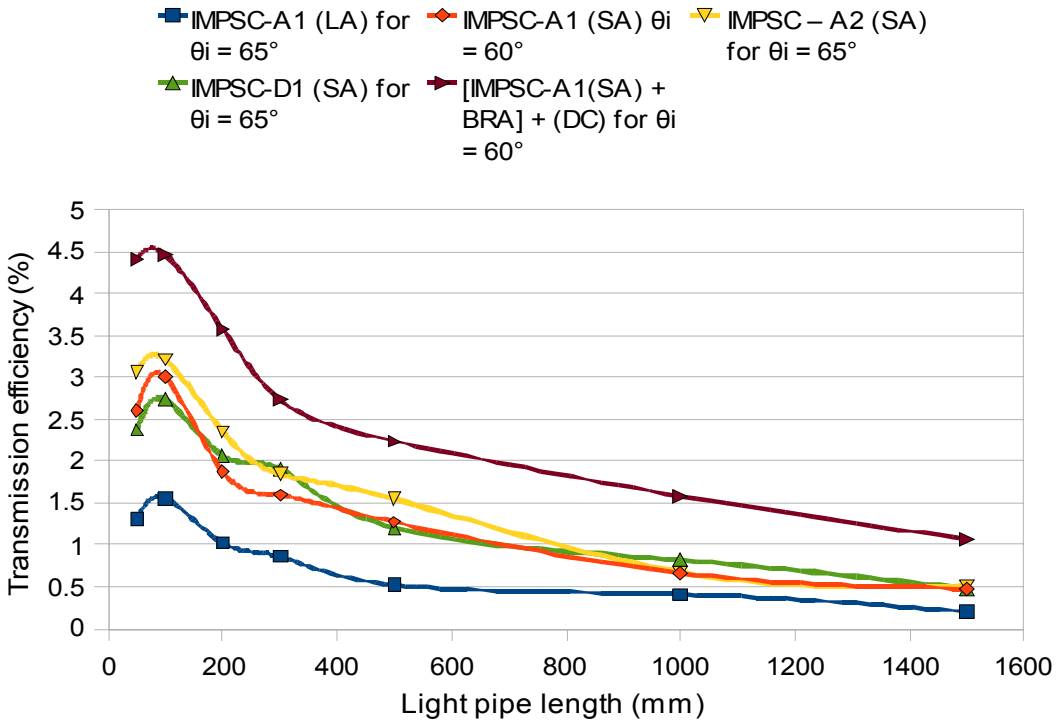

Figure 7.40 – Peak illuminance output E_{out} (lx) – above – and corresponding peak transmission efficiency TE (%) – below – both as a function of the light pipe length (mm). Laboratory tests set-up parameters: incident angle θ_i of direct light (300-1100nm) at the meridional plane discriminated for each system. Comparisons between several IMPSC systems laser-cut PMMA prototypes (5mm thick).

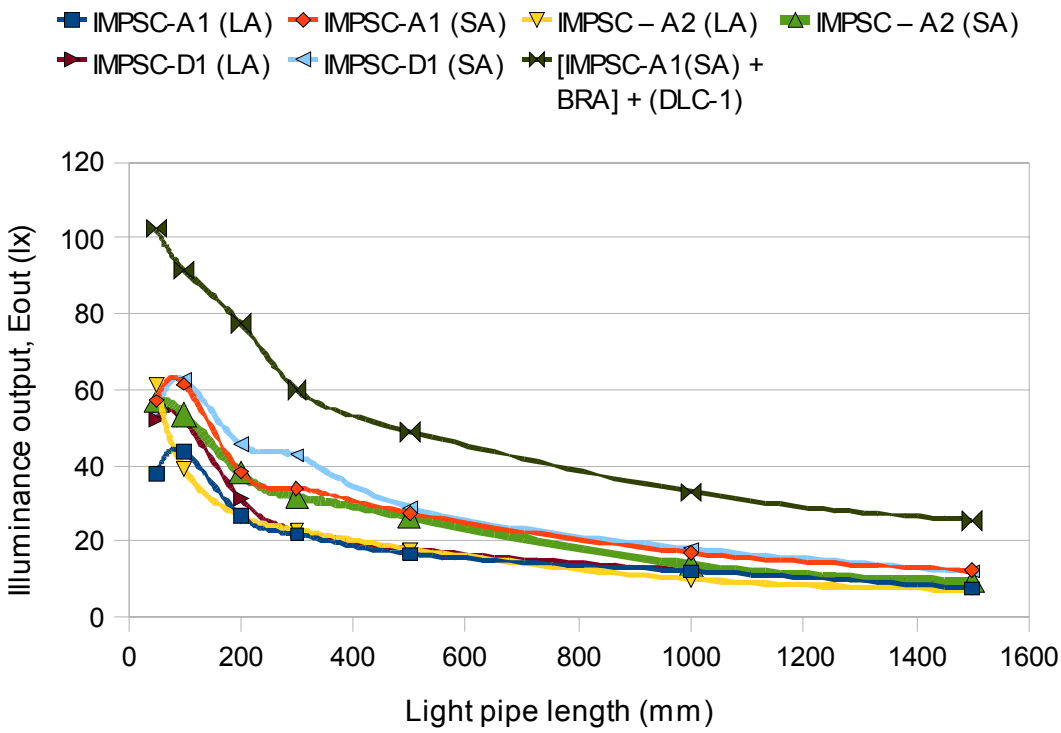

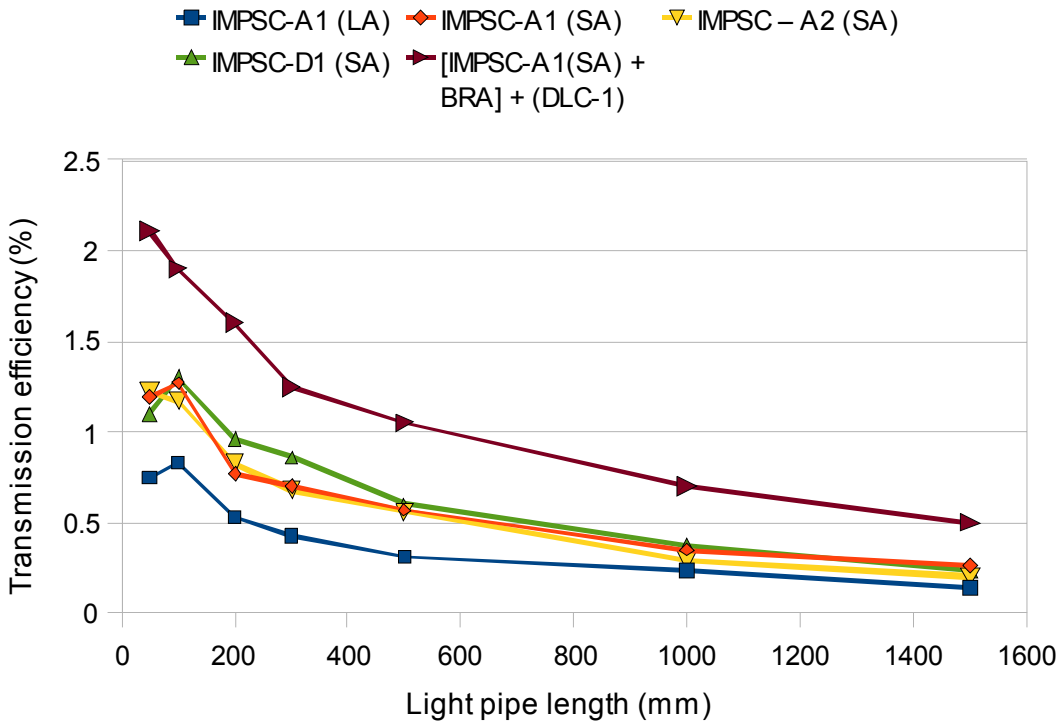

Figure 7.41 – Average illuminance output E_{out} (lx) – above – and corresponding average transmission efficiency TE (%) – below – both as a function of the light pipe length (mm). Laboratory tests set-up parameters: incident angle θ_i of direct light (300-1100nm) varying from 5° to 75° at the systems meridional plane. Comparisons between several IMPSC systems laser-cut PMMA prototypes (5mm thick).

7.7.3 Outdoor tests of IMPSC systems

Figure 7.42 presents lateral-view of the basic outdoor experiment set-up configuration. The IMPSC-A2(LA) system was positioned vertically, supported by a set of auxiliary holders and rigid support structure. The device was orientated to allow direct sunlight to enter through its entrance aperture. The exit aperture was located above a “window” cut at the centre of a protective screen cap. Solar radiation emerging from the IMPSC exit aperture passes though the “window” and enters a hollow cylindrical light pipe integrator (300mm long; Ø = 50mm). The light pipe was made of a commercial polyester-aluminium sheet, with specular reflectance about 80-85%. A photometer (Extech EA-31 illuminance meter) with cosine corrector (white-plastic diffuser dome) was positioned at the low-end section of the hollow cylindrical light pipe.

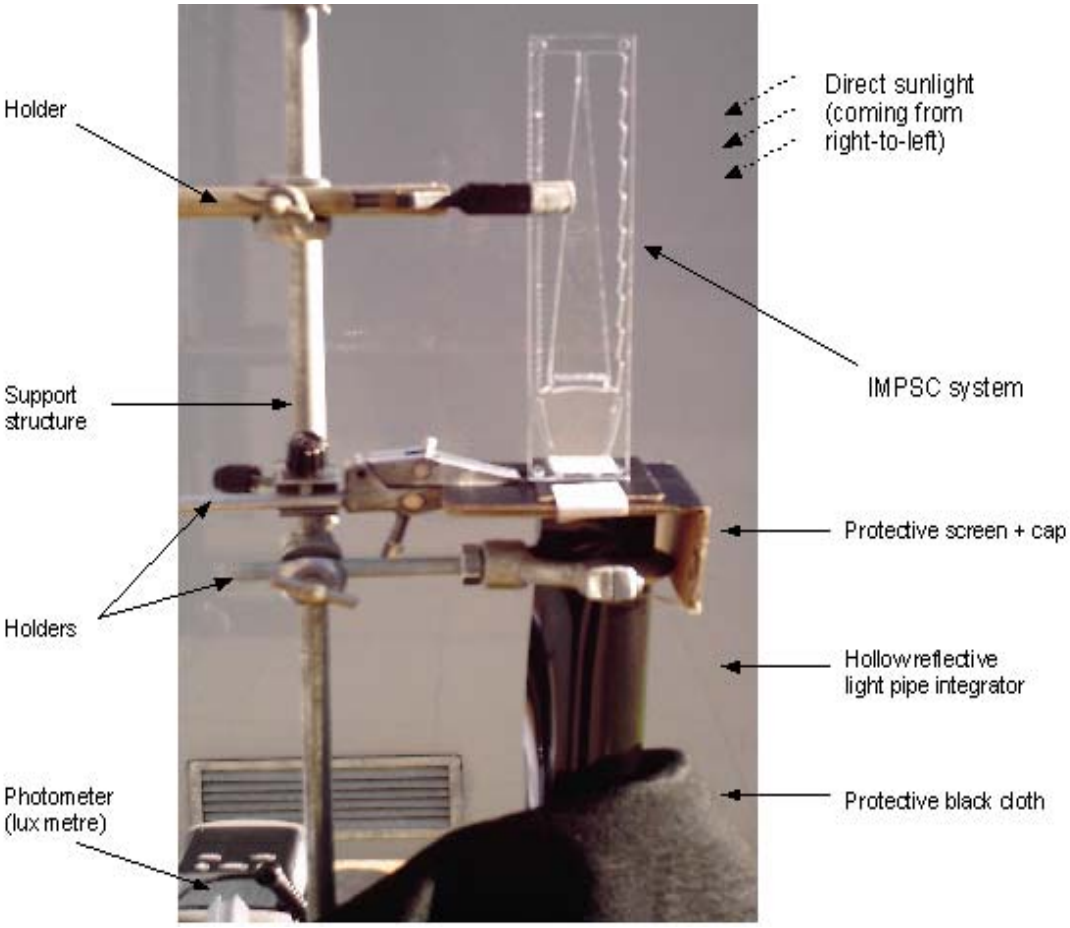

Figure 7.42 – Outdoor experiment set-up configuration for IMPSC systems. System parameters: aluminium hollow light pipe (length L = 300mm; diameter Ø = 50mm).

Figure 7.43 presents the results of the outdoor experimental tests for the IMPSC-A2(LA) demonstration prototype (as seen in Figure 7.42, above). Measured vertical/façade global illuminance (E_{in}) varied from 40000lux to 60000lux.

Figure 7.44 presents the results of the outdoor tests for the IMPSC-D1 system. The experiment set-up configuration was similar to the set-up displayed in Figure 7.42. Measurements were taken on the 17th of January, (low-winter sun, peak h_s = 18°), at Brunel University Campus, Uxbridge, London, UK (51° 33' 0" North, 0° 29' 0" West). The frontal surface (entrance aperture) was directed towards the South. Measurements were taken during a period of 3 hours, from 11:00 am to 14:00 pm.

Figure 7.44(a) displays the vertical/façade illuminance (lx) measurements according to British Standard BS 8206-2:2008 and CIE international standard CIE S 011/E:2003. Figure 7.44(b) shows the Illuminance output E_{out} (lx) of the IMPSC-D1 system measured at the end of a folded aluminium sheet light pipe 300mm long and 50mm in diameter. Figure 7.44(c) shows the illuminance transmission efficiency T_E of the IMPSC-A2(LA) system calculated as the percentage value of the illuminance measured at the entrance aperture and illuminance at the exit aperture of the system, as previously described in Chapter 3.

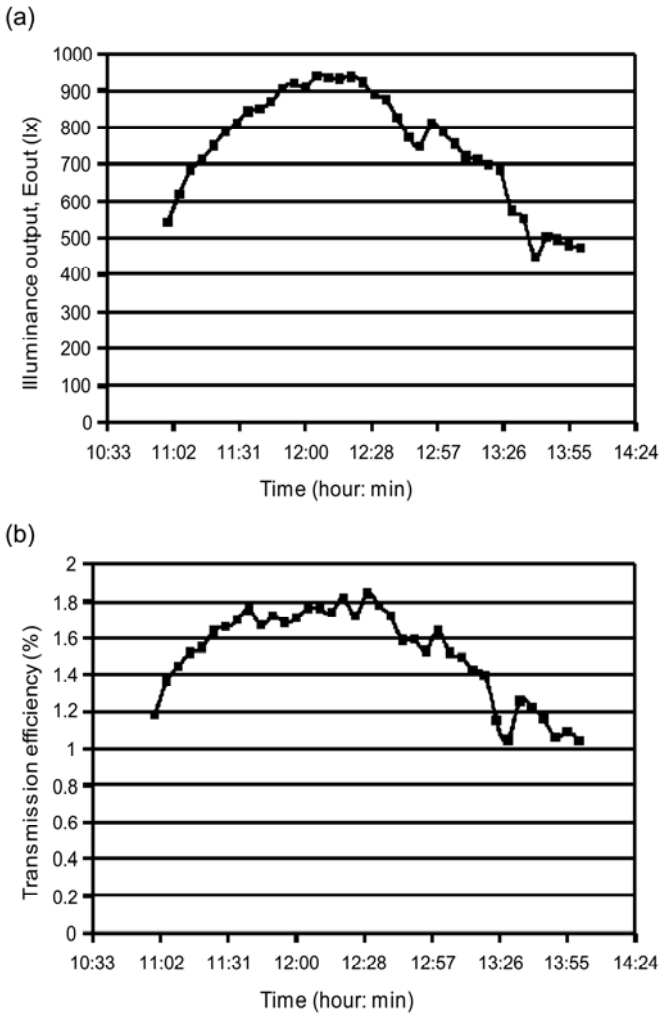

Figure 7.43 - Results of the outdoors experimental tests for IMPSC-A2(LA) system. Conducted at Brunel University Campus, Uxbridge, London, UK on the 17th of January 2009. Direction: South. Peak solar altitude angle h_s = 18° (low winter sun).

(a)

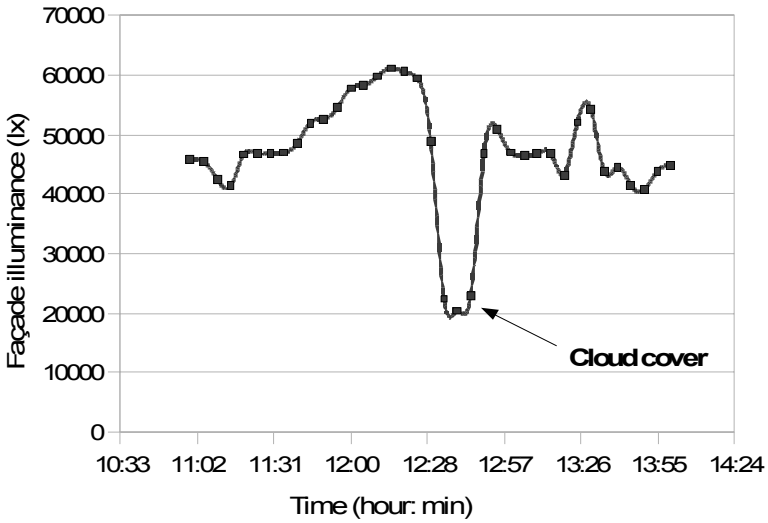

(b)

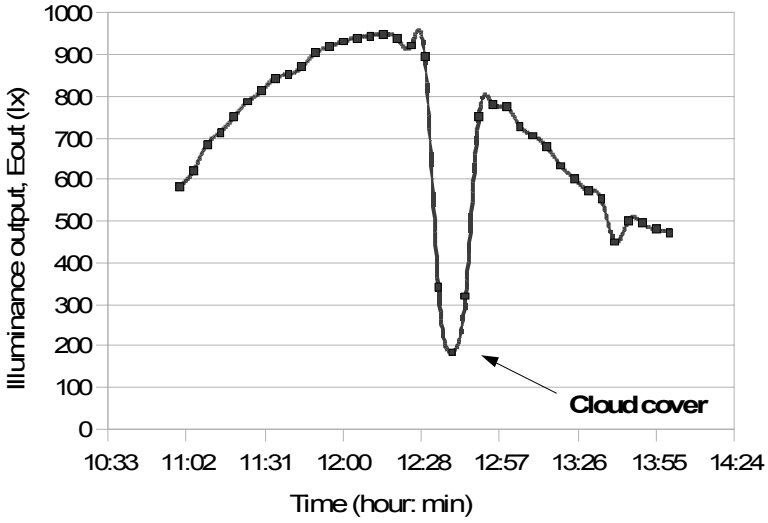

(c)

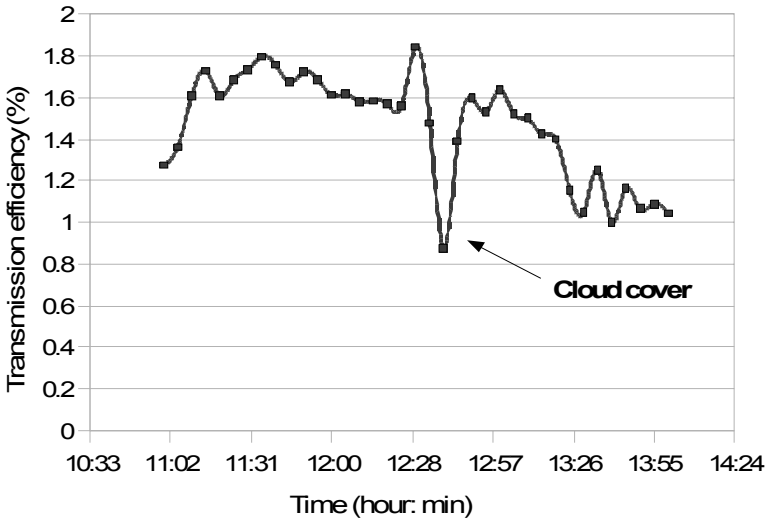

Figure 7.44 – Outdoor experimental tests results for IMPSC-D1(LA) system. Graphs: (a) façade illuminance (lx) as a function of time (hour: minutes); (b) illuminance output, E_{out} (lx) as a function of time (hour: minutes); and (c) transmission efficiency (%) as a function of time (hour: minutes).

7.8 Results and discussion on the IMPSC systems

The integrated multi-prismatic solar collector (IMPSC) introduces a series of original optical arrangements that integrates two sets of parallel prismatic arrays with at least one independent symmetrical integrated light guide (SILG), with a continuous linear profile, located in-between the prismatic arrays. The SILG geometry resembles an “inverted V” and is defined by the apex angle α_{SILG} located at the top-end of its structure. Light is trapped by means of TIR inside the light guide (SILG).

Due to the geometry of the light guide (SILG), the angular distribution $\Delta\theta$ of light trapped by TIR is improved by the angular increment $\alpha_{SILG/2}.N_{TIR}$, where $\alpha_{SILG/2}$ corresponds to half apex angle of the light guide (SILG) and N_{TIR} the number of total internal reflections. A series of polygonal light-extractors located at the low-end section of the light guide improves the extraction of light by decreasing the incident angle θ_i of a light ray at the extractors interface till it is lower than the critical angle θ_c (in the case of the PMMA prototypes $\theta_c \approx 42°$, for $\lambda = 555nm$).

The IMPSC concept provides a system with at least two different ranges of acceptance angles θ_{accept} by assigning different values for each set of parallel prismatic array apex angle α_{PA}. The inclusion of a concentration section at the low-end section of the IMPSC increases the geometric concentration ratio to at least $C_R = 12.5X$, whereas the MPSC systems geometric concentration ratio were around $C_R \approx 5.6X$.

Computer simulations indicate that the IMPSC basic optical configuration provides a transmission efficiency up to $T_E = 26.8\%$, leading to an effective optical concentration ratio of at least 3.25X (considering: $\alpha_{PA} = 24°$; $\alpha_{SILG} = 8°$; $\theta_i \approx 58°$; $\lambda = 555nm$; and refractive index n = 1.491).

IMPSC demonstration prototypes made of clear PMMA (n =1.491) and manufactured by laser ablation process, yield peak transmission efficiencies up to $T_E \approx 5\%$ for an incident artificial light source ($\lambda = 300nm$-$1100nm$) at the entrance aperture meridional plane considering an incidence angle θ_i varying from $\theta_i = 5°$ to $\theta_i = 75°$.

It has been experimentally demonstrated that the acceptance angle θ_{accept} of the IMPSC/RINSC system is directly related to the value of the prismatic arrays apex angles α that is positioned as the “entrance aperture” of the system. Prismatic arrays with smaller apex angles α are more suitable for building geographic locations and/or orientation of lower incident angles θ_i of direct sunlight, whereas prismatic arrays with smaller apex angles α are more suitable for locations of high incident angles θ_i of direct sunlight.

7.9 Summary and conclusions of Chapter 7

The IMPSC concept has been introduced and analysed. The main parameters have been presented and discussed. Computer simulations measured transmission efficiencies up to T_E = 26.8%, whereas laboratory experimental tests with laser-cut demonstration prototypes yield peak transmission efficiencies around $T_E \approx 5\%$.

Some important issues from this chapter are highlighted as follows:

- Ray-tracing analysis has shown that the presence of extractors located at the low-end section of the light guide (SILG) provides a feasible solution to extract light from the light guide. The extractors also serve to "correct" the angular distribution $\Delta\theta$ of light as it is extracted from the light guide (SILG).
- The inclusion of the deconcentrator light cone (DLC) at the beginning of the light pipe provided a simple and efficient way to significantly increase the transmission efficiency T_E of the IMPSC + light pipes system. Results have shown that the transmission efficiency T_E of the system can be doubled in this situation.
- The optical layout configurations of the IMPSC systems as presented in this chapter provides higher geometric concentration ratios C_R than the previous MPSC systems presented in Chapter 6: IMPSC geometric concentration ratios $C_R \geq 12X$; MPSC geometric concentration ratios was $C_R \approx 5X$ to 6X.

One of the main problems with the IMPSC optical configurations relates to its acceptance angle θ_{accept} and the incident angle θ_i of direct light at the frontal surface of the light guide (SILG). As seen in the literature review, Fresnel-reflections (or dielectric reflections) increase with the increase of the refractive index n and the incidence angle θ_i. For solid-dielectric materials with a mean refractive index around 1.50, such as soda-lime glass or PMMA (n =1.491), Fresnel reflection losses becomes more significant for $\theta_i > 60°$, representing around 10% of losses at the incidence interface (see Figure 2.12, pp.25). For higher incidence angles $\theta_i \approx$ 18 - 20% losses for $\theta_i = 70°$ and > 40% for $\theta_i > 80°$.

Therefore, a possible effective design strategy to improve the efficiency of the RINSC/IMPSC system is to explore design alternatives that minimises and/or "recycles" Fresnel reflections losses that happen inside the RINSC/IMPSC optical system. Special attention should be given in order to minimise Fresnel reflection losses at the systems solid-dielectric light guide (SILG) surface/interface. This design goal is the starting point for the next chapter.

Note that a journal paper related to the IMPSC systems has been submitted before the submission of this thesis (Pelegrini et al, 2009b).

Chapter 8 - Vertically Integrated Nonimaging Solar Collectors

8.1 Introduction

This chapter introduces the Vertically Integrated Nonimaging Solar Collectors (VINSC). The VINSC concept is a sub-category of the RINSC systems based on the basic theory and design principles presented in Chapter 4.

As discussed earlier, it is possible to reduce Fresnel-reflections at the frontal surface of the light guide by increasing its apex angle α_{SILG}. However, this has negative implications such as the increase in the light guide thickness, which would also lead to a decrease in the geometric concentration ratio C_R and result in a less compact system. Therefore, it is argued here that it is necessary to explore alternative optical configurations in order to minimise Fresnel-reflection losses of incident light at the entrance surface of the light guide.

The main design problems investigated with the VINSC configuration were:

- How to combine several prismatic elements with different acceptance angles θ_{accept} into an integrated system structure with a single light guide?
- How to design a configuration that minimises Fresnel-reflection losses at the entrance surface of the integrated light guide?

8.2 The Vertically Integrated Nonimaging Solar Collectors (VINSC) concept

The main goals established for the VINSC optical design were:

- To provide a geometric configuration that could potentially reduce Fresnel-reflection losses at the entrance surface of the system's light guide; and
- To increase the acceptance angle θ_{accept} of the system.

Figure 8.1 displays a vertical-section view of the geometric optical profile of a possible configuration for the VINSC system. This configuration is named here as VINSC-A1 system. The main features and parts that compose the VINSC-A1 system are highlighted.

As presented in Figure 8.1, the VINSC-A1 has a set of three prismatic arrays with different acceptance angles θ_{accept}. They are defined here as: (A) low-section prismatic array; (B) mid-section prismatic-array; and (C) top-section prismatic array. Each prismatic array section is optimised for a specific acceptance angle θ_{accept} which is defined by the value of the apex angle α of the prismatic elements of each section.

Figure 8.2 presents a series of ray-tracing analysis to illustrate the differences between the acceptance angles θ_{accept} of each prismatic array section. Note that Fresnel reflections and scattering losses were not considered in the simulations shown in Figure 8.2 in order to make it easier to visualise the working principle.

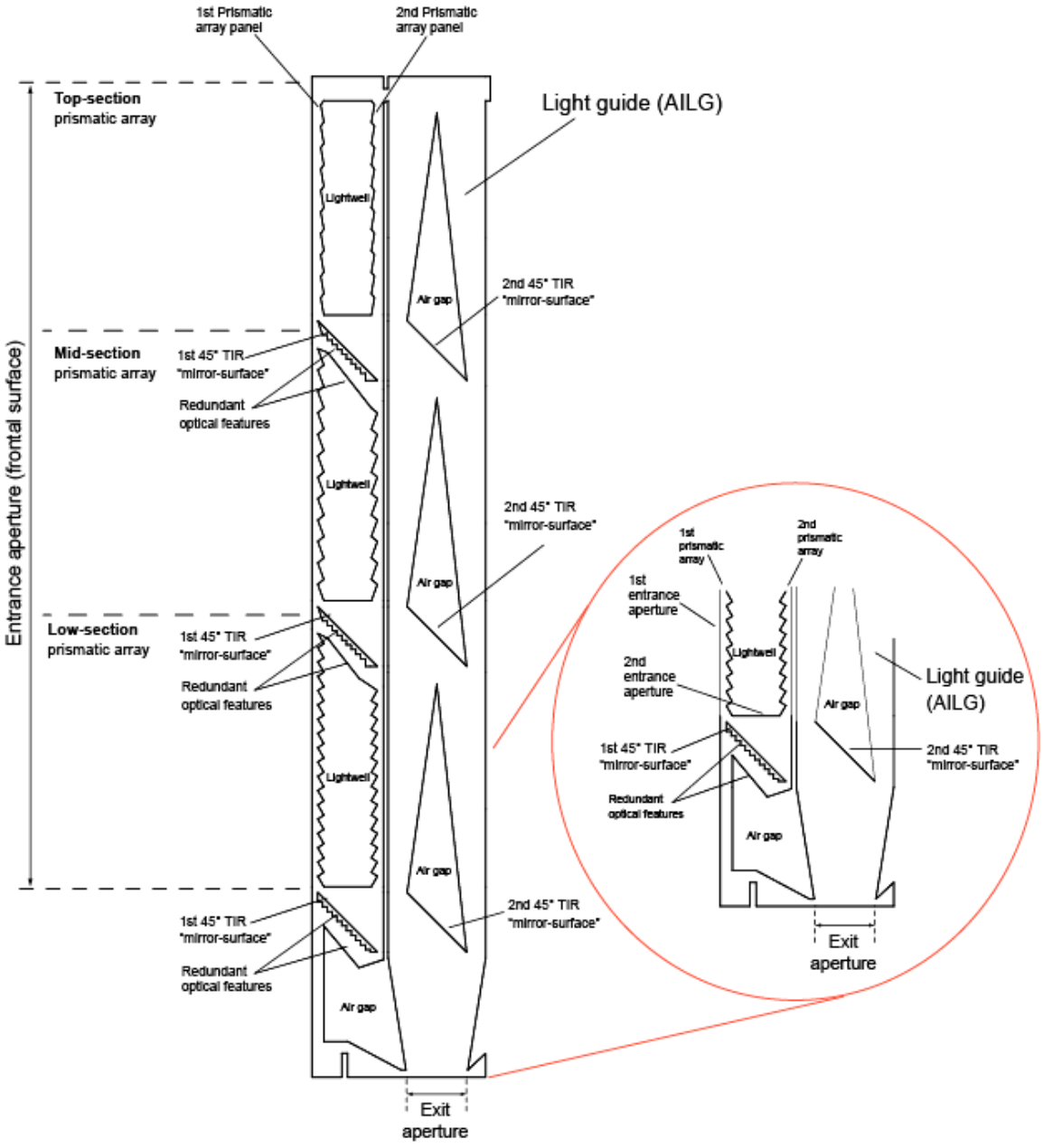

Figure 8.1 - Vertical-section view of optical profile of the VINSC-A1 system. In this example: low-section prismatic arrays apex angles α = 30°; mid-section prismatic arrays apex angles α = 20°; top-section prismatic arrays apex angles α = 10°.

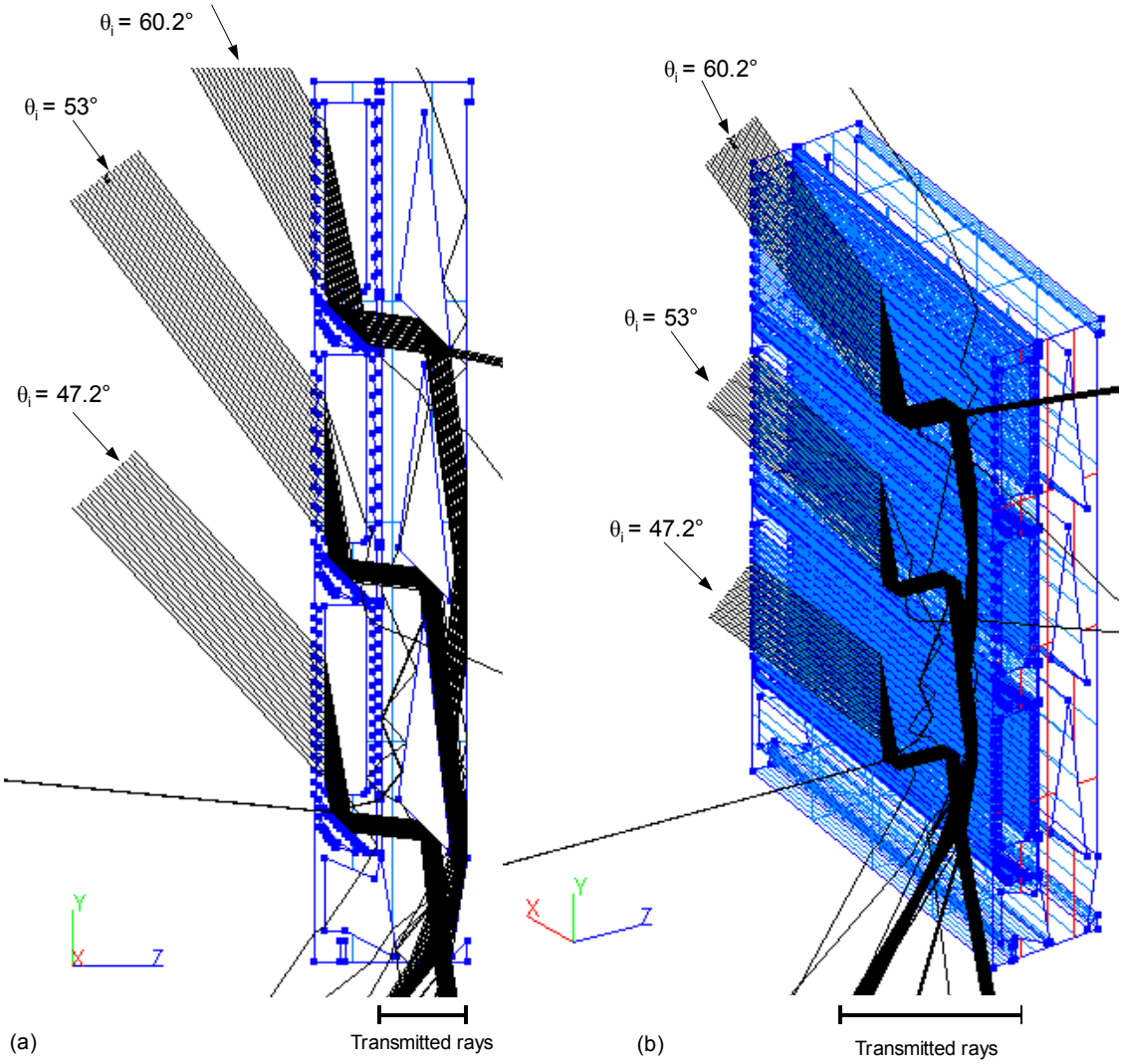

Figure 8.2 – Ray-tracing analysis demonstrating the working principle of the VINSC-A1 system. Vertical-section view is shown in (a); perspective view is shown in (b). Fresnel reflections and scattering were not considered in the simulation.

In this particular simulated example, the measured values for the optimum acceptance angles θ_{accept} are, approximately: 47° for the low-section prismatic array; 53° for the mid-section prismatic array; and 60° for the top-section prismatic array. It is important to stress that these values are obtained considering: a collimated beam of monochromatic light (λ = 555nm) incident at the meridional plane; and a solid-dielectric material (PMMA) with refractive index n = 1,491. The interception position, that is, the part of the entrance aperture where incident light "intercepts" the system, has also an important influence on which portion of this light will enter the system.

Figure 8.3 presents a sequence of ray-tracing analysis to demonstrate how the VINSC-A1 system works under a continuous variation of incident light intercepting its entire frontal area (entrance aperture). In this simulation, a collimated beam of 1000 rays of monochromatic light (λ = 555nm) was directed towards the frontal surface (entrance aperture) of the VINSC-A1 system. The specified refractive index was n =

1,491. The incident angle θ_i varies from: 47° in (a), 53° in (b), 60° in (c) and 63° in (d). Note that the first three of these incident angles (θ_i = 47°, 53° and 60°) coincide, respectively, with the optimum acceptance angle θ_{accept} for the low-section, mid-section and top-section of the frontal prismatic arrays, as described earlier. Hence, the portion of incident rays that intercept each of the prismatic arrays sections inside their acceptance angle θ_{accept} is transmitted to the exit aperture.

In Figure 8.3(d), the incident angle θ_i = 63° is larger than the acceptance angle θ_{accept} of all prismatic array sections (low, mid and top prismatic sections). Consequently, most of the incident rays will be rejected by the system due to total internal reflection (TIR) inside the frontal prismatic array structures. This suggest that such configuration of prismatic arrays can be applied to harvest sunlight at low incident angles (θ_i < 30°) and medium incident angles (30°≤ θ_i ≥ 60°), and reject it at higher incident angles (θ_i > 63°, in this case). This may be a desirable design strategy to reduce building thermal loads by blocking unwanted solar radiation in the summer, for example.

Note that the VINSC concept is not limited to only three groups of prismatic arrays. More prismatic array sections can be added in order to increase the collector frontal area and harvest more sunlight. However, solar radiation collected from the top-section prismatic array will suffer higher attenuation inside the light guide due to the fact that the optical path length (OPL) to the exit aperture is greater.

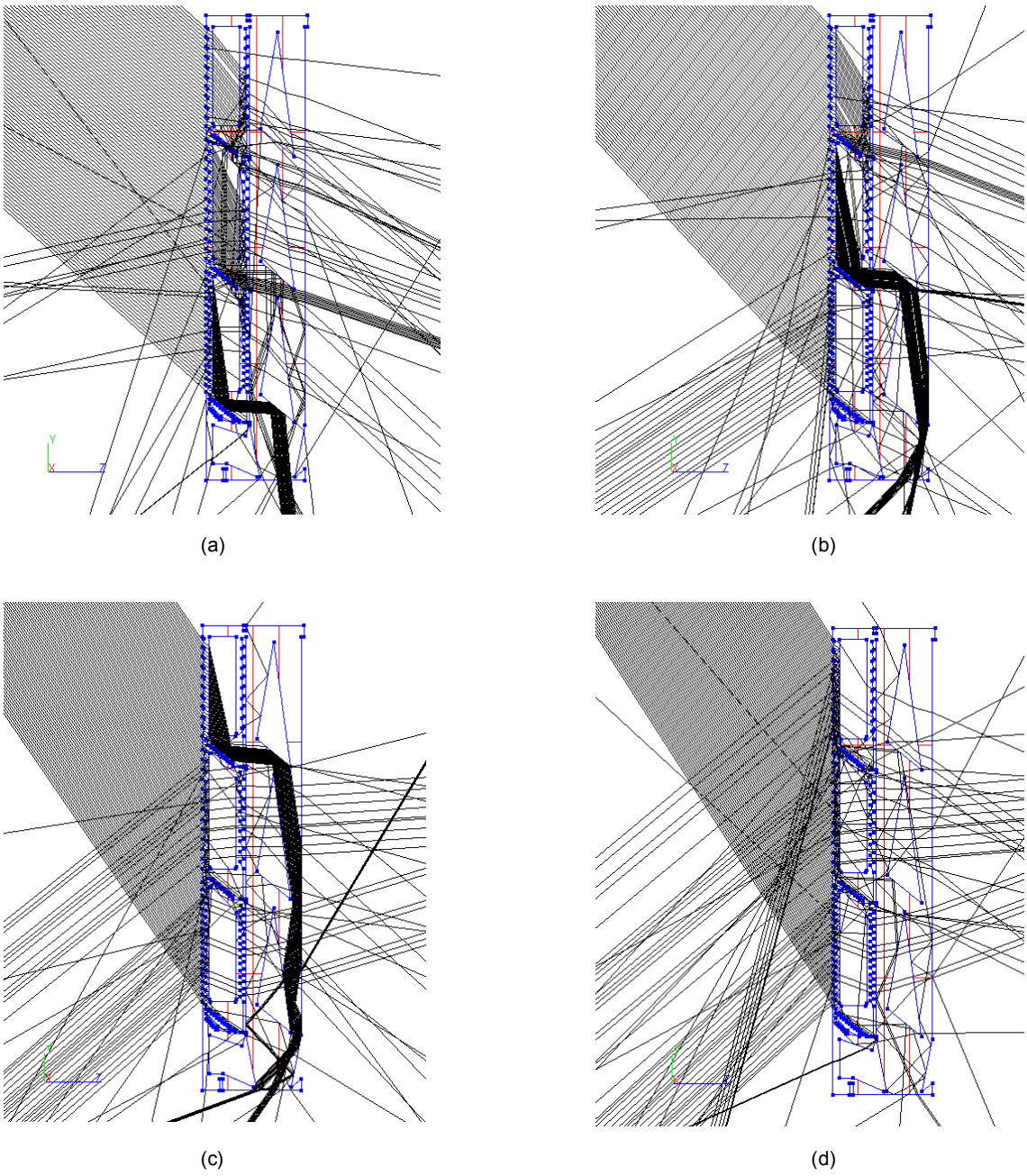

Figure 8.3 – Ray-tracing analysis demonstrating the three acceptance-angles of the VINSC-A1 system basic working principle. Incident light (λ = 555nm) is directed from left-to-right.

8.3 Preliminary design studies and ray-tracing analysis

As seen in the literature review, Fresnel-reflection losses increases with the increase of the incident angle θ_i of light at the surface/interface of a solid-dielectric material (Hecht, 1998). Hence, an attempt to reduce Fresnel-reflections in the RINSC/VINSC systems was to address the problem by reducing the incident angle θ_i of light expected to be coupled into the solid-dielectric light guide. A series of preliminary design studies were conducted to investigate possible geometric configurations to minimise Fresnel-reflection losses (Figure 8.4).

In the ray-tracing simulations displayed in Figure 8.4 a beam of collimated monochromatic light (λ=555nm) was directed towards the optical design studies. The goal was to couple the incident light into a parallel solid-dielectric light guide. Prismatic elements and geometric changes in the profile-section of the light guide were simulated. Simulations considered the use of clear acrylic PMMA with a refractive index n = 1,491 as the solid-dielectric material of the system.

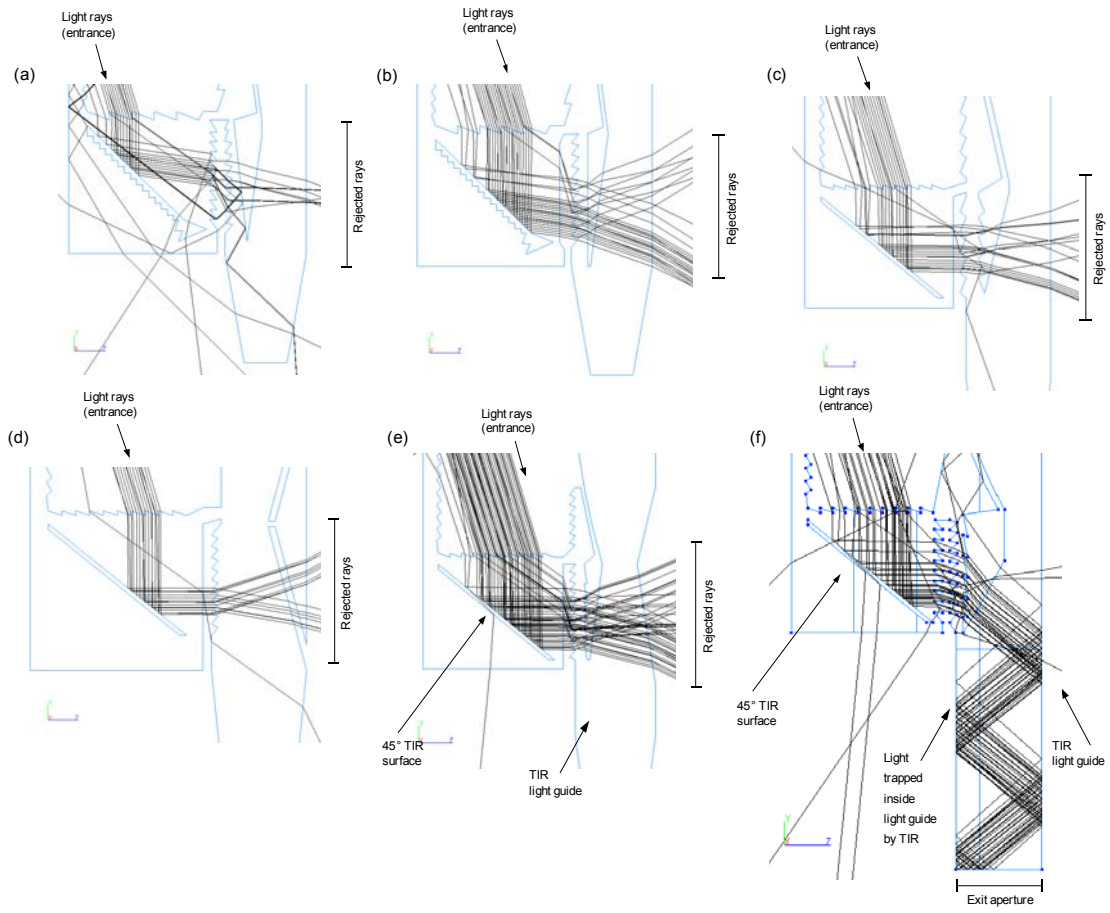

Figure 8.4 – Series of design studies (section view) and ray-tracing for light coupling into the light guide.

The introduction of the 45°-TIR corner inside the light guide had both positive and negative consequences. The positive aspect was that it changes the direction of incoming light through around 90° (Figure 8.4). This makes it possible to couple light inside the light guide and direct it towards the systems exit aperture with minimum attenuation, since the expected light path to the exit aperture will approach a straight line parallel to the systems vertical optical axis. However, the negative aspect was that the said straight line light path will be partially interrupted by the presence of the next 45°-TIR surface situated along its path.

Note in Figure 8.5 that no significant Fresnel-reflection losses are identified along the path of the main light beam (concentrated lines) at the interface/entrance of the light guide (Figure 5.8d).

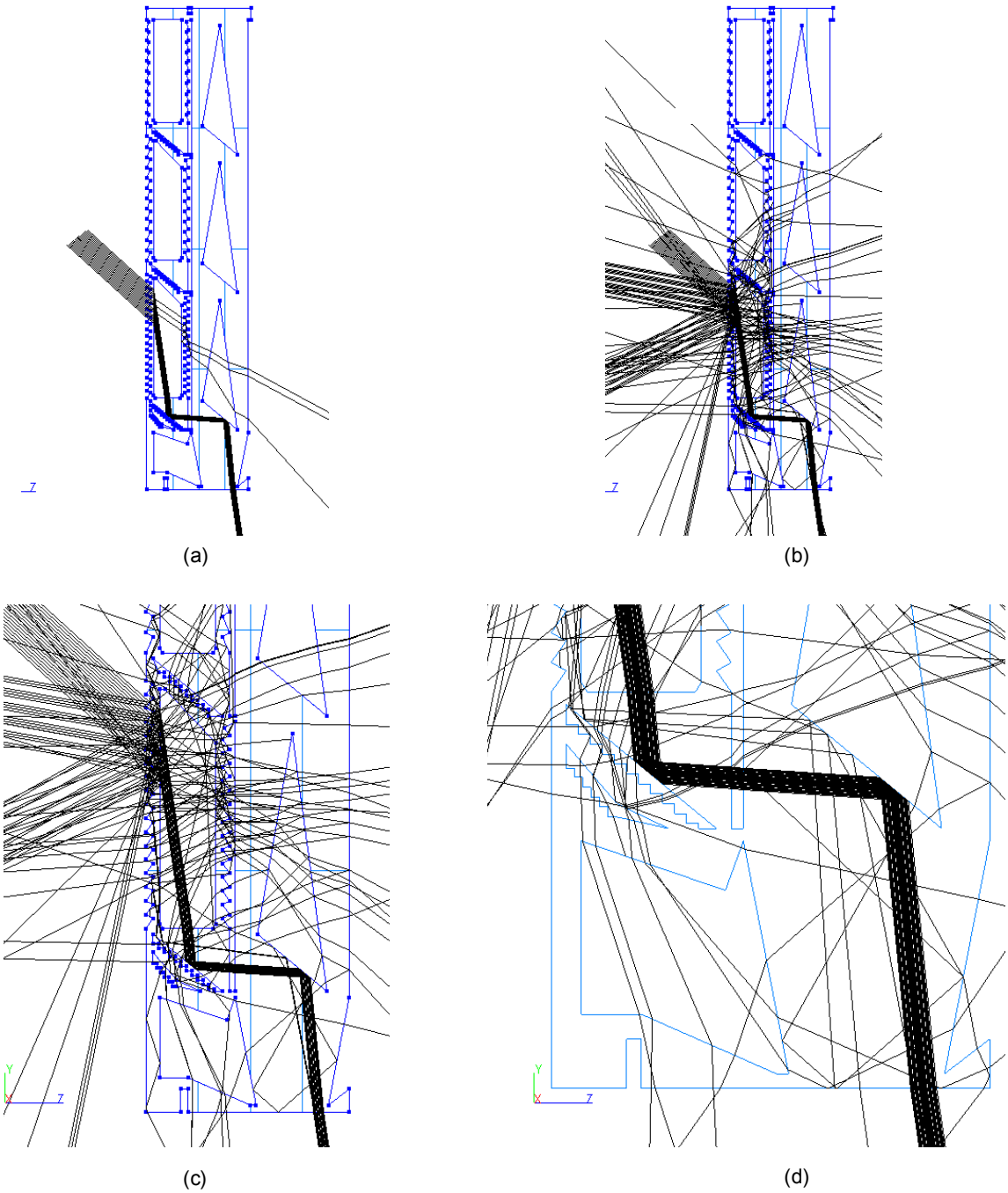

Figure 8.5 – Ray-trace analysis simulating Fresnel-reflection losses with VINSC-A1 system (section-cut profile view). Collimated monochromatic light (λ = 555nm) is projected from left to right at incident angle θ_i = 47.7°. In image (a) no Fresnel-reflections are considered; in image (b) Fresnel-reflection losses are considered. Images (c) and (d) are zoom-in of previous image (b).

8.4 Main geometric features and parameters

8.4.1 Prismatic arrays set (entrance aperture)

As seen in Figure 8.1, the VINSC is composed by a sub-set of three sections of two parallel prismatic-arrays with a distance between them. Each sub-section has its own array of prisms with specific apex angle (α) and base angle (β) values.

In principle, the entrance aperture of the VINSC system is its entire frontal surface. The first prismatic array (PA-1) constitutes the entrance aperture of the system. In the case of the VINSC-A1 system (example), the top-section prisms apex angle measures α_{top} = 10°; the mid-section prisms apex angle measures α_{mid} = 20°; and low-section prisms apex angles measures α_{low} = 30°. Note that the selected values of the apex angles α were chosen only as an example.

The second prismatic array (PA-2) basic function is to try to recycle part of the light that otherwise would escape from the light guide system and re-direct it again towards the 45°TIR surface.

8.4.2 Asymmetric integrated light guide (AILG)

Due to its geometric construction, the light guide of the VINSC system basic configuration is named asymmetric integrated light guide (AILG) - (see Figures 8.1 and 8.2). Light will remain trapped inside the AILG as long as the incident angle θ_i at the AILG walls are equal or larger than the critical angle θ_c of the solid-dielectric material of the AILG in relation to its surrounding medium.

8.4.3 Redundant optical features

The term “redundant optical features” is applied to define the optical elements and surfaces inside the VINSC system that are apparently redundant. The basic function of these features is to recycle part of the rays that otherwise would escape from the system.

The redundant optical features are located in “unoccupied areas” inside the VINSC system volumetric space configuration that otherwise would remain empty or with no function at all (see Figure 8.1). Since the VINSC systems can be made-out of a single solid-dielectric material, and manufactured by processes such as injection moulding process (or casting process, for glass), the addition of redundant optical features is expected not compromise the costs and manufacturing process.

8.5 Computer simulations and ray-trace analysis

Figure 8.6 plots the results for ray-tracing analysis for the VINSC-A1 system with a refractive index n =1, 491. The simulation considered a beam of collimated monochromatic light (λ = 555nm) incident at the meridional optical plane of the system, representing the solar altitude h_s angular displacement. Incident monochromatic light started with an energy power of 1.0, representing 1lm. Fresnel-reflection losses were not considered in this simulation. Note that the lumens output can also considered as the transmittance efficiency T_E of the system.

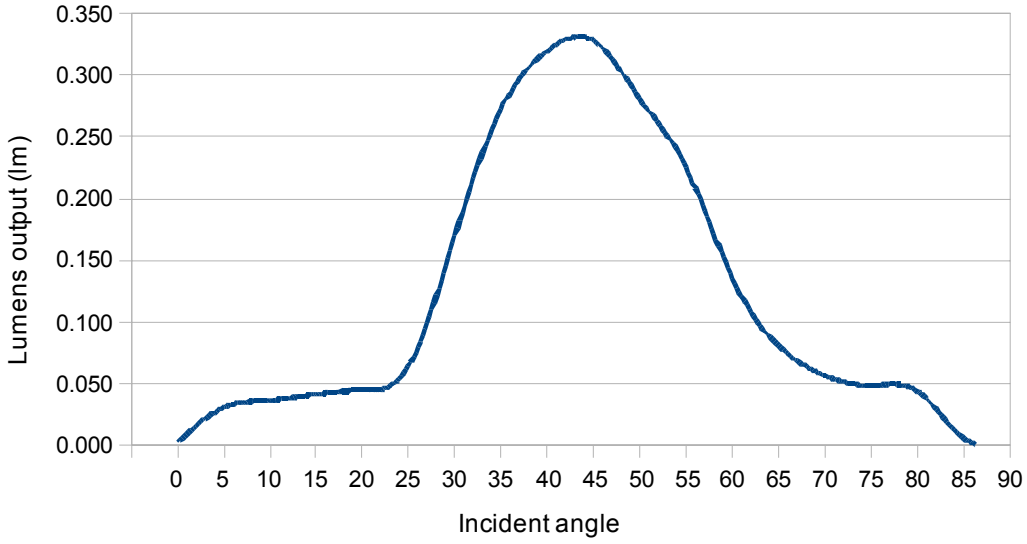

Figure 8.6 – Results of OptiCAD® ray-trace analysis conducted with VINSC-A1 system.

8.6 VINSC systems laser-cut demonstration prototypes

The VINSC demonstration prototypes were manufactured with the laser cutter machine. The VINSC prototypes were manufactured using a sheet of clear PMMA, commercial grade 3mm thick, in contrast with the prototypes presented in the previous chapters that are 5mm thick. The intention was to verify if the thickness of the PMMA sheet could have a significant influence on the quality of the surface finishing provided by the laser ablation process.

A series of VINSC systems laser-cut PMMA prototypes are displayed in Figure 8.7. It is important to stress that all prototypes represent a vertical-section (slice) of the VINSC system containing its optical profile (optical meridional plane).

The alternative designs to the original VINSC-A1 system (Figure 8.1) include the parabolic-type profile (VINSC-3, in Fig.8.7), and the hyperbolic-type profile (VINSC-2 and VINSC-4, in Fig. 8.7).

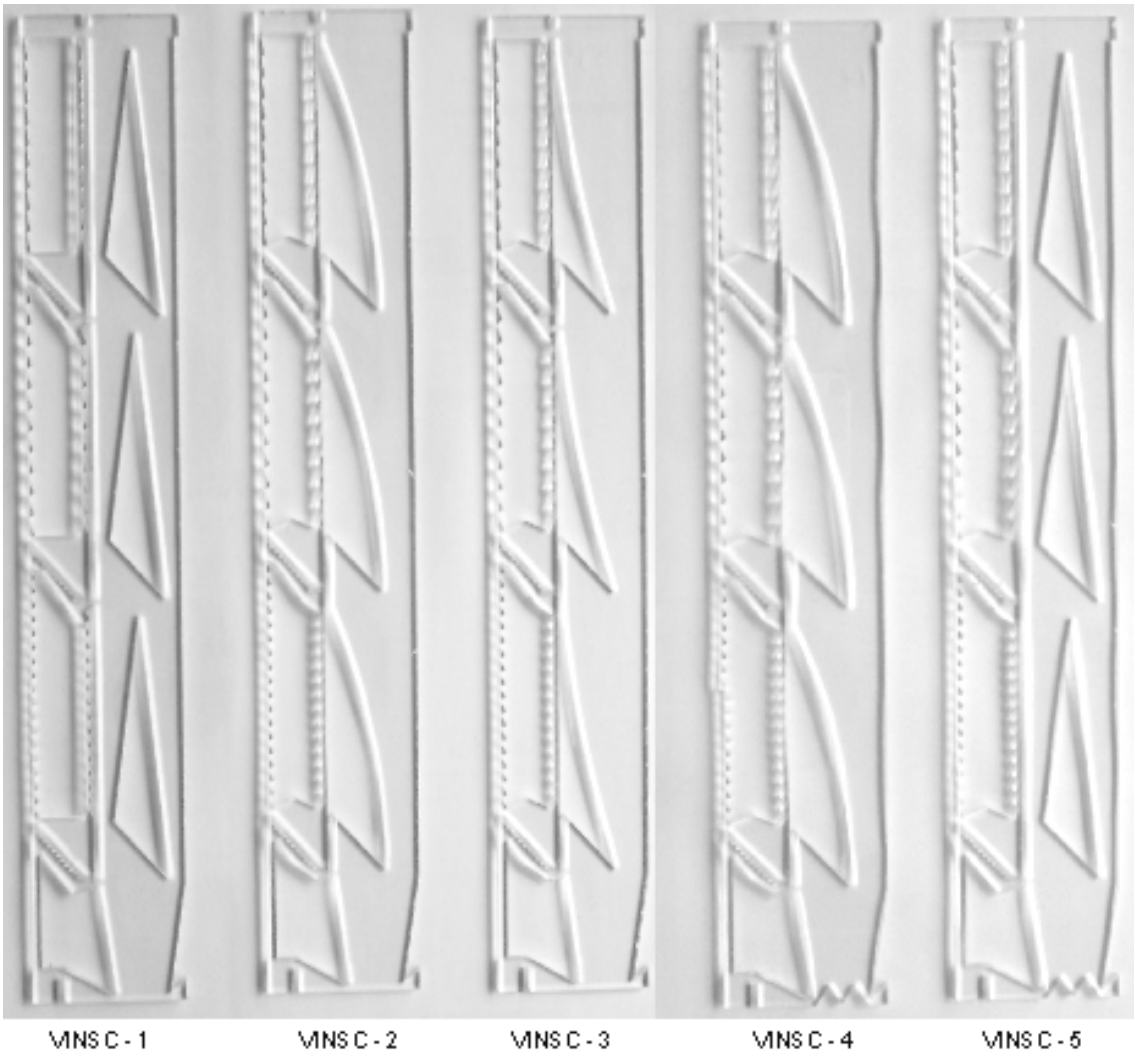

Figure 8.7 – VINSC systems laser-cut PMMA prototype sections, 3mm thick.

8.7 VINSC prototypes surface analysis

As already observed and analysed in the previous chapters, the application of the laser ablation process to manufacture the prototypes resulted in severe damage to their surface. As mentioned in the previous section, it was expected that the VINSC demonstration prototypes, made out of a 3mm thick clear PMMA sheet, could provide surfaces with higher optical quality. However, this was not observed in the final prototypes. Smaller features presented the worst surface finishing. Polishing was not so useful due to technical limitations in accessing these surfaces.

Figure 8.8 presents a series of examples of surface finishing with low quality provided by the laser ablation process. The images correspond to the section cut area of a 3mm thick PMMA laser-cut prototype. Figure 8.9 shows a detailed view of a

redundant optical feature on the VINSC prototypes. Notice the areas of melted-solidified PMMA caused by the laser ablation process (Figure 8.9).

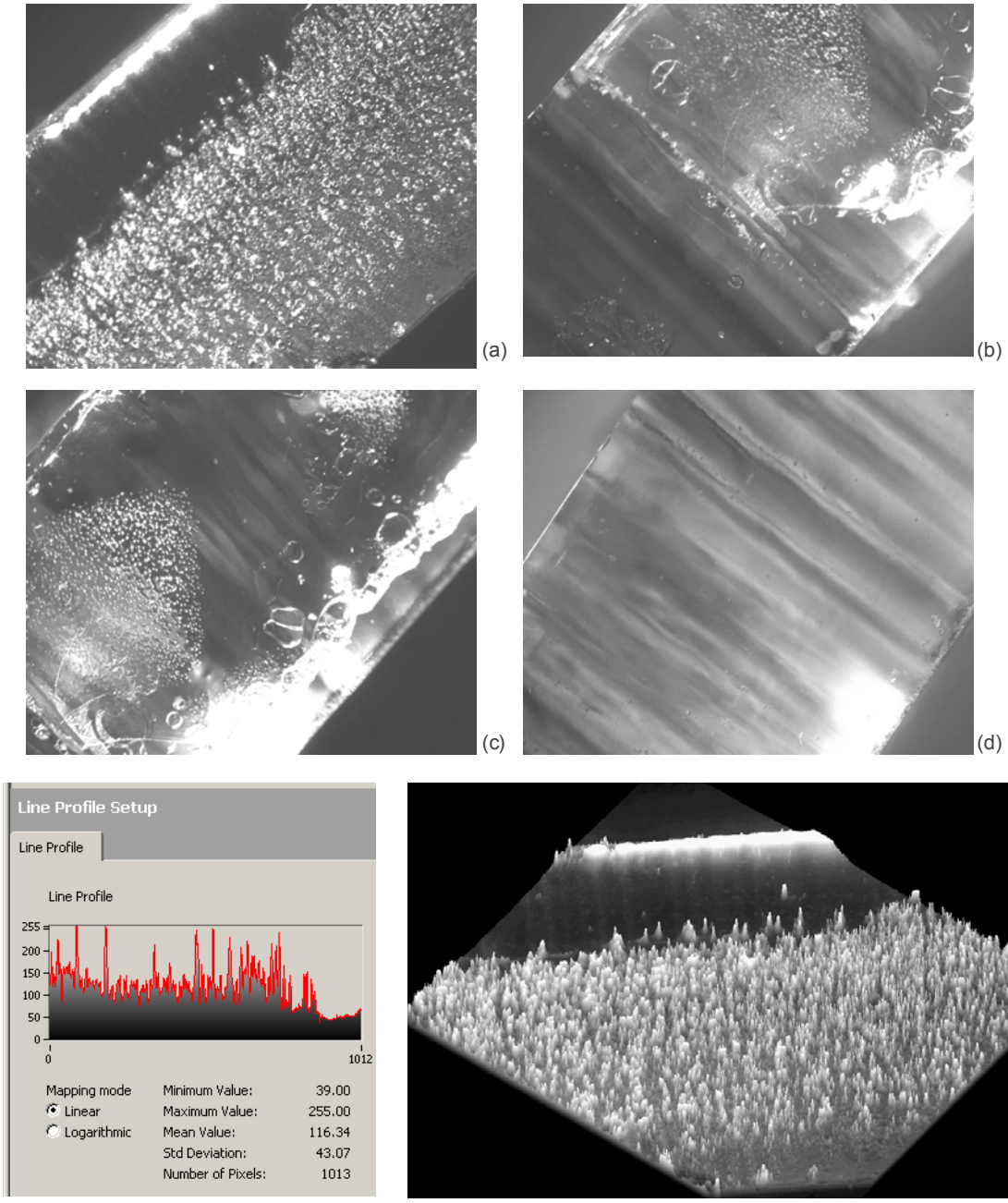

Figure 8.8 – Examples of surface finishing with low quality provided by the laser ablation process. VINSC laser-cut prototypes: PMMA, 3mm thick. Images (a), (b), (c) and (d) width corresponds to approximately 4mm.

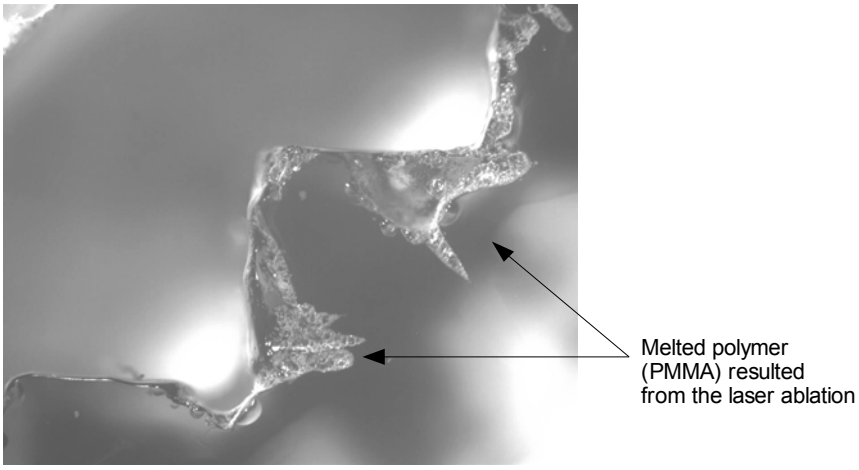

Figure 8.9 – Surface analysis of redundant optical feature. Image width corresponds to ≈ 4mm.

8.9 Outdoor experimental tests of the VINSC laser-cut prototype

A series of outdoor experimental tests were conducted in order to evaluate the performance of the VINSC systems under direct sunlight. Due to time constraints and weather conditions, most of the outdoors tests were conducted during the winter time, when the Sun is at its lowest altitude in the sky.

The outdoor experimental test configuration set-up for the VINSC systems is presented in Figure 8.10. A stack of three PMMA 3mm thick VINSC-A1 system laser-cut section was used. The three 3mm thick parts were fixed together resulting in a final system with a frontal aperture area of 9mm by 320mm (height).

The outdoor experiment configuration displayed in Figure 8.10(a) follows basically the same set-up as the ones presented in the previous chapters. In the configuration shown in Figure 8.10(b) a 1m long hollow tubular-folded aluminium sheet reflective light pipe integrator was used instead of the 300mm long applied in the previous configuration (Figure 8.10a). Both light pipes have a diameter of 50mm.

A photometer (Extech EA-31 illuminance meter) with cosine correction diffuse dome is positioned at the exit end of the hollow light pipes integrators (Figure 8.10a; 8.10b) to measure the illuminance output E_{out} (lx) emerging from the VINSC-A1 system exit aperture. At the same time another photometer (Extech EA-33) was positioned next to the experiment set-up to measure the vertical/façade illuminance input E_{in} (see Figure 8.10b). All outdoors experimental tests were conducted at Brunel University campus, Uxbridge, London, United Kingdom. Geographic coordinates: 51° 33' 0" North, 0° 29' 0" West. Figure 8.11 plots the results of the first series of outdoor experimental test with the VINSC-A1 system, conducted during a period of 3 hours (11:00 – 14:00 hs, local GMT time) on the 15/01/09 (low winter sun).

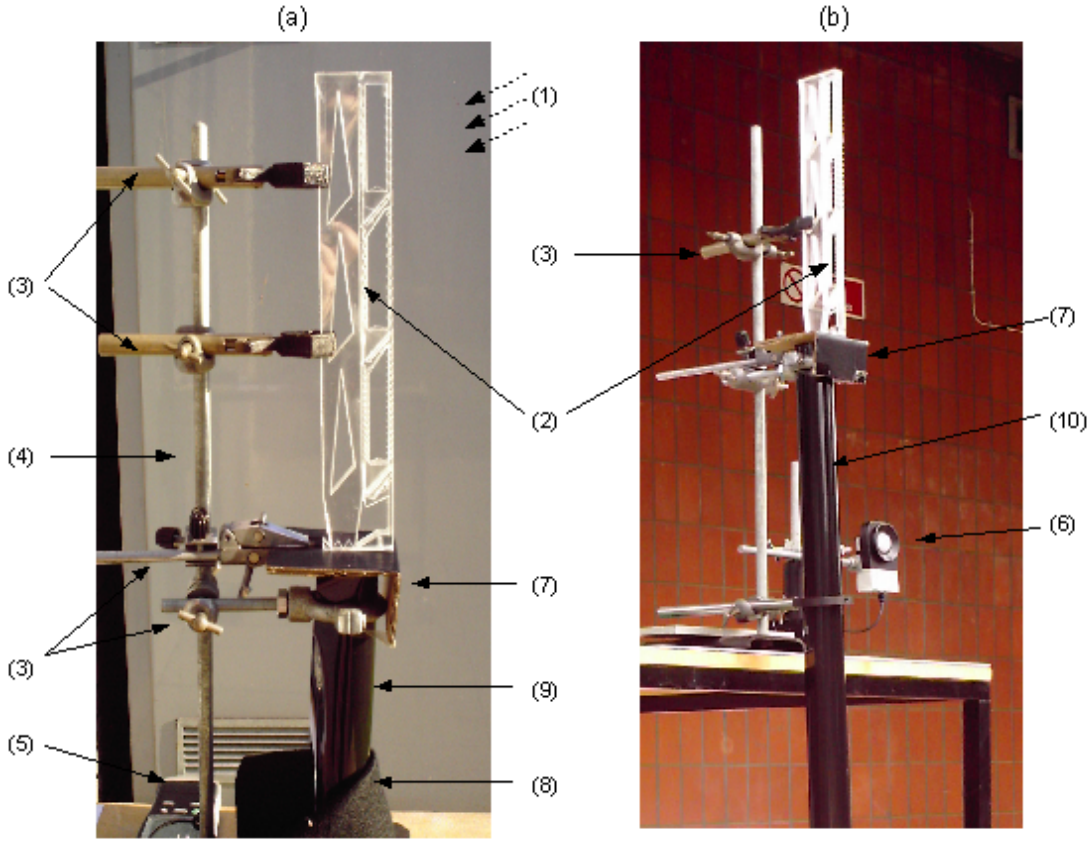

(1) Direct sunlight (coming from right-to-left); (2) VINSC system; (3) Holders; (4) Support structure; (5) Photometer (lux metre); (6) Photometer used to measure ground and vertical illuminance of direct sunlight; (7) Protective screen cap; (8) protective black cloth; (9) Hollow reflective light pipe integrator 300mm long; (10) Hollow reflective light pipe integrator 1m long.

Figure 8.10 – Two outdoors experiment set-up for the VINSC systems. In (a), lateral view of the VINSC-A1 system coupled to 300mm long hollow aluminium light pipe integrator. In the experiment set-up configuration presented in (b), a 1m long hollow aluminium light pipe is used.

The results for the direct illuminance output E_{out} (lx) for the VINSC-A1 prototypes (Figure 8.11b) shows that the system responds quite well to variations in the vertical/façade illuminance input E_{in} (Figure 8.11a). The illuminance output E_{out} peaked around 1400lx, yielding a peak transmission efficiency T_E of about 2% (Figure 8.11c). Note that both the illuminance output E_{out} and the transmission efficiency T_E increases when the incident angle θ_i of direct sunlight approaches the meridional plane of the VINSC-A1 system and decreases after that. However, it is important to note that the solar altitude angle h_s during the test was below the optimum acceptance angle θ_{accept} of the VINSC-A1 demonstration prototype.

(a)

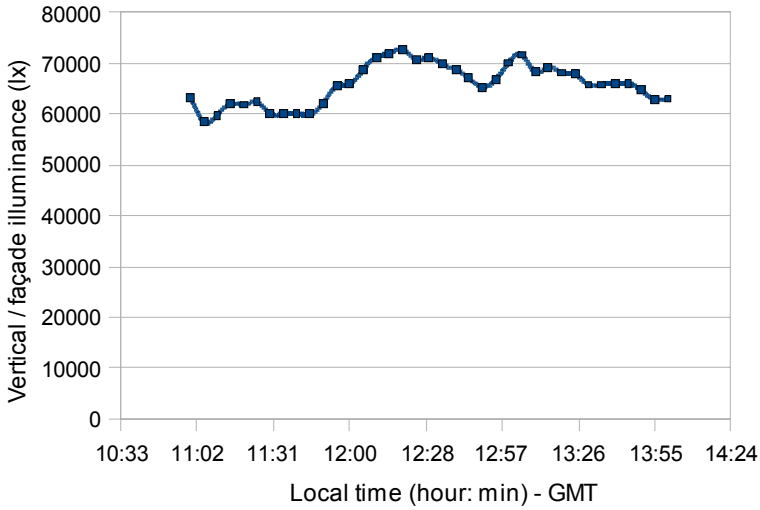

(b)

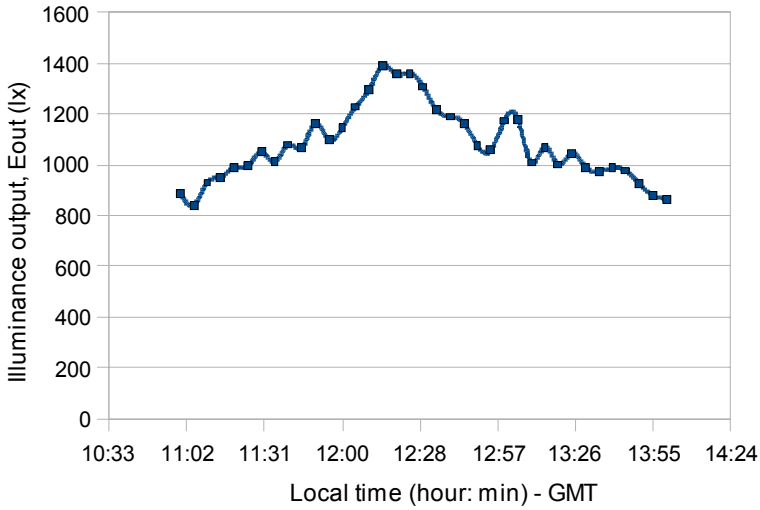

(c)

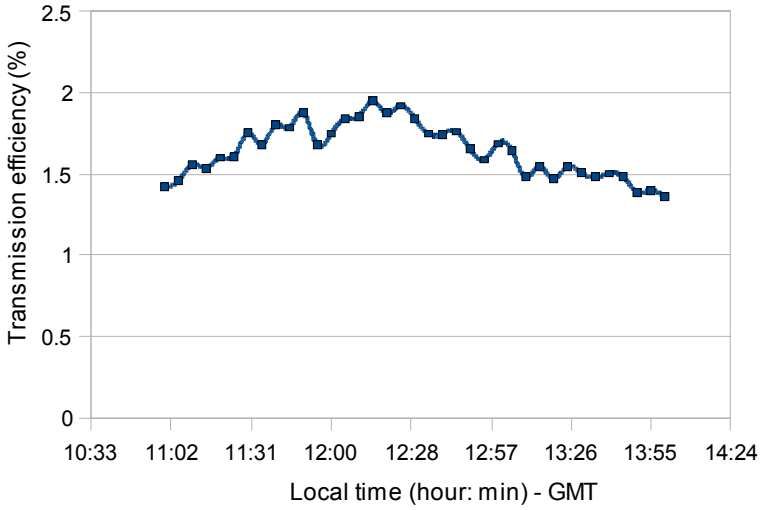

Figure 8.11 – Outdoor experimental tests results for VINSC-A1 system (3x3mm; PMMA). Graph (a) plots the vertical/façade global illuminance (lx) as a function of time; (b) plots the transmitted illuminance output (lx) of the system as a function of time; (c) plots the transmission efficiency T_E (%) of the system.

Figure 8.12 plots the illuminance output E_{out} results for the VINSC-A1 demonstration prototype considering five different orientations: East (E), South-East (SE), South (S), South-West (SW) and West (W). Measurements were taken during the same day (14th of March) by rotating the experiment set-up towards the five specified directions (indicated by a magnetic compass). Figure 8.13 presents the total sum (or combined results, considering overlaps) of the results previously shown in Figure 8.12. Figure 8.14 and Figure 8.15 present stereographic projections of the results previously displayed in Figures 8.12 and 8.13, respectively. These results demonstrate that it is possible to increase the overall efficiency of the system by optimising the orientation of a series of VINSC/RINSC solar collectors and by combining the illuminance output E_{out} from these systems.

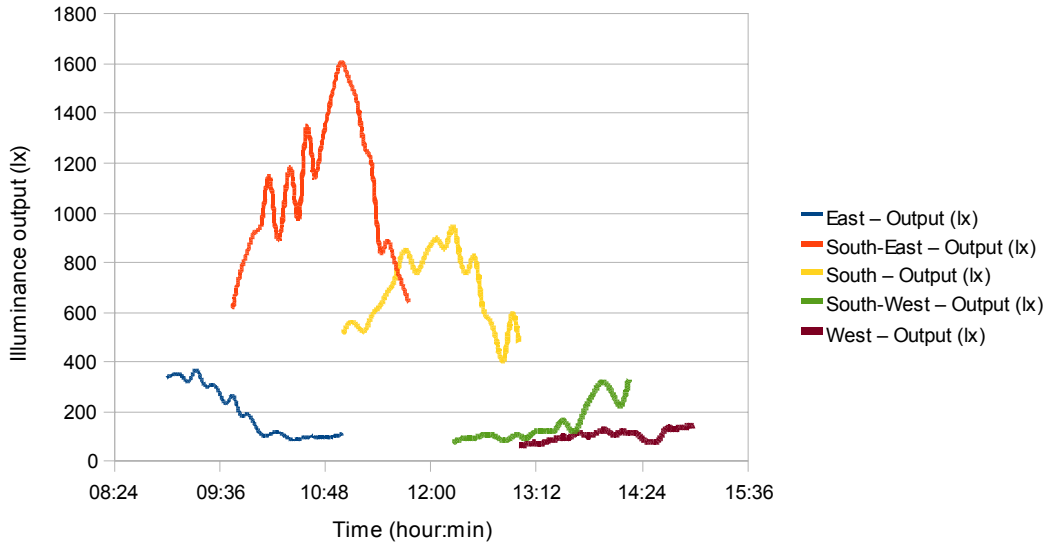

Figure 8.12 – Illuminance output E_{out} of outdoor experimental testes with of VINSC-A1 system.

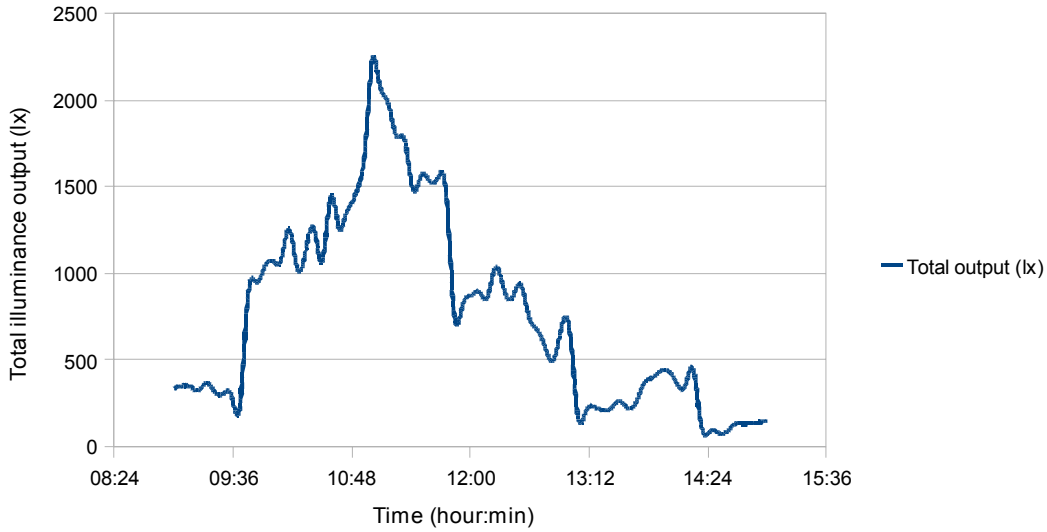

Figure 8.13 – Combined result (total sum, considering overlapping) of the Illuminance output E_{out} results previously displayed in Figure 8.12.

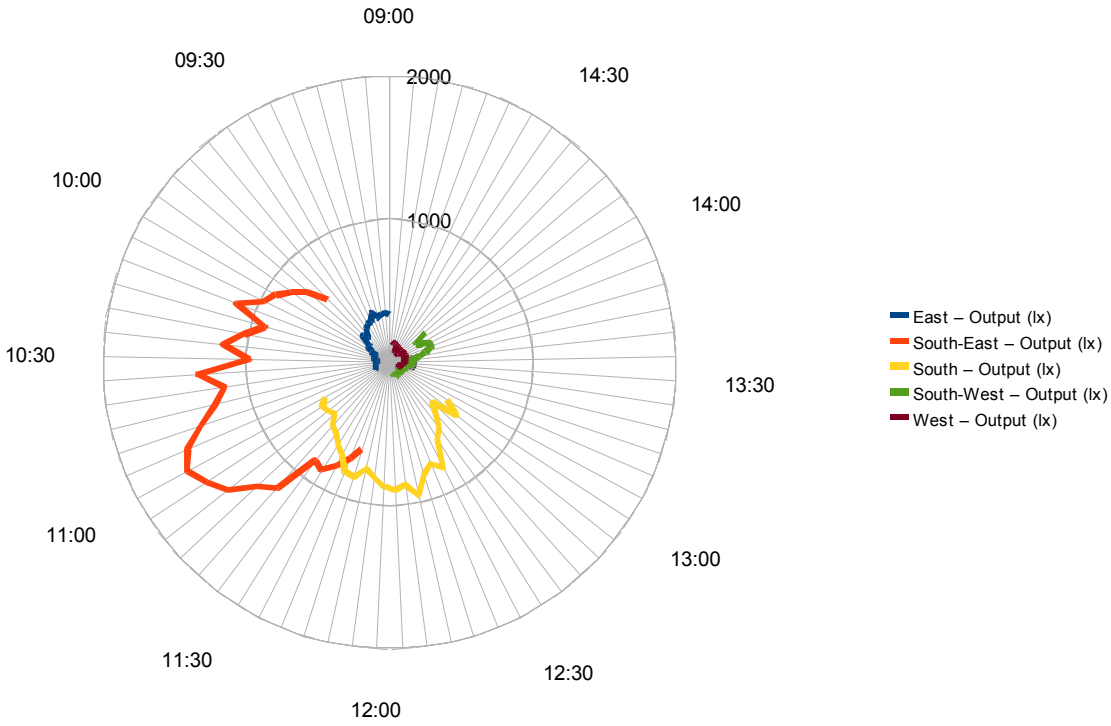

Figure 8.14 – Stereographic projection of the outdoor test results of the illuminance output E_{out} for the VINSC-A1 system previously presented in Figure 8.12.

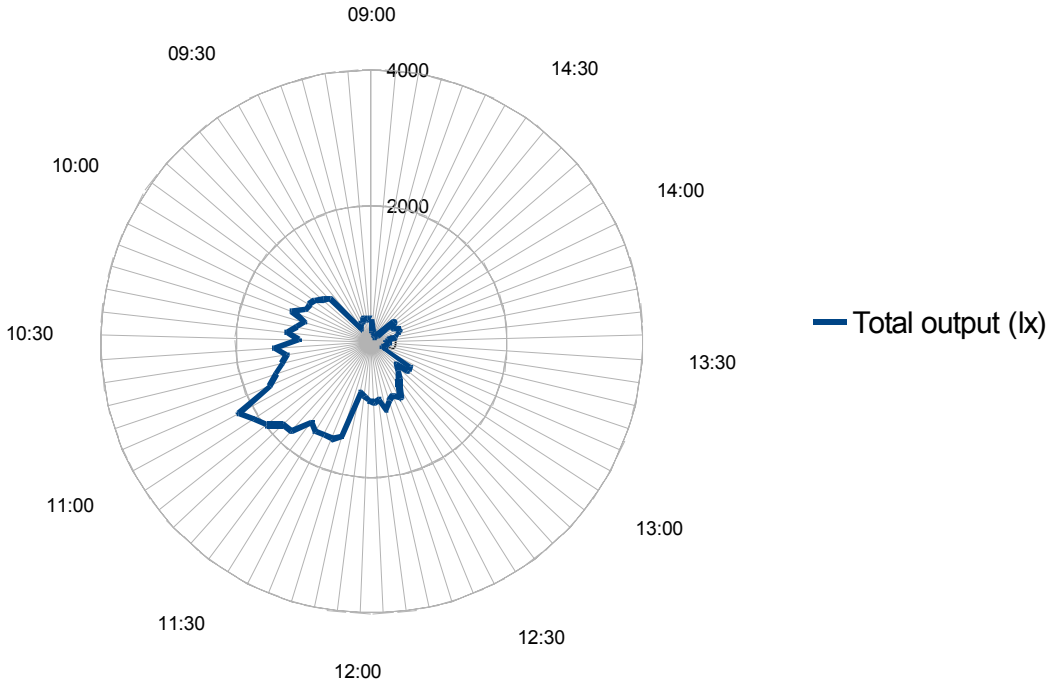

Figure 8.15 - Stereographic projection plotting the hour-distribution of the total sum of the illuminance output E_{out} (lx) of the VINSC-A1 system prototype previously presented in Figure 8.13.

8.10 CAD-CAE preliminary simulations for injection moulding

A series of simulations to analyse the feasibility of using injection moulding to mass-manufacture the VINSC systems was performed using CAD-CAE Moldflow® software. The VINSC-A1 system was used for a computer simulation preliminary study. Two materials were considered in the simulations: clear PMMA and polycarbonate (PC), both commercial grades.

Quality in injection moulding is directly dependent on the homogeneous filling of the moulds cavities (Strong, 1996, pp.307; Courbebaisse and Garcia, 2002). A fundamental issue to achieve this relates to the correct location of the injection gates. The injection gate is the point through which the melted fluid-material (in this case, polymers PMMA and PC) enters the mould cavities (Strong, 1996, pp.307).

According to Courbebaisse and Garcia (2002) and Chen and Liu (1999), a preliminary study to identify the location of the injection gate(s) should be considered with regard to the geometry of the mould cavities (Strong, 1996, pp.307).

The injection gates were located at four different positions on the lateral side of the VINSC-A1 structure (Figure 8.16). The locations of the injection gates in the computer simulation considered:

- The software parameters and options (Moldflow®: www.modlflow.com);
- The geometry of the parts under analysis (VINSC systems);
- The extraction of the final product from the mould;
- References in the literature (Weng et al, 2009; Courbebaisse and Garcia, 2002; Chen and Liu, 1999; Strong, 1996).

Figure 8.16 displays the injection moulding simulations conducted with Moldflow® software. The simulation shows how the distribution of injected material inside the mould cavities of the VINSC-A1 system varies in accordance to location of the injection gate. Still in Figure 8.16, the 3D perspective of the VINSC-A1 mould is presented as an example to illustrate how the Moldflow® software calculates the time (measured in seconds) it takes to fill the entire cavity of the mould.

Figure 8.17 presents the results of the Moldflow® simulations for the VINSC-A1 system considering the four injection gate locations as previously shown in Figure 8.16. Figures 8.17a and 8.17b shows the injection time (i.e. the time that it takes to fill the entire mould cavities) varying in accordance to the location of the injection gate (locations shown in Figure 8.16). The software only accused that there could be a potential injection problem if the material used was PC and the selected injection gate was the no.3, as shown in Figure 8.17a. This happened due to the long time it took (> 27s) to fill the mould. All other simulations were considered feasible by the programme.

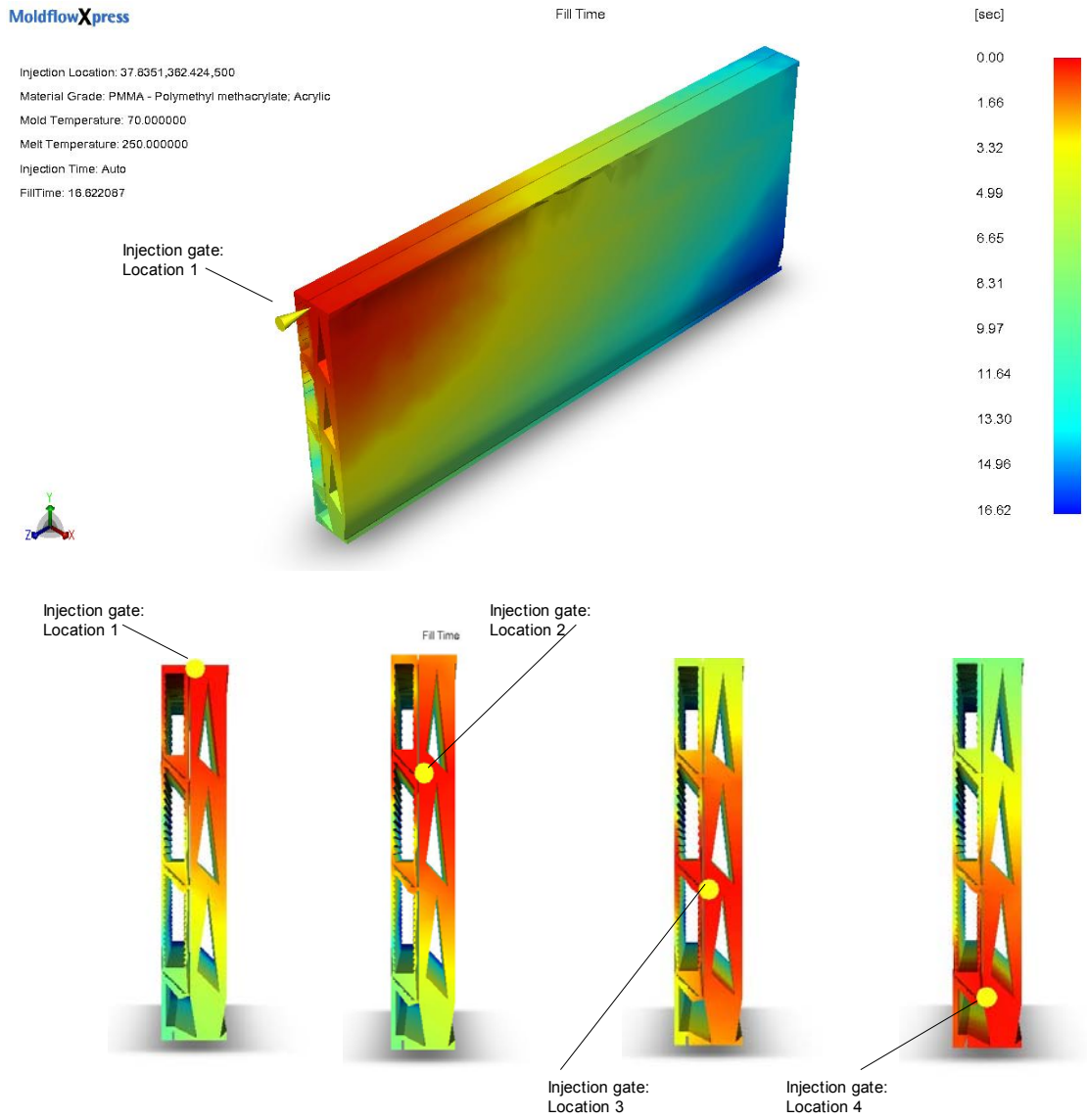

Figure 8.16 – CAD-CAE Moldflow® injection moulding simulation for the VINSC-A1 system.

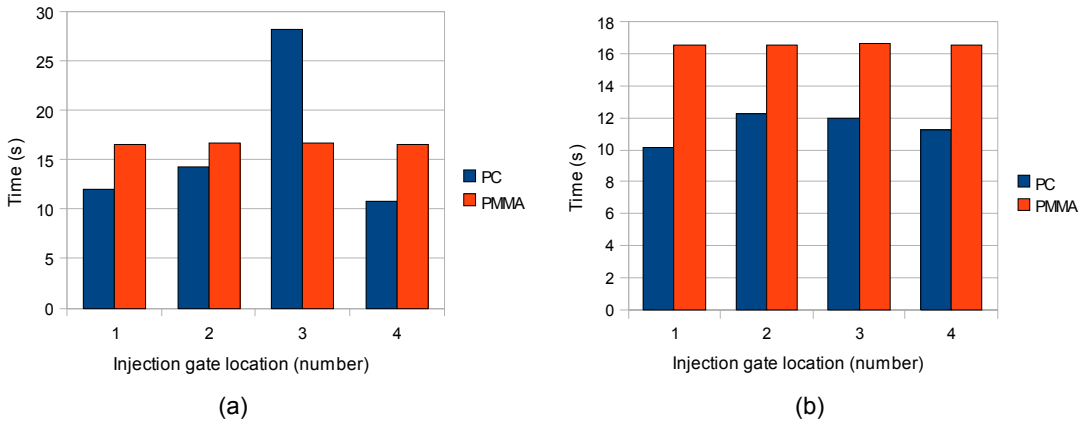

Figure 8.17 – Results of the Moldflow® injection moulding simulation according to injection gate location as specified previously in Figure 8.16. Injection time (measured in seconds, s) as a function of the injection gate location, for commercial grades of clear polycarbonate (PC) and clear PMMA. System: VINSC-A1.

Note that the melt temperature of the polymer has an important influence on the injection moulding process (Weng et al, 2009; Ashby, 2007). Polymers with higher melt temperature lead to lower viscosity. As a result there is also a reduction in cavity pressure and shear stress inside the mould (Weng et al, 2009). Weng et al (2009) has shown that residual stress at the immediate area located around the injection gates can result in the effect of birefringence[6].

Despite the fact that injection moulding is a relatively simple manufacturing process, the behaviour of injected molten polymer inside the moulds cavities is quite complex. As a consequence of this, the final quality of surface finishing, material distribution and wall thickness, among other parameters of injected moulded components, are highly dependent on the realisation of extended preliminary tests executed to fine-tune and select the optimum combination of manufacturing process parameters (Strong, 1996; O'Driscoll, 2002; Ashby, 2007). They also depend on the quality and geometry of the moulds, the injection machine capabilities and the accumulated know-how from the machine operators (Tsai et al, 2008; Edwards, 1998; Courbebaisse and Garcia, 2002). Hence, it is important to stress that the injection moulding simulation presented here should be seen as a preliminary study.

8.11 Results and discussion on the VINSC systems

The VINSC system provides an original optical configuration that was conceived with the intent to minimise Fresnel reflection losses at the entrance interface of its asymmetrical integrated light guide (AILG).

The VINSC system includes a set of at least three prismatic arrays with different apex angles α, increasing the overall acceptance angle θ_{accept} of the system in the incidence angle interval of $25° \leq \theta_i \geq 70°$ (at its optical meridional plane). The optical layout of the light guide AILG allows the coupling of light at an incident angle θ_i close to the normal axis of the entrance interface section. As a result, Fresnel reflections losses are minimised at the entrance interface of the light guide AILG. Ray-tracing analysis conducted with OptiCAD® software indicates that Fresnel reflections at the related AILG entrance interface section are kept below 5% (for n=1.491 and λ = 555nm). This result is in good agreement with the theory presented in the literature review (Chapter 2; Section 2.6.5: see Figure 2.12).

The VINSC optical configurations presented in this work provides a geometric concentration ratio of at least C_R = 12.8X. Computer simulations conducted with

[6] Birefringence is also known as double refraction (Hecht, 1998).

OptiCAD® software indicate that peak transmission efficiencies $T_E > 34\%$ are possible at an incident angle $\theta_i \approx 45°$ of monochromatic light ($\lambda = 555nm$) at the VINSC-A1 system optical meridional plane. For comparison, the simulated IMPSC systems (Chapter 7) peak transmission efficiencies yield results of $T_E \approx 27\%$.

Outdoor experimental tests conducted during the winter time (low solar incidence angles) with a VINSC-A1 system demonstration prototype (laser-cut, PMMA) yield illuminance transmission efficiencies T_E around 1.5% to 2%. Illuminance output E_{out} peaking from $E_{out} \approx 1400lx$ (measured on the 15.01.09) to $E_{out} \approx 1600lx$ (measured on the 14.03.09), and also varying in accordance to the positioning and orientation (E, S-E, S, S-W, W), indicates that the VINSC-A1 demonstration prototype responds well to variations of the solar incidence angle (h_s; γ_s).

8.12 Summary and conclusions of Chapter 8

The VINSC concept provides a possible configuration where Fresnel-reflection losses at the entrance interface of the light guide AILG are minimised to around 5% to 10%. This is done by providing a geometric configuration where the incident angle θ_i of an incoming ray approaches the normal of the light guide AILG entrance section interface.

Injection moulding simulations and preliminary studies indicate the possibility to manufacture the VINSC-RINSC systems by mass-manufacturing processes such as injection moulding. Simulations considering PMMA and polycarbonate (PC) materials in the injection process indicate that the VINSC system can potentially be manufactured using a single mould, leading to costs reduction in tooling and machinery.

Chapter 9 - Results and Contributions to Knowledge

9.1 Introduction

This chapter presents a general discussion on the main results of this work and describes its original contributions to knowledge. Comparisons between the RINSC systems and the state-of-the-art in solar collectors and solar concentrators are drawn. Considerations on the application of the laser ablation prototyping process and the prototypes surface quality are also made.

9.2 Discussion on the main results and comparative analysis

The results of the experimental tests conducted with the demonstration prototypes have indicated that the RINSC systems can provide transmission efficiencies T_E at least comparable with current luminescent solar concentrators (LSC) technologies ($T_E \approx 6\%$ to $T_E \approx 8\%$) described in the literature (Earp et al, 2004; Slooff et al, 2008; Sanderson, 2008; Rowan et al, 2008). It is also important to notice that the peak transmission efficiencies T_E of the RINSC systems (varying from $T_E \approx 2\%$ to $T_E \approx 8\%$) are also comparable with the daylight factor (DF) recommended by lighting and building standards (CIE, 2003; British Standard BS 8206-2:2008). In the literature it has been shown that a DF of 2% to 5% is sufficient for most indoor activities (CIE, 2003; Li and Cheung, 2006; Li, 2007; Li et al, 2008; British Standard BS 8206-2:2008).

The PSC systems provided a high geometric concentration ratio C_R = 25X. However, the peak transmission efficiencies T_E of the PSC demonstration prototypes were very low: around $T_E \approx 0.12\%$ (measured at a distance d = 1000mm) to $T_E \approx 0.5\%$ (measured at a distance d = 50mm). This generated the need to find better solutions to increase the efficiency and the acceptance angle θ_{accept} as well. This need led to the development of the MPSC concept.

The basic design of the MPSC system provided a geometric concentration ratio of $C_R \approx 5.6X$. The MPSC demonstration prototypes yield peak transmission efficiencies

T_E from 6% to 8% for incident radiant energy (λ = 300nm - 1100nm) at the entrance aperture meridional plane varying from $\theta_i = 5°$ to $\theta_i = 75°$.

The IMPSC systems were derived from the MPSC basic concept. The inclusion of a concentration section at the low-end section of the IMPSC increased the geometric concentration ratio to at least $C_R \approx 12.5X$, whereas the MPSC systems geometric concentration ratio was around $C_R \approx 5.6X$. Computer simulations indicated that the IMPSC basic optical configuration can provide transmission efficiencies T_E up to 26.8%, leading to an effective optical concentration ratio of at least 3.25X (considering: $\alpha_{PA} = 24°$; $\alpha_{SILG} = 8°$; $\theta_i \approx 58°$; λ = 555nm; and refractive index n = 1.491). IMPSC demonstration prototypes yield transmission efficiencies up to $T_E = 5\%$ for an incident artificial light source (λ = 300nm-1100nm) at the entrance aperture meridional plane considering an incidence angle θ_i varying from $\theta_i = 5°$ to $\theta_i = 75°$.

The VINSC optical configurations provided a geometric concentration ratio of at least $C_R \approx 12.8X$. Computer simulations conducted with the VINSC systems indicated that peak transmission efficiencies $T_E > 34\%$ are possible for an incident angle $\theta_i \approx 45°$ of monochromatic light (λ =555nm) at the system optical meridional plane.

The RINSC systems described in this work can lead to optical configurations with higher geometric concentration ratio C_R than current nonimaging concentrators. As discussed in the literature review, the classical CPC nonimaging concentrator is limited to a geometric concentration ratio C_R between 3 and 5 (Chaves and Collares-Pereira, 2000, pp.270). CPC-type devices with a geometric concentration ratio $C_R > 5$ are unpractical because they become too tall with the increase of the concentration ratio (Welford and Winston, 1978; Chaves and Collares-Pereira, 2000, pp.270). The reflective asymmetric CPC for building façade integration analysed by Mallick et al (2006) has a geometric concentration ratio C_R of 2.32. Solid-dielectric wedge-type concentrators, such as the systems analysed by Maruyama and Osako (1999) and Chien et al (2009), usually have a geometric concentration ratio C_R between 2.5 and 5.

Table 9.1 compares some of the systems introduced in this thesis with the state-of-the-art in nonimaging concentrators described in the literature. Table 9.2 summarises the main results of the laboratory experimental tests conducted with the laser-cut demonstration prototypes.

Table 9.1 – Comparison between the geometric concentration ratio C_R of some of the RINSC systems demonstration prototypes and current technologies in nonimaging concentrators.

RINSC systems prototypes	CR	State-of -the-art nonimaging concentators	CR
PSC-A	25	(a) Classic CPC	3 to 5
MPSC-X1	5.6	(b) Dielectric-filed CPC	3 to 5
MPSC-S1	5.6	(c) Solid-dielectric wedge-type concentrators	2.5 to 5
PSC-B1	7.5	(d) Reflective asymmetric CPC	2.32
IMPSC-D	10	(e) DTIRC	3 to 6
IMPSC-A	12.5		
VINSC	12.8		

References: (a) Chaves and Collares-Pereira (2000, pp.270); (b) Welford and Winston (1978); (c) Maruyama and Osako (1999) and Chien et al (2009); (d) Mallick et al (2006); (e) Ning et al (1987).

Table 9.2 – Peak transmission efficiencies of RINSC systems demonstration prototypes with higher performance. Numerical data selected from laboratory experimental tests results.

RINSC systems	Peak transmission efficiencies T_E (%) (Measurement distance: light pipe lenght, in mm)					
	50	100	500	1000	1500	Avarege
MPSC – X1(2P)	5.98	3.63	1.84	1.3	0.88	2.73
MPSC – X2(2P)	7	4.27	2.33	1.77	1.5	3.38
MPSC – S1(SA)	7.89	2.68	1.22	1.14	0.95	2.78
IMPSC-A1 (SA)	3.08	3	1.3	0.73	0.58	1.74
IMPSC-A1 (LA)	1.81	1.56	0.55	0.54	0.25	0.95
IMPSC-A1 (SA)+BRA+DLC	4.8	4.5	2.6	1.7	1.13	2.95
IMPSC-A2 (SA)	3.1	3.37	1.55	0.71	0.52	1.85
IMPSC-D1 (SA)	2.56	3.64	1.36	0.9	0.52	1.8

9.2 Considerations on the laser ablation prototyping process

In general terms, the laser ablation process didn't provide the surface finishing expected for the demonstration prototypes. Thermal expansion caused by the heat of the laser generated several types of surface and sub-surface defects. Solidified molten plastic, air-bubbles and cracks are some examples of the features generated along the path of the laser-cut.

It is necessary to consider that the surface and sub-surface defects has a double-negative impact on light capture and transmission potential. Firstly, surface scattering occurs when a beam of light enters the system. Secondly, volume (bulk) scattering occurs for rays propagating inside the system by TIR. The effect of surface and sub-surface defects on the transmission of light inside solid dielectric mediums has been previously related to an increase in losses due to backscattering inside solid-dielectric planar waveguides (Hunsperger, 1995; Ladouceur and Poladain, 1996). This

means that a significant portion of the rays propagating inside the light guide escaped due to manufacturing errors on the surface and the formation of air-bubbles and other inclusions inside the bulk of the material due to thermal stress caused by the laser ablation process.

However, it is important to stress, that despite the surface and sub-surface defects, the laser-manufactured demonstration prototypes successfully proved the RINSC concepts introduced in this thesis.

9.3 Contributions to knowledge

The main contributions to knowledge resulted from this research are defined as:

(1st) A novel category of nonimaging solar collector devices named Refractive Integrated Nonimaging Solar Collectors (RINSC) has been presented. The RINSC category provided the basic schematic design layout-concept from which it was possible to integrate several geometrical optical features into a single-structure solid-dielectric embodiment. The RINSC systems were generated by designing an "optical profile section" (ROPS) on the lateral side of a solid-dielectric volume. The basic geometrical optics schematic layout was characterised by having the exit aperture and the entrance aperture located in perpendicular planes. The basic layout and design parameters provided a frame-work for the design of compact optical geometries. The RINSC category, as presented and analysed in this work, was sub-divided into four sub-categories: (1) the Prismatic Solar Collector (PSC); (B) the Multi-Prismatic Solar Collector (MPSC); (3) the Integrated Multi-Prismatic Solar Collector (IMPSC); and (4) the Vertically Integrated Nonimaging Solar Collector (VINSC). Each RINSC sub-category was defined by a set of geometric optical features integrated in an original optical configuration.

(2nd) The Prismatic Solar Collector (PSC) concept demonstrated that it is possible to use a single solid-dielectric prismatic array panel with combined light guide to harvest and trap incident light by means of total internal reflection (TIR).

(3rd) The Multi-Prismatic Solar Collectors (MPSC) expanded the PSC concept by provided an original optical arrangement characterised by a series of parallel prismatic arrays with combined light guide integrated into an enclosed optical system. It demonstrated that the introduction of a succession of parallel prismatic arrays can lead to larger acceptance angles θ_{accept} and higher transmission efficiencies T_E than the previous PSC systems.

(4th) The Integrated Multi-Prismatic Solar Collectors (IMPSC) introduced a series of original optical arrangements that integrated two sets of parallel prismatic arrays with at least one independent symmetrical integrated light guide (SILG), with a continuous linear profile, located in-between the prismatic arrays. The SILG geometry resembles an “inverted V” and was defined by its apex angle α_{SILG} located at the top-end of its structure. Light can be trapped by means of TIR inside the light guide (SILG). Due to the geometry of the SILG, the angular distribution $\Delta\theta$ of light trapped by TIR is improved by the angular increment $\alpha_{SILG/2}.N_{TIR}$, where $\alpha_{SILG/2}$ corresponds to half apex angle of the SILG and N_{TIR} the number of total internal reflections. A series of polygonal light-extractors located at the low-end section of the light guide SILG improved the extraction of light from the light guide SILG by decreasing the incident angle θ_i of a light ray at the extractors interface till it is lower than the critical angle θ_c (in the case of the PMMA demonstration prototypes: $\theta_c \approx 42°$, for $\lambda = 555nm$). The IMPSC basic concept provided an optical system with at least two different ranges of acceptance angles θ_{accept} by assigning different values for each set of prismatic array apex angle α_{PA}.

(5th) The Vertically Integrated Nonimaging Solar Collector (VINSC) provided an original optical arrangement to minimise Fresnel reflection losses at the entrance interface of a vertically orientated solid-dielectric asymmetrical integrated light guide (AILG) that runs parallel to the prismatic arrays structure (entrance aperture). The VINSC system included a set of at least three prismatic arrays with different apex angles α, increasing the overall acceptance angle θ_{accept} of the system in the incidence angle interval of $25° \leq \theta_i \geq 70°$ (at the optical meridional plane). The optical layout of the AILG allows the coupling of light at an incident angle θ_i close to the normal axis of the AILG entrance section interface. As a result, Fresnel reflections losses can be minimised at the entrance interface of the light guide AILG, contributing to an increase in the system transmission efficiencies T_E.

(6th) Design, prototyping and experimental test of a novel device conceived to analyse the angular distribution $\Delta\theta$ of light emerging from the exit aperture of the solar-collectors demonstration prototypes. The device, named Angular Distribution Imaging Device (ADID), applies a series of fibre-optical cables concentrically attached to a dome-shaped structure to collect the light that emerges from the exit aperture of solar collectors. The end-section of each fibre-optical cable is attached to a flat surface component. A digital camera can be pointed towards the flat surface in order to visualize the end-section of the fibre-optical cables and extract qualitative information about the spatial distribution of light emerging from the solar collector exit aperture.

Chapter 10 - Conclusion and Future Work

10.1 Conclusion

A novel technological category of solar collector devices, named Refractive Integrated Nonimaging Solar Collectors, has been introduced and analysed. The RINSC systems have demonstrated that it is possible to design compact low-cost solid-dielectric nonimaging solar-daylighting-collector devices that combine several optical elements (such as prismatic arrays, solid-dielectric light guides, light extractors and concentrator sections) into a single-structure embodiment.

Due to their integral design, made out of a single material/component, and relatively simple geometry, it is argued that the RINSC systems presented in this thesis are suitable to be manufactured by mass-production processes, such as injection moulding and/or extrusion. This has significant advantages in reducing manufacturing costs while at the same time assuring the quality/efficiency of the final product.

The optical configurations and compact embodiment of the RINSC systems, in which the entrance aperture and the exit aperture are located in perpendicular planes, allows them to be integrated into a building façade without creating any protrusion. The low-cost design, compactness and mass-manufacturing potential construction of the RINSC systems indicate that they could lead to solar collector systems with high building integration potential.

It is important to stress that the design and development of the innovative optical systems introduced in this thesis were backed-up with extensive computer ray-tracing analysis, prototyping, laboratory and outdoor experimental tests.

10.2 Recommendations for future work

The following topics are recommended for future work:

(A) Improvement and optimisation of the geometric design and design variations of the RINSC systems and sub-categories. For example:

Considering the results of the experimental tests, the PSC is the less efficient system developed in this research. The peak efficiency measured was only $T_E \approx 0.5\%$.

However, further geometric modifications such as the customised specification of the prismatic array apex angle α for a particular building geographic and site location may optimise the system and improve its performance. Since it is the most simple and low-cost system of the RINSC system analysed in this thesis, the PSC system may find application as a kind of hybrid glazing.

As demonstrated, the MPSC concept allows the development of a significantly higher number of studies and design variations than the previous PSC system, since it has a larger number of parameters to change and improve. It is recommended the optimisation of the prismatic arrays and the specification of the prisms apex angle α in order to adapt the MPSC system for specific building geographic and site location.

The improvement of the optical configuration of the IMPSC systems could consider the optimisation of the symmetrical integrated light guide apex angle α_{SILG} in order to improve the angular distribution Δθ of light propagating inside the system. The geometric design and base angle β of the extractors section should also be optimised in accordance with the angular distribution Δθ of light propagating inside the symmetrical integrated light guide SILG. Design variations of the concentrator section at the low-end section of the IMPSC system are also worth investigating. Concentrator sections with “hyperbolic-type profiles” may provide more compact geometries. The designs of hyperbolic geometries for nonimaging concentrators has been previously analysed by authors such as Welford and Winston (1978) and Ning et al (1987a). Variations of the entrance surface of the concentrator section of the IMPSC system should also be considered. An increase of the curvature radius of the entrance surface, for example, can lead to a decrease in the distance of the focal line plane, resulting in a more compact system. Other possibilities could include the generation of an aspheric-type surface profile (Smith, 2000, pp.547) or even a Fresnel-type surface profile (Fresnel Technologies, 2001). These design alternatives could be very interesting to provide higher concentration for solar photovoltaic cells attached directly to the exit aperture of the IMPSC/RINSC system.

Possible geometric variations for the VINSC systems could consider increasing the length of the prismatic arrays sections and modifications of the asymmetrical integrated light guide (AILG) geometries. A feasible design variation could eliminate the two interfaces between the light guide AILG entrance section and the 45° TIR surface that precedes it. It is expected that the overall transmission efficiencies T_E should increase in at least 5% by eliminating the transmission losses at these interfaces.

(B) RINSC systems designed to “use” Fresnel reflections losses. The RINSC systems developed and analysed in this work are based around the optical phenomenon of total internal reflection (TIR). A possible alternative design strategy could focus on the development of geometric optical configurations that improve the “use” of Fresnel reflections losses that happen inside the system.

(C) The development of robust computer algorithms that consider the geographic location of the building, façade/roof orientation, nearby sun-obstructions (e.g. taller buildings), daily/annual angular solar displacement (h_s, γ_s) availability of sunshine and local weather patterns, could provide support to optimise and customise the optical layout of the RINSC systems for a specific location.

(D) Improved materials and manufacturing processes, including:

Manufacture of RINSC systems using other solid-dielectric materials, such as: polycarbonate (PC), commercial glass (soda-lime), low-iron glass, PMMA+glass composite materials (Ashby et al, 2007) and transparent ceramics (Krell et al, 2009).Investigation and application of solid dielectric materials with lower attenuation and scattering losses (Ashby, 2007).

Deeper investigation of alternative manufacturing processes suitable for the RINSC systems, including: injection moulding, casting and extrusion, among other possibilities. Three main issues should be considered: (A) costs (tooling; machinery; manufacture); (B) bulk material homogeneity provided by the manufacturing process (e.g.: as a result of the injection pressure/temperature); (C) surface finishing quality provided by the manufacturing process.

(E) Building integrated solar-optics skin. The inclusion of RINSC-type optics directly integrated into building façade components and materials could lead to a kind of optical structure embed into the building envelope (or skin). This research approach offers an interesting possibility where the design strategy of solar collectors/concentrators shifts from the development of isolated systems (as done nowadays), to a more integrated view which encompasses the building as a whole. This could lead to buildings where large areas of its outside surfaces (e.g. facades and roof) are able to harvest part of the incident solar radiation. Ultimately, the building could become a large solar collector system.

References

Addington, M. 2003. Energy, Body, Building. Harvard Design Magazine, 18, 1-6.

Andersen, M.; de Boer, J. 2006. Goniophotometry and assessment of bidirectional photometric properties of complex fenestration systems. Energy and Buildings, Vol. 38, pp. 836–848.

Andre, E.; Schade, J. 2002. Daylighting by Optical Fibre, Master Dissertation, Lulea University of Technology.

Andreev, V. M. et al. 2004. Concentrator PV modules and solar cells for TPV systems. Solar Energy Materials and Solar Cells, 84, 3-17.

Andrews, C.J.; Krogmann, U. 2009. Technology diffusion and energy intensity in US commercial buildings. Energy Policy, 37, 541–553.

Ando Electric Co.Ltd. 1998. AQ6317B Optical Spectrum Analyser instruction manual.

Ando Electric Co Ltd., available at: http://www.ando.co.jp – [accessed 12th August 2008].

Antón, I. et al. 2003. Characterization of optical collectors for concentration photovoltaic applications. Progression in Photovoltaics: Research and Applications, 11, 387-405.

Ashby, M.; Shercliff, H.; Cebon, D. Materials: Engineering, science, processing and design. Butterworth-Heinemann & Elsevier, Burlington, MA, 2007.

Askeland, D.R.; Phulé, P.P. The Science and Engineering of Materials. Books/Cole – Thomas Learning, Pacific Grove, CA, 2003.

ASTM Standard G173-03, 2003, “Standard Tables for Reference Solar Spectral Irradiances: Direct Normal and Hemispherical on 37° Tilted Surface”, ASTM International, West Conshohocken, PA, 2003, DOI: 10.1520/G0173-03E01.

BAA Heathrow Local Air Quality Action Plan 2007-2011 (2007). Available at: http://www.heathrowairport.com/assets//B2CPortal/Static%20Files/Action_Plan.pdf [accessed 20th February 2009].

Bazilian, M.D. et al. 2001. Photovoltaic concentration in the building environment. Solar Energy, 71, 57-69.

Berson, D.M. 2003. Strange vision: ganglion cells as circadian photoreceptors. Trends in Neurosciences, 26, 314-320.

Block, K. 2006. Renewable energy policies in the European Union. Energy Policy, 34, 251–255.

Bodart, M. et al. 2008. Photometry and colorimetry characterization of materials in daylighting evaluation tools. Building and Environment, 43, 2046-2058.

Bodart, M., De Herde, A., 2002. Global energy savings in offices building by the use of daylighting. Energy and Buildings, 34, 421-429.

British Glass Manufacturers Confederation, available at: http://www.britglass.org.uk – [accessed 20th June 2009].

British Standard BS 667:2005: Illuminance meters – Requirements and test methods.

British Standard BS 8206-2:2008: Lighting for Buildings, Part 2: Code of practice for daylighting.

British Standard BS 8887-1:2006: Design for manufacture, assembly, disassembly and end-of-life processing (MADE) – Part 1: General concepts, process and requirements.

British Standard BS EN 12464-1:2002: Light and lighting – Lighting of work places – Part 1: Indoor work places.

British Standard BS EN 13119:2007: Curtain walling – Terminology.

British Standard BS EN ISO 9488:2000: Solar Energy – Vocabulary.

British Standard BS ISO 10110-4:1997: Optics and optical instruments - Preparation of drawings for optical elements and systems, Part 4: Material imperfections – Inhomogeneity and striae.

British Standard BS ISO 10110-8:1997: Optics and optical instruments - Preparation of drawings for optical elements and systems, Part 8: Surface texture.

British Standard BS ISO 23539:2005: Photometry – The CIE system of physical photometry.

British Standard BS ISO 80000-7:2008: Quantities and units – Part 7: Light.

British Standard BS ISO 15392:2008: Sustainability in building construction – General principles.

British Standards, BS ISO 15686-5:2008: Buildings and constructed assets - Service-life planning - Part 5: Life-cycle costing.

Buie, D.C.W. Optical Considerations in Solar Concentrating Systems. Doctoral thesis. University of Sydney, 2004.

Callow, J. Daylighting Using Tubular Light Guide Systems. Doctoral thesis. University of Nottingham, 2003.

Campos, J.; Pons, A.; Corredera, P. 2003. Spectral responsivity scale in the visible range based on single silicon photodiodes. Metrologia, 40, S181-S184.

Canziani, R. et al. 2004. Daylight and energy performances of a new type of light pipe. Energy and Buildings, 36, 1163–1176.

Cariou, J.M., et al. 1986. Refractive-index variations with temperature of PMMA and polycarbonate. Applied Optics, 25, 334-336.

Carter, D.J. 2002. The measured and predicted performance of passive solar light pipe systems. Lighting Research & Technology, 34: 39-52.

Chandra, M. 1996. Luminous efficacy of solar radiation and evaluation of natural illumination: A review. Energy Conservation Management, 37, 1623-1634.

Chaves, J.; Collares-Pereira, M. 2000. Ultra Flat Ideal Concentrators of High Concentration. Solar Energy, 69, 269-281.

Chaves, J.; Collares-Pereira, M. 2002. Ideal concentrators with gaps. Applied Optics, 41, 1267-1276.

Chemisana, D. et al. 2009. Comparison of Fresnel concentrators for building integrated photovoltaics. Energy Conversion and Management, 50, 1079–1084

Cheng, Y.K.; Chern, J.L. 2006. Irradiance formations in hollow straight light pipes with square and circular shapes. Journal of the Optical Society of America A, 23, 427-434.

Chen, Y-M.; Liu J-J. 1999. Cost-effective design for injection molding. Robotics and Computer

Integrated Manufacturing, 15, 1-21.

Chien, M-C; Tung, Y.L.; Tien, C-H. 2009. Ultracompact backlight-reversed concentration optics. Applied Optics, 48, 4142-4148.

Chirarattananon, S.; Chedsiri, S.; Renshen, L. 2000. Daylighting through light pipes in the tropics. Solar Energy, 69, 331-341.

CIE- Commission Internationale de l'Eclairage, available at: http://www.cie.co.at - [accessed 10th April 2006].

CIE-Commission Internationale de l'Eclairage. CIE 1988 2° Spectral luminous efficiency function for photopic vision, No. 86. Vienna, Commission Internationale de l'Eclairage, 1990.

CIE-Commission Internationale de l'Eclairage: Spatial Distribution of Daylight – CIE Standard General Sky. CIE S 011/E:2003, ISO 15469:2003(E), Vienna, 2003.

Collares-Pereira, M. et al. 1977. Lens-mirror combinations with maximal concentration. Applied Optics, 16, 2677-2683.

Courbebaisse, G.; Garcia, D. 2002. Shape analysis and injection molding optimization. Computational Materials Science, 25, 547-553.

Cutler, B. et al. 2008. Interactive selection of optimal fenestration materials for schematic architectural daylighting design. Automation in Construction, 17, 809-823.

Darula, S. et al. 2005. Reference luminous solar constant and solar luminance for illuminance calculations. Solar Energy, 79, 559-565.

Davim, J.P. et al. 2008. Some experimental studies on CO2 laser cutting quality of polymeric materials. Journal of Materials Processing Technology, 198, 99-104.

de Cardona M.S. et al, 1985. Outdoor evaluation of luminescent solar concentrator prototypes. Applied Optics, 24, 2028-2032.

de Vries, B.J.M. et al. 2007. Renewable energy sources: Their global potential for the first-half of the 21st century at a global level: An integrated approach. Energy Policy, 35, 2590-2610.

Dhanasekar, B. et al. 2008. Evaluation of surface roughness based on monochromatic speckle correlation using image processing. Precision Engineering, 32, 196-206.

Diaz-Rainey, I.; Ashton, J.K. 2008. Stuck between a ROC and a hard place? Barriers to the take up of green energy in the UK. Energy Policy, 36, 3053– 3061

Dislich, H. 1979. Plastics as Optical Materials. Agnew.Chem.Int.Ed.Engl. 18, 49-59.

Doulos, L.; Tsangrassoulis, A.; Topalis, F. 2008. Quantifying energy savings in daylight responsive systems: The role of dimming electronic ballasts. Energy and Buildings, 40, 36-50.

Durak, A. et al. 2007. Impact of lighting arrangements and illuminances on different impressions of a room. Building and Environment, 42, 3476-3482.

Durán, J.C.; Nicolás, R.O. 1987. Comparative optical analysis of cylindrical solar concentrators. Applied Optics, 26, 578-582.

Earp, A.A.; Smith, G.B.; Franklin, J.; Swift, P.D. 2004(a). Optimisation of a three-colour luminescent solar concentrator daylighting system. Solar Energy Materials and Solar

Cells, 84, 411-426.

Earp, A.A.; Smith, G.B.; Swift, P.D.; Franklin, J. 2004(b). Maximising the light output of a luminescent solar concentrator. Solar Energy, 76, 655-667.

Edmond Optics®, available at: http://www.edmundoptics.com – [accessed 10th Sept. 2009].

Edmonds, I.R.; Greenup, P.J. 2002. Daylighting in the tropics. Solar Energy, 2, 111-121.

Edwards, K.L. 2002. Towards more strategic product design for manufacture and assembly: Priorities for concurrent engineering. Materials & Design, 23, 651-656.

Efthimiopoulos, T; Kiagias, H.; Christoulakis, S.; Merlemis, N. 2008. Bubble creation and collapse during excimer laser ablation of weak absorbing polymers. Applied Surface Science, 254, 5626-5630.

EIA. International Energy Outlook 2009. EIA/DOE, available at: http://www.eia.doe.gov/oiaf/ieo/pdf/0484(2009).pdf - [accessed 18th August 2009].

Eicker, U. Solar Technologies for Buildings. John Wiley & Sons, Chichester, UK, 2003.

Elias, H-G. An Introduction to Plastics. 2nd Edition, Wiley-VCH, 2003.

Elmualim, A.A., 1999. Evaluation of dichroic material for enhancing light pipe/natural ventilation and daylighting in an integral system. Applied Energy, 62, 253-266.

Ewen, J.M. 1897. Design for a prism-plate. U.S. Patent Design No. 27,345.

Extech®, available at: http://www.extech.com - [accessed 08th June 2006].

Fend, T. et al. 2003. Comparative assessment of solar concentrator materials. Solar Energy, 74, 149-155.

Feuermann, D. et al. 2002. Solar fiber-optic mini-dishes: First experimental results and field experience. Solar Energy, 72, 459-472.

Feuermann, D.; Gordon, J.M. 1999. Solar fibre-optic mini-dishes: a new approach to efficient collection of sunlight. Solar Energy, 65, 159-170.

Fontoynont, M. 2002. Perceived performance of daylighting systems: lighting efficacy and agreeableness. Solar Energy, 73, pp.83-94.

Fournier F.; Rolland, J. 2008. Optimization of freeform lightpipes for light-emitting-diode projectors. Applied Optics, 47, 957-966.

Fraas, L.M., et al, 1983. Concentrated and piped sunlight for indoor illumination. Applied Optics, 22, 578-582.

Freeman, M.H. Optics. 10th Edition, Butterworths, London, 1990.

Freewan, A.A. et al. 2009. Interactions between louvers and ceiling geometry for maximum daylight performance. Renewable Energy, 34, 223-232.

Fresnel Technologies. 2001. Fresnel lenses brochure, available at: http://www.fresneltech.com/pdf/FresnelLenses.pdf

Fröhlich, C. 2006. Solar irradiance variability since 1978: Revision of the PMOD Composite during Solar Cycle 21. Space Science Reviews, 125, 53-65.

Galasiu, A.D.; Veitch, J.A. 2006. Occupant preferences and satisfaction with the luminous environment and control systems in daylit offices: a literature review. Energy and Buildings, 38, 728-742.

Gao, H.Y. et al. 2006. Total internal reflection-refraction beam expander. Optics Communications, 260, 699-702.

Garcia-Botella, A. et al. 2006. Elliptical Concentrators. Applied Optics, 45, 7622-7627.

Geary, J.M. Introduction to Optical Testing. SPIE Press – The International Society for Optical Engineering, Bellingham, Washington, 1993.

Geary, J.M. Introduction to Lens Design: with practical ZEMAX examples. Willmann-Bell, Richmond, Virginia, 2007.

Gerchikov, V. et al. 2005. Modelling attenuation versus length in practical light guides. LEUKOS, 1, 47-59.

Goldemberg, J. 2006. The promise of clean energy. Energy Policy, 34, 2185–2190.

Goldschmidt, J.C., et al, 2009. Increasing the efficiency of fluorescent concentrator systems. Solar Energy Materials and Solar Cells, 93, 176-182.

Goodman, N.B. et al. 1976. Solid-dielectric compound parabolic concentrators: On their use with photovoltaic devices. Applied Optics, 15, 2434-2436.

Gordon, J.M.; Feuermann, D. 2005. Optical performance at the thermodynamic limit with tailored imaging designs. Applied Optics, 44, 2327-2331.

Gordon, J.M.; Rabl, A. 1992. Nonimaging compound parabolic concentrator-type reflectors with variable extreme direction. Applied Optics, 31, 7332-7338.

Gratia, E.; De Herde, A. 2003. Design of low energy office buildings. Energy and Buildings, 35, 473-491.

Greivenkamp, J.E. Field Guide to Geometrical Optics. SPIE, Washington, 2003.

Gross, S. et al. 2007. PMMA: A key macromolecular component for dielectric low-κ hybrid inorganic-organic polymer films. European Polymer Journal, 43, 673-696.

Gunerhan, H.; Hepbasli, A. 2007. Determination of the optimum tilt angle of solar collectors for building applications. Building and Environment, 42, 779-783.

Gupta, A. et al. 2001. Design of efficient lightpipes for illumination by an analytical approach. Applied Optics, 40, 3640-3648.

Hatwaambo, S. et al. 2008. Angular characterization of low concentrating PV-CPC using low-cost reflectors. Solar Energy Materials & Solar Cells, 92, 1347-1351.

Hecht, E. Optics. Addison Wesley Longman, Reading, MA, 1998.

Hestnes, A.G. 1999. Building Integration of Solar Energy Systems. Solar Energy, 67, 181-187.

Himawari®, available at: http://www.himawari-net.co.jp/e_page-index01.html - [accessed 24th July 2005].

Hovila, J. New Measurement Standards and Methods for Photometry and Radiometry. Doctoral dissertation, Helsinki University of Technology, 2005.

Huang, C.H. et al. 2002. Calculation of the absorption coefficients of optical materials by measuring the transmissivities and refractive indices. Optics & Laser Technology, 34, 206-211.

Hunsperger, R.G. Integrated Optics: Theory and Technology. 4th edition, Springer-Verlag, Berlin, 1995.

Huygens, C. Treatise of Light. Dover Publications, New York, 1962 (re-edited).

IEA. Daylight in buildings: a source book on daylighting systems and components. International Energy Agency, 2000.

Ihm, P., Nemri, A., Krarti, M. 2009 Estimation of lighting energy savings from daylighting, Building and Environment 44: 509– 514.

Jacovides, C.P. et al. 2000. Spectral solar irradiance and some optical properties for various polluted atmospheres. Solar Energy, 69, 215-227.

Jenkins, D., Muneer, T. 2003. Modelling light-pipe performances – a natural daylighting solution. Building and Environment, 38, 965-972.

Jenkins, D.; Muneer, T. 2004. Light-pipe prediction methods. Applied Energy, 79, 77-86.

Jenkins, D.; Newborough, M. 2007. An approach for estimating the carbon emissions associated with office lighting with a daylight contribution. Applied Energy, 84, 608-622.

Jentsch M.F.; Bahaj A.S.; James, P.A.B. 2009. Climate change future proofing of buildings: Generation and assessment of building simulation weather files. Energy and Buildings 40, 2148–2168.

Kandilli, C. et al. 2008. Exergetic assessment of transmission concentrated solar energy systems via optical fibres for building applications. Energy and Buildings, 40, 1505-1512.

Kandilli, C.; Ulgen, K. 2009. Review and modelling the systems of transmission concentrated solar energy via optical fibres. Renewable and Sustainable Energy Reviews, 13, 67-84.

Kaushika, N. D.; Reddy, K. S. 2000. Performance of a low cost solar paraboloidal dish steam generating system. Energy Conversion and Management, 41, 713-726.

Kaushika, N.D.; Sumathy, K. 2003. Solar transparent insulation materials: A review. Renewable and Sustainable Energy Reviews, 7, 317-351.

Kerker, M. The Scattering of Light and Other Electromagnetic Radiation. Academic Press, New York, 1969.

Kiatgamolchai, S.; Chamni, E., 2008. Theory and experiment of a two-dimensional cone concentrator for sunlight. Solar Energy, 82, 111-117.

Kim, Y.; Han, G.Y.; Seo, T. 2008. An evaluation on thermal performance of CPC solar collector. International Communications in Heat and Mass Transfer, 35, 446-457.

Kitai, M.S.; Semchishen, V.A. 1996. Melting of polymers during UV laser ablation. Quantum Electronics 26, 517-519.

Kittler, R.; Darula, S. 2002. Parametric definition of the daylight climate. Renewable Energy, 26, 177-187.

Krell, A. et al. 2009. Transparent compact ceramics: Inherent physical issues. Optical Materials, 31: 1144–1150.

Ladouceur, F.; Poladian, L. 1996. Surface roughness and backscattering. Optics Letters, 21, 1833-1835.

Lee, E.S.; Selkowitz, S.E. 2006. The New York Times Headquarters daylighting mockup: Monitored performance of daylighting control system. Energy and Buildings, 38, 914-

929.

Lehmann, P. 1999. Surface-roughness measurement based on the intensity correlation function of scattered light under speckle-pattern illumination. Applied Optics, 38, 1144-1152.

Leslie, R.P. 2003. Capturing the daylight dividend in buildings: why and how? Building and Environment, 38, 381-385.

Li, D.H.W. 2007. Daylight and energy implications for CIE standard skies. Energy Conservation and Management, 48, 745-755.

Li, D.H.W., et al. 2008. An analysis of luminous efficacies under the CIE standard skies. Renewable Energy, 33, 2357 – 2365.

Li, D.H.W.; Cheung, G.H.W. 2006. Average daylight factor for the 15 CIE standard skies. Lighting Research and Technology, 38, 137-152.

Li, D.H.W.; Lam, J.C.; Wong, S.L. 2005. Daylighting and its effects on peak load determination. Energy, 30, 1817-1831.

Liebert, A.; Manieski, R. Scattering: Encyclopedia of Optical Engineering, Vol.3. Edited by Driggers, R.G. Marcel Dekker Inc, New York, 2003, pp. 2545-2552

Lifante, G. et al. 1983. Solar concentrators using total internal reflection. Applied Optics, 22, 3966-3970.

Lin, H. et al. 1994. Temperature and wavelength dependent transmission of optically transparent glass fibre poly (methyl methacrylate) composites. Journal of Materials Science, 29, 5193-5198.

Loe, D.L. 2003. Quantifying lighting energy efficiency: a discussion document. Lighting Research Technology, 35, 319-329.

Loe, D.L. 2009. Energy efficiency in lighting – considerations and possibilities. Lighting Research and Technology, 41, 209–218.

Lorenzo, E. 1981. Chromatic aberration effect on solar energy systems using Fresnel lenses. Applied Optics, 20, 3729-3731.

Luque, A. 1986. Nonimaging optics in photovoltaic concentration. Physics Technology, 17, 118 -124.

Mallick, T.K. et al. 2007. Power losses in an asymmetric compound parabolic photovoltaic concentrator. Solar Energy Materials & Solar Cells, 91, 1137-1146.

Mallick, T.K.; Eames, P.C.; Norton, B. 2006. Non-concentrating and asymmetric compound parabolic concentrator building façade integrated photovoltaics: An experimental comparison. Solar Energy, 80, 834-849.

Mancisidor, I.M.deA., et al. 2009. European Union's renewable energy sources and energy efficiency policy review: The Spanish perspective, Renewable and Sustainable Energy Reviews 13, 100–114.

Mansour, A.F. 1998. Optical efficiency and optical properties of luminescent solar concentrators. Polymer Testing, 17, 333-343.

Mansy, K. 2004. A user-friendly procedure to visualize the hourly quantitative performance of daylighting systems. Solar Energy, 77, 373-380.

Martin, N.; Ruiz, J. M. 2001. Calculation of the PV modules angular losses under field conditions by means of an analytical model. Solar Energy Materials and Solar Cells, 70, 25-38.

Maruyama, T.; Osako, S. 1999. Wedge-shaped light concentrator using total internal reflection. Solar Energy Materials & Solar Cells, 57, 75-83.

Masui, H.; Nakamura, S.; DenBaars, S.P. 2008. Analytical light-ray tracing in two-dimensional objects for light-extraction problems in light-emitting diodes. Applied Optics, 47, 88-92.

Matusiak, B. 2004. Lighting systems in smart energy efficient buildings (report on the state-of-the-art), SINTEF Civil and Environmental Engineering.

Matuska, T.; Sourek, B. 2006. Façade solar collectors. Solar Energy, 80, 1443-1452.

Maxey, L.C., et al. 2008. Hybrid Solar Lighting: Final Technical Report and Results of the Field Trial Program. Oak Ridge National Laboratory, UT-Battelle LLC and U.S. Department of Energy, available at: http://www.ornl.gov/sci/btc/pdfs/maxey_doc12657_hsl_08.pdf - [accessed 10th February 2009].

Maxia, V. et al. 1973. Angular distribution of light transmitted by a cylindrical guide. Applied Optics, 12, 98-102.

McMullan, R. Environmental Science in Building, Palgrave, New York, 2002.

Messenger, R.; Ventre, J. Photovoltaic Systems Engineering. CRC Press, Boca Raton, FL, 2000.

Miñano, J.C.; Gonzalez, J.C. 1992. New method of design of nonimaging concentrators. Applied Optics, 31, 3051-3060.

Mohelnikova, J. 2009. Tubular light guide evaluation. Building and Environment, 44, 2193 –2200.

Moldflow®, available at: http://www.moldflow.com – [accessed 3rd November 2008].

Monodraught®, available at: http://www.monodraught.com - [accessed 25th June 2005].

Mouroulis, P; Macdonald, J. Geometrical Optics and Optical Design. Oxford University Press, New York, 1997.

Nabil, A., Mardaljevic, J. 2006. Useful daylight illuminances: a replacement for daylight factors. Energy and Buildings, 38, 905-913.

Nardin, B. et al. 2002. Injection moulding simulation results as an input to the injection moulding process. Journal of Materials Processing Technology, Vol.130-131, 310-314.

National Instruments®, available at: http://www.ni.com - [accessed 19th February 2008].

Nazzal, A.A. 2005. A new evaluation method for daylight discomfort glare. International Journal of Industrial Ergonomics, 35, 295–306.

Nicoletti, M. 1998. Architectural expression and low energy design. Renewable Energy, 15, 32-41.

Nikolov, I.D.; Ivanov, C.D. 2000. Optical plastic refractive measurements in the visible and the near-infrared regions. Applied Optics, 39, 2067-2070.

Nilsson, J. Optical Design and Characterization of Solar Concentrators for Photovoltaics. Licentiate thesis, Lund University, 2005.

Ning, X. et al (1987a). Dielectric totally internally reflective concentrators. Applied Optics, 26, 300-305.

Ning, X. et al (1987b). Optics of two-stage photovoltaic concentrators with dielectric second stages. Applied Optics, 26, 1207-1212.

NIST. Measurement Services: Photometric Calibrations, Special Publication 250-37, 1997.

Nuwayhid, R. Y.; Mrad, F.; Abu-Said, R. 2001. The realization of a simple solar tracking concentrator for university research applications. Renewable Energy, 24, 207-222.

O'Driscoll, M. 2002. Design for manufacture. Journal of Materials Processing Technology, 122, 318-321.

Ohno, Y. Measurement Procedures (Chapter 5): in DeCusatis, C: Handbook of Applied Photometry. AIP Press, Optical Society of America (OSA) and Springer-Verlag, New York, 1998.

Okoro, O.I.; Madueme, T.C. 2006. Solar energy: A necessary investment in a developing country. International Journal of Sustainable Energy, 25, 23-31.

Olders, H. 2003. Average sunrise time predicts depression prevalence. Journal of Psychosomatic Research, 55, 99-105.

Omer, A.M. 2008. Focus on low carbon technologies: The positive solution. Renewable and Sustainable Energy Reviews, 12, 2331-2357.

OptiCAD®, available at: http://www.opticad.com - [accessed 29th Sept. 2005].

OptiCAD Corporation. OptiCAD®: Optical analysis program user's guide, version 10, 2006.

OpticStar®, available at: http://www.opticstar.com - [accessed 2nd Sept. 2008].

Osbourn, D. Introduction to Building. 2nd ed. Addison Wesley Longman, Essex, UK, 1997.

Parans®, available at: http://www.parans.com - [accessed 10th Sept. 2009].

Pauley, S.M. 2004. Lighting for the human circadian clock: recent research indicates that lighting has become a public health issue. Medical Hypotheses, 63, 588-596.

Pearsall, N.M. 1998. The design and performance of photovoltaic facades in the UK. Renewable Energy, 15: 552-557.

Peippo, K. et al. 1999. Multivariate optimization of design trade-offs for solar low energy buildings. Energy and Buildings, 29: 189-205.

Pelegrini, A.V.; Harrison, D.; Shackleton, J. 2007. Splitting the solar spectrum for daylighting and water heating applications. Proceedings of the International Conference Portugal SB07 Sustainable Construction Materials and Practices, IOP Press, 2007, pp.451-458.

Pelegrini, A.V.; Harrison, D.; Evans, P. 2009a. Prismatic solar collectors for core-daylighting in buildings. Renewable Energy (accepted paper).

Pelegrini, A.V.; Harrison, D.; Evans, P. 2009b. Integrated multi-prismatic solar collector: A novel concept of nonimaging concentrator optics. Solar Energy Materials and Solar Cells (submitted paper).

Pérez-Lombard, L. et al. 2007. A review on buildings energy consumption information. Energy and Buildings. Performance Simulation Association, 16, 42-44.

Pérez-Lombard; L., Ortiz; J., Pout, C. 2008. A review on buildings energy consumption

information. Energy and Buildings, 40, 394–398.

Prasad, D.; Snow, M. Designing with solar power: a source book for building integrated photovoltaics (BiPV) / editors. Earthscan, London, 2005.

Probst, M.C.M.; Roecker, C. 2007. Towards and improved architectural quality of building integrated solar thermal systems (BIST). Solar Energy, 81, 1104-1116.

Rabl, A. 1994. Edge-ray method for analysis of radiation transfer among specular reflectors. Applied Optics, 33, 1248-1259.

Rabl, A.; Winston, R. 1976. Ideal concentrators for finite sources and restricted exit angles. Applied Optics, 15, 2880-2883.

Rahoma, U.A. 2001. Clearness index estimation for spectral composition of direct and global solar radiations. Applied Energy, 68, 337-346.

Rao, C.B.; Raj, B. 2003. Study of engineering surfaces using laser-scattering techniques. Sadhana, 28, 739-761.

Reijenga, T.H. PV in Architecture: in Luque, A. and Hegedus, S. (eds.): Handbook of photovoltaic science and engineering. John Wiley & Sons, Chichester, England, 2003.

Reinhart, C.; Selkowitz, S. 2006. Daylighting: Light, form, and people. Energy and Buildings, 38, 715-717.

Ries, H. 1982. Thermodynamic limitations of the concentration of electromagnetic radiation. Journal of the Optical Society of America, 72, 380-385.

Ries, H. et al. 1997a. Extracting concentrated guided light. Applied Optics, 36, 2869-2874.

Ries, H. et al. 1997b. Performance limitations of rotationally symmetric nonimaging devices. Journal of the Optical Society of America, 14, 2855-2862.

Ries, H.; Rabl, A. 1994. Edge-ray principle of nonimaging optics. Journal of the Optical Society of America, 11, 2627-2632.

Robledo, L.; Soler, A. 2001. Luminous efficacy of direct solar radiation for all sky types. Energy, 26: 669-677.

Rosemann, A. et al. 2008a. Cost-effective controlled illumination using daylighting and electric lighting in a dual-function prism light guide. Lighting Research Technology, 40, 77-88.

Rosemann, A. et al. 2008b. Development of a cost-effective solar illumination system to bring natural light into the building core. Solar Energy, 82, 302-310.

Rosemann, A.; Kaase, H. 2005. Lightpipe applications for daylighting systems. Solar Energy, 78, 772-780.

Rosenfeld, A.H.; Selkowitz, S.E. 1977. Beam daylighting: an alternative illumination technique. Energy and Building, 1, 43-50.

Rowan, B.C. et al. 2008. Advanced material concepts for luminescent solar concentrators. IEEE Journal of Selected Topics in Quantum Electronics, 14, 1312-1322.

Ruiz, B.J.; Rodriguez, V.; Bermann, C. 2007. Analysis and perspectives of the government programs to promote the renewable electricity generation in Brazil. Energy Policy, 35, 2989–2994.

Sametoglu, F. 2007. Relation between the illuminance responsivity of a photometer and the

spectral power distribution of a source. Optical Engineering, 46, 093607(1)–093607(12).

Sanderson, K. 2008. Efficiency records claimed for solar devices. Nature, available at: http://www.nature.com/news/2008/081208/full/news.2008.1281.html - [accessed 5th January 2009].

Schanda, J. et al. 2002. Does lighting need more photopic luminous efficiency functions? Lighting Research and Technology, 34, 69-78.

Scharlack, R. S. 1977. All-dielectric compound parabolic concentrator. Applied Optics, 16, 2601-2602.

Schmidt-Kloiber, H.; Schoeffmann, H. 1986. Metallic hollow cones as light concentrators. Applied Optics, 25, 252-257.

Schneider, W.E; Young, R. Spectroradiometry Methods (Chapter 8): in DeCusatis, C: Handbook of Applied Photometry. AIP Press, Optical Society of America (OSA) and Springer-Verlag, New York, 1998.

Selkowitz, S. 1998. The elusive challenge of daylighted buildings: A brief review 25 years later. Daylighting '98 Conference Proceedings, May 11-13, Ottawa, Ontario, Canada.

Serra, R. 1998. Chapter 6: Daylighting. Renewable and Sustainable Energy Reviews, 2, 115-155.

Sezgen, O.; Koomey, J.G. 2000. Interactions between lighting and space conditioning energy use in US commercial buildings. Energy, 25, 793-805.

Shannon, R.R. The Art and Science of Optical Design. Cambridge University Press, Cambridge, 1997.

Shen, J. et al. 2005. Subsurface damage in optical substrates. Optik, 116, 288-294.

Sierra, C.; Vazquez, A.J. 2005. High solar energy concentration with a Fresnel lens. Journal of Materials Science, 40, 1339 – 1343.

Slooff, L.H., et al. 2008. A luminescent solar concentrator with 7.1% power conversion efficiency. Phys. Stat. Sol. (RRL), 2, 257–259.

Smith, G.B. 2004. Materials and systems for efficient lighting and delivery of daylight. Solar Energy Materials & Solar Cells, 84, 395-409.

Smith, W.J. Modern Optical Engineering. SPIE Press & McGraw-Hill, New York, 2000.

Smith, W.J. Practical Optical System Layout and Use of Stock Lenses. McGraw-Hill, New York, 1997.

SolidWorks®, available at: http://www.solidworks.com - [accessed 15th July 2005].

Solux®, available at: http://solux.net - [accessed 28th July 2008].

Strong, A.B. Plastics - Materials and Processing. Prentice-Hall / Simon & Schuster Company, Englewood Cliffs, New Jersey, 1996.

SVV Technologies Innovations®, available at: http://www.svvti.com - [accessed 15th March 2007].

Swanson, R.M. 2000. The promise of concentrators. Progress in Photovoltaics: Research and Applications, 8, 93-111.

Swift, P.D.; Smith, G.B. 1995. Cylindrical mirror light pipes. Solar Energy Materials and Solar

Cells, 36, 159-168.

Swift, P.D.; Smith, G.B.; Franklin, J. 2006. Hotspots in cylindrical mirror light pipes: description and removal. Lighting Research and Technology, 38, 19-31.

Taylor, A.E.F. Illumination Fundamentals. Rensselaer Polytechnic Institute, 2000.

Thormark, C. 2002. A low energy building in a life cycle—its embodied energy, energy need for operation and recycling potential. Building and Environment, 37, 429 – 435.

Timinger, A. et al. 2000. Optical assessment of nonimaging concentrators. Applied Optics, 39, 5679-5684.

Tsangrassoulis, A. et al, 2005. On the energy efficiency of a prototype hybrid daylighting system. Solar Energy, 79, 56-64.

van Sark, W.G.J.H.M., et al. 2008. Luminescent Solar Concentrators – A review of recent results. Optics Express, 16, 21773-21792.

Vasylyev, S. Nonimaging Reflective Lens Concentrator. Paper presented at the International Conference on Solar Concentrators for the Generation of Electricity or Hydrogen, May 1-5, 2005, Scottsdale , AZ.

Wadsworth, F.L.O. 1903. Illuminating Structure. U.S. Patent No.717,783.

Walker, R.A. 1972. Optical systems for defining the viewing and measuring fields in luminance radiance meters. Applied Optics, 11, 2060-2068.

Webb, A.R. 2006. Considerations for lighting in the built environment: non-visual effects of light. Energy and Buildings, 38, 721-727.

Weber, W.H.; Lambe, J. 1976. Luminescent greenhouse collector for solar radiation. Applied Optics, 15, 2299-2300.

Welford, W.T.; Winston, R. The Optics of Nonimaging Concentrators: Light and Solar Energy. Academic Press, London, 1978.

Weng, C. et al. 2009. Numerical simulation of residual stress and birefringence in the precision injection moulding of plastic microlens arrays. International Communications in Heat and Mass Transfer, 36, 213-219.

Winston, R. 1970. Light collection within the framework of geometrical optics. Journal of the Optical Society of America, 60, 245-247.

Winston, R.; Miñano, J.C.; Benitez, P. Nonimaging Optics. Elsevier Academic Press, London, 2005.

Yalukova, O.; Sarady, I. 2006. Investigation of interaction mechanisms in laser drilling of thermoplastic and thermoset polymers using different wavelengths. Composites Science and Technology, 66, 1289-1296.

Zacharopoulos, A. et al. 2000. Linear dielectric non-imaging concentrating covers for PV integrated building facades. Solar Energy, 68, 439-452.

Zain-Ahmed, A. et al. 2002. The availability of daylight from tropical skies – a case study of Malaysia. Renewable Energy, 25, 21-30.

Zygo®, available at: http://www.zygo.com - [accessed 05th January 2009].

Appendix

Appendix 1 – Selected design studies and prototyping examples

Appendix 2 – Comparative surface analysis

Appendix 3 – Alternative design concepts and prototyping

Appendix 4 – Publications and submitted works (ABSTRACTS)

Appendix 1 - Selected design studies and prototyping examples

This appendix presents a selection of some examples of the design studies and other design variations of the RINSC systems that were developed during this research but were not included in the main text of this thesis.

Figure A1.1 presents a computer ray-tracing analysis conducted with OptiCAD® to demonstrate the transmitted rays through a hollow light guide coupled to a Prismatic Solar Collector (PSC). Simulation parameters: refractive index n = 1.50; incident monochromatic light (λ = 555nm) with θ_i = 40° at the system meridional plane.

Figure A1.2 shows a ray-tracing analysis with a preliminary design study for the IMPSC system in which the exit aperture is located at the low-end section of the system parallel to the entrance aperture plane. Simulation parameters: refractive index n = 1.50; incident monochromatic light (λ = 555nm) with θ_i = 28° at the system meridional plane.

Figure A1.3 shows a sequence of ray-tracing analysis demonstrating a preliminary design study for the IMPSC-D system with two integrated light guides. Note that the exit aperture is also located at the low-end section of the system parallel to the entrance aperture plane. Simulation parameters: refractive index n = 1.50; incident monochromatic light (λ = 555nm) with θ_i = 56° at the system meridional plane.

Figure A1.4 presents a ray-tracing analysis demonstrating a preliminary design study for the IMPSC system with three parallel integrated light guides. Simulation parameters: refractive index n = 1.50; incident monochromatic light (λ = 555nm) with θ_i = 52° at the system meridional plane.

Figure A1.5 presents a sequence of ray-tracing analysis demonstrating one of the preliminary design studies related to a possible variation of the IMPSC system.

Figure A1.6 shows the IMPSC-A2 demonstration prototypes manufactured by laser ablation process (material: PMMA; thickness: 5mm). Note in Figure A1.6 (A) the formation of a “concentrated / focused area” of light transmitted by the system. Note in Figure A1.6 (B) the effect of the prismatic array in deflecting incidence direct sunlight at the entrance aperture.

(A)

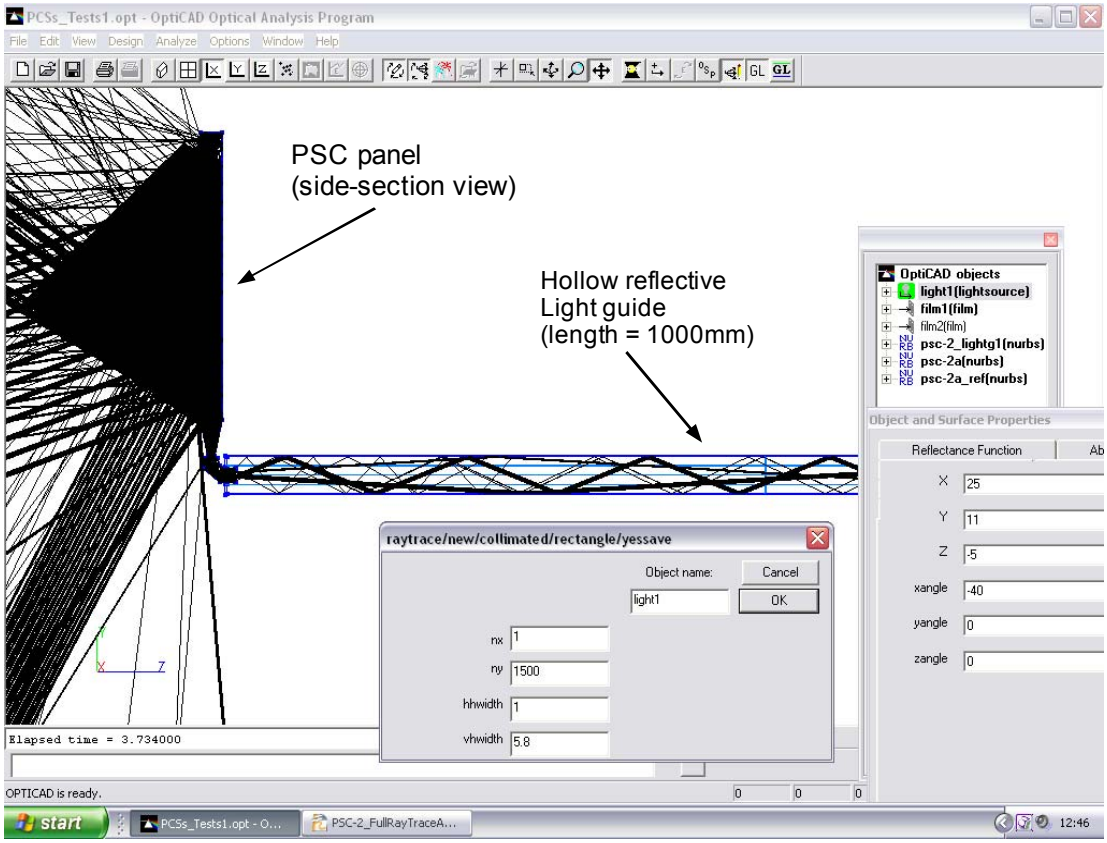

(B)

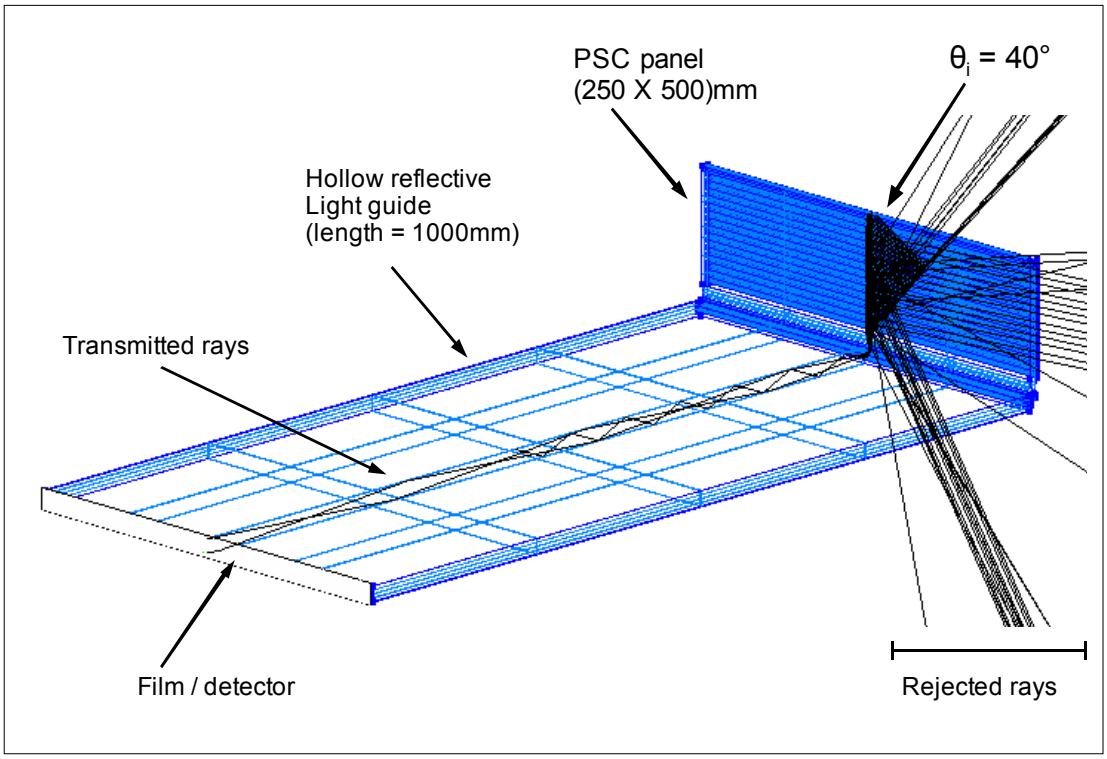

Figure A1.1 – Ray-tracing analysis demonstrating transmitted rays through a hollow light guide coupled to a prismatic solar collector (PSC) CAD model.

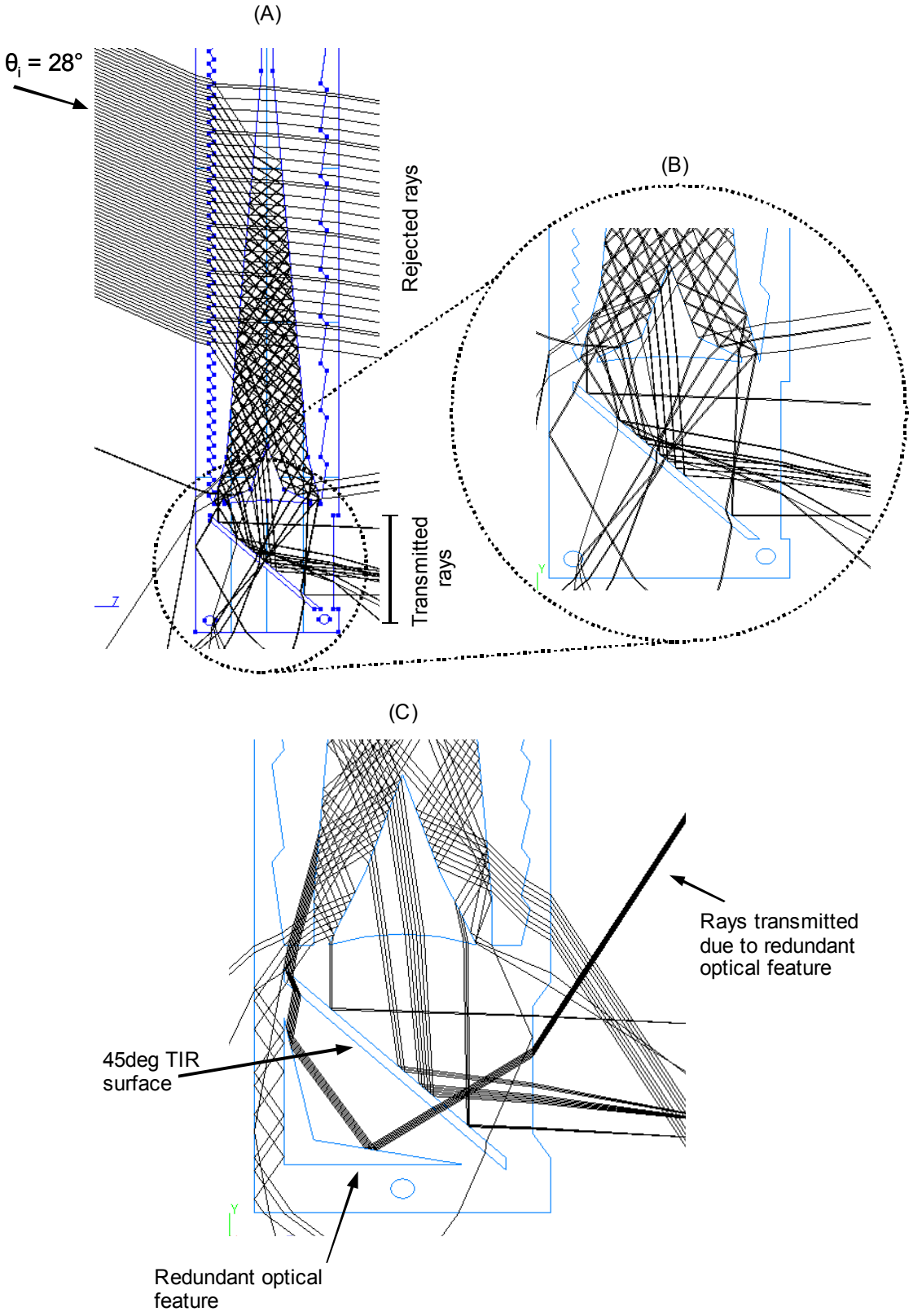

Figure A1.2 – Ray-tracing analysis demonstrating a preliminary design study for the IMPSC system in which the exit aperture is located at the low-end section of the system parallel to the entrance aperture plane.

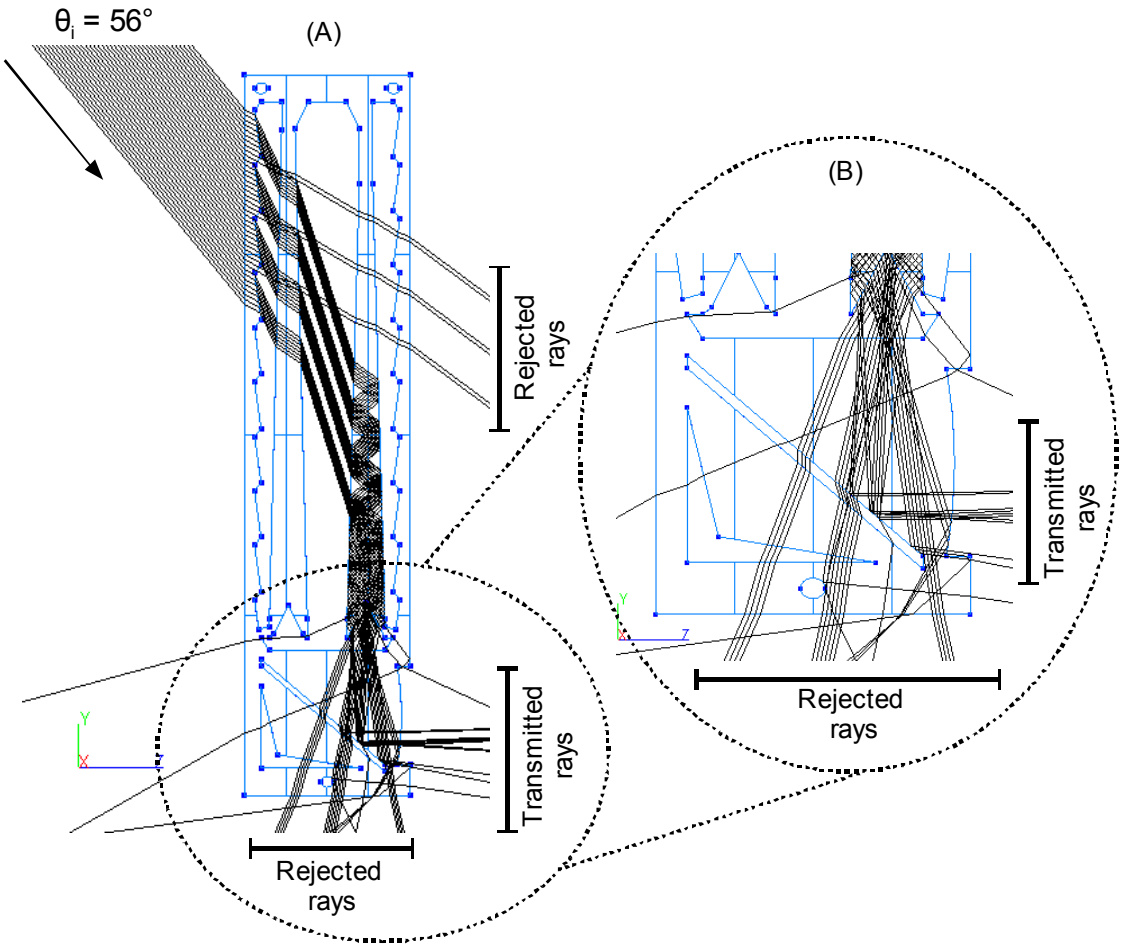

Figure A1.3 – Ray-tracing analysis demonstrating a preliminary design study for the IMPSC-D system with two integrated light guides.

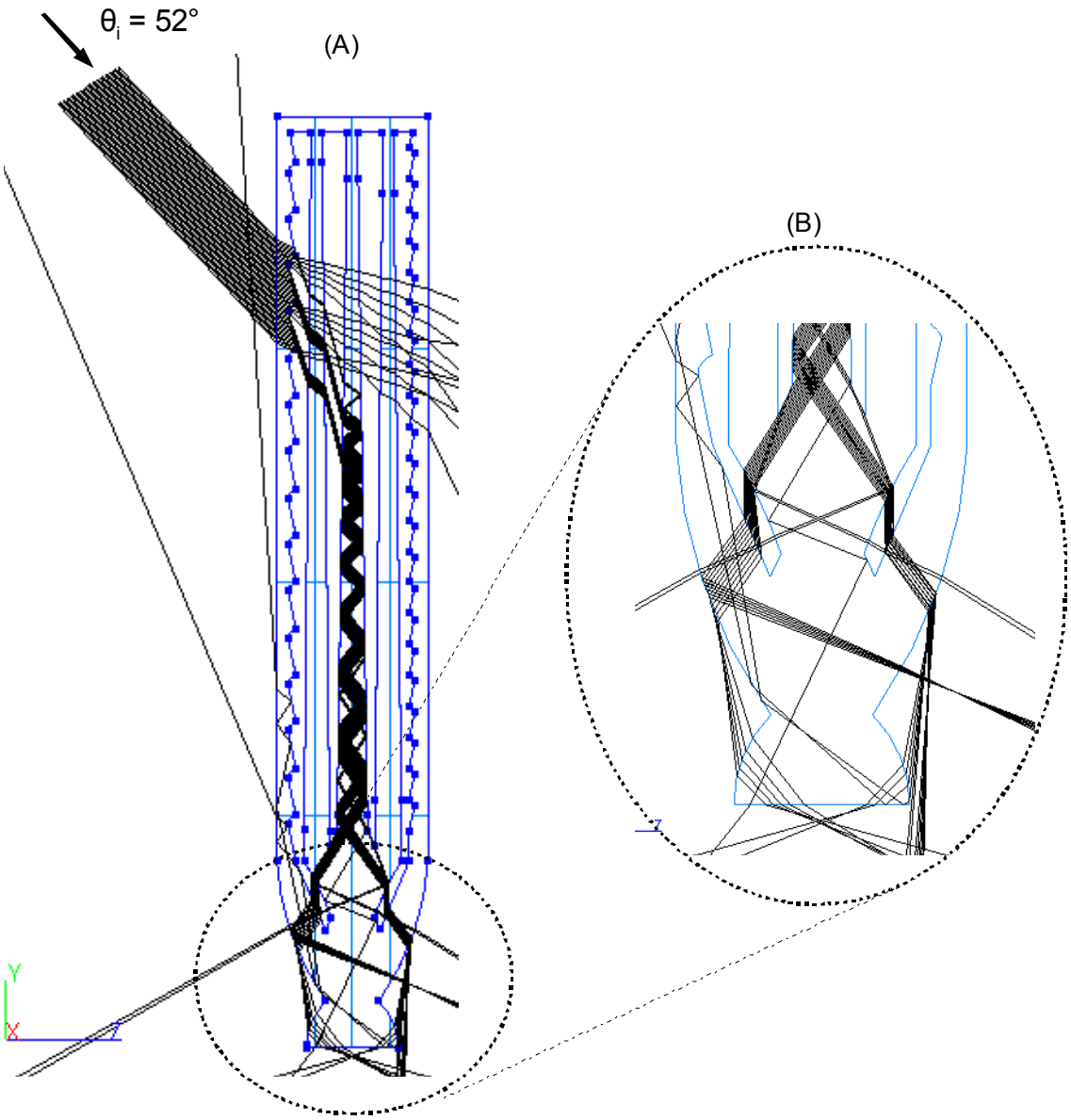

Figure A1.4 – Ray-tracing analysis demonstrating a preliminary design study for the IMPSC system considering the inclusion of a third integrated light guide.

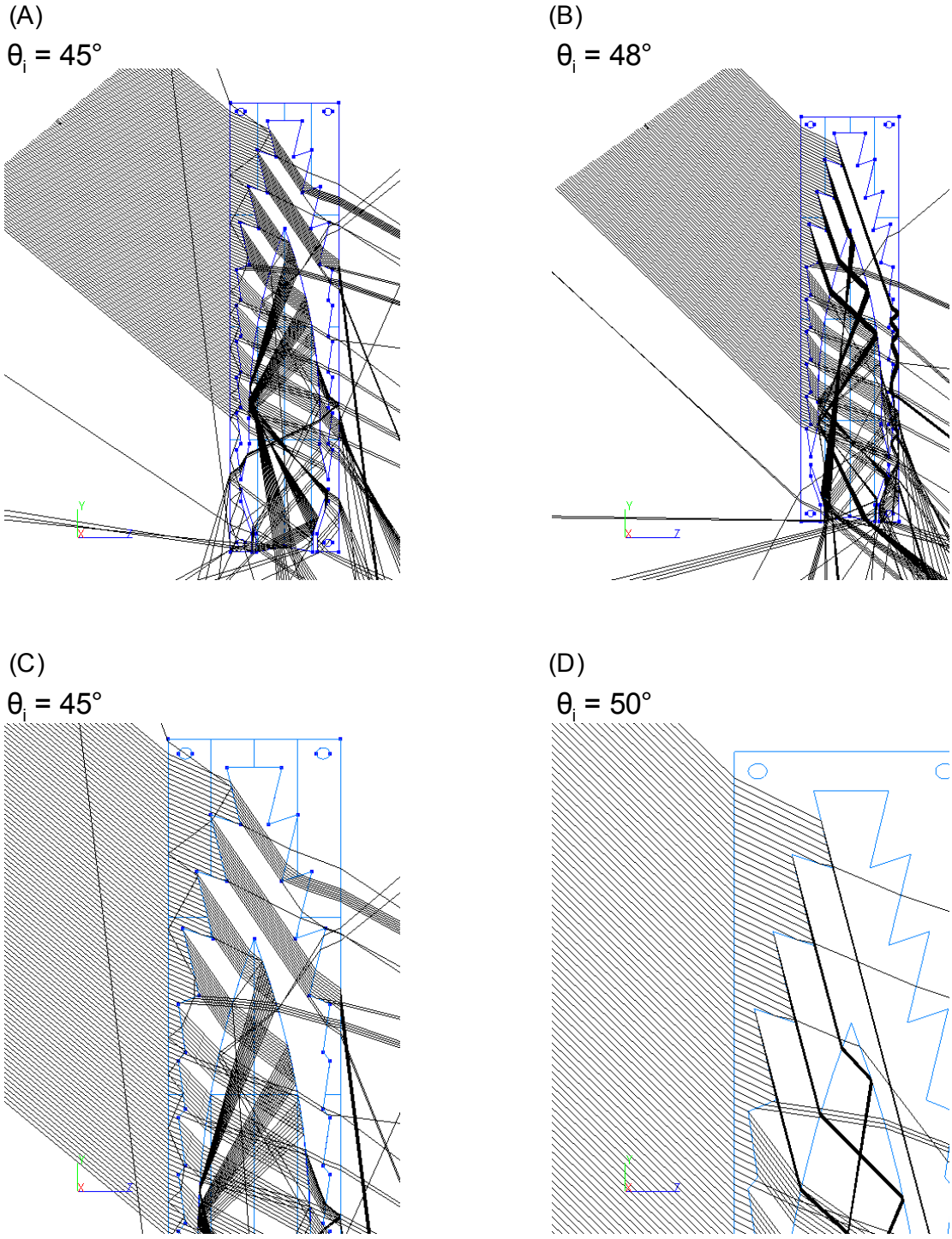

Figure A1.5 – Sequence of ray-tracing analysis demonstrating a preliminary study for a variation of the IMPSC system.

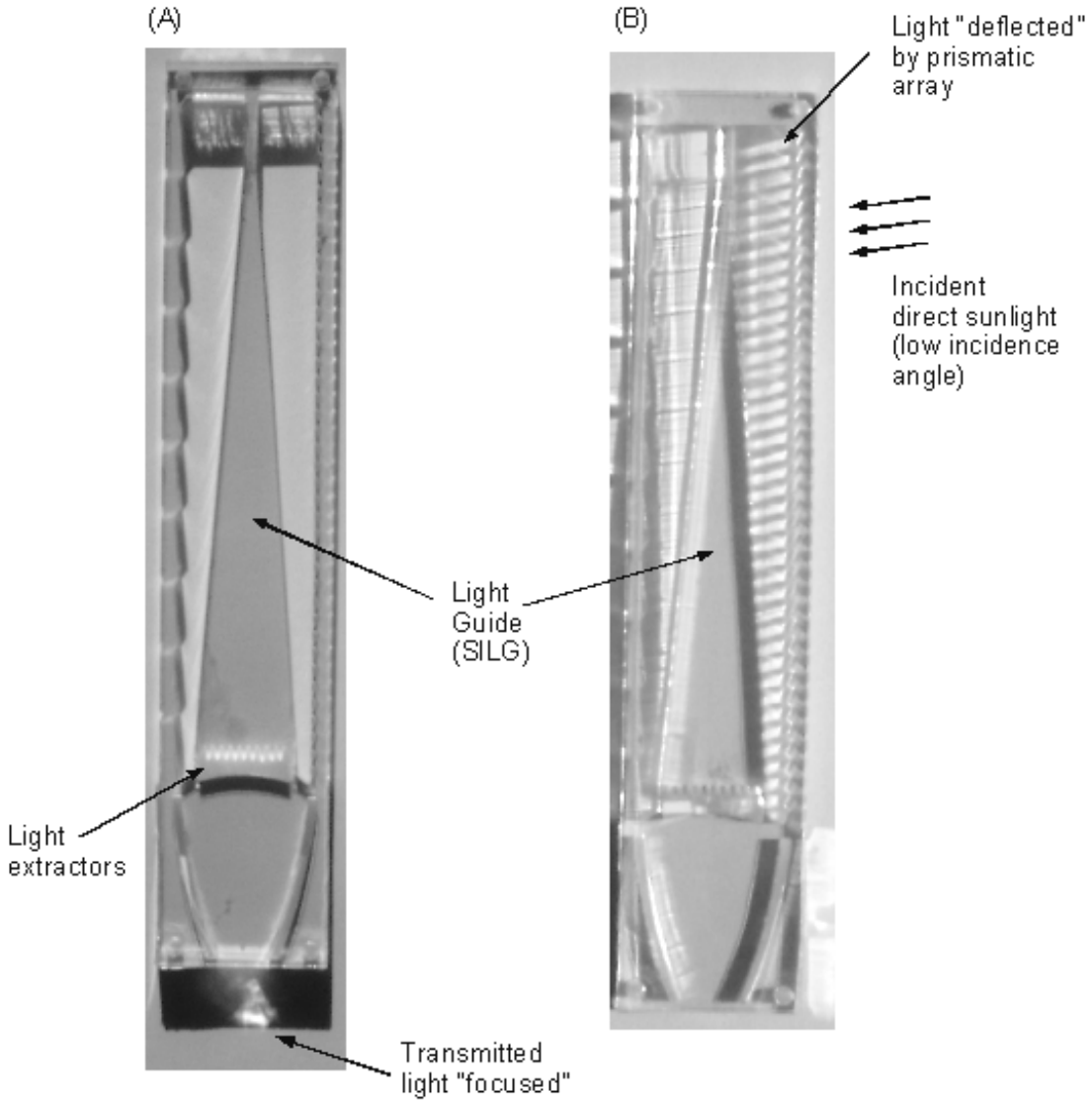

Figure A1.6 – IMPSC-A2 demonstration prototypes manufactured by laser ablation process (material: PMMA; thickness: 5mm).

Appendix 2 - Comparative surface analysis

This appendix presents a qualitative surface analysis to compare the average surface quality of the demonstration prototypes, manufactured by the laser ablation process, with a commercial lens made of PMMA and manufactured by injection moulding process. Note the difference between the optical profiles of both figures.

Figure A2.1 shows a qualitative analysis of the average quality of the external surfaces of the RINSC demonstration prototypes manufactured by the laser ablation process. Figure A2.2 displays a section of the surface of a commercial lens made of PMMA and manufactured by injection moulding process. Note the difference between the optical profiles of Figure A2.1 (B) and Figure A2.2 (B)

(A)

(B)

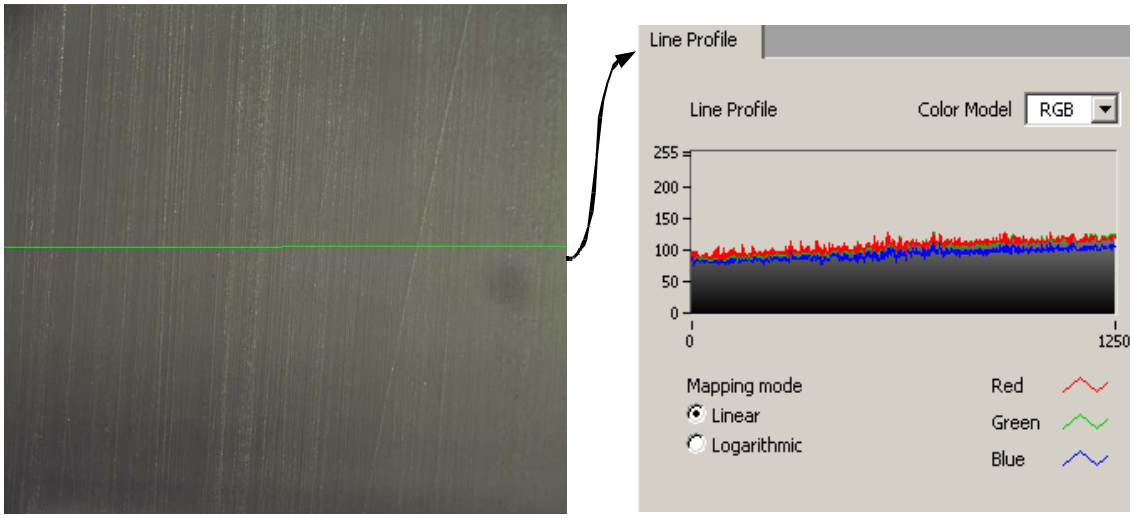

(C)

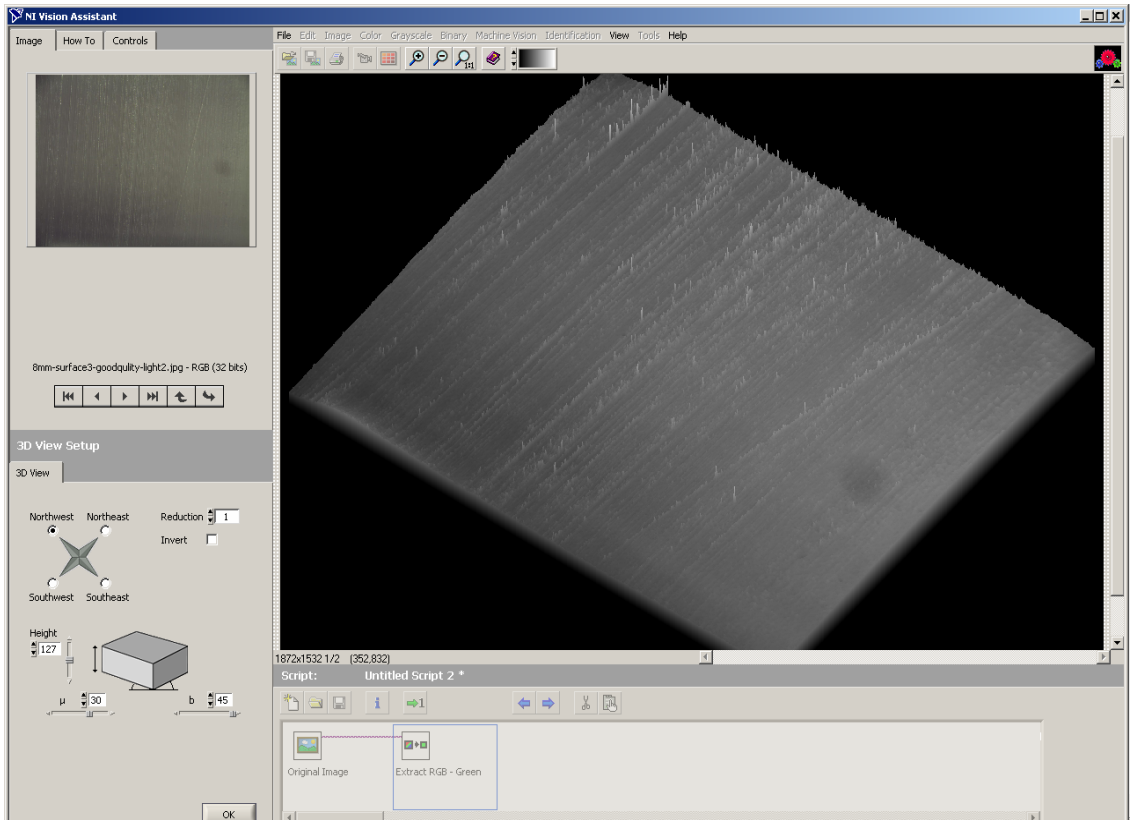

Figure A2.1 – Average roughness quality of the external surfaces of the RINSC demonstration prototypes manufactured by laser ablation process.

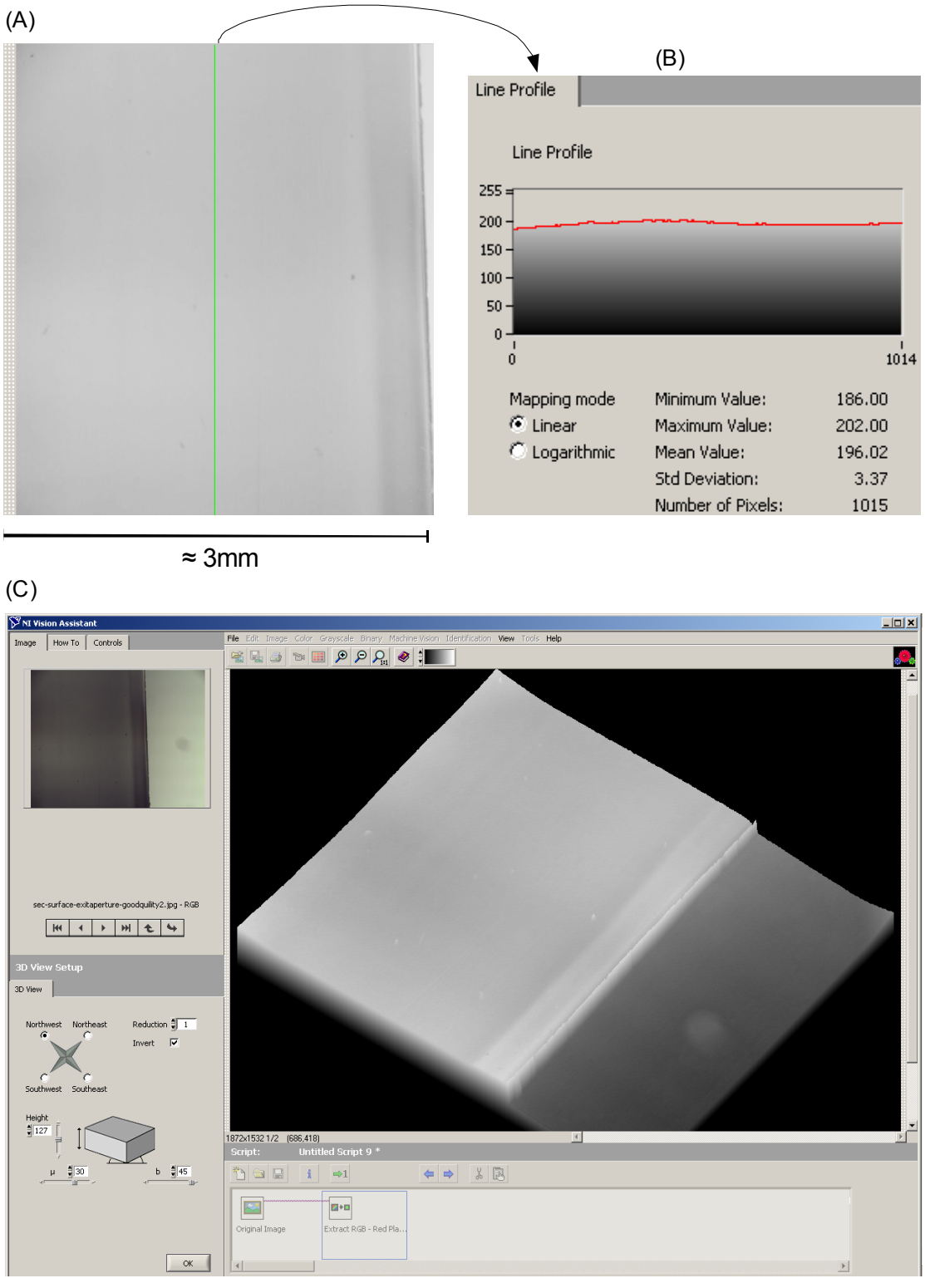

Figure A2.2 – Comparative reference showing a section of the surface of a commercial lens made of PMMA and manufactured by injection moulding process.

Appendix 3 - Alternative design concepts and prototyping

Two alternative design concepts that were also conceived and developed during this research are presented in this appendix.

The first concept, shown in Figures A3.1 to A3.3, presents a refractive-optics system that combines a CPC-type array with a planar light guide, both integrated into a single solid-dielectric structure. Figure A3.3 presents a series of demonstration prototypes made of PMMA (5mm thick) and also manufactured by laser ablation process.

The second concept, shown in Figure A3.4, is a compact nonimaging solar collector based on reflective-optics, rather than refractive-optics. This system was named folded-reflective-optics solar collector (FROSC). Computer ray-tracing analysis conducted with OptiCAD® demonstrates the working principle of this concept.

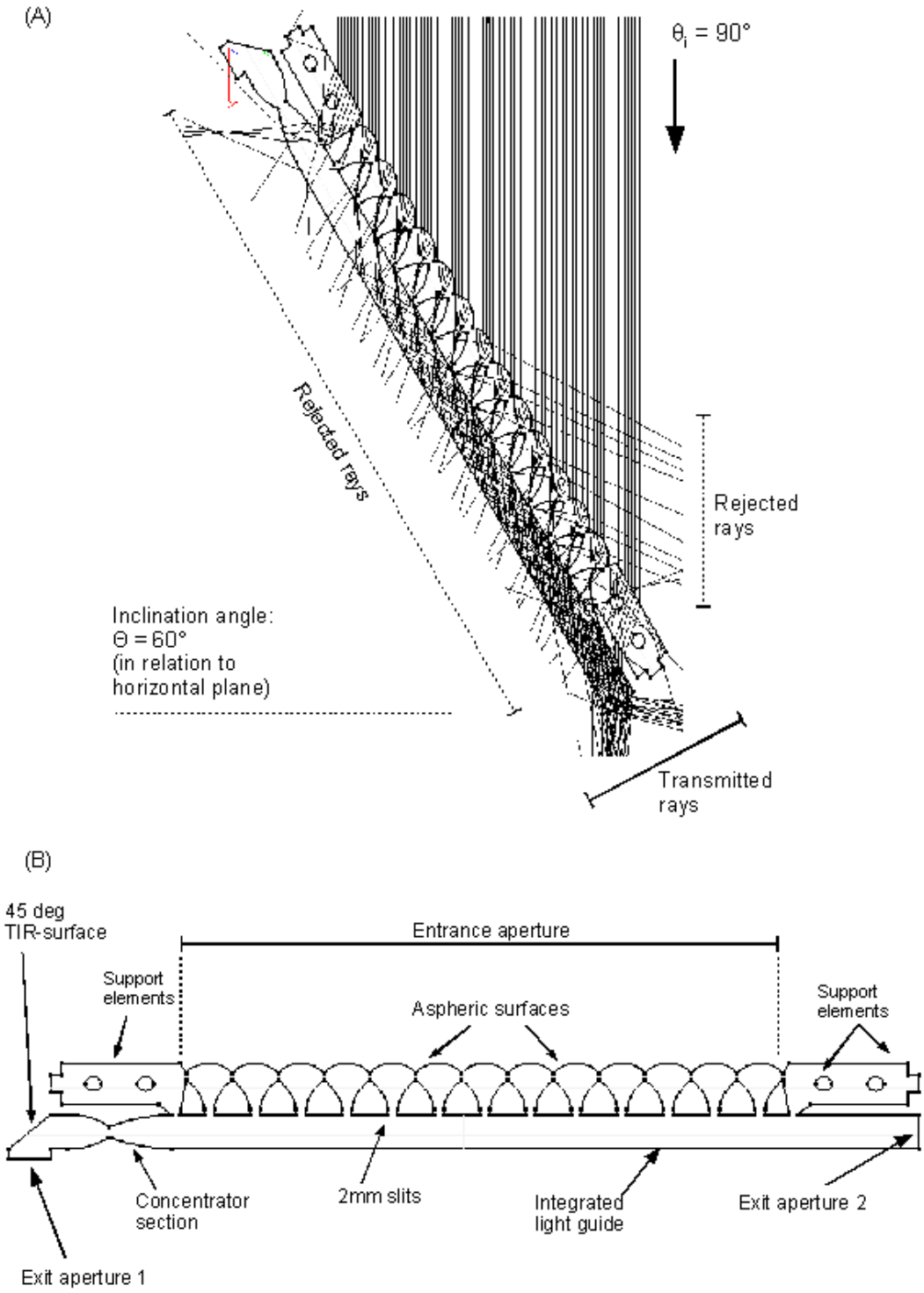

Figure A3.1 – An alternative design concept for a RINSC system conceived for tilted roofs.

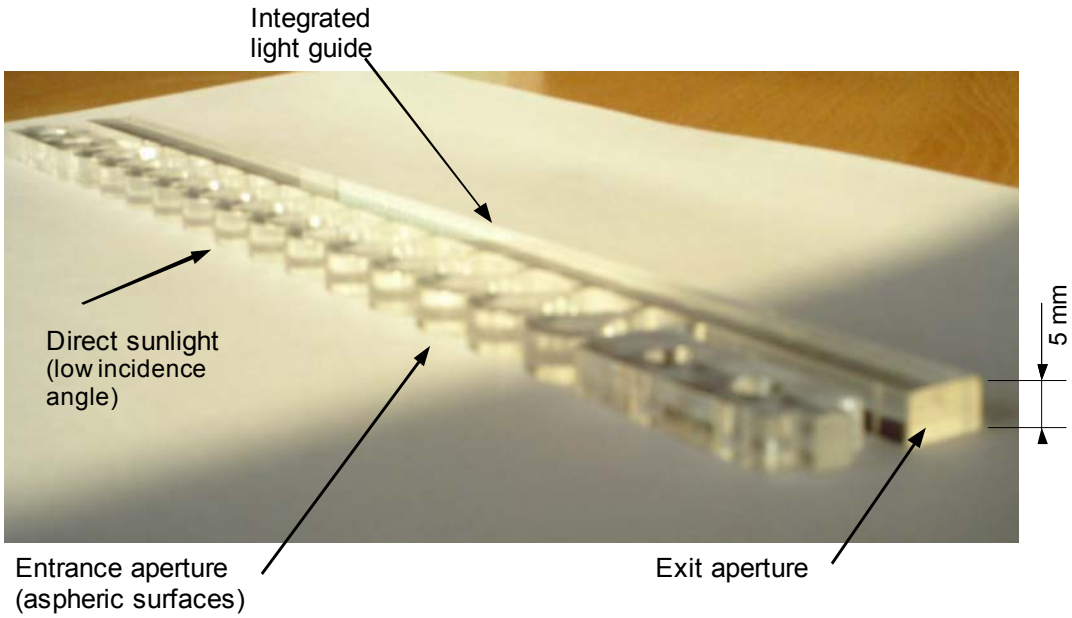

Figure A3.2 – Demonstration prototype for the alternative design concept for a RINSC system adapted for tilted roofs (as previously shown in Figure A3.1).

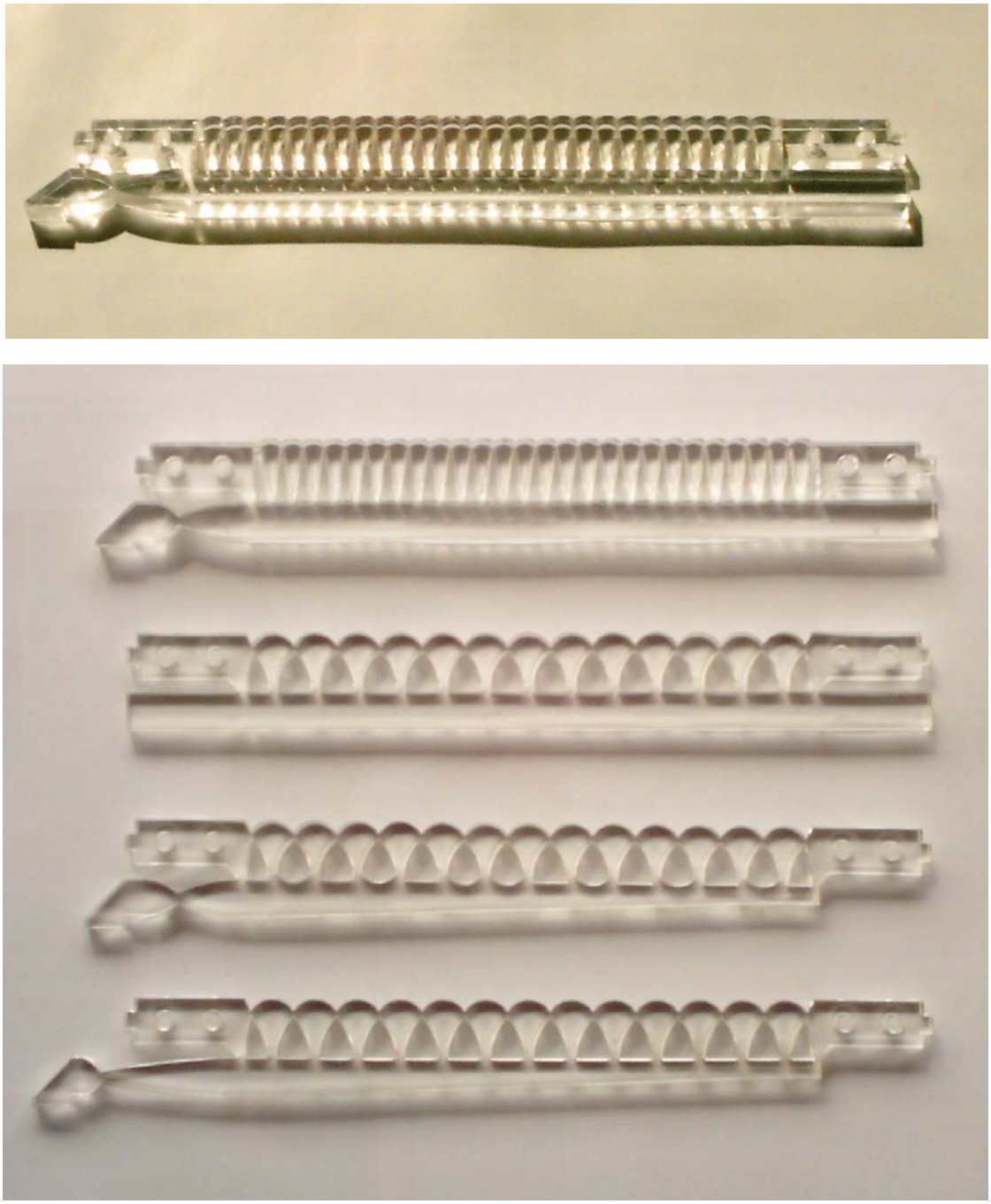

Figure A3.3 – Demonstration prototype for the alternative design concepts for a RINSC system adapted for tilted roofs.

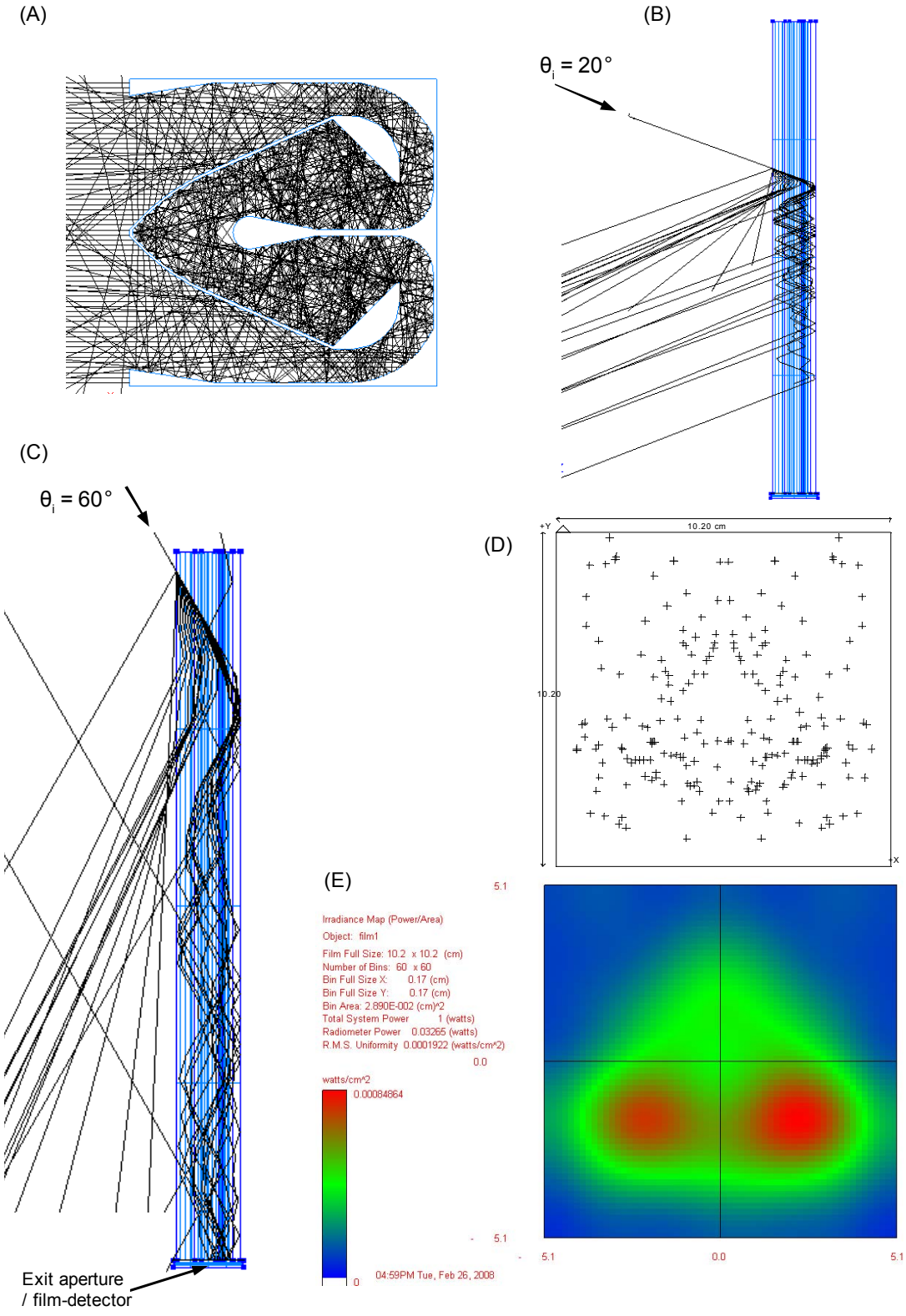

Figure A3.4 – Ray-trace analysis for the folded-reflective-optics solar collector (FROSC).

Appendix 4 – Publications abstracts

Three abstracts from papers completed before the examination of this thesis are attached in this appendix section. The first two are directly related to the RINSC systems. The third abstract, from a conference paper, presents the main results related to the first part of this research.

Attached papers abstracts are presented in the following order:

(A) Journal paper (ABSTRACT): **"Prismatic solar collectors for core-daylighting in buildings"**
Authors: Alexandre V. Pelegrini, David Harrison, Peter Evans
Status: accepted research paper

(B) Journal paper (ABSTRACT): "**Integrated multi-prismatic solar collector: A novel concept of nonimaging concentrator optics"**
Authors: Alexandre V. Pelegrini, David Harrison, Peter Evans
Status: **submitted research paper** (waiting for journal response – until the submission date of this thesis)

(C) Conference paper (ABSTRACT): "**Splitting and managing the solar spectrum for energy efficiency and daylighting"**
Authors: Alexandre V. Pelegrini, David Harrison, John Shackleton
Status: published in the proceedings and presented at the international conference "*Portugal SB07 Sustainable Construction, Materials and Practices: Challenge of the Industry for the New Millennium*", ISBN 978-1-58603-785-7, IOS Press, 2007.

Observation: this paper presents the results of the first part of this doctorate research, prior to the development of the RINSC systems presented in this thesis.

Elsevier Editorial System(tm) for **Renewable Energy**

Manuscript Draft (ABSTRACT)
Manuscript Number:

Title: Prismatic solar collectors for core-daylighting in buildings

- **Article Type:** Research Paper

- **Keywords:** Solar collectors; Daylighting systems; Prismatic panels; Sustainable buildings

- **Corresponding Author:** Mr Alexandre Vieira Pelegrini, MEng, BSc
- Corresponding Author's Institution: Brunel University

- **First Author:** Alexandre V Pelegrini, MEng, BSc
- **Order of Authors:** Alexandre V Pelegrini, MEng, BSc ; David Harrison, PhD; Peter Evans, PhD

Abstract: In this paper we present a device that applies prismatic structures and total internal reflection to divert and capture solar radiation for natural illumination and clean-energy applications in buildings. We call this device a prismatic solar collector. With a compact configuration the prismatic solar collector can be adapted or integrated into a building façade with minimum interference with the buildings architecture. A series of prototypes made out of clear polymethyl-methacrylate were manufactured by a laser cut process. Ray-trace analysis and experimental tests were carried out. Results show that these devices could provide an alternative low-cost solution to harvest and deliver sunlight for natural illumination in core building areas among other possible applications.

Elsevier Editorial System(tm) for **Solar Energy Materials and Solar Cells**

Manuscript Draft (ABSTRACT)
Manuscript Number: SOLMAT-D-09-00555

Title: Integrated multi-prismatic solar collector: A novel concept of nonimaging concentrator optics

- **Article Type:** Regular Manuscript

- **Keywords:** nonimaging optics, solar concentrators, prismatic arrays, light trapping, total internal reflection, solar collectors.

- **Corresponding Author:** Alexandre Vieira Pelegrini, MEng
- Corresponding Author's Institution: Brunel University

- **First Author:** Alexandre Vieira Pelegrini, MEng
- **Order of Authors:** Alexandre Vieira Pelegrini, MEng; David Harrison, PhD; Peter Evans, PhD.

Abstract: A novel concept of a static nonimaging solar collector is introduced and analysed. The concept, named integrated multi-prismatic solar collector (IMPSC), is a low-cost solid-dielectric nonimaging system that integrates several optical elements into a single-structure embodiment. Its working principle is based on refractive-optics and total internal reflection (TIR). The IMPSC optical system has a compact geometric configuration in which the exit aperture is perpendicular to the entrance aperture. Field and laboratory experimental tests with a demonstration prototype, made of clear polymethyl-methacrylate (PMMA) manufactured by laser ablation process, yield peak transmission efficiencies from 1.8% up to 5%. Computer simulated transmission efficiency peaked above 26%, leading to an effective concentration ratio of 3.25. The IMPSC system is designed for building integration. In this paper we analyse the performance of the IMPSC to harvest direct sunlight for natural illumination in buildings. Adaptations for solar-photovoltaic applications are also considered. Basic theory and considerations for future improvements are also presented.

Suggested Reviewers:

Antonio Luque Dr.
Universidad Politécnica de Madrid (UPM)
luque@ies-def.upm.es
Member of the Editorial Board of Solar Energy Materials & Solar Cells.

Volker Wittwer Dr.
Fraunhofer Institute for Solar Energy Systems
volker.wittwer@ise.fraunhofer.de
Member of the Editorial Board of Solar Energy Materials & Solar Cells.

A. Rohatgi Dr.
Georgia Institute of Technology
Ajeet.rohatgi@ece.gatech.edu
Member of the Editorial Board of Solar Energy Materials & Solar Cells.

Splitting and managing the solar spectrum for energy efficiency and daylighting

A.V.Pelegrini, D.Harrison, J.Shackleton
School of Engineering and Design, Brunel University, London, United Kingdom

ABSTRACT:

"This paper analyses the possibilities and benefits of splitting the solar spectrum for natural illumination and heating water applications in buildings. A design concept for a solar spectrum splitting device is presented. It considers the use of a dichroic cold-mirror to separate the infrared from the visible light. The device is attached to a low-cost solar collector that can be integrated into a building façade or roof. An experiment to test the efficiency of the system is carried out. As a result, "cool" visible light carrying almost no heat can be transported by fiber-optic cables to increase natural illumination in core areas of buildings, while the infrared is used to heat water. Lighting efficiency and water heating efficiency are estimated" (Pelegrini et al, 2007).

Observation:

This abstract was extracted from the paper "Splitting and managing the solar spectrum for energy efficiency and daylighting", published in the proceedings and presented at the international conference "*Portugal SB07 Sustainable Construction, Materials and Practices: Challenge of the Industry for the New Millennium*", ISBN 978-1-58603-785-7, IOS Press, 2007. The conference was held in Lisbon.

Note that the paper presents the results of the first part of this doctorate research, prior to the development of the RINSC systems presented in this thesis.

Splitting and managing the solar spectrum for energy efficiency and daylighting

A.V.Pelegrini, D.Harrison, J.Shackleton
School of Engineering and Design, Brunel University, London, United Kingdom

ABSTRACT: This paper analyses the possibilities and benefits of splitting the solar spectrum for natural illumination and heating water applications in buildings. A design concept for a solar spectrum splitting device is presented. It considers the use of a dichroic cold-mirror to separate the infrared from the visible light. The device is attached to a low-cost solar collector that can be integrated into a building façade or roof. An experiment to test the efficiency of the system is carried out. As a result, "cool" visible light carrying almost no heat can be transported by fiber-optic cables to increase natural illumination in core areas of buildings, while the infrared is used to heat water. Lighting efficiency and water heating efficiency are estimated.

1 INTRODUCTION

Energy consumption in buildings accounts for almost 40% of the total energy produced in Europe. Despite innovations and the development of more energy-efficient appliances and building systems, energy demand continues to rise due to the fact that there are more buildings being constructed and higher comfort levels are required by occupants. As highlighted by Osbourn (1997, pp.4), today "a modern building is expected to be a life-support machine". In this context, the efficient use of solar radiation becomes a fundamental issue in the design of sustainable and low-energy buildings.

The energy impact of solar radiation in buildings is well investigated in the literature. Lighting management with artificial lighting dimming as a function of daylighting can result in lighting energy savings from 20% to 70%, depending on several factors such as the building design, positioning and local climate conditions. Overall building energy consumption can be reduced by10% to 30% if daylighting is used strategically. One of the main problems with achieving this goal is that the heat from the solar radiation needs to be extracted before it enters the building, so that additional savings can result from reducing air conditioning loads. In hot climates solar heat gain can account for over 50% of the total building envelope cooling load (Krarti et al 2005, Bodart & Herde 2002, Perez-Lombard et al. 2007).

In a modern economic perspective one can think of sunlight as a free service provided by nature. Even on a cloudy day the available light intensity outside a building envelope is enough to illuminate almost every indoor task. But to use the whole potential of solar radiation for building services applications one has to consider the separation of the solar spectrum into its basic components, visible light (VIS), infrared (IR) and ultraviolet (UV). If done properly, this approach can result in several benefits. For example, visible light can be used for natural illumination while the IR part of the spectrum can be redirected for other applications.

This paper analyses the possibilities and benefits of splitting the solar spectrum for natural illumination and heating water applications in buildings. A design concept for a solar spectrum splitting device and a low-cost solar collector are presented. Lighting efficiency and water heating efficiency are estimated.

2 SOLAR RADIATION AND DAYLIGHTING IN BUILDINGS

2.1 *Solar radiation and building services*

The solar irradiance on a perpendicular plane outside the Earth atmosphere is calculated as 1353 W/m2. This value is known as the solar constant. On the top of the atmosphere around 48% of solar radiation is in the visible range (380nm to 780nm), 6.4% is ultraviolet irradiance (<380nm), and 45.6% is infrared radiation (above 780nm). In power terms this corresponds to 660 W/m2 related to the visible range, 92.6 W/m2 to ultraviolet, and 614.4 W/m2 corresponds to infrared irradiance. On the planet surface the intensity of solar irradiance will vary greatly due to losses in the atmosphere (Eicker 2003, pp.16).

The major goal of solar radiation management inside a building is to use sunlight to its fullest, separating the spectrum (visible light, ultra-violet and infrared), controlling and directing it according to different building systems needs. Table 1 presents some possible applications for the solar spectrum components in building services applications. Note that the solar components "to avoid" for each application is also highlighted.

Table 1. Applications for solar radiation in building services.

Application	Part solar spectrum needed	Part solar spectrum to avoid
Natural illumination	Visible light (VIS)	IR
Space heating	Infrared (IR)	--
Hot water	IR	--
Photovoltaic (PV) - (generate electricity)	VIS	IR
Thermophotovoltaic (TPV) - (generate electricity)	IR	--
Organic Photovoltaic (OPV) – (generate electricity)	Full spectrum	--
Air purification	Ultraviolet (UV)	--
Water purification	Ultraviolet (+IR)	--
Natural ventilation (stack-effect)	IR	--

2.2 *Benefits of daylighting*

When thinking about solar radiation one automatically thinks about natural lighting. Daylighting is the complete design process and application of natural light to its fullest inside buildings (Karlen & Benya 2004, p.31). If it is done properly it can create interesting dynamic interiors, support human health and activities, improve work and learning performance, reduce environmental impact, and reduce energy demand. If done improperly, it causes discomfort glare and demands excessive energy to extract the generated heat (Leslie 2002, p.381, Fontoynont 2002).

Beyond the impact on energy saving and costs reduction, researchers have also found that natural light can provide a healthier indoor environment. Recent research shows that lighting has a more profound implication on human health and well-being that was once suspected (Berson 2003, Webb 2006). Pauley (2004) argues that natural light is the best to balance the circadian clock and also that indoor lighting should employ lights with wavelengths shifted toward the yellow and orange wavelengths. Olders (2003) report on the positive impact of daylighting on the treatment of depression and seasonal affect disorders (SAD).

2.3 *Solar spectrum splitting technologies and materials*

Imenes & Mills (2004) present a very comprehensive review of the literature on spectral beam splitting technologies for solar concentrating systems. Although the main focus of their review highlights the applications for photovoltaic and thermophotovoltaic energy conversion, most of the principles can also be applied to daylighting systems. The authors classify current beam splitting methods in the following categories: (1) transmissive and reflective methods; (2) refractive and absorptive filtering methods; (3) luminescent filtering methods; (4) holographic filtering methods.

Dichroic materials, cold mirrors and hot mirrors can also be applied to separate the solar spectrum. Dichroic materials are manufactured on a glass or plastic base on which alternate lay-

ers of transparent materials are laid. The amount and values of the wavelength transmitted or reflected depend on the thickness and refractive index of each layer. It reflects visible light and transmits the IR, being also referred as a "cold mirror". Changing the order of the layers reflects the IR and transmits the visible light. In this configuration it is referred as a "hot mirror". Magnesium fluoride/zinc sulphide and tantala/silica oxides are some examples of dichroic layers. (Elmualim et al. 1999, pp.255). Dye et al (2003) report a full-spectrum solar concentrator system that also applies a dichroic cold mirror to separate the infrared from this visible light. In this system the IR is directed towards a thermophotovoltaic (TPV) cell array to generate electricity, while the visible light is used for natural illumination or photobioreactors.

3 SYSTEM DESIGN AND PROTOTYPING

3.1 *Optical system configuration and dichroic cold mirror device*

To separate the infrared from the visible light we used a dichroic cold mirror made of borosilicate (LEBG) float glass, 50x50mm and 3mm thickness. Operating at an angle of 45 degrees it reflects over 90% of visible light (425-650nm) while around 85% of the infrared (800-1200nm) is transmitted through.

The cold mirror was mounted at an angle of 45 degrees inside a device specially designed for it. The device is attached to the solar collector. Figure 1 illustrates how the system is expected to work. A flux of collimated sunlight, concentrated by the solar collector, is directed towards the cold mirror. Visible light (VIS) is reflected down while the infrared (IR) passes through. Collimation is a fundamental requirement for the efficient separation of the solar spectrum using a dichroic cold mirror. This means that incoming rays must be parallel so that sunlight intensity is maximized. If most of the incoming light flux is not collimated the infrared and visible light will not be separated.

A photometer (light meter) is connected to the visible light exit, measuring the light level (illuminance, lx) output of the system. The projected area of the cold mirror (50x50mm, positioned at 45 degrees) over the visible light exit is 50x36mm. The same projected area covers the infrared exit. It is important to note that the cold mirror projected area of 50x36mm will de used later on in this paper to calculate the lighting efficiency of the system (luminous intensity and illuminance).

At the infrared exit an aluminum container with 500ml of water is kept isolated inside a larger container. The internal and external walls of the larger container are covered with thermal insulation. An infrared reflective coating covering the internal walls of the container helps to keep the infrared trapped inside. The aluminum container is painted in black. A small window on the side of the larger container can be opened to take measurements of the water temperature using an infrared thermometer (Fig.1).

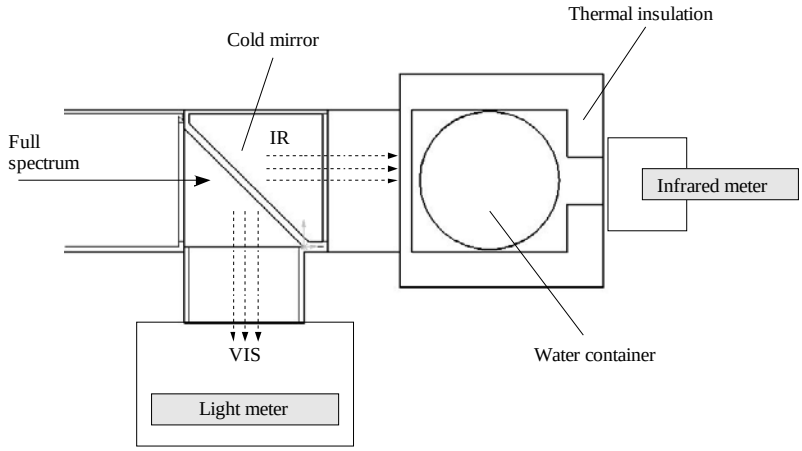

Figure 1. Schematic representation of the device used to separate the infrared (IR) and the visible light (VIS).

3.2 *Design and mock-up prototyping of the solar collector*

Our intention for this experiment was to develop a low-cost passive (non-tracking) solar collector, rather than a high cost system tracking system. CAD software was applied to design the system and preliminary virtual simulations were done using OptiCAD, an optic-design specialist software. Using ray-tracing analysis tools it was possible to optimize the system and define the best acceptance angle for solar incidence.

The final solar collector mock-up was optimized for the experiment location (London, UK: 51 38' N; 07' W) and has an acceptance angle of 50 degrees. Positioned at an angle of 45 degrees and facing south it achieves its highest efficiency range from 12:00h to 13:30h. It has a frontal area of 440x200mm which represents around 1/11 square meter. In other words, an array of eleven solar collectors (440x200mm) occupies an area of one square meter.

A fundamental requirement for the system was to maximize the reflectivity of the visible light and the infrared inside the solar collector. This is an essential issue in a system that intends to use both visible light and infrared. For this reason it was important to choose reflective materials, coatings and optical components that worked well for both visible light and infrared. We used Mylar to cover the internal surfaces of the solar collector. This material reflects both visible light and infrared with an efficiency of 90-95%. Figure 2 shows perspectives and side views of CAD drawings of the proposed solar collector.

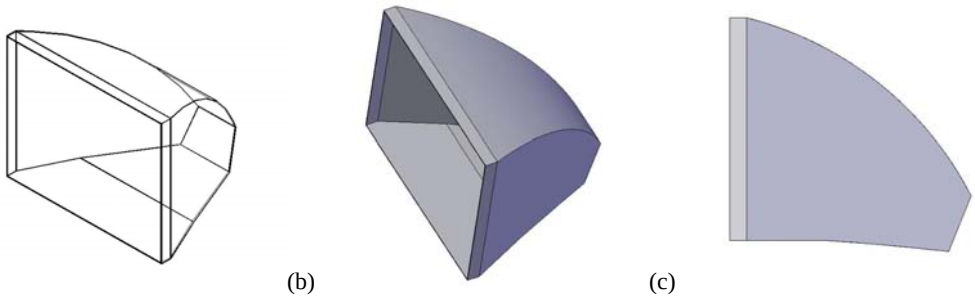

(a) (b) (c)

Figure 2. CAD drawings of the solar collector. Perspective views (a) and (b). Side view (c).

4 EXPERIMENTS AND RESULTS

4.1 *Experiment set-up*

Two experiments were realized in London (51 38' N; 07' W), both in late April 2007. The mock-up prototype of the designed solar collector was installed indoors, above a double-glazing window facing south. The area of the collector received direct sunlight from around 10:30 in the morning to 16:30 in the afternoon. In the first experiment the collector was positioned at an angle of 30 degrees in relation with the ground floor. For the second experiment the angle was increased to 45 degrees so that the frontal area of the collector was facing the sun during a longer period. Table 2 presents a summary of the conditions for each experiment.

Table 2. Solar collector set-up, weather conditions and sky illuminance for experiments 1 and 2.

Experiment	Solar collector set-up		Weather conditions	Sky Illuminance (lx)		Hours
	Orientation	Positioning		Max.	Min.	
Experiment 1 (25.04.2007)	South	30 degrees	Variable, sun spells Partial cloud, rain	70000	1000	3 hours
Experiment 2 (30.04.2007)	South	45 degrees	Bright sunny, No clouds	>100000	30000	5 hours

4.2 *Data gathering and results*

Measurements of visible light output and temperature variation in the 500ml water container were taken every 10 minutes. Visible light was measured using two photometers (Extech Light Meter EA31 and Extech Light Meter EA33). An infrared thermometer (Extech 42529) was used to measure variations in the water temperature.

Figure 3 and Figure 4 plots the results from the first experiment. Figure 5 and Figure 6 plots the results from the second experiment. Two major variables were responsible for the great differences between the results. One is the positioning angle of the solar collector (30 degrees in the first experiment and 45 degrees in the second). The other variable was the weather conditions. Cloudy weather with few sunny spells was predominant during the first day of experiment, while a sunny day with blue sky and no clouds was a gift for the second experiment.

The light level output of the system is presented as "system lux" in Figure 3, for experiment 1, and Figure 5, for experiment 2. The "sky lux" term refers to the light level values of the sky illuminance, measured by positioning the photometer in a horizontal position under direct sunlight.

Temperature variations of the 500ml water container are presented in Figure 4, for experiment 1, and Figure 6, for experiment 2. The temperature of the water container that receives infrared radiation from the solar collector is noted in the legend of Figure 4 and Figure 6 as "Temp.C1", marked with a square in the graph. "Temp.C1" is the water container presented firstly in Figure 1. "Temp.C2" and "Temp.C3" refers to two other 500ml water containers that were used as reference. The container "Temp.C2" was positioned under direct sunlight, while the container "Temp.C3" was kept in the shade at room temperature. The three water containers start with the same temperature, 21 degrees Celsius, in both experiments.

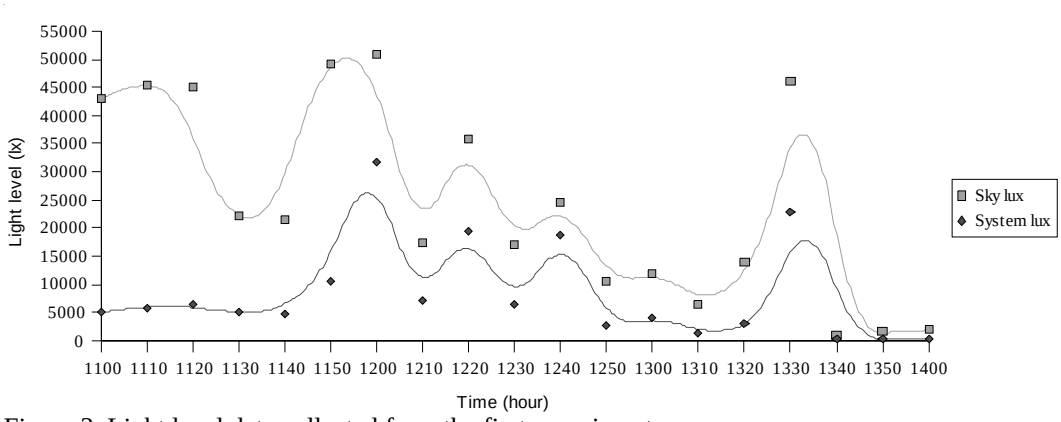

Figure 3. Light level data collected from the first experiment.

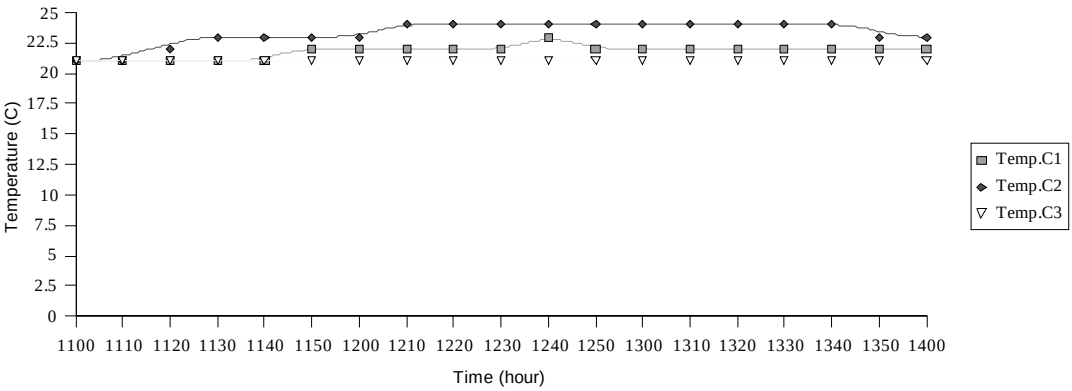

Figure 4. Temperature data collected from the first experiment.

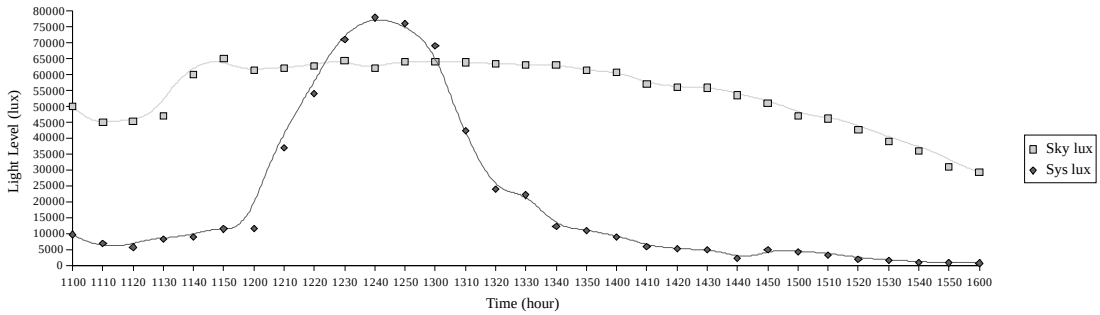

Figure 5. Light level data collected from the second experiment.

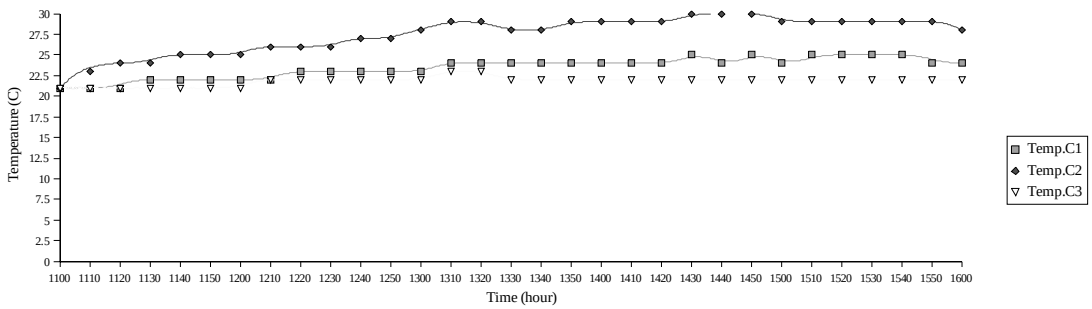

Figure 6. Temperature data collected from the second experiment.

4.3 *Estimating lighting efficiency*

Lighting efficiency is analyzed here in terms of the luminous output of the system considering the data collected from the two experiments. Calculations result from an estimation of the performance of a system with the same configuration but with a frontal area of one square meter.

Table 3 and Table 4 present the estimated performance for a system with a frontal area of one square meter. Data is extracted from Figure 3 and Figure 5 and rearranged in time periods of 30 minutes. This procedure helps to estimate the average performance of the system at different periods of time and under different weather conditions. The columns under the term "system efficiency" present the average value of the luminous flux (in lumens). To calculate the transmission efficiency we estimate that all lumens output is concentrated directly into a bundle of acrylic (PMMA) fiber optical cables (core diameter of 1mm, attenuation 0.21 dB/m). Light transmission efficiency through the fiber optical cables are estimated to be 75% after 5m, 40% after 10m, and only 10% after 20m. Values are approximated.

Considering the values presented in Table 4 we calculate that, at its peak efficiency (from 12:30 to 13:00), the system is capable to illuminate an area of 10m² with an illuminance level of 112lx (after 5m), 60lx (after 10m) and 15lx (after 20m).

Table 3. Luminous flux out put and estimation of the transmission efficiency for experiment 1.

Time	System efficiency (Exit output)	Light transmission efficiency for 1mm PMMA fiber optical cable		
		After 5m (75%)	After 10m (40%)	After 20m (10%)
	Lumens	Lumens	Lumens	Lumens
1100 – 1130	114	85.5	45.6	11.4
1130 – 1200	268	201	107.2	26.8
1200 – 1230	332	249	133	33.2
1230 – 1300	163	122.3	65.2	16.3
1300 – 1330	159	119.3	63.6	15.9
1330 – 1400	123	92.2	49.2	12.3

Table 4. Luminous flux output and estimation of the light transmission efficiency for experiment 2.

Time	System efficiency (Exit output)	Light transmission efficiency for 1mm PMMA fiber optical cable		
		After 5m (75%)	After 10m (40%)	After 20m (10%)
	Lumens	Lumens	Lumens	Lumens
1100 – 1130	156	117	62.4	15.6
1130 – 1200	206	154.5	82.4	20.6
1200 – 1230	887	665.3	354.8	88.7
1230 – 1300	1502	1126.5	601	150.2
1300 – 1330	804	603	321.6	80.4
1330 – 1400	278	208.5	111.2	27.8
1400 – 1430	127	95.3	50.8	12.7
1430 – 1500	83	62.2	33.2	8.3
1500 – 1530	57	42.8	22.8	5.7
1530 – 1600	20	15	8	2

4.4 *Estimating water heating efficiency*

The system water heating efficiency was measured considering the difference between the temperature of the water in the container that received direct infrared from the system (Temp.C1, from Figures 4 and 6), and the temperature of the reference water container that was kept isolated at room temperature (Temp.C3, from Figures 4 and 6). Table 5 shows the average and the peak temperature differences measured in the experiments.

Although only a small change in temperature was measured, it is important to note that the system sustained the temperature difference for more than two hours in the first experiment (that lasted only 3 hours) and for four and a half hours in the second experiment (that lasted 5 hours).

We estimate that a 1m² array of solar collectors (with the same configuration as the one described in this paper, and under the same weather conditions) would be able to sustain an increase of up to 3 degrees Celsius in 5 litre of water during at least one and half hours. To increase 3 degree Celsius in the temperature of 50 litre of water would require a solar collector array with an area of 10m².

Table 5. Water heating efficiency for experiments 1 and 2.

Time	Experiment 1 Temperature difference (Celsius)		Experiment 2 Temperature difference (Celsius)	
	Average	Peak	Average	Peak
1100 – 1130	-	-	-	1 (at 11:30)
1130 – 1200	1	1 (at 11:50)	1	-
1200 – 1230	1	-	1	-
1230 – 1300	1	2 (at 12:40)	1	-
1300 – 1330	1	-	1	2 (at 13:30)
1330 – 1400	1	-	2	-
1400 – 1430	-	-	2	3 (at 14:30)
1430 – 1500	-	-	3	-
1500 – 1530	-	-	3	-
1530 – 1600	-	-	3	-

5 DISCUSSION AND CONCLUSION

Solar radiation can result in a more positive contribution to buildings systems and services if visible light and infrared are separated. The system presented in this paper is capable to deliver up to 1120lm through 5m of fiber optical cables. Although this is considered a low luminous flux, it is still able to illuminate an area of 10m² with 112lx (after 5m). We estimate that an array of solar collectors with 3m² to 5m² will be able to deliver up to 560lx of natural light (with no infrared) to an area of 10m² located 5m deep into the building. This is enough for almost all

tasks realized in educational and office buildings, for example (CIBSE, 2002).

The strategy for the solar collector was to design a low-cost passive (non-tracking) system that could be easily integrated into a buildings façade or roof top. Our intention for this experiment was to develop a low-cost (and low-efficiency) system, rather than a high efficiency-high cost system. The solar collector acceptance angle can be optimized for different site locations considering the positioning of the building on the Earth surface (longitude and latitude). It also can be optimized according to the façade where it is positioned (facing south, west, east or north).

Some small improvements in the system could increase its performance significantly. Using a better cold mirror (with infrared transmission of up to 2500nm) it may be possible to increase the water temperature. We expect to at least double the efficiency of the system while keeping costs low.

Acknowledgments

This project is funded in part by CNPq, Brazilian National Council for Scientific and Technology Development.

REFERENCES

CIBSE, 2002. *Code for Lighting*. Oxford: Butterworth-Heinemann.

Berson, D.M. 2003. Strange vision: ganglion cells as circadian photoreceptors. *Trends in Neurosciences* 26(6): 314-320.

Bodart, M. & De Herde, A. 2002. Global energy savings in offices building by the use of daylighting. *Energy and Buildings* 34: 421-429.

Dye, D. et al. 2003. Optical design of an infrared non-imaging device for full-spectrum solar energy systems. *Proceedings of International Solar Energy Conference, Hawaii, USA, 15-18 March 2003*.

Eicker, U. 2003. *Solar Technologies for Buildings*. Chichester, England: John Wiley & Sons.

Elmualim, A.A. 1999. Evaluation of dichroic material for enhancing light pipe/natural ventilation and daylighting in an integral system. *Applied Energy* 62: 253-266.

Fontoynont, M. 2002. Perceived performance of daylighting systems: lighting efficacy and agreeableness. *Solar Energy* 73(2): 83-94.

Imenes, A.G. & Milles, D.R. 2004. Spectral beam splitting technology for increased conversion efficiency in solar concentrating systems: a review. *Solar Energy Materials & Solar Cells* 84:19-69.

Karlen, M. & Benya, J. 2004. *Lighting Design Basics*. Hoboken, New Jersey: John Wiley & Sons.

Krarti, M. et al. 2005. A simplifies method to estimate energy savings of artificial lighting use from daylighting. *Building and Environment* 40: 747-754.

Leslie, R.P. 2003. Capturing the daylighting dividend in buildings: why and how? *Building and Environment* 38: 381-385.

Olders, H. 2003. Average sunrise time predicts depression prevalence. *Journal of Psychosomatic* 55: 99-105.

Osbourn, D.1997. *Introduction to Building*. Essex, England: Addison Wesley Longman.

Pauley, S.M. 2004. Lighting for the human circadian clock: recent research indicates that lighting has become a public health issue. *Medical Hypotheses* 63: 588-596.

Perez-Lombard, L. et al. 2007. A review on buildings energy consumption information. *Energy and Buildings* (article in press).

Webb, A.R. 2006. Considerations for lighting in the built environment: non-visual effects of light. *Energy and Buildings* 38: 721-727.